

Spring 2019

HORIZONTAL FLOW LOOP DESIGN FOR THE STUDY OF DRILL STRING ROTATION EFFECTS ON CUTTINGS TRANSPORT

David C. Rathgeber

Follow this and additional works at: https://digitalcommons.mtech.edu/grad_rsch

Part of the [Petroleum Engineering Commons](#)

HORIZONTAL FLOW LOOP DESIGN FOR THE STUDY OF DRILL
STRING ROTATION EFFECTS ON CUTTINGS TRANSPORT

by

David Clifford Rathgeber

A thesis submitted in partial fulfillment of the
requirements for the degree of

Master of Science in Petroleum Engineering

Montana Tech

2019



Abstract

Exploration and Production companies are continually focusing more time, energy and resources into Extended Reach Drilling in order to maximize reservoir production while minimizing both environmental impact and development costs.

These long laterals (2:1 Measured Depth: True Vertical Depth) are often more difficult to drill and can be severely impacted by inadequate drilling practices. Cuttings transport efficiency is a critical parameter of Extended Reach Drilling operations, and poor wellbore cleaning can lead to excessive torque, drag, and several other serious downhole problems.

Although many studies have been performed that identify the importance of drill string rotation on cuttings movement, there is still much to be learned about the correlation between rotation and hole cleaning. This increase in transport cuttings efficiency is more pronounced in larger diameter holes, where often sudden increases in transport efficiency occur when drill string rotation nears both 120 and 180 RPM.

This document presents a design of a flow loop capable of emulating downhole flow conditions and high RPM drill string rotation in a large diameter wellbore, which would allow for the study and better understanding of this phenomenon. This design will also be the first that allows drill string interchangeability and adjustment of drill string centerline within the casing, further increasing research capabilities. A comprehensive computational fluid dynamics (CFD) model has also been designed. This model will be used alongside the flow loop and will be refined and validated by future flow loop experiments. This flow loop and CFD model can be used to develop working correlations and provide real world predictive models.

A strong comprehension of these step changes in cuttings removal rates could allow for the development of new technology or drilling practices that could replicate this effect, increasing transport efficiency dramatically. With the ever-increasing importance of successful Extended Reach Campaigns, companies are relying heavily on technological and operational breakthroughs to push the envelope of Extended Reach.

Keywords: Extended reach, cuttings transport, drilling, horizontal, rotation, CFD

Dedication

I wish to thank my Mom Leslie and Dad Donald for their continued love and support through my time on this research. In addition, I would like to thank my Fiancée, Sonia and our kids, Trent, Corwin and Penelope, for being incredibly supportive and understanding during my studies. I would never have been able to do it without you!

Acknowledgements

I would like to thank Dr. Lee Richards, Dr. Peter Lucon, Brandon Foster and Matt Malin for their guidance throughout this project. Brandon Foster for his assistance granting me access to invaluable educational experiences leading to the further design of the flow loop presented in this document. Dr. Lucon for his invaluable assistance in granting me access to the appropriate CFD modeling software and offering guidance in selecting components for the flow loop. Matt Malin for his assistance in completing flow loop experiments on the Montana Tech campus 2-inch flow loop.

Table of Contents

ABSTRACT	II
DEDICATION	III
ACKNOWLEDGEMENTS	IV
LIST OF TABLES.....	X
LIST OF FIGURES.....	XII
LIST OF EQUATIONS	XV
GLOSSARY OF TERMS	XVIII
GLOSSARY OF EQUATION TERMS	XIX
1. INTRODUCTION	1
1.1. <i>Problem Statement</i>	3
1.2. <i>Limitations</i>	4
2. LITERATURE REVIEW.....	6
2.1. <i>Forward</i>	6
2.2. <i>Current State of Extended Reach Drilling</i>	9
2.2.1. Introduction	9
2.2.2. The Importance of Extended Reach	15
2.2.3. Extended Reach Defined	17
2.3. <i>Extended Reach Drilling Constraints</i>	21
2.3.1. Mechanical Constraints Overview	22
2.3.1.1. Drill String.....	22
2.3.1.2. Casing.....	26
2.3.1.3. Rig Capability.....	27
2.3.1.4. Well Profile.....	28

2.3.2.	Formation Constraints Overview.....	29
2.3.2.1.	Cement.....	30
2.3.2.2.	Drilling Mud Rheology and ECD	32
2.3.2.3.	Cuttings Management.....	34
2.4.	<i>Extended Reach Cuttings Transport Evaluation</i>	<i>40</i>
2.4.1.	Modeling	41
2.4.1.1.	Newtonian and Non-Newtonian Fluids	44
2.4.1.2.	Non-Newtonian Fluid Flow in Annulus.....	54
2.4.1.3.	Stabilized Flow	57
2.4.1.4.	Pressure Loss in Non-Newtonian Flow	59
2.4.1.5.	Non-Newtonian Annulus Flow Modeling	62
2.4.1.6.	Empirical Correlations	63
2.4.1.7.	Critical Cuttings Transport Velocity Model	65
2.4.1.8.	Layer Model	67
2.4.1.9.	Computational Fluid Dynamics Modeling	69
2.4.2.	Experimentation.....	71
2.5.	<i>Literature Review Conclusion and Recommendations</i>	<i>76</i>
3.	PROCEDURE AND METHODOLOGY.....	78
3.1.	<i>Problem Identification.....</i>	<i>78</i>
3.1.1.	CFD Modeling.....	79
3.1.1.1.	Model Geometry.....	79
3.1.1.2.	Meshing	80
3.1.1.3.	Preprocessing - Setting up Domain	81
3.1.1.4.	Preprocessing - Setting up Physics	81
3.1.1.5.	User Defined Data	83
3.1.1.6.	Solving.....	83
3.1.1.7.	Postprocessing and Results.....	84
3.1.2.	Experimental Data.....	84
3.1.3.	Vertical Flow Loop Model.....	85

3.1.3.1.	Simulation Design	85
3.1.4.	Horizontal Flow Loop Model	90
3.1.4.1.	Inlet and Outlet Design	90
3.1.4.2.	Test Section Dimensions	91
3.1.4.3.	Test Section Design	92
3.2.	<i>Flow Loop Design</i>	92
3.2.1.	Overview	92
3.2.1.1.	Test Section	92
3.2.1.2.	Test Section Pump	94
3.2.1.3.	Power Section	103
3.2.1.4.	Cuttings Management	105
3.2.1.5.	Fluids Management	105
3.2.1.6.	Data Acquisition, Monitoring and Controls Systems	106
4.	RESULTS	109
4.1.	<i>Experimental Results</i>	109
4.1.1.	Single Phase Results	109
4.1.1.1.	Simulation Results	110
4.1.1.2.	Hardware and Simulation Time	111
4.1.2.	Multiphase Results	112
4.1.2.1.	Hardware and Simulation Time	114
4.2.	<i>Flow Test Section</i>	114
4.2.1.	Flow Inlet	115
4.2.2.	Flow Outlet	123
4.2.3.	Test Window	126
4.2.4.	Test Window Length	127
4.3.	<i>Return Line</i>	128
4.4.	<i>Flow Loop Volume Requirements</i>	129
4.5.	<i>Test Section Ends</i>	129
4.6.	<i>Flow Loop Pumps</i>	129

4.6.1.	Test Section Pump	129
4.6.2.	Fluid circulation pump	133
4.7.	<i>Power Sections</i>	134
4.7.1.	Pipe Rotation	134
4.7.2.	Pipe Assembly/Disassembly	135
4.8.	<i>Fluids Management System</i>	136
4.8.1.	Storage and Mixing Equipment	136
4.8.2.	Flow and circulation lines	138
4.8.2.1.	Drain System	138
4.8.2.2.	Filling/Circulation System	140
4.9.	<i>Cuttings Management System</i>	141
4.9.1.	Cuttings Separation	141
4.9.2.	Cuttings Storage and Injection	143
4.10.	<i>Data Acquisition, Monitoring and Controls systems</i>	144
4.10.1.	Monitoring Systems	144
5.	DISCUSSIONS AND CONCLUSIONS	148
5.1.	<i>Design Implications</i>	148
5.2.	<i>Flow Loop Design Summary</i>	149
5.3.	<i>Future Work</i>	153
5.3.1.	Flow Loop Design Refinement	153
5.3.1.1.	Equipment Design and Selection	153
5.3.1.2.	Operating Guidelines, HSE	157
5.3.2.	CFD Model Refinement	157
5.3.2.1.	Vertical Flow Loop Models	158
5.3.2.2.	Horizontal Flow Loop Models	159
6.	REFERENCES CITED	161
7.	APPENDIX	172
7.1.	<i>Rig Pricing</i>	172

7.2.	<i>Additional Mixture Velocity Equations.....</i>	174
7.3.	<i>Velocity Ratio Data</i>	175
7.4.	<i>Flow Loop Data</i>	176
7.5.	<i>Vertical Flow Loop Experimental Data.....</i>	178
7.6.	<i>SpaceClaim User Manual</i>	185
7.7.	<i>Supplemental Drilling Fluid Data.....</i>	192
7.8.	<i>Montana Tech Flow Loop Spaceclaim P&ID.....</i>	193
7.9.	<i>Horizontal Flow Loop Inlet Spaceclaim P&ID's.....</i>	194
7.10.	<i>Inlet/Outlet Mesh Data</i>	197
7.11.	<i>Vertical Flow Loop Mesh Data</i>	205
7.12.	<i>Test Section Flow Loop Mesh Data</i>	211
7.13.	<i>Flow Normalization Plot, 60 ft.</i>	219
7.14.	<i>Drill Pipe Data Table.....</i>	220
7.15.	<i>Drive Motor Specifications</i>	224
7.16.	<i>Fully Rotational Toque Bucking Machine.....</i>	226
7.17.	<i>Spectra Stim</i>	228

List of Tables

Table I: List of flow loops and their dimensions (Li & Luft, 2014).....	73
Table II: Drilling Mud Properties	83
Table III: Flow Loop Experiment Averages Summary	85
Table IV: Fluent solver settings for multiphase flow	86
Table V: Fluent model settings for multiphase flow	86
Table VI: Fluent phase settings for multiphase flow	87
Table VII: Fluent boundary properties for multiphase flow	87
Table VIII: Fluent solver settings for multiphase flow.....	89
Table IX: Expected Fluid Property Ranges	96
Table X: Flow Loop Test Section Flow Ranges.....	97
Table XI: Expected Torque Values.....	105
Table XII: Single Phase Simulation Results.....	110
Table XIII: Calculated results, single-phase.....	111
Table XIV: Standalone computer specifications	111
Table XV: Simulation run times	111
Table XVI: Multiphase flow experiment results	112
Table XVII: Montana Tech cyberinfrastructure	114
Table XVIII: Summary of Fluid Velocities	118
Table XIX: Inlet Parameter Summary	123
Table XX: Outlet Parameter Summary.....	126
Table XXI: Test section length summary	127
Table XXII: Return line specifications	128

Table XXIII: Flow loop volume summary	129
Table XXIV: General Suitability of Wetted Materials	132
Table XXV: Flow loop pump requirements	132
Table XXVI: API Make-up torque recommendations.....	135
Table XXVII: Minimum tank capacity	137
Table XXVIII: Shale shaker vs Mudcube.....	142
Table XXIX: Mudcube specifications	142
Table XXX: Fluid velocities summary	143
Table XXXI: Cuttings management system specifications	144
Table XXXII: Pressure transducer set location along test window	145
Table XXXIII: Summary of data monitoring systems.....	147
Table XXXIV: Flow loop design parameters summary	150
Table XXXV: CFD Models summary	152
Table XXXVI: Summary of future design work for flow loop	154
Table XXXVII: Multiphase method assignments.....	159
Table XXXVIII: Floating Rig Price Estimates.....	172
Table XXXIX: Jack up Rig Price Estimates.....	173
Table XL: Flow Loop Sources.....	176
Table XLI: Drilling Fluid Rheometer Data	192

List of Figures

Figure 1: Wytch Farm Development Radius	10
Figure 2: BP Extended Reach Categories compared to 2:1 Departure: TVD ratio (Mason & Judzis, 1998)	18
Figure 3: Ellipse of Uncertainty.....	26
Figure 4: Acting forces on a drilled cutting (Egenti, 2014).....	42
Figure 5: Cuttings transport flow regimes (Egenti, 2014)	43
Figure 6: Rheology comparison by shear response (expected curves).....	46
Figure 7: Shear stress layers	47
Figure 8: Rheogram of a Newtonian fluid (Cooking Oil, 294K) (Chhabra & Richardson, 2008)	48
Figure 9: Trend of a typical Hershel-Buckley fluid.....	52
Figure 10: Velocity ratio parameters	56
Figure 11: Velocity ratio profiles.....	57
Figure 12: Three-phase flow model.....	67
Figure 13: Two-phase flow model.....	68
Figure 14: Eccentricity Test Run Locations	90
Figure 15: Centrifugal Performance Curve (Capacity vs. Total Head)	100
Figure 16: Centrifugal Performance and Efficiency Curve	101
Figure 17: Single phase simulations pressure drop.....	110
Figure 18: Experimental results, 15 scfm air and 10 gpm water rates.....	112
Figure 19: Experimental results, 35 scfm air and 10 gpm water rates.....	113
Figure 20: Experimental results, 60 scfm air and 10 gpm water rates.....	113

Figure 21: Flow Loop Test Section Inlet Designs (45°, reverse 45°, 90° and dual 90°) with 8-inch ID	115
Figure 22: Flow Normalization by Fluid Characteristics (45°, 8-inch inlet)	117
Figure 23: Varied Shear Between Fluids	118
Figure 24: Velocity Normalization on 90° inlet (8 inch)	119
Figure 25: Velocity Normalization on 45° inlet (8 inch)	120
Figure 26: Velocity Normalization on 90° inlet (5 inch)	120
Figure 27: Velocity Normalization on 45° inlet (5 inch)	121
Figure 28: Velocity Normalization on reverse 45° inlet (8-inch)	122
Figure 29: Velocity Normalization on dual-90° inlet (8-inch).....	122
Figure 30: End-effects, heavy OBM, 90° outlet (8-inch).....	124
Figure 31: End-effects, light WBM, 90° outlet (8-inch).....	125
Figure 32: End-effects, water, 90° outlet (8-inch)	125
Figure 33: Inlet and outlet elbow identification.....	128
Figure 34: FORUM Energy Services fully rotational torque machine	136
Figure 35: Venturi jet pump design	137
Figure 36: Drain line front view	139
Figure 37: Drain line side view.....	139
Figure 38: Side view, fill line to inlet	140
Figure 39: Top view, fill line to inlet.....	141
Figure 40: Transducer locations on casing	145
Figure 41: Workbench Window.....	185
Figure 42: SpaceClaim Default Sketch Plane.....	186

Figure 43: SpaceClaim Options Menu.....	187
Figure 44: Circle Sketch, 2-inch ID, 2.325 OD	188
Figure 45: Design Tab	188
Figure 46: Cylinder pull.....	189
Figure 47: Volume extract tool.....	190
Figure 48: Material Assignment	191
Figure 49: Velocity Normalization on 90° inlet (8-inch, 60 ft.)	219

List of Equations

Equation

(1)	2
(2)	36
(3)	47
(4)	47
(5)	48
(6)	48
(7)	49
(8)	49
(9)	50
(10)	50
(11)	50
(12)	50
(13)	51
(14)	52
(15)	52
(16)	56
(17)	57
(18)	58
(19)	58
(20)	58
(21)	59

(22)	59
(23)	60
(24)	60
(25)	60
(26)	60
(27)	61
(28)	61
(29)	61
(30)	61
(31)	61
(32)	61
(33)	62
(34)	62
(35)	64
(36)	65
(37)	66
(38)	69
(39)	78
(40)	82
(41)	87
(42)	96
(43)	98
(44)	101

(45)	101
(46)	102
(47)	102
(48)	102
(49)	102
(50)	103
(51)	104
(52)	104
(53)	110
(54)	174
(55)	192
(56)	192
(57)	192

Glossary of Terms

Term	Definition
ERD	Extended Reach Drilling
MERW	Mega Extended Reach Wells
E&P	Exploration & Production
RSS	Rotary Steerable System
MLT	Multi-Lateral
BUR	Build Up Rate
BHA	Bottom Hole Assembly
NPT	Non-Productive Time
FPSO	Floating Production, Storage & Offloading
DPBS	Drill Pipe Bearing Sub
DSTR	Drill String Torque Reduction
AC	Anti-Collision
NPDD	Non-Rotating Drill Pipe Protector
ECD	Equivalent Circulating Density
ESD	Equivalent Static Density
SMB	Synthetic-Based Mud
OBM	Oil-Based Mud
WBM	Water-Based Mud
TD	Target Depth
TVD	Total Vertical Depth
MD	Measured Depth
TUDRP	Tulsa University Drilling Research Projects
LPAT	Low Pressure Ambient Temperature
CDV	Critical Deposition Velocity
CTFV	Critical Transport Fluid Velocity
GNF	Generalized Newtonian Fluid
EE	Eulerian-Eulerian
EL	Eulerian-Lagrangian
CFD	Computer Fluid Dynamics
HPHT	High Pressure High Temperature
RPM	Revolutions Per Minute
ACTF	Advanced Cuttings Transport Flow loop
API	American Petroleum Institute
YP	Yield Point
CCD	Charged Coupled Device
PIV	Particle Image Velocimetry
P-HAR	Pipe-Hole Area Ratio

Glossary of Equation Terms

Term	Definition
EMW	Equivalent Mud Weight
p	Frictional pressure-drop
TVD	True Vertical Depth
g	Gravitational acceleration
F	Force applied
A	Area
τ_{xy}	Shear Stress
Δv	Change in Velocity
Δy	Change in Length
γ_{xy}	Shear Rate
η	Dynamic Viscosity
μ	Kinematic Viscosity
ρ	Density
m	Power Law Fluid Consistency Index
n	Flow Behavior Index
μ_0	Zero Shear Viscosity
μ_∞	Infinite Shear Viscosity
λ	Curve Fitting Parameter
k	Curve Fitting Parameter
n^*	Flow Behavior Index
α	Measure of Degree of Shear Thinning Behavior
ξ	Velocity Ratio
ω	Rotational Angular Velocity
U	Bulk Axial Velocity
R_I	Inner Cylinder Radius
R_O	Outer Cylinder Radius
Ta	Taylor Number
κ	Radius Ratio R_I/R_O
T	Rotational Reynolds Number
Le	Entrance Length
D	Diameter
Re	Reynolds Number
Q	Flow Rate
δ	Degree of Eccentricity
r_w	Wellbore Radius
C_e	Eccentricity Correction Factor
f	Friction Factor
D_a	Annulus Diameter
D_{dp}	Drill Pipe Diameter
f_L	Frictional Pressure Loss
i	Hydraulic Pressure Gradient

i_L	Hydraulic Pressure Gradient
C	Volumetric Concentration of Cuttings
k_2	Experimental Constant
s	Solid/Fluid Density Ratio
V_{SL}	Moore's Slip Velocity of Cuttings
d_s	Particle Diameter
CTFV	Critical Transport Fluid Velocity
V_c	Cuttings Velocity
V_μ	Particle Slip Velocity
C_{ang}	Change in Wellbore Angle from Vertical
C_{size}	Change in Cuttings Size
C_{mwt}	Change in Mud Weight
α	A_s/A_t Ratio
U_s	Suspended Cuttings Velocity
U_b	Cuttings Bed Velocity
p'	Modified Pressure
Co	Courant Number
h_A	Total Head Loss
h_R	Pipe Friction Loss
h_L	Head Loss
N	Impeller Speed
h_{sp}	Static Pressure Head
h_{vp}	Vapor Pressure Head
h_s	Reservoir Elevation Head
h_f	Suction Head Loss
T	Torque
WK^2	Moment of Inertia
ΔN	Change in Speed
T	Time
C	Hazen-Williams Coefficient

1. Introduction

Efficient cuttings removal is a critical component of successful Extended Reach Drilling (ERD) operations (Egenti, 2014). Many studies have evaluated factors that affect cuttings transport in horizontal and extended reach drilling applications, but uncertainties remain. Past studies have mainly focused on understanding how drilling fluid properties and flow rates affect cuttings removal, but not much is understood regarding how drill pipe rotation affects cuttings transport (T.R. Sifferman & Becker, 1992) (Tomren, Iyoho, & Azar, 1986). It has been observed that increased drill string rotation within high inclination wellbores improves cuttings transport (most notable in smaller cuttings), but not much is yet known as to how or why this rotation improves removal (Alfsen, Blikra, & Tjotta, 1995a).

Through both laboratory studies and real-world data, a direct correlation can be made between drill string RPM (revolutions per minute) and cuttings removal in high inclination wellbores. Further, a sudden spike in cuttings removal is often observed around 120 RPM, and again around 180 RPM (Mims, Krepp, & Williams, 2007), particularly in large diameter wellbores ($\geq 12.25''$). This phenomenon is not well understood, and further research needs to be conducted to determine why these RPM zones cause a significant increase in cuttings removal.

As extended reach drilling continues to push the boundaries of technology, companies are continually looking for ways to optimize their drilling programs. A better understanding of the effects of drill string rotation on cuttings transport could improve operational efficiency and help reduce NPT caused by hole cleaning related events. There is also a potential that this better understanding may lead to methods that can reduce torque and drag in ERD operations. Some researchers have concluded that these higher torque and drag values are often due a high volume of small cuttings, which are more difficult to transport (Sanchez, Azar, Bassal, & Martins, 1997).

These small cuttings settle on the low side of the horizontal section of a wellbore and create a cuttings bed that can prevent landing casing, or even drilling to target depth (Duan et al., 2006) if not properly managed. An increase in cuttings removal efficiency through drill string rotation could also aid in reducing required flow rates, lowering Equivalent Circulating Density (ECD). ECD's are generally much higher in ERD due to the higher MD/TVD ratio. This ratio amplifies the frictional pressure drop in the annulus, creating a large equivalent mud weight (EMW, Equation 1, p = frictional pressure drop, TVD = true vertical depth, g = gravity). In pressure sensitive formations, moderation of effective circulating density is critical for minimizing formation damage and fracturing. A better understanding of drill pipe rotation on cuttings removal in horizontal wellbores would offer optimization opportunities in several areas of a drilling program. One phenomenon, fluid spiraling, increases ECD's in small diameter wellbores. This could be minimized if the process was better understood.

$$EMW = \frac{p}{TVD \cdot g} \quad (1)$$

In order to design and propose an adequate flow loop, a complete understanding of downhole fluid mechanics must be achieved. Although many horizontal flow loops exist that allow for replication of similar flow regimes, pressures, and temperatures (Tomren et al., 1986) (Sanchez et al., 1997)(T.R. Sifferman & Becker, 1992), the goal of this study is to develop a horizontal flow loop design that will allow for the study of drill string rotation effects on cuttings transport in ERD applications. There are currently no flow loops in operation that are specifically designed with the goal of recreating high RPM pipe rotation in large diameter hole, therefore, this design must take considerable care to ensure appropriate length to recreate extended reach wellbore conditions, while enabling the insertion and modification of an active drill string/bottom hole assembly. By gaining a strong understanding of the conditions that are to

be replicated, proper sizing and power delivery systems can be implemented into the flow loop design. This will ensure accurate down-hole simulations can be designed for experimental studies.

In addition to designing a properly sized flow loop, proper data analysis hardware must be utilized to accurately measure the movement of cuttings and fluid within the wellbore. By ensuring precision and accuracy in measurement, a strong collection of data will be obtained, allowing comprehensive and conclusive research to be done. Further, an accurate method of measuring the actual fluid flow will need to be integrated, allowing visualization of the actual fluid mechanics downhole.

1.1. Problem Statement

The purpose of this Thesis is to present a comprehensive design proposal for a large-scale horizontal flow loop capable of simulating downhole flow conditions and high RPM drill string rotation. Although many flow loops exist around the world (See Table I, Section 2.4.2 and Appendix 6.3), none have purposefully designed to simulate pipe rotation effects in large diameter ($\geq 12.25''$) wellbores. Therefore, no current flow loops can effectively recreate the substantial increase in cuttings transport efficiency at both the 120 RPM and 180 RPM range that is observed in real-world drilling practices. In addition to its ability to recreate these downhole conditions, this flow loop will be equipped with the proper visualization and analysis hardware and software that will allow for a comprehensive understanding of how drill string rotation affects cuttings transport in horizontal wellbores. Previous studies have indicated that drill string rotation has a positive effect in cuttings transport (H Ilkin Bilgesu, Mishra, & Ameri, 2007; Duan et al., 2006; Egenti, 2014), but these studies provide not definitive answers regarding what specific effects the drill pipe rotation is providing. Although pressure and temperature play

strong roles in downhole mechanics, the purpose of this flow loop is to study the effect of drill pipe rotation on cuttings transport, and as such, it will not be designed for HPHT (High-Pressure High-Temperature) operation.

1.2. Limitations

The scope of this Thesis has created limitations into the detail of physical design of the flow loop. Significant time during research was allocated to developing an accurate and detailed computational fluid dynamics (CFD) model to assist in sizing the test section of the flow loop. In order to validate the CFD models used in the design of the proposed flow loop, several models of the existing vertical flow loop on the Montana Tech campus were designed. These models were then compared with experimental trials run in both single-phase (water) and multiphase (water/air) regimes, to ensure multiphase simulations for the flow loop (liquid/solid) were properly designed.

This CFD modeling was a critical component in the overall design of the flow loop. Prior to determining the overall length of the flow loop test section, proper modeling techniques were performed to determine flow normalization from the inlets, as well as any turbulence caused by the test section outlet. Due to the non-Newtonian nature of drilling fluid, simple calculations were not enough and powerful CFD models were required to determine minimum lengths from the inlet and outlet.

Given the complexity of modeling software, the CFD model does not exhibit variable eccentricity of the drill string during rotation, and models were designed with the drill string in static locations, rotating as a rigid body (diagrams of drill pipe location can be found in the Methods section).

The physical flow loop design contains dimensions, expected equipment, and basic operational parameters. Although possible locations for the flow loop were considered, these locations and installation costs were omitted from the scope of this Thesis.

2. Literature Review

2.1. Forward

From the introduction of rotary drilling techniques by the Baker brothers in 1882, to Exxon Neftegas drilling the world's longest Extended Reach well in 2017, rotary and directional drilling has developed substantially since its need was initially realized in the early 1920's to meet the world's increasing energy needs. Prior to this time, wells were only thought to be drilled in a vertical direction, but after several wells unknowingly drifted off course and off lease, several lawsuits established a need to know wellbore position (Mitchell & Miska, 2011).

Initial attempts to monitor wellbore deviation were slow and inaccurate. The acid bottle technique, originally developed in the 1800's, consisted of lowering a glass jar filled with acid down the wellbore. The glass jar would sit at the bottom of the well, and after some time, the bottle would become etched (Devenish, Dirksen, Dow, & Maingot, 2015). Later in the 1920's, Totco invented the mechanical drift recorder but it was also notoriously unreliable. Both methods still lacked the ability to deliver azimuth as well. It wasn't until 1926, when Sperry introduced the first gyroscopic based technology to accurately measure inclination and azimuth on 3 separate axes. Drillers could now accurately determine wellbore position.

Near the end of the 1920's, deliberately drilled directional wells began to emerge, with the implementation of hardwood wedges to "steer" the drill bit. By 1930, the first recorded directional wells appeared on the coast of Long Beach, California, which were aimed at exploiting subsea reserves off the shoreline. Directional wells became commonplace and were drilled by using permanently installed steel whip stocks.

Although general drill string technology continually increased throughout the 1940's and 50's with the introduction of non-magnetic drill collars, stabilizers and stiff collars, directional control remained poor with roller cone assemblies.

A major breakthrough occurred in drilling technology in 1958, when Dyna-Drill introduced the first downhole drilling motor based on René Moineau's principle of the Progressive Cavity pump. This motor, combined with a bent housing sub, allowed drillers the first opportunity to "slide" the bottom hole assembly (BHA) in a desired location, while using the drive of the motor to rotate the drill bit. Coupled with magnetic single-shot tools, directional wells became much more accurate. However, due to the placement of the bent sub, any sliding operations required tripping the assembly in and out of the hole, as the sub would cause high stresses on the BHA if any attempt to rotate was made.

In 1969, wireline run magnetic steering tools were introduced, which became a common method of directional surveying through the 1970's. Although real-time measurements could be made, these surveys would have to be run at every connection.

The 1980's saw the next big breakthrough in directional drilling technology, when the first bent housing, adjustable motors were introduced. Measurement while drilling (MWD) tools also entered the industry, however both techniques were very expensive, and it wasn't until the end of the 1980's when directional and horizontal wells became more economical and viable to Exploration and Production (E&P) companies (Devenish et al., 2015).

As directional wells gained popularity within the industry, the term "Extended Reach" was created to describe horizontal wells that extended further than 5,000ft (1,500m) from its surface location. As drilling and surveying technology advanced and allowed further reach of horizontal legs, the term was modified to a ratio of 2:1 horizontal to vertical displacement,

meaning the wells Target Depth (TD) would be 2 times farther from its surface location than it was deep (Jerez, Dias, & Tilley, 2013).

As well trajectories became increasingly more complex, the term was once again modified to its current definition of a ratio of measured depth (MD) to true vertical depth (TVD). Wells were also more specifically categorized, as Low Reach (1:1), Medium Reach (1.5:1), Extended Reach (2:1) (Coley, 2015). The current definition of extended reach wells has grown to include wells that may not have a step-out of at least 2:1 but have characteristics that make them difficult to drill. Some of these technological challenges include:

- Wells with an unwrapped reach greater than 25,000 feet;
- 3D wells (complex well design);
- Wells which approach the limits of what has been achieved by the industry to date in terms of horizontal displacement at a given TVD;
- Directional wells that challenge the capabilities of the rig (Agbaji, 2011);
- Deepwater extended reach drilling wells (Mims et al., 2007).

With the introduction of Rotary Steerable Systems (RSS) in the late 1990's, the development of Extended Reach Drilling took off, with drilling operations being able to combat some of the constraints that made long wells previously impossible to drill (Devenish et al., 2015).

Today, E&P companies are constantly pushing the limits of extended reach drilling and battling many of the issues that are encountered as wells continue to grow in lateral length. The world's longest extended reach well, drilled by Exxon Neftegas Limited in 2015, is part of the Sakhalin-1 Project. The Sakhalin-1 project has continuously pushed the boundaries of extended reach drilling, with its latest record setting well O-05RD in 2017. With a total measured depth of

49,213 feet (15,004 meters) long with a horizontal reach of 46,347 feet (14,130 meters) at 8,610 feet (2,625 meters) TVD. Wells such as this have prompted the term “Ultra-Extended Reach” to define wells with a step-out of over 40,000 feet (12,192 meters) (Mitchell & Miska, 2011).

2.2. Current State of Extended Reach Drilling

2.2.1. Introduction

In the 1990’s, Extended Reach Drillings (ERD) gained significant industry attention through the Wytch Farm development in Poole Harbour, by BP (formerly British Petroleum, British multinational oil and gas company). The region, a well-known and very popular tourist destination off the coast of Southern England, hosts the Sherwood Sandstone Reservoir at 1,585m (5,200ft) TVD, with reserves estimated at 436 million barrels of oil (Knott, 1998). The original plans to construct an artificial platform in Poole Bay raised significant concerns regarding the potential environmental and socio-economic damage to the region (Devenish et al., 2015), but thanks to technological advances within the drilling industry, BP chose instead to develop the reservoir through a series of shallow step-out wells from a mainland site. The decision was beneficial economically and environmentally, reducing rig and platform costs during both drilling and production operations. It also translated into a savings of approximately \$150 million in development costs (Payne, Cocking, & Hatch, 1994), eliminating many of the additional issues that can be encountered in offshore drilling operations, such as increased environmental risks and development time.

Over the course of the 6-year, 17 well development of Wytch Farm, teams at BP repeatedly met the challenge of drilling increasingly long and difficult ER wells. BP steadily developed the field through increasing step-outs, ranging from under 5,000m (16,400ft) to record setting wells over 10,000m (32,000ft) (Figure 1). Ultimately, M16z (not pictured) would

become the worlds' longest well with a TD of 36,992 feet (11,278 meters); a record that remained unbroken for almost a decade. This feat was achieved through the development of new technology, excellent planning, and continuously pushing the technical limit to maximize performance delivery (Meador, Allen, & Riley, 2000).

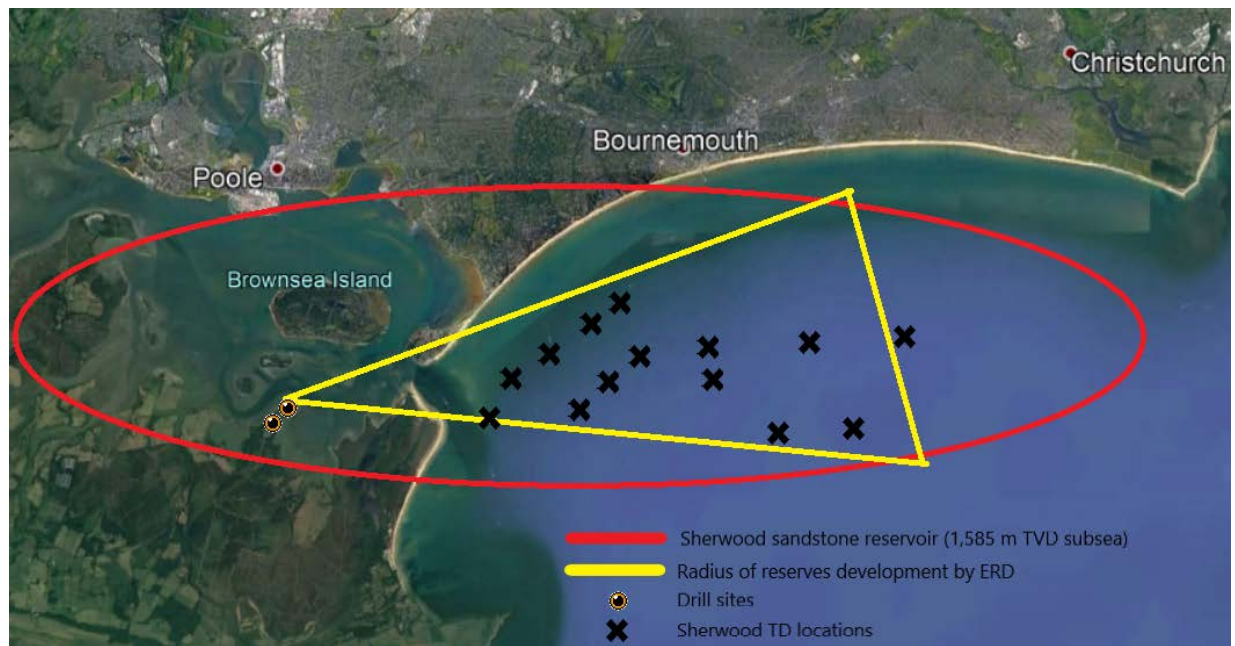


Figure 1: Wytch Farm Development Radius

Wytch Farm served as a testing grounds for the refinement of current drilling technology, and the development of new equipment and methods. These difficult wells raised many issues for BP engineers. Drill string problems such as torque, drag and buckling arose due to the shallow step-out and extended reach. Controlling hydraulics and hole-cleaning capabilities were key, as inefficient cuttings transport is a main factor for excessive torque and drag in extended reach drilling (Duan et al., 2008). Additionally, proper rheological parameters of drilling fluid

were critical in maintaining a successful wellbore, as fluid losses, hole instability and hydration of formation shales would cause major issues if left unchecked (Cocking, Bezant, & Tooms, 1997). Casing and cementing operations proved to be very difficult, with heavy casing being difficult to run to bottom without buckling or surging the wellbore, and high ECD's from pumping cement were extremely difficult to overcome. The team approached the wells in a graduating-step-way, learning from each previous well and taking significant time to properly plan each operation on every well. These step-method, combined with RSS development, casing flotation and others helped successfully overcome some of the issues encountered (Meader et al., 2000). Under any extended reach drilling application, well trajectory design also plays a critical role in the success of the well. Along with other logistical challenges, survey and logging accuracy is paramount in the extended reach sections for these wells. The engineering team at BP would use this logging data in real-time to geo-steer and make any adjustments necessary. Through the life of the project, the team would refine each new well plan based on learnings from previous wells, making corrections such as adjusting the tangent section to reduce torque and drag (Cocking et al., 1997).

BP's team developed the program to maximize learning and increase performance through the slow increase of step-outs on each advancing well. This focus on learning allowed continued success through each increasingly difficult well. Major problems that could have occurred had the team attempted much longer reach wells sooner in the field development were avoided thanks to this step up approach (Cocking et al., 1997).

Through the development of existing ERD knowledge, and the application and refinement of new technology, the Wytch Farm Development was the beginning of what is now a substantial part of oil and gas exploitation. Extended reach drilling is being used to develop

mature fields such as the United Kingdom Continental Shelf (UKCS) in the North Sea more economically. As these reservoirs have increased development, accessing un-swept areas of the reservoir becomes more difficult, requiring increasingly complex well profiles. Newly developed RSS technology that was being used at Wytch farm was also unlocking previously un-swept reserves in the North Sea. Complex 3D well profiles, a facet of extended reach, were now possible thanks to this technology (Saeverhagen, Thorsen, Gard, & Jones, 2008). Drilling equipment was being pushed to its limits through the aggressive build-up rates (BUR) and steering accuracy required to hit the small targets (Krueger, Sharpe, Attridge, & Ruzska, 2017). This heavily developed field has had great success through more than 110 sub-sea wells, including 53 multi-lateral wells (MLT), making anti-collision of highest priority (Saeverhagen et al., 2008). Several complex “corkscrew” wells were successfully drilled without incident, due in part to successful planning and execution, and with technology originally developed and refined at Wytch Farm.

Extended Reach Technology continued to develop and become more economically vital to E&P companies into the 21st century. The Campos Basin, off the coast of Brazil, is considered to be one of the world’s most important deep water oil and gas developments, housing almost 80 percent of Brazil’s overall oil output (Paes, Ajikobi, & Chen, 2005). The BC-10 block asset, joint operated by Shell (50%), Petrobras (35%) and ONGC (15%) hosts some of the industry’s most difficult deep water extended reach wells. An extremely complex faulted reservoir at a relatively shallow depth below the mud line (2,800ft [850m]) posed significant operator challenges (Stockwell, Zambrano, Bezerra, & Arevalo, 2010). The Campos Basin contains a heavy crude, and the optimal drainage option for these wells is horizontal. Deepwater drilling is an extremely expensive operation, and the success and profitability of a well are highly

dependent on drilling costs. Optimizing drilling operations by utilizing the best extended reach drilling techniques is a critical factor in assuring positive economic return. Drilling challenges Shell encountered during its drilling operations consisted of vibration related failures regarding the drill string, and hydraulics related issues. To elaborate, drill string vibrations would slow Rate of Penetration (ROP), cause accelerated wear to the BHA and drill bit, and distort MWD readings. Hole problems from hydraulics included lost circulation and formation influx, hole stability problems and poor drill cuttings removal (Paes et al., 2005). These problems were initially severe, but as Shell continued to develop the field, were mitigated and managed to lower overall Non-Productive Time (NPT). This led to the economic success of the BC-10 block, and a better understanding of managing deep water extended reach wells.

Currently, the Chayvo, Odoptu, and Arkutun Dagi fields in Northern Russia are at the forefront of Extended Reach Drilling. ExxonMobil, lead operator on the Sakhalin-1 project, has been utilizing extended reach drilling technology to successfully exploit the thin, 65ft (20m) oil column of the field. The field development began in 2003, and is continuing to this day, continuously setting extended reach records (Gupta, Sanford, Mathis, DiPippo, & Egan, 2013). ExxonMobil's extensive ERD experience, along with continuously developed tools and techniques that first saw extended reach use at Wytch Farm, has allowed the operator to drill multiple record breaking wells, from longest well to longest horizontal reach (Gupta, Yeap, Fischer, Mathis, & Egan, 2014). Orlan-05RD, the most recently drilled well in the Sakhalin project, once again set the world record for an extended reach well, with a projected TVD of 8,611ft (2,625m) and measured depth of 49,213ft (15,000m) (Official numbers have not yet been released).

BP continues to try and develop fields by using the same Extended Reach technology it found success with at Wytch farm, in fields such as the Alaska Liberty development. Much like Wytch farm, the initial design involved the construction of an artificial island and standalone development pad. Prior to the 2010 Deepwater Horizon oil spill, BP modified their development plan to instead expand the pre-existing Endicott Satellite Drilling Island, shifting the well profiles to Ultra-Extended Reach Drilled (u-ERD). This strategy was developed by the CEO, as ExxonMobil had recently become a leader in ERD technology and BP was attempting to return to the top of ERD operations. BP determined that the ideal recovery of this light-oil field would be through waterflooding and developed a plan for upwards of 6 wells (4 producers, 2 injectors), with departures ranging from 34,000 to 44,000ft (10,360 – 13,400m). These wells are all on outer boundary of the U-ERD envelope and require a purpose-built rig to drill. As these wells are 4 to 5 times longer than the conventional wells of the area, no rigs could be upgraded or modified to handle the extreme power requirements of these wells. Much like Wytch Farm and other ERD operations, BP would need to design these drilling programs to handle the expected torque, ECD's, and directional capability (BP Exploration, 2007). Unfortunately, after the Macondo incident, BP faced increased pressure from both State and Federal government bodies to scrap the Liberty uERD program. BP withdrew their formally approved Development and Production Plan (DPP) from the Mineral Management Service in May of 2014, and ownership of the field was then sold to Hilcorp LLC in November of 2014 (BOEM, 2017). At present time, the project is still under review before approval, and Hilcorp has submitted its amended DPP this past May to the Bureau of Ocean Energy Management (BOEM). Hilcorp plans on returning to the original plan of constructing a drilling and production island to recover the reserves, as they do not have the existing infrastructure that BP did (Hilcorp, 2017).

2.2.2. The Importance of Extended Reach

Extended Reach Drilling (ERD) is becoming an increasingly crucial technique in developing oil and gas reserves economically. Reserves that were previously unreachable conventionally are now becoming accessible to operators. Extended reach drilling allows an operator to access more of a reserve from a single location, while also lowering its operational footprint and often using existing infrastructure (M. W. Walker, 2012). The Liberty Development Plan aimed to capitalize on its preexisting Endicott facility instead of constructing a new man-made island to exploit the Liberty Field. The economic benefits of eliminating the need to build a new production facility, pipeline, and dedicated island for drilling and production operations is substantial, both in operator cost and development time.

In an environmental sense, the use of extended reach allows an operator to have a much smaller environmental footprint. In the case of Wytch Farm, BP was able to preserve the environmentally sensitive and popular Poole Harbour area by drilling from a mainland location further away. Liberty also planned to maintain the ecologically sensitive area of northern Alaska by eliminating the construction of an additional man-made island. In today's social and political climate, E&P companies are facing increased public scrutiny for maintaining high environmental standards. In the wake of the Deepwater Horizon incident, increased environmental regulations are forcing companies to develop reservoirs through minimal environmental disturbance. ERD technology is allowing continued access to these reserves in a more environmentally friendly way.

Another facet of Extended Reach technology has allowed operators to access deep water reservoirs that were previously too costly to develop. Mega-Extended Reach-Wells (MERW) are extended reach wells that are drilled from a shallow-water platform, targeting deep water reservoirs from one satellite location. These wells face a multitude of extreme ERD problems,

largely due to unconsolidated formations and low overburden pressures (Chen & Gao, 2016). However, the cost savings in utilizing a shallow water jack-up rig in comparison to a deep water semi-submersible or drillship is substantial. Floating rigs currently run an average day rate between \$200,000 - \$443,000USD/day, wherein jack-up rigs average between \$48,000 - \$123,000USD/day (Riglogix, 2017). Over the course of a 100 day well, this can result in a cost savings ranging from \$8,000,000USD to almost \$40,000,000USD (7.1). The cost savings continue long after drilling operations are complete, as well. Subsea wells are extremely expensive to operate and maintain, and if wells need a workover in the future, mobilization and workover costs can be significantly higher in deep water. Shallow “dry-tree” installations allow for much easier access throughout the life of the well.

In deep water reservoirs that cannot be reached from shallow water locations, ERD technology has become even more crucial to assuring economic success. The costs of the drilling operation are critical in maximizing financial gains from the reservoir, and detailed planning of each well is necessary to minimize any Non-Productive Time (NPT) that could increase costs (Paes et al., 2005). The Campos Basin, offshore Brazil, is an example in which ERD technology was implemented to maximize reservoir coverage from a minimal number of locations. Due to the deep-water nature of this reservoir (upwards of 6,500ft [2,000m]), special subsea pumping facilities and the use of Floating Production, Storage and Offloading (FPSO) ships are implemented at high costs. Having a central drilling site that will produce a vast amount of the reservoir reduces the chances of requiring multiple FPSO's, drastically reducing production costs. The complex lithology of the Campos Basin forced the operator to develop intricate 3D well profiles to maximize reservoir drainage (Stockwell et al., 2010). The

successful implementation of ERD technology allowed the operator to successfully maximize reservoir coverage economically.

The cost savings of implanting ERD can be seen not only in drilling cost reduction, but in overall development and production plans. Wytch Farm allowed BP to save over \$150,000,000USD in development costs by eliminating the need to construct an artificial island. This also accelerated the drilling program by 3 years, and substantially lowered the project's environmental footprint (Payne et al., 1994).

When oil prices drop below \$60USD/STB, operators look at finding every opportunity to drill more economic wells. The use of smaller, more mobile rigs is becoming another viable avenue for cost-savings. These rigs are being contracted to drill increasingly complex wells that often reach or exceed the rigs normal expectations. These wells require careful planning and constant monitoring as any issues that arise can become significant problems for smaller rigs being pushed to their limits. Critical parameters that must be monitored during drilling include hole condition, ECD's, hole cleaning and torque and drag (Suggett & Smith, 2005) These are all standard Extended Reach complications, however encountering such problems at the limits of a rig can lead to serious and expensive issues.

2.2.3. Extended Reach Defined

The industry has generally given a basic definition to ERD, and most published papers state that an extended reach well has a MD/TVD ratio of 2:1 or more (Bhalla, 1996)(Rubiandini R.S., 2008)(Jerez et al., 2013). Ultra-reach wells have similar definitions, ranging from a ratio of 5:1 or more (Modi, Mason, Tooms, & Conran, 1997) to a step out of 40,000ft (12,195m) (Mitchell & Miska, 2011). However, the use of this ratio, or step out length, does not necessarily equate to increasing difficulty. Some Deepwater wells, such as one drilled by an operator in

West Africa, had a ratio of only 2.5, but offered many significant challenges of a difficult extended reach well, such as BHA/survey management, vibration and hole cleaning (A. Wilson, 2015)(Jerez et al., 2013). Due to this inconsistency, several companies with a great deal of extended reach developments define extended reach in much more detail. BP expands on the MD/TVD ratio by further defining 3 levels of well design, based on TVD. Step-out wells with a TVD of approximately 5,000ft (1,525m) are considered shallow, with the highest step-outs generally encountered (over 32,000ft [10,000m]). Intermediate wells are classified as wells with an average TVD of 10,000ft (3,050m), with step-outs on average being slightly less (26,000ft [8,000m] +). Finally, deep level wells have much deeper TVD's, approximately 15,000ft (4,575m) or more, with step-outs being in the 23,000ft (7,000m) range (Mason & Judzis, 1998). This approach doesn't comply with the previously defined 2:1 ratio, as deep wells do not necessarily reach the minimum defined ERD departure level (Figure 2).

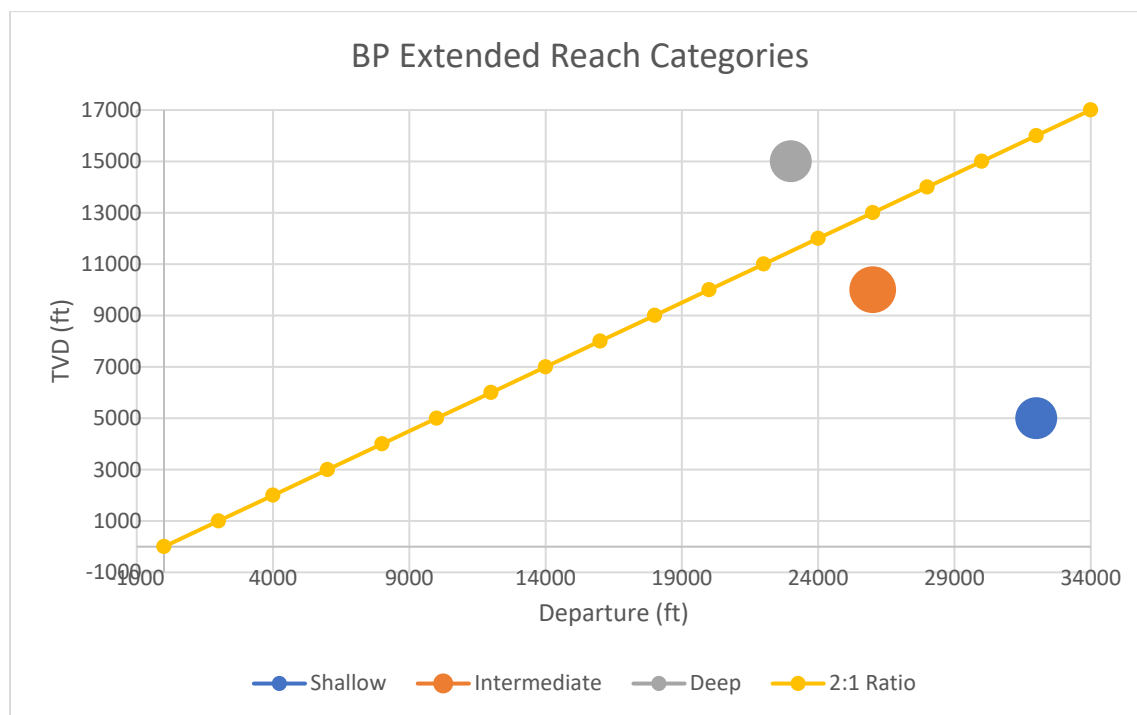


Figure 2: BP Extended Reach Categories compared to 2:1 Departure: TVD ratio (Mason & Judzis, 1998)

K&M Technology (herein referred to as K&M), a consultancy company specializing in the design and execution of extended reach and complex wells, has the most elaborate identification system for extended reach wells. This categorization understands that the ratio definition does not accurately portray the difficulty or complexity of these wells. K&M has developed a system to classify extended reach wells by well profile and design complexities specific to each operation. Unlike BP, who categorized extended reach wells into 3 levels, K&M begins by identifying 2 types of extended reach wells: very shallow wells, and very long wells. Further building on these 2 well profiles, well designs can also be implemented as each have their own unique set of extended reach challenges. The designs identified by K&M are: Complex well design, Deepwater extended reach wells, and limited rig capability (Mims et al., 2007).

BP further assesses difficulty of ERD operations by dividing operational limits into 2 broad categories: mechanical and formation-related (Mason & Judzis, 1998). Mechanical limits cover any physical restraint, from rig power to casing and drill pipe strength. Formation-related limits can consist of all limits encountered due to reservoir or formation conditions, such as stability, fracture gradient and pore pressures. Another school of thought discusses limits in regard to constraints, that can be influenced by 3 design categories: drill string design, casing design and hydraulics design (Rubiandini R.S., 2008). Drill string design is a critical component to any extended reach project, as the friction that occurs due to drag in the extended lateral sections can be substantial. Proper design of a drill string is paramount in achieving success. Casing design is another critical component to any extended reach program, as casing is generally the highest load the rig will handle, and friction and buckling stresses become more severe. Hydraulic design considers the development and management of drilling fluid and the

rig circulation system, as it is a critical component in hole cleaning, maintaining hydrostatic pressure, and ensuring wellbore stability.

Complex well designs, such as the more recent offshore wells in the North Sea, offer significant challenges. This complex and maturing region is filled with many fault blocks and structures throughout. These faults, combined with the necessity for smaller reservoir targets to successfully maximize drainage of potentially producing formations, require the design of well plans for small targets. One of these wells has a complex corkscrew design, with a $5^\circ/100\text{ft}$ azimuth turn of 255° while maintaining an 88° inclination. A similar well in the area, such as one requiring a 200° azimuth curve at $8.5^\circ/100\text{ft}$ while holding a 90° inclination (Krueger et al., 2017), truly display that the MD/TVD ratio does not dictate extended reach difficulty. These extremely complex well designs push the technological limits while still offering an “unwrapped” departure that qualifies as an extended reach well, with increased challenges.

Deepwater extended reach wells, such as the Ostra wells in Parques das Conchas, off the coast of Brazil, challenge operators by combining both extended reach limitations with deep water challenges. With generally shallow reservoir depths below the mudline, shallow kick-off points were required in unconsolidated formations. Low drilling margins and low fracture gradients all played major roles in the success of these wells (Stockwell et al., 2010).

Additionally, a long riser section can add significant weight to a drill string, increasing buckling risks when combined with shallow or aggressive build rates. Casing operations, which generally are the heaviest load a rig will hoist, become more difficult due to the addition of the long (5,000ft+) riser section. Drilling fluid properties can also be adversely affected by the drastic temperature changes that may occur between the reservoir and the cold riser, and special calculations must be undertaken to ensure that equivalent static density, the determinant in

hydrostatic pressure, is correct (Zamora, Broussard, & Stephens, 2000). The generally low water temperatures encountered during deep water drilling operations (40°F, 5°C) can substantially increase fluid viscosity, and in turn increase effective circulating density (ECD). With narrow drilling margins, the importance of maintaining a low ECD is critical, and must be kept in check (van Oort, Lee, Friedheim, & Toups, 2004).

K&M firmly believes that extended reach drilling can also be categorized by limited rig capability. This means that a well may be deemed an extended reach well, and encounter the issues that would arise on many other extended reach wells, if the drilling rig is being pushed to its limits during operation (Mims et al., 2007). In the current economic climate, companies are constantly looking to save costs on drilling and completing new wells, and by choosing a smaller rig, money can be saved if proper planning is done to mitigate any newly expected risks.

2.3. Extended Reach Drilling Constraints

Successful ERD operations must manage several challenges through the life of a well, from the critical planning stage to drilling and completion. These challenges can largely be categorized by either mechanical or formation-related constraints (Mason & Judzis, 1998). From these two major categories, a multitude of more specific limitations can be identified. All these limitations must be addressed during the planning stage, and constantly monitored during drilling operations to ensure successful wells. These problems are much more severe in ERD operations than in conventional drilling operations, as the extended length tends to cause these issues to compile. Through the development of the Wytch Farm field, tangent angles were modified from 83° to 81° from wells M2 to M3 and M5. This small change, over the 16,400ft (5,000m) tangent, significantly reduced drag during sliding operations (Cocking et al., 1997). This very small change is an example of how small changes can have large consequences in ERD wells.

2.3.1. Mechanical Constraints Overview

Mechanical limits experienced during extended reach drilling consist of anything that has a physical restraint in a drilling operation. This includes drill pipe and casing design, which affect torque handling capabilities, collapse, burst and buckling strength. Overall rig capability, from hoisting ability, top-drive torque, and maximum pumping parameters are also factors in this category. Real-time mechanical constraints that are encountered during drilling operations, such as survey management, drill string vibration and contact loads (riser and casing wear during drilling operations) are mechanical constraints that can be controlled through proper procedure, and maintenance. Torque, drag, and buckling are all factors that go into the development of drill pipe and casing plans, however they are closely monitored and mitigated during drilling operations through drilling fluid rheology and drilling procedure.

2.3.1.1. Drill String

During extended reach drilling operations, the drill string can be exposed to extremely high torque and drag friction factors. These friction factors are largely the result of cuttings accumulation from hole cleaning difficulty and wellbore eccentricities in long lateral sections. Although dog leg severity (DLS) is a major factor in torque and drag, properly planned and executed ER wells are careful in minimizing DLS. Operators must take extreme care in designing a proper wellbore that minimizes tortuosity, as this can be a major factor in torque loads. The difference of even a degree in a tangent section can affect drag loads significantly, over a long distance (Cocking et al., 1997). As the horizontal sections of these wells grow, the resisting friction factors between the drill string and the bottom of the wellbore increase. This increased friction leads to high torque loads from rotating the drill string, and substantial axial-forces from pushing to place an adequate weight-on-bit (WOB). Most conventional drill strings

do not see much relief from buoyancy effects, as gravitational forces from drill string weight are strong. Although higher mud weights can increase drill string buoyancy and reduce hook load, reaction forces coupled with friction coefficients between the drill string and the bottom of the wellbore. These forces work against the torque applied by the rig, requiring more surface force (Hareland, Lyons, Baldwin, Briggs, & Bratli, 1998). Additionally, directional control is a crucial part of ERD, and Bottom Hole Assembly (BHA) selection plays a vital part in the success of a well.

2.3.1.1.1. Drill Pipe Selection

The robustness of the drill string is a critical factor in extended reach drilling, as the requirement of a round trip to replace a failed drill string can be a time-intensive and costly process, upwards of six days (M. W. Walker, 2012). Although there are several other tools and techniques that allow operators to lower torque and drag, properly designed drill string technology is a critical component in achieving success in ERD projects (Jellison, Chandler, Payne, & Shepard, 2007). Several methods have been tested in the past, some with more success than others. The implementation of drill pipe bearing subs (DPBS) and non-rotating drill pipe/casing protectors (NDPP) only offered limited gains, and posed problems such as loading at weak spots and stripping potential (Nixon, Nims, Rodman, & Swietlik, 1996).

The most common solution to torque problems in ERD involves upsizing and upgrading drill pipe. Generally, ER drill strings range between 5 7/8 inches and 6 5/8 inches. These strings are made with high-strength steel to resist expected torque, while still allowing adequate flow-rates to clean a hole properly and not exceed ECD factors. Many times, torsional capacity of drill pipe is limited by the tool joint, so Extreme-Torque connections such as double-shoulder tool-joints can offer up to 70% more working torque capability than standard API pipe (Jellison,

Payne, Shepard, & Chandler, 2003). More recent advances have allowed extended reach records to be set in Brazil, using VAM Express connections, which offer upwards of 200% more average torque capacity than some standard API connections (Osório et al., 2013). Torque and drag management tools such as Drill String Torque Reduction (DSTR) subs can also play a role in reducing drill string torque. DSTR's can reduce drill string torque, and often lower casing wear on ER Wells (Nixon et al., 1996). DSTR's, however, are not often used in ERD wells.

As previously mentioned, large diameter steel drill pipe causes increased torque and drag issues due to gravitational forces in horizontal sections. One solution that many operators are now turning to involve utilizing lower density materials in their drill string. Materials such as aluminum, titanium and carbon-fiber are being introduced to create strong drill pipe with a fraction of the weight. These materials can offer substantial benefits, including a higher strength to weight ratio as overall weight is significantly reduced, to superior corrosion resistance (Jellison et al., 2007). The unfortunate downside to selecting these materials is increased cost; however, running the more exotic material strings as part of a tapered drill string below steel can reduce torque and tension loads significantly, and allow longer wells do be drilled with less capable rigs (Foster & Krepp, 2007).

2.3.1.1.2. BHA Selection

One critical factor in ERD is the ability to accurately steer the BHA at extreme lengths. Several technologies have been implemented to assist in the delivery of ER wells. At Wytch farm, the development of the PowerDrive RSS prototype allowed the operator to continually steer the wells past the torque and drag limits set by a conventional BHA. At a certain length, axial drag becomes too high to successfully steer a BHA with a conventional, bent-housing motor (Meader et al., 2000). RSS technology allows the operator to steer the BHA actively

while continuing to rotate the drill string. This offers many benefits, from dramatically reduced axial drag, to increased cuttings removal efficiency. Additional benefits of RSS technology were implemented in offshore wells, where “point-the-bit” designs allow for aggressive builds in unconsolidated formations, something that was much more difficult to obtain with conventional BHA’s (Stockwell et al., 2010). RSS technology continues to develop, and new high-Build Up Rate (BUR) RSS systems are allowing operators to complete highly aggressive and complex wells in mature fields (Krueger et al., 2017).

Logging and directional measurement are also key components to ERD, and accuracy at these significant depths and/or lengths is much more difficult to obtain. In more developed fields, anti-collision (AC) becomes a more serious problem. Being able to accurately determine where the well is at all times is vital to ensuring safe distance to neighboring wellbores. At extreme lengths, cumulative MWD interference can become a severe problem, causing an increased ellipse of uncertainty (Figure 3), particularly in the east-west direction. In the early days of uERD wells, magnetic surveying was second to gyro technology (Payne et al., 1994). However, as gyro technology has its own unique set of problems (fragility, drift), and MWD technology currently rivals (and in some cases surpasses) gyro technology for use in ERD wells. In extended reach wells, survey management is a fundamental. Due to the extended reach of these wells, the accumulation of errors and uncertainties must be managed in order to successfully hit a geological target (Jerez et al., 2013). Previously BHA assemblies placed MWD tools a significant distance behind the bit, leading to very tight tolerances and delayed measurements of actual wellbore placement. To mitigate this, the implementation of Logging While Drilling (LWD) tools provided real-time data close to the bit, warning of any changes in

lithology (Allen, Tooms, Conran, Lesso, & Slijke, 1997). With current RSS technology, this issue is no longer significant, as many have their own surveying instruments close to the bit.

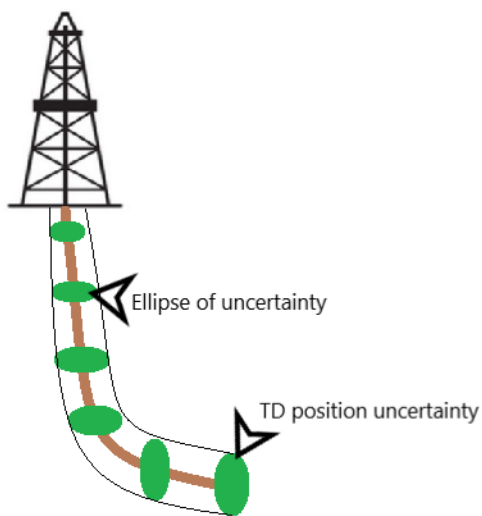


Figure 3: Ellipse of Uncertainty

2.3.1.2. Casing

Casing design for ERD wells is a critical optimization case. Although it is possible to design a casing string that will withstand all expected loads, careful consideration must be taken to minimize the cost of these strings. Casing strings are often the most expensive item in a well, and must be designed to withstand many different loads through the entire life of a well, and operators spend significant time in ensuring costs are minimal (Roque & Maidla, 1995). In drilling operations, early casing strings can be subject to drill string wear through ER drilling and rotation. In long laterals, torque, drag and buckling stresses play a large factor in landing a casing successfully. A casing's ability to be "floated" to TD must also be considered, and its

ability to handle different fluids such as air, or a low density spacer (Jaffe, Maidla, Irrgang, & Janisch, 1997). Designing a casing that can withstand all these factors within the rigs handling capabilities becomes a difficult process when also factoring in cost. Casing wear can be minimized through other mitigation techniques such as non-rotating drill pipe protector (NDPP) subs, but these tools can cause costly NPT if they fail prematurely (Nixon et al., 1996). Ultimately, casing design is a critical component to any ER well, and operators must consider a myriad of factors in the design process.

2.3.1.3. Rig Capability

One of the most significant factors in the success of an extended reach well is the capability of the rig. Ensuring a rig has appropriate circulation system power, top drive and hoisting power are all critical components in managing ERD constraints. In the current economic climate, it is being observed that there are two facets of ERD wells being drilled. The specific design of ERD rigs is allowing previously unreachable or uneconomic reserves to be accessed, restricted either by depth or environmental concerns. Additionally, through ERD planning techniques, less capable rigs are being pushed to their limits drilling wells that could be more easily handled by larger rigs, in the effort to reduce costs (Suggett & Smith, 2005).

With increasing budget constraints and environmental concerns, many companies are now looking at designing fit-for-purpose ERD rigs for large-scale projects such as Liberty in Alaska (formerly BP), the Sakhalin I Project (Yastreb rig, Exxon Neftegas) and the North Caspian Sea (arctic class drilling barge rig Sunkar, for Joint Venture Operations). New ERD rig designs incorporate more torque and pick-up capacity, more fluid and cuttings handling capability, and higher mud system pressure requirements, all while minimizing their footprint. With ERD operations aiming to have smaller well pads with tight wellhead spacing, these rigs

must be maneuverable between wells with minimal downtime (Husband, Bitar, & Quinlan, 2007).

Due to the extreme scale of ERD operations, other considerations must be considered when designing these purpose-built rigs. Due to the extensive length of ER wells, tubular handling and storage becomes a large-scale operation. The rig layout must be able to store the significant amount of drill pipe required, through both vertical (racking stands in the derrick) or horizontal setbacks. ERD pads often have simultaneous operations (SIMOPS) occurring at any given time, and access to any and all equipment is paramount to efficient and safe drilling, completions and production operations (Husband et al., 2007)

2.3.1.4. Well Profile

Well profiles play a pivotal part in the design and implementation of ERD operations. As many ERD wells have a significant tangent section in order to access the reservoir targets. Furthermore, in many ERD cases, wellbore placement is critical due to tight or fractured reservoir conditions. The Exxon Neftegas Sakhalin-1 project is focused on accessing a thin oil column under an environmentally sensitive waterway. Vertical uncertainty that varied as little as 4 meters impacted expected production over the first 10 years upwards of 10%, and a 6 meter vertical offset from the mid-oil column reduced total expected recovery by 30% (Gupta et al., 2013). In the Campos Basin, well plans required an aggressive build section in unconsolidated formation, something not attainable with conventional mud motors. Interbedded shales, siltstones and limestone layers added increased complexity as all formations offered different directional responses (Stockwell et al., 2010). These types of complexities are often encountered in any ERD operation.

Operators will often use a variety of simulators and computer modeling programs to develop the most ideal directional plan. Although torque levels are generally more dependent on overall length than tangent angle (Modi et al., 1997), it was discovered that drag could be a considerable issue in the tangent section if designs were varied by even 1 degree. At Wytch Farm, it was found that increasing the tangent angle would minimize torque during rotary drilling, however drag was significantly higher for sliding operations (Cocking et al., 1997). In modern ERD operations RSS technology is most often used, and sliding is not required for directional control. This use of RSS tools often allows steeper tangent angles, lowering torque.

Detailed modeling techniques used by operators help to simulate other operational conditions. BHA specific simulators can be applied to determine optimum drilling parameters and BHA assemblies (Jerez et al., 2013). These simulators can also simulate expected torque and drag values throughout the wellbore, allowing for additional optimization. These values are critical in ensuring they will not exceed the design capabilities of the rig or tubular system to be used (Kamaruddin, Md Zin Che'ap; , Sering, Good, & Khun, 2000).

2.3.2. Formation Constraints Overview

Formation constraints cover a wider range of limits and technical issues. There are a vast array of constraints and limits that must be managed, all centered around drilling fluid system management. Both equivalent static density (ESD) and equivalent circulating density (ECD) are critical parameters in managing the often narrow drilling margins between fracture and pore pressures (Bogdanov et al., 2012)(Zamora et al., 2000). Most ERD wells use a higher density mud, to aid in wellbore stability (Rubiandini R.S., 2008). These fluid characteristics are also critical in cementing operations, where the density and viscosity of a cement slurry is often much higher than the drilling fluid. ECD's must be managed through techniques such as reducing

pump rate and adding retardants to the cement, friction factors, or using foam-based cement slurries to reduce density. Other hazards that can be reduced by mud system design/maintenance include differential sticking, lost circulation, friction coefficients and hole cleaning (Glebov et al., 2014). These factors, however, are not solely dependent on the mud system. Pump management, connection practices, and tripping practices all play significant factors in managing wellbore stability. Cuttings removal is a critical aspect of successful extended reach wells, as they are a major contributor to drag. Previously, flowrate was considered the primary parameter in hole cleaning on ERD wells (Payne et al., 1994), and ECD's became the most limiting factor in longer lateral sections (Bogdanov et al., 2012). However, more recent endeavors have proven that rotary speed and patience are more significant for success in hole cleaning. ECD's are generally less sensitive to flowrate in larger diameter hole sizes ($\geq 12''$), and in smaller diameter holes ($\leq 8.5''$), where ECD is more sensitive to flow rate, those sections are easier to clean with lower flowrates.

2.3.2.1. Cement

Cementing casing or liner in deviated wellbores poses a significant challenge over vertical wells, and these problems are often exponentially more substantial in ERD. Due to the large diameter of casing in comparison to a drill string, ECD's are often substantially higher due to the flow area restriction alone. This can lead to formation fracturing and lost circulation (Glebov et al., 2014). Improper hole cleaning, which further lowers the effective wellbore diameter, can increase ECD's more, so operators must ensure that the wellbore is properly circulated clean prior to any casing operations. Due to the increase diameter of casing, lower pump rates are often required to maintain acceptable ECD's, and they may not be adequate for hole cleaning. In ERD, final casing strings are liners that are hung at the shoe of the last

complete casing string. This is done to lower costs, reduce ECD's, and increase pumping ability, as these strings are run and set via drill pipe.

In addition to ensuring a prepared wellbore prior to casing operations, cement design is a crucial part of many ERD operations. In some cases, such as the BC-10 block of the Campos basin, gravel pack completions are run (Paes et al., 2005). Sakhalin-1 wells utilize liner strings consisting of screens, blank pipe and inflow control devices that are set with packers in an open hole (M. W. Walker, 2012), eliminating the need for cemented liner or casing. However, in many cases such as Wytch Farm, final production liner or casing is cemented in place. Due to narrow drilling margins that are often encountered, cementing operations can be very difficult to complete without losses through formation fracturing. Cement design programs can optimize slurry to minimize any fracture risks, however in some cases, this will not eliminate fracture risk. Wytch Farm engineers required that cement have all the isolating qualities of a full weight slurry and could not run lighter weight slurries such as foam. The team determined that a low density oil sweep be pumped prior to the cement, effectively lowering ECD within acceptable ranges (Cocking et al., 1997).

Casing centralization is of significant concern as well, as improperly designed centralization can lead to an increase in torque and drag, by increasing the radius of rotation and casing deflection, while also potentially packing off casing with uncirculated drill cuttings (Sanchez, Brown, & Adams, 2012). The need for proper centralization is significant in deviated wellbores, as casing is likely to be on the bottom of the wellbore, leading to improper zonal isolation. This improper centering can lead to channeling as in the annulus, further reducing zonal isolation (Cai, Gao, Zhang, Cui, & Guo, 2014).

Proper design of casing and centralizers are a significant part of adequate cement jobs, as to ensure proper cement distribution with minimal channeling, liner/casing should be rotated. The additional torque that occurs during cement operations is often escalated by the addition of centralizers, and high-torque thread connections must be able to withstand these forces. In the case of Wytch Farm, high-torque liner connections combined with high torque capacity liner hangers were used to minimize torque concerns, and two zinc-alloy solid centralizers were run per joint to ensure concentric cement placement (Cocking et al., 1997).

2.3.2.2. Drilling Mud Rheology and ECD

Managing the rheology and density of drilling mud in ERD operations is often a considerable challenge. ECD's play a critical role in formation management and is often a limiting factor in ERD departure. Due to often narrow drilling margins between fracture gradients and pore pressures, higher density mud with low rheology must often be actively managed through proper flow rates, drill string sizing and ROP. However, sometimes these modifications aren't enough, and in the case of wells being drilled in the Korchagina field in the North Caspian Sea, the solution was to increase hole size from 8.5 inches (215.9mm) to 9.5 inches (241.3mm). This increase in hole diameter lowered ECD by 2.2 lb/gal (220 kg/m³, 0.22 Specific Gravity (SG)), which allowed the operator to continue drilling without fear of formation fracture. This significant change, however, required changing operational parameters for hole cleaning and ROP control (Bogdanov et al., 2012). In addition to increasing hole size, carefully designed OBM was utilized to maximize cuttings transport and hole stability given the flow rates and ROP planned. With these changes in place, the last well from this project was drilled 28 days faster than the originally planned 84.

Rheological parameters can also play a significant factor in managing ECD's particularly in deep water ERD operations. Deepwater drilling environments can often see temperatures as low as 40 degrees Fahrenheit (5 degrees Celsius) in the long riser sections. This low temperature can often affect the rheology of drilling mud, increasing viscosity dramatically and in turn increasing ECD's and surge pressures (van Oort et al., 2004). In many offshore and ERD operations, Synthetic Based Muds (SBM) or Oil Based Muds (OBM) are often used to their high lubricity, ability to stabilize reactive clays and preserve hole stability and resist contamination (Cameron, 2001). Although these are all highly sought-after benefits, one significant downside to OBM's and SBM's is their increased susceptibility to rheological changes with temperature fluctuations compared to Water Based Muds (WBM) (Zamora et al., 2000). The most effective way to lower ECD's are to have a thin rheology. Unfortunately, the critical aspect of cuttings removal is heavily dependent on rheology, and too thin a rheology may lead to improper hole cleaning (van Oort et al., 2004). This in turn will effectively raise ECD through an increase in average mud density from small cuttings, and by lowering the effective diameter of the wellbore through cuttings beds (Feifei Zhang, Filippov, Miska, & Yu, 2017). The introduction of flat-rheology mud systems has shown in several scenarios to be very successful in minimizing increased ECD risks due to temperature and pressure fluctuations. Two wells drilled in the Yurkharvoskoye field in the Arctic Yamal peninsula of Russia, utilized a flat-rheology SBM to successfully reach TD without any issues (Glebov et al., 2014). Although these wells were mainland drilled and did not experience the significant temperature fluctuations due to water, the Permafrost of the area applied a geothermal gradient of approximately 11 degrees Fahrenheit per 100 ft (3 degrees Celsius per 100 meters). Although bottom-hole temperature was difficult to estimate reliably due to the heterogeneity of rock, it was enough of a fluctuation to substantially

affect rheological properties (Zadvornov et al., 2015). Extensive field data has also shown the benefit of flat-rheology SBM. The success it has had in the Gulf of Mexico has led to the overwhelming acceptance within the industry (van Oort et al., 2004).

2.3.2.3. Cuttings Management

Cuttings management is one of the most critical components to a successful ERD campaign, and arguably the most important function of a drilling fluid. Improper hole cleaning can lead to drilling and completions problems, from formation fracturing resultant from increased ECD's, stuck pipe from bridging and packing off, to excessive torque and drag. Cuttings management can be measured through carrying capacity during flow, and its ability to suspend cuttings when static. It has been observed that mud qualities such as lower viscosity and gel strengths, and higher density are advantageous in removing cuttings from a wellbore (Williams Jr. & Bruce, 1951). For transporting cuttings, the two main easily controllable parameters affecting cuttings transport are flow rate and fluid rheology. Drill string rotation and eccentricity, wellbore size and inclination, cuttings size and density, formation breakdown, drilling rate and fluid density also play important roles in cuttings transport. These additional factors, however, are reliant on many other drilling parameters and cannot practically be designed to optimize cuttings transport (Mohammadesalehi & Malekzadeh, 2001). For example, although higher density drilling fluids are more beneficial to cuttings removal, the primary design behind optimal density is to maintain an overbalance within the wellbore. As density increases, Rate of Penetration (ROP) declines due to increased solids content preventing the bit from contacting uncut formation. Increased density will also increase ECD's which could cause formation fracturing and lost circulation if not within required drilling margins. Drill string rotation plays critical role in cuttings transport, particularly in ERD wells. However, the speed

of rotation (RPM) is often limited by torque and vibration encountered within the wellbore (Gupta et al., 2014), as well as downhole tool capability.

Wellbore inclination plays a significant role in cuttings transport efficiency. Previous studies have noted that as wellbore inclination angle approaches as little as 10°, the behavior of cuttings movement begins to change (Martin, Georges, Bisson, & Konirsch, 1987). Further studies have noted much more difficulty in eliminating cuttings beds between the inclinations of 35° and 50°, as the cuttings beds will slide back to the bottom when flow has stopped (Tomren et al., 1986). Other experimental research identified the highest difficulty in cuttings transport to be in the range of 40° to 60° (Ford, Peden, Oyenevin, Gao, & Zarrough, 1990)(Peden, Ford, & Oyenevin, 1990). Peden et.al did mention that the ‘critical angle’ in which the highest velocity is required is dependent on other parameters such as rheology, annular clearance and transport mechanism. Sifferman and Becker saw significant cuttings bed build up began between 60° and 90°, concluding that this may be the most difficult inclination range to clean (T.R. Sifferman & Becker, 1992), however they found that cuttings bed measurements were difficult to measure at inclinations below 60 degrees due to them sliding down the wellbore when pumping was stopped. This observation is a strong indication of the higher risk of packing off in inclined wellbores, as cuttings can build up over flat-time.

2.3.2.3.1. Vertical Annulus Cuttings Transport

In vertical wellbores, cuttings transport efficiency is primarily based on settling velocity. Empirical correlations developed by Moore (1974), Chien (1971) and Walker and Mayes (1975) are generally accepted for determining fluid and pumping parameters (Mitchell & Miska, 2011). An experimental study completed by Sifferman, Myers, Haden and Wahl, on drill cutting transport in vertical annuli concluded several factors that are still used in vertical wellbore design

today. They observed that a minimum annular velocity of 0.83 ft/sec provided satisfactory cuttings transport, based on most drilling mud rheology. They also observed that increased viscosity benefits cutting transport efficiency, and that drill pipe rotation had only a slight effect on cutting transport (Thomas R Sifferman, Myers, Haden, & Wahl, 1973).

General modeling for cuttings transport in vertical wells is based off the mechanistic model, developed by Clark and Bickham. They observed, through laboratory testing, that in vertical and near vertical annuli, cuttings are almost uniformly distributed throughout the annular cross-section and settle downhole against the flowing mud (Clark & Bickham, 1994).

$$V_{mix} = \frac{0.0475v_s}{0.05 - c_0} \quad (2)$$

(2) Displays the calculation to determine minimum mixture velocity required for a specified cuttings concentration. Minimum mixture velocity (V_{mix}) is the minimum allowable circulation velocity required maintain a cuttings concentration at or below 5% in a vertical/near-vertical annulus. In this equation, c_0 is the fraction cuttings concentration (value less than 5% (Pigott, 1941)) and v_s is the settling velocity (Mitchell & Miska, 2011). A detailed breakdown of these variables and how they are determined can be found in 7.2.

Although almost all wells have a vertical component to contend with regarding cuttings transport (slant wells occasionally being one exception when spud angle is above 35°), this field has been thoroughly studied, and is well understood. Cuttings movement in vertical annuli is only a more significant concern in deep water wells, where long, low-temperature affected risers can vastly affect the rheology of drilling fluid, and in turn effect cuttings transport. These problems have been largely mitigated through the use of flat-rheology SMB, and the use of riser-

booster pumps (Zamora et al., 2000). In general, cuttings transport through the vertical section of a well is considered the least difficult.

2.3.2.3.2. Deviated Annulus Cuttings Transport (35° - 60°)

As the deviation of a wellbore increases, the risk of cuttings bed development also increases. This cuttings bed is the accumulation of cuttings build up on the low-side of the wellbore, usually caused by inadequate flowrate or improper rheology, lowering the carrying capacity of the drilling mud. This cuttings accumulation can be of significant concern within the range of 35° to approximately 60° (studies vary), Within this range, cuttings beds have a higher tendency to slide back down to the bottom of the wellbore, increasing likelihood of stuck pipe, packing-off, or other similar problems during periods of non-circulation (Pilehvari, Azar, & Shirazi, 1999). A large-scale experimental study of cuttings transport through the Tulsa University Drilling Research Projects (TUDRP), undertaken by P.H. Tomren, A.W. Iyoho, and J.J. Azar, did considerable testing at all angles of inclination. They discovered a dramatic change in particle behavior, resulting in a very high low side-wellbore cuttings concentration, at lower flow rates (<3 ft/sec). Turbulent flow and pipe rotation would disrupt the cuttings beds, allowing for better transport, however the cuttings were seen to be shot axially, not necessarily traveling up the wellbore (Tomren et al., 1986). Although turbulent and transitional flow often occurs around BHA's and stabilizers, in field situations, most wellbore flow is considered laminar in typical drilling operations. This is due to the laminar nature found for a significant portion of the wellbore (around drill pipe and in casing). Tomren found that laminar flow was unsuccessful in transporting cuttings, until the development of the cuttings bed was significant enough to reduce the annular volume and increase velocity. When flow rates were increased above 3 ft/sec, slug-pattern cuttings transport was observed, possibly indicating a change to transitional or turbulent

flow. This created a cyclical pattern, in which cuttings beds would develop, increasing annular velocity. This increased velocity would erode the cuttings beds, and increase annular volume once again reducing velocity, allowing the development of a new cuttings bed. The study also found that for angles between 35° and 50°, the highest risk for cuttings to slide down and accumulate on the low side of the wellbore occurred. This issue was exasperated by drill pipe eccentricity, in which it would tend to settle on the low side of the wellbore, encouraging fluid flow to the upper half, leaving the bottom stagnant (Mitchell & Miska, 2011).

Although flow rate is the overlying and dominant factor in cuttings transport at this inclination, fluid rheology also plays an important factor. Contrary to the positive-negative relationship of yield point (YP) value to cuttings concentration in vertical wells, the higher YP becomes less impactful as deviation increases. An additional study observed that as inclination increased, turbulent flow encouraged cuttings transport more than laminar flow; higher YP fluids tended to offer more laminar flow, and a more immediate development of cuttings beds (Okrajni & Azar, 1986). This observation is repeated in many studies regarding cuttings transport in deviated and horizontal wellbores and is an important factor in the design of a drilling program for ERD. Management of cuttings transport is super-critical in this area, as with ERD operations, a considerable amount of drilling time occurs past this build section of the well. If cuttings transport is not managed, there will be a much higher risk of cuttings bed accumulation to occur at approximately 60°, when cuttings beds have been shown to stop sliding.

2.3.2.3.3. Deviated Annulus Cuttings Transport (61° - ~90°)

As wells increase in deviation, the risks of cuttings beds sliding diminishes (T.R. Sifferman & Becker, 1992), however the development of these beds persists and can become detrimental. Two of the primary risks of cuttings bed accumulations in ERD are the increase in

torque and drag on the drill string, and a potential increase in ECD due to smaller annular diameter; however, in cuttings beds have not been proven to significantly increase ECD's until substantial bed height, potentially due to high-side fluid channeling. One significant issue that arises in ERD is due to the extensive length and time cuttings are in the wellbore, they can be ground down into finer and finer particles, making transport more difficult and causing solids contamination within the active mud system. Unlike large cuttings, whose main parameter for removal is flow rate, small cuttings transport is highly dependent on rheology and drill pipe rotation. These smaller cuttings are often very cohesive and can easily accumulate and cause stuck drill pipe. Unfortunately, the cumulative studies of the effects of cuttings size on transport are diverse and contradictory, most likely due to incomparable conditions (Duan et al., 2006). A PhD study completed by Ahmed observed that the required critical velocity for removing cuttings would increase significantly as cuttings sizes smaller than 1.5 mm in diameter, but this velocity would level off and decrease as cuttings grew to 1.5 mm in diameter and larger (Ahmed, 2001). Additionally, Walker and Li observed that cuttings larger than 0.76 mm are more difficult to clean, but became easier to clean under 0.76 mm (S. Walker & Li, 2000). These observations suggest that cuttings size can cause significant difficulty in determining ideal drilling parameters (flow rate, ROP, RPM). An important note on this study, however, is that the size of cuttings has not been found to be of significant importance in practical applications.

Almost all recent studies note the importance of drill string rotation in aiding cuttings removal in horizontal wellbores. Early studies put less significance on rotation than other factors such as flow rate and thixotropy (Martin et al., 1987). However, as directional wells became more difficult, long, and popular, the importance of drill pipe rotation became apparent. Several studies have focused specifically on the effects of drill pipe rotation in cuttings transport

(Loureiro, Paula, Serafim, & Martins, 2004; Sanchez et al., 1997). These studies have observed several factors that affect cuttings removal, such as the presence of Taylor vortices (Lockett, Richardson, & Worraker, 2000), various flow patterns and their effects on cuttings beds (Loureiro et al., 2004) and the general consensus that increasing rotation speed will enhance hole cleaning (Philip, Sharma, & Chenevert, 1998; Sanchez et al., 1997; Yoho, 1980). However, there is no consensus on the reason why rotation has this effect on hole cleaning, and a study must be performed to determine why. Furthermore, no replication of the cuttings transport efficiency step-change around 120 RPM observed in the field.

2.4. Extended Reach Cuttings Transport Evaluation

In order to gain a better understanding of cuttings transport, particularly in horizontal and deviated wells, researchers have used mathematical modeling to simulate downhole conditions, and flow loops to recreate flow patterns. Mathematical modeling has allowed a better understanding of how cuttings may behave at various flow rates and inclinations, from vertical to horizontal; however, due to the transient nature of cuttings, these models are often quite limited, as they can only consider a single section of hole, often with a constant hole geometry (Naganawa & Nomura, 2006). Many flow loops have also been designed, such as the Low-Pressure Ambient Temperature (LPAT) flow loop at the Tulsa University Drilling Research Projects (TUDRP) facility, to observe in greater detail how cuttings behave under a variety of conditions. Both methods have allowed for a better understanding of how cuttings behave within the wellbore, but there is still much that can be learned. Many studies have indicated the positive effect that drill pipe rotation has in horizontal wellbores (Sapru, 2001)(Sanchez et al., 1997)(Pilehvari et al., 1999). Unfortunately, there is still minimal understanding of how drill string rotation truly aids cuttings transport. It is clear through these studies and field data that

high-speed rotation plays a key role in cuttings transport, but more needs to be done to understand the dynamic effects of this rotation (Pilehvari et al., 1999).

2.4.1. Modeling

Cuttings transport modeling has been an important area in drilling since the introduction of rotary drilling. Prior to the 1980's, a need for understanding of cuttings transport was apparent, and several mathematical models were developed to aid in assuring good hole cleaning in vertical annuli. Moore, Chien, Walker and Mayes performed several experimental runs in flow loops and developed correlations for determining mud properties and flow rates in vertical wells (Mitchell & Miska, 2011). Unfortunately, these correlations are not effective as wellbore inclination increases much past 10° from vertical.

Cuttings transport studies saw a significant shift from vertical wellbore analysis to inclined modeling in the 1980's, as directional wells began to outnumber vertical wells (Mohammadesalehi & Malekzadeh, 2011). It became immediately apparent cuttings behave differently as inclinations increase, and vertical models could not be applied in deviated and horizontal wellbores.

The general unstable and transient nature of cuttings transport in deviated wellbores make mathematical modeling difficult, as there are many factors that affect cuttings transport. Each cutting experiences several forces (Figure 4) and flow patterns (Figure 5) that play an important role in determining cuttings transport (Egenti, 2014).

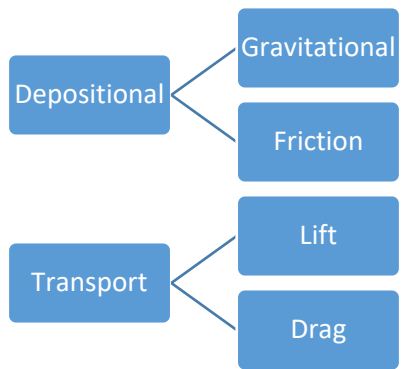


Figure 4: Acting forces on a drilled cutting (Egenti, 2014)

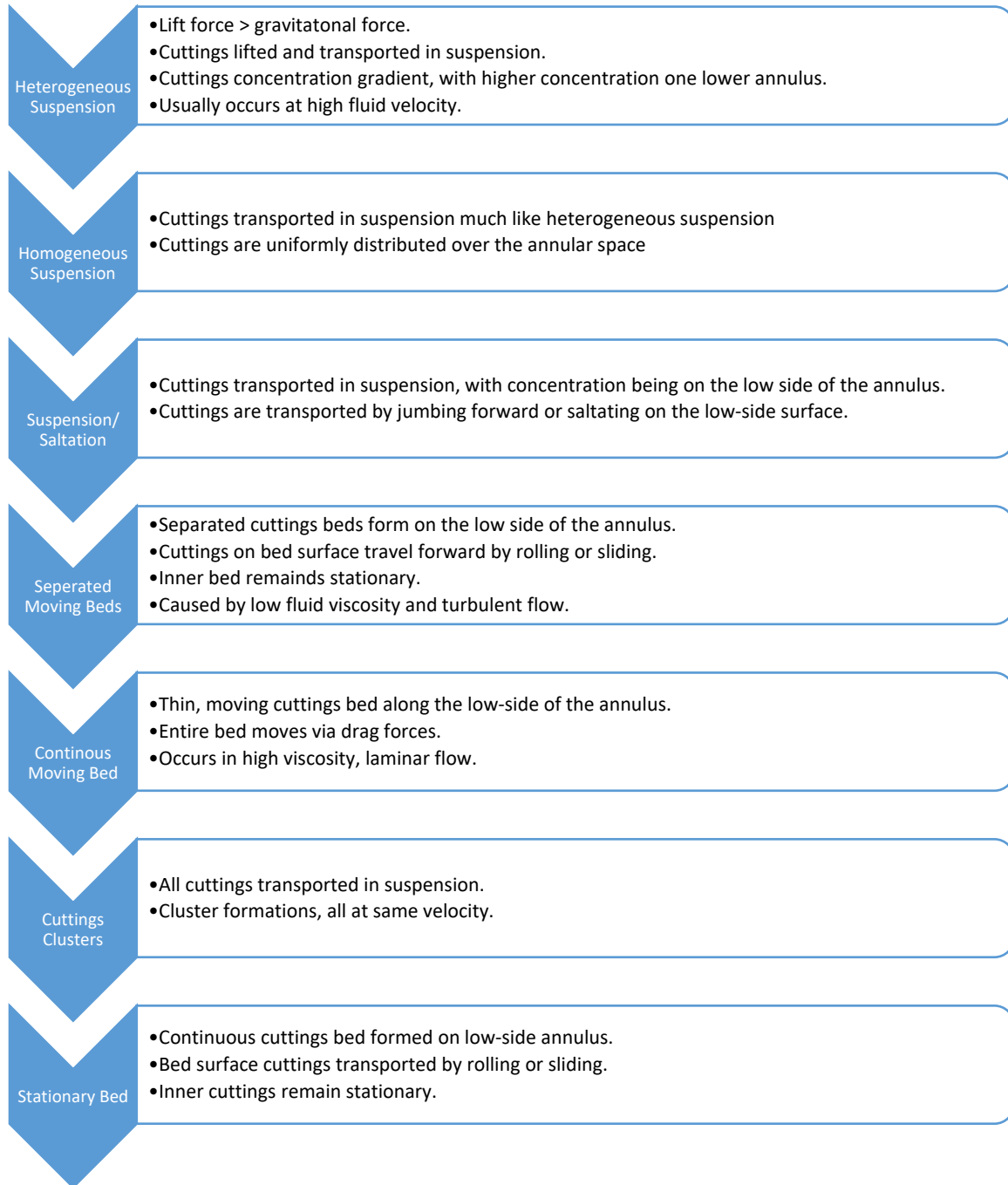


Figure 5: Cuttings transport flow regimes (Egenti, 2014)

With the many factors that come into play in modeling cuttings transport, it was understood that simple correlations aren't practical for anything other than specific parameters. They are developed under selected conditions and do not apply outside of those boundaries. Along with empirical correlations developed from large scale experimental tests, different mathematical models were applied in hopes to further describe the nature of cuttings transport. The critical transport velocity model allowed a basic understanding of what minimum flow rates were required in order to eliminate the development of cuttings beds, but do not account well for non-Newtonian fluids, or other wellbore factors such as wellbore eccentricity. Layer-modeling was introduced in the 1970's to describe slurry transport, and it was later applied to cuttings transport. Two and three-layer models were developed under both steady-state and transient conditions, offering a clearer interpretation of cuttings transport and a better determination of cuttings bed levels.

With the development of more powerful computer simulators, the introduction of computational fluid dynamics modeling further increased the ability of engineers in modeling and predicting cuttings flow, with a variety of important parameters included (wellbore eccentricity, pipe rotation, non-Newtonian flow). These models have helped researchers immensely in the understanding of cuttings transport, however there is still much to learn and improve upon.

2.4.1.1. Newtonian and Non-Newtonian Fluids

When discussing study of fluid flow and fluid characteristics, there are multiple facets that must be considered. Generally, fluids are divided into 2 main categories based on their reactive nature to pressure (compressible or incompressible). Incompressible fluids are further characterized by their response to shearing and can be considered either Newtonian or non-

Newtonian in nature. The drilling industry utilizes a wide variety of fluids some of which are compressible, however most are incompressible. Drilling fluids that are considered compressible are gases, and in drilling cases, nitrogen, air, and other gaseous state drilling fluids are used in a variety of applications such as air drilling for unconsolidated surface holes, to full underbalanced drilling in delicate or sensitive formations.

The primary focus of this section is to describe the differences between incompressible Newtonian and non-Newtonian fluids and flow properties, and to highlight any important studies and relevance to the drilling industry. Drilling fluids are often considered non-Newtonian due to their non-linear shear stress/shear rate trends. It is important to identify the differences between Newtonian and non-Newtonian flow characteristics, to outline the proper approach for analysis.

Additionally, drilling fluids utilize the Hershel-Buckley method for determining shear rate. This method is further discussed in 2.4.1.1.2.

2.4.1.1.1. Shear Modeling in Drilling fluid

The study of flow in wellbore annulus during drilling operations has been ongoing since fluid was first used. However, as drilling fluids were developed, new models and approaches were required in order to more accurately understand the dynamics. Drilling fluids are most often non-Newtonian, shear-thinning (pseudoplastic) in nature, and popular models for evaluation include the Bingham-plastic model, the Hershel-Buckley model and the Power law model. API RP13D, the American Petroleum Institute's section discussing drilling fluid hydraulics modeling, recommends the Hershel-Buckley model over all other models. Figure 6 displays the differences in how each model's shear stress differs in a relation to shear rate. The Hershel-Buckley model displays the same characteristics as the Power law in that as shear rate increases, shear stress decreases (shear thinning). However, it also has an initial shear stress

higher than zero, much like the Bingham plastic model. This allows a more accurate representation of a drilling fluids gel-strength, in which it requires an initial shear stress before it begins to flow, and that it will shear more easily as more stress is applied.

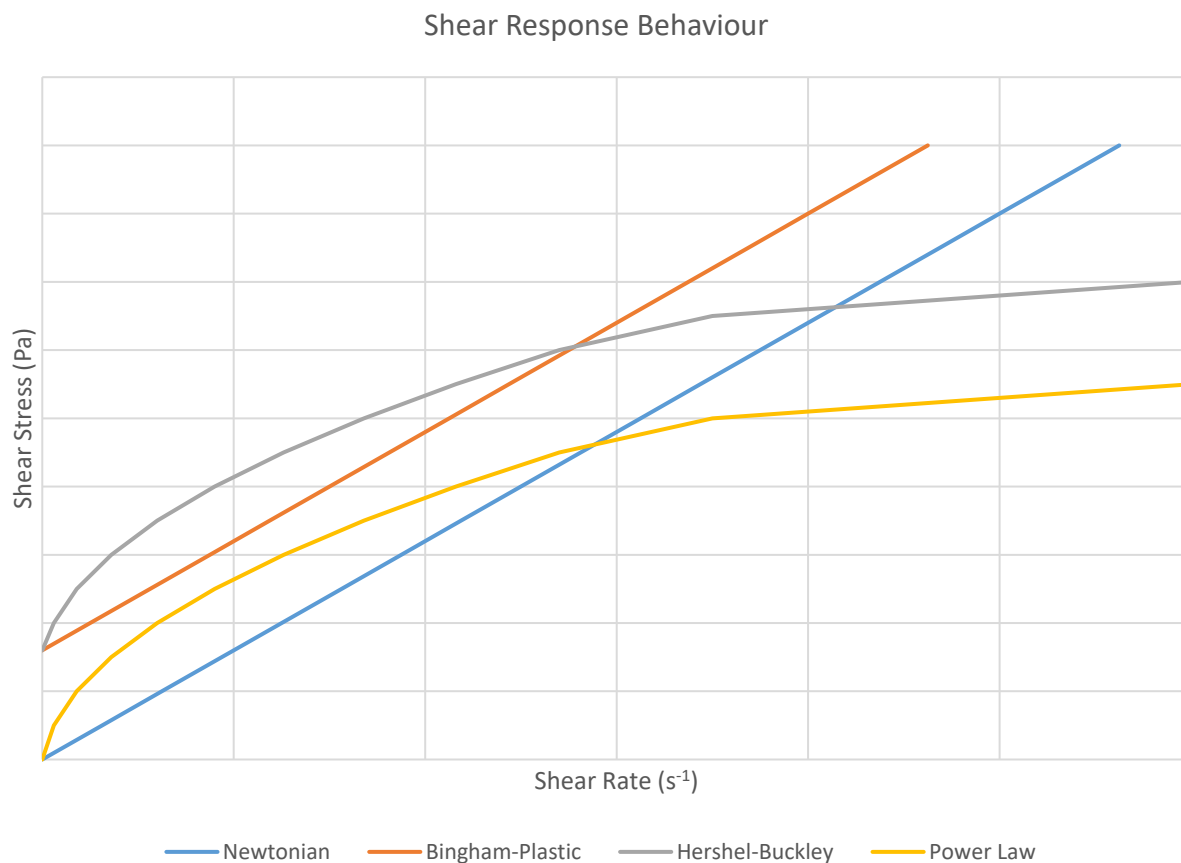


Figure 6: Rheology comparison by shear response (expected curves)

2.4.1.1.2. Shear Stress/Rate Relationship

Two of the most significant properties that define both Newtonian and non-Newtonian fluid flow are shear rate and shear stress, and their relationship to one another. Shear stress is defined as a force tending to cause deformation of a material by slippage along a plane (or planes) parallel to the imposed stress (Britannica, 2018). An example would be if a force was

applied along the top of a stack of papers, the shear force would be the force it would take to move each paper forward from the paper below. As the layers get further away from the force, the layer moves less and less, until the stationary surface area is reached, and no fluid movement is encountered (Figure 7). The magnitude of shear stress is directly related to dynamic viscosity ‘ η ’ when considering the force in fluids, wherein an increased viscosity will see higher shear stress than a lower viscosity.

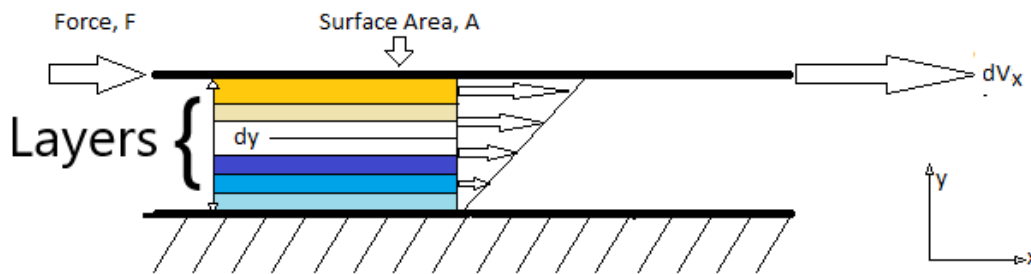


Figure 7: Shear stress layers

The general shear stress equation is defined in (3), where F is equal to the force applied, A is equal to the area the force is applied to, and τ_{yx} is equal to the shear stress (subscript x referring to the direction normal to the shearing surface, and subscript y referring to the direction of the force and the flow) (Chhabra & Richardson, 2008).

$$\frac{F}{A} = \tau_{yx} \quad (3)$$

Shear stress is often plotted in reference to shear rate. Shear rate (herein identified as $\dot{\gamma}_{xy}$) is a measure of the change in velocity in respect to distance (4), and is also referred to as the velocity gradient (Mott, 2006).

$$\frac{\Delta v}{\Delta y} = \text{Shear Rate } (\dot{\gamma}_{xy}) \quad (4)$$

As previously stated, shear stress is directly related to the dynamic viscosity of the fluid in motion. By multiplying dynamic viscosity by the velocity gradient, shear stress is obtained in fluid dynamics (5).

$$\frac{F}{A} = \tau_{yx} = \eta \left(-\frac{dV_x}{dy} \right) = \eta \dot{\gamma}_{xy} \quad (5)$$

To identify the relationship between shear stress and shear rate, measurements are plotted on charts often referred to as rheograms or flow charts (Figure 8).

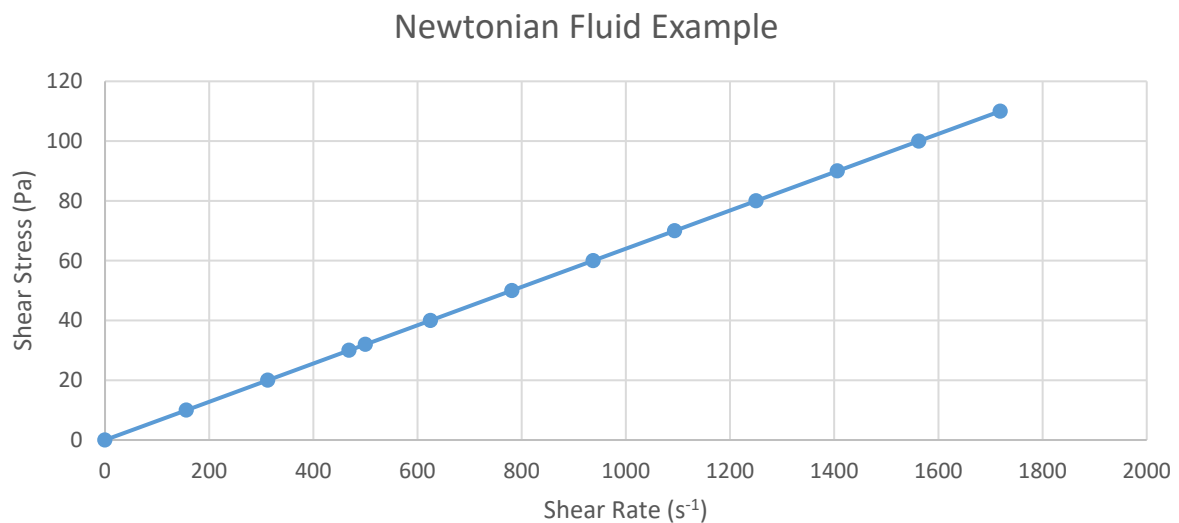


Figure 8: Rheogram of a Newtonian fluid (Cooking Oil, 294K) (Chhabra & Richardson, 2008)

Kinematic viscosity is another form of describing fluid viscosity, in reference to density (6). Kinematic velocity (μ) is derived as the ratio of dynamic viscosity and density (ρ)

$$\frac{\eta}{\rho} \quad (6)$$

In Newtonian fluids, the relationship between shear stress and shear rate is linear at constant pressures and temperatures. It is also referred to as the constant of proportionality (7), or Newtonian viscosity and will be represented by μ . The more generalized term of shear stress divided by shear rate is called apparent viscosity.

$$\mu = \frac{\tau}{\dot{\gamma}} \quad (7)$$

In non-Newtonian fluids, the apparent viscosity is not constant at a given temperature and pressure. Unlike Newtonian fluids, it is dependent on several flow conditions. Non-Newtonian fluids can be categorized into 3 distinct classes:

1. Generalized Newtonian Fluids (GNF): these fluids rate of shear is determined only by the value of shear stress at one point and one instant (8). These fluids are also called time-independent fluids.

$$\dot{\gamma} = f(\tau) \quad (8)$$

2. Time-dependent fluids: These fluids have a shear stress/rate relationship that is dependent on the length of shear time, as well as their kinematic history. These fluids can be either thixotropic (shear thinning time-dependent) or rheopectic (shear thickening time-dependent).
3. Visco-elastic fluids: these fluids possess the elastic qualities of a solid (particularly at low shear rates), while at the same time demonstrating fluid viscosity characteristics.

2.4.1.1.2.1. Generalized Newtonian Fluids

GNF's can be further subdivided into three types:

1. Shear-thinning (pseudoplastic fluids) are the most common type of non-Newtonian behavior, and it is recognized by a decrease in apparent viscosity as increased shear rate. The power law model (9) is one of the most widely used models to evaluate the relationship between shear stress and shear rates of shear thinning fluids. In the power law equation, 'm' (fluid consistency index) and 'n' (flow behavior index) are empirical parameters, for flow behavior index values below 1, shear thinning behavior is observed, and above 1, shear thickening is observed. Other models, such as the Carreau viscosity equation (10) (μ_0 = zero shear viscosity, μ_∞ = infinite shear viscosity, λ = curve fitting parameter, n^* = curve fitting parameter), Cross viscosity equation (11) (k = curve fitting parameter) and the Ellis fluid model (12) (α = measure of the degree of shear thinning behavior) are also popular methods for modeling shear thinning fluids. (Chhabra & Richardson, 2008)

$$\mu = \frac{\tau_{yx}}{\dot{\gamma}_{yx}} = m(\dot{\gamma}_{yx})^{n-1} \quad (9)$$

$$\frac{\mu - \mu_\infty}{\mu_0 - \mu_\infty} = \{1 + (\lambda\dot{\gamma}_{yx})^2\}^{(n^*-1)/2} \quad (10)$$

$$\frac{\mu - \mu_\infty}{\mu_0 - \mu_\infty} = \frac{1}{1 + k(\dot{\gamma}_{yx})^n} \quad (11)$$

$$\mu = \frac{\mu_0}{1 + (\tau_{yx}/\tau_{1/2})^{\alpha-1}} \quad (12)$$

2. Viscoplastic fluid: This type of fluid must have its yield stress exceeded before it begins to deform and/or flow. This results in 2 different regions: an unyielded zone where the fluid is at rest, or moves as a rigid object, and a second region where it moves as a viscous fluid (Kefayati, Tang, & Chan, 2018). The most basic and often used model for describing viscoplastic fluids is the Bingham plastic model (13). This model considers that certain sections of a flow may not necessarily achieved their shear stress yield point. In addition, the flow and shear are different dependent on distance from the pipe or annulus wall, and iterative calculations must often be performed to gain an understanding of flow rate and shear at different zones.

$$\tau = \tau_y = \tau_{wi} - \gamma_a \frac{dp_f}{ds} \quad (13)$$

The Herschel-Buckley fluid model (Figure 9) assigns 3 constants to generalize the Bingham plastic model. The general equation is (14), and can bears some resemblance to the power law model (9), in which both ‘m’ and ‘n’ are empirical numbers, and τ_o^H is dependent on τ_{yx} ($|\tau_o^H| < |\tau_{yx}| = (14)$, $|\tau_o^H| > |\tau_{yx}| = \gamma_{yx} = 0$).

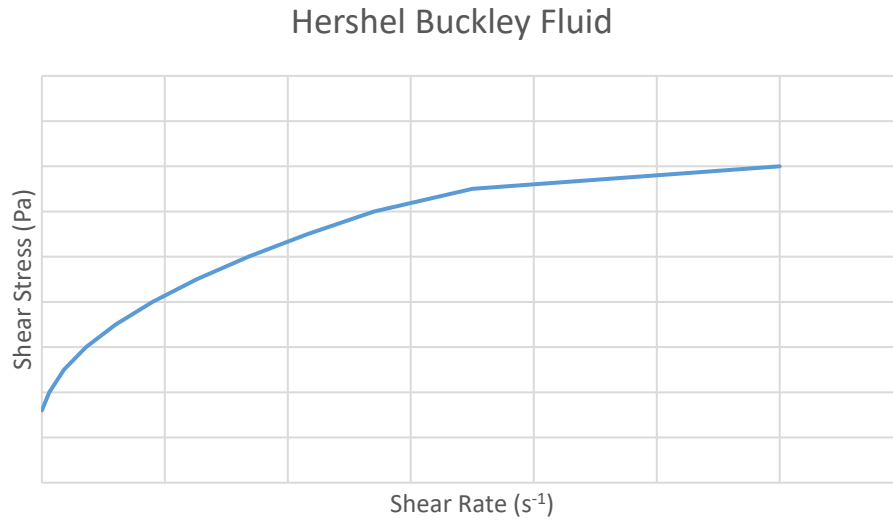


Figure 9: Trend of a typical Hershel-Buckley fluid

$$\tau_{yx} = \tau_0^H + m(\dot{\gamma}_{yx})^n \quad (14)$$

The Casson fluid model is a third method for evaluating shear thinning fluids and is used primarily in the foodstuffs and biological materials industry. It is defined by (15). Much like the Herschel-Buckley model, τ_0^C is compared to the absolute value of τ_{yx} ($|\tau_0^C| < |\tau_{yx}| = (13)$, $|\tau_0^C| > |\tau_{yx}| = \dot{\gamma}_{yx} = 0$).

$$(|\tau_{yx}|)^{1/2} = (|\tau_0^C|)^{1/2} + (\mu_c |\dot{\gamma}_{yx}|)^{1/2} \quad (15)$$

3. Shear-thickening (dilatant) fluids: these fluids show similar characteristics to pseudoplastic fluids regarding a lack of yield stress, however opposite to an observed decrease in viscosity with shear rate, dilatant fluids see an increase in apparent viscosity.

2.4.1.1.2.2. Time-Dependent Fluids

Many drilling fluids, such as polymer-based systems, exhibit time-dependent shearing, in which as the fluids are sheared at a relatively steady rate over a given time, their apparent viscosity decreases. This act is called thixotropy, and is observed only in time-dependent, non-Newtonian fluids (no correlation has ever been seen in GNF's). One important note on these fluids is that apparent viscosity can often be restored if the shearing action is reduced, or altogether removed, allowing the fluid to return to its initial state. This behavior differs from typical shear thinning/thickening behavior as it represents a constant shear rate over time causing the thinning, as opposed to an increase shear rate discussed previously.

Much like the difference between pseudoplastic and dilatant fluids, rheopexy is the term used to describe a fluid that sees an increase in viscosity as a constant shear rate is applied over time. This behavior is very seldom seen and very few fluids possess this type of characteristic. Bovine synovial fluid is one example of a fluid that exhibits rheopexy (Oates, Krause, Jones, & Colby, 2006).

2.4.1.1.2.3. Visco-Elastic Fluids

Drilling fluids are often designed to exhibit visco-elastic properties, as many drilling fluids must develop a gel-strength for solids suspension during static time. In fluid terms, the elasticity of a fluid can be described as its ability to return to an original state after some deformation. When considering a visco-elastic fluid, the apparent viscosity will offer up a resistance to flow, however the elastic component of the fluid will encourage a fluid to “step-back” after it stops flowing, exhibiting some elasticity.

2.4.1.2. Non-Newtonian Fluid Flow in Annulus

Given that drilling fluid is primarily non-Newtonian, particularly when drilling with incompressible fluids in extended reach or high inclination wells, there are a multitude of factors that influence fluid flow. Non-Newtonian fluid flow is affected by a variety of parameters, from wellbore geometry, shear rate, and drill string rotation, and is often contaminated with drilling solids, as well as formation fluids (oil, gas, water). These parameters can alter the flow patterns of multiphase drilling fluid, causing instability and turbulence.

A study completed by Dewangan and Sinha analyzed the effects that eccentricity has on multiphase flow instability. The study considered only fully developed annular flow and used a Newtonian fluid model as a carrier flow (fluid transporting cuttings). With these parameters, they observed 4 key findings:

1. Transition flow increases in likeliness from the bottom of the annulus to the top, regardless of azimuthal direction it travels (clockwise or counterclockwise). This observation helps explain why higher velocity flow channeling occurs on the high side (top portion of a horizontal annulus) of a wellbore in horizontal drilling operations.
2. Radius ratios eccentric ratios and dimensions of the annulus all have a significant effect on the critical flow rate values, as well as the critical Reynolds number.
3. The presence of a secondary phase lowers any possibility of a transition phase occurring and this transition phase is more likely to occur close to the inner (drill string) radius than the outer (annulus) radius. This result indicates that the drill string rotation has an effect on flow transition (Dewangan & Sinha, 2016).

The study completed by Dewangan and Sinha supports drill pipe rotation has a direct effect on flow turbidity and that higher fluid velocities develop into a channel on the high side of

the wellbore. The results of this study are not based on Non-Newtonian fluids, which are used in drilling operations to circulate the wellbore. Therefore, results of the study cannot be used to draw conclusions on the observed conditions in drilling operations.

A previous study performed by Escudier et.al. identifies the critical differences encountered between Newtonian and non-Newtonian fluids in a wellbore, particularly when inner-cylinder rotation is a factor. The study cross-examines different fluid models for comparison (Herschel-Buckley, Power-Law, Carreau, Cross). It also identifies two separate flow regimes in horizontal wellbores with inner cylinder rotation, the primary axial flow through the annulus, and a secondary, cross-plane flow. Escudier makes the critical note that in Newtonian fluids, these two flow regimes are independent of each other. However, non-Newtonian fluids demonstrated a complete dependence on one another, creating three flow types:

1. Axial dominated ($\xi < 1$)
2. Mixed ($1 < \xi < 10$)
3. Rotation dominated ($\xi > 10$)

These flow types are determined by the dimensionless velocity ratio ξ (16), in which ω is the rotational angular velocity of the inner cylinder (in radians/sec), U is the bulk axial velocity of the fluid (m/s), and R_I is the outer drill string (inner cylinder) radius (m)(Figure 10).

(Escudier, Oliveira, & Pinho, 2002)

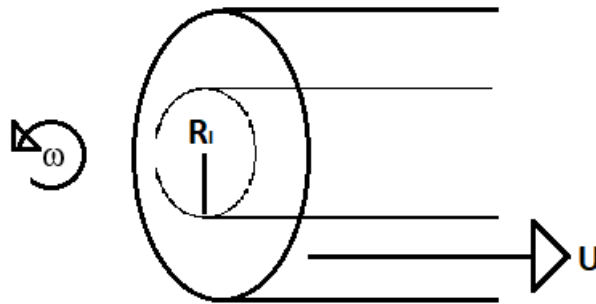


Figure 10: Velocity ratio parameters

$$\xi = \frac{\omega R_i}{U} \quad (16)$$

The velocity ratio equation was applied to determine the velocity ratios for three drill pipe sizes (5-inch, 5.5-inch, 5.875-inch), over an RPM range of 0-200.

Figure 8 displays that flow is in axial dominated flow for all strings until approximately 180 RPM, at which point the larger strings exceed a velocity ratio of 1.0 and become mixed. Under conventional drilling and rotating conditions (0-180 RPM), the velocity ratio remains well below 10. Therefore, based on this relation in practice rotational dominated flow should not be present. 7.3 outlines numerical results from Figure 8.

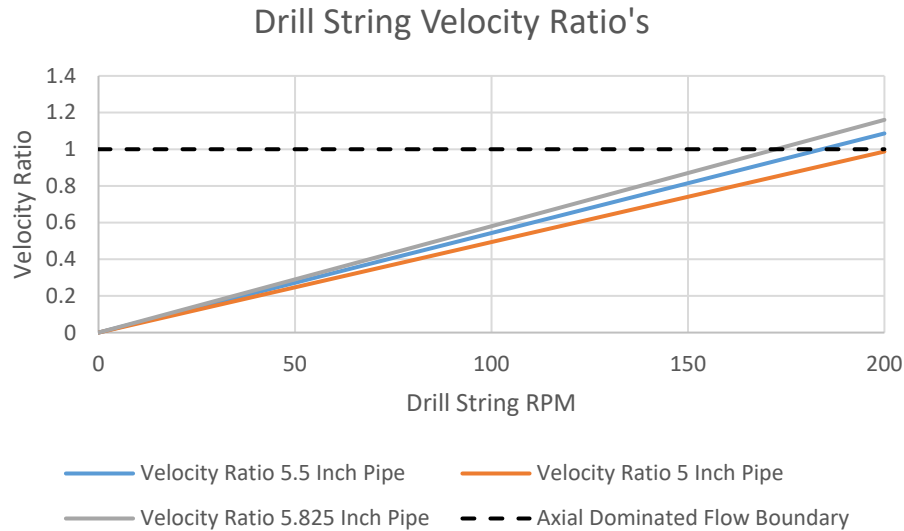


Figure 11: Velocity ratio profiles

Escudier et al. recognized that axial and cross-sectional flow patterns are coupled. Escudier et al. noted that with shear-thinning (pseudoplastic) non-Newtonian fluids, the influence of the bulk Reynolds number Re (19) is significant and complex in that peak axial fluid velocity tends to decrease as the Taylor number Ta (dimensionless value pertaining to inertial forces from rotating fluid related to viscous forces, (17)) increases (as seen in Newtonian flow), but is also influenced by Re . Unlike Newtonian flow, the location of this peak axial velocity is dependent on both the Re value and Ta value (κ is the radius ratio R_I/R_O).

$$Ta = \left(\frac{1}{\kappa} - 1 \right) T^2 \quad (17)$$

2.4.1.3. Stabilized Flow

Many studies have been performed that assume that flow has stabilized in an annulus. However, the study of developing flow is a critical parameter to adequate sizing of the flow loop.

As drilling fluid and cuttings enter the flow loop test section, they undergo a significant change in flow area, and a change in direction. Additionally, a rotating inner cylinder may further complicate fluid normalization, as flow will be subject to both axial and cross-sectional flow (as discussed in the previous section).

In order to determine the proper length for flow to develop, entrance length L_e must be calculated (18),(19). Flow must be first identified as Laminar or Turbulent, by calculating the bulk Reynolds Number (20) through a variety of means. Historically, the flow of Newtonian fluids with a Reynolds number equal to or less than 2100 is considered laminar, and equal to or above 3000 turbulent. This leaves a volatile range between 2000 and 3000 that leads to unpredictable flow but is generally considered transitional or turbulent.

$$\frac{L_e}{D} = 0.05Re_D \rightarrow \text{Laminar Flow} \quad (18)$$

$$\frac{L_e}{D} = 50 \rightarrow \text{Turbulent Flow} \quad (19)$$

$$Re_D = \frac{VD}{\nu} = \frac{\rho VD}{\mu} = \frac{4Q}{\pi D \nu} = \frac{4\dot{m}}{\pi D \mu} = \frac{2\rho U \delta}{\mu_F} \quad (20)$$

In a drilling annulus with non-Newtonian fluids, however, is significantly more complex. When considering time-independent (GNF) fluids, the type and degree of non-Newtonian behavior has a significant impact on the determination of a critical Reynolds number. Ryan and Johnson (Ryan & Johnson, 1959) Identified that for power-law fluids, Reynolds numbers can be determined using the flow behavior index (21). This equation, along with studies performed by others (Mishra & Tripathi, 1971) have had difficulty aligning with several experimental studies performed (Dodge & Metzner, 1959; Rudman, Blackburn, Graham, & Pullum, 2004). As such, it is still a safe assumption to associated laminar flow below a Reynolds number of 2100, and turbulent above.

$$Re_{MR} = \frac{6464n}{(3n + 1)^2} (2 + n)^{(2+n)/(1+n)} \quad (21)$$

When attempting to determine flow boundaries in an annulus, additional properties become prevalent and complex. Both axial (Re_D) and rotational Reynolds numbers (T , (22)) must be considered as both flow regimes are coupled. This adds a layer of complexity to determining flow normalization, as transitional flow can be adversely affected by the inner pipe rotation. It must be noted that the inner pipe eccentricity is of significant effect, and is often on the low side of the wellbore in horizontal drilling. Although drill string position is not exact at any given time during rotation, it can be maintained to allow for strong estimates of flow normalization when determining both primary (axial) and secondary (helical/cross sectional) flow regime normalization.

$$T = \frac{\rho\omega R_I \delta}{\mu_F} \quad (22)$$

Several studies have been completed by researchers such as Escudier et.al. and Ferras et.al. that outline several numerical and analytical methods for studying the flow of non-Newtonian and viscoelastic fluids in a wellbore. These studies have allowed for the elimination of some affects that can be experienced when rotation, such as Taylor vortices.

2.4.1.4. Pressure Loss in Non-Newtonian Flow

During drilling operations, drilled cuttings are transported by the drilling fluids by the act of hydraulic transport. When considering pressure-drop due to frictional flow, it is important to note that there are 2 categories. One category consists of the fine, more evenly dispersed

particles (low gravity solids), and the second category consists of larger, more dense particles (high gravity solids) (Chhabra & Richardson, 2008). Eccentricity also has a large effect on expected pressure loss due to friction in a wellbore, wherein a higher eccentricity results in lower friction loss. This differential is more significant in Newtonian fluids; however, it is still noticeable in non-Newtonian flow in an annulus.

2.4.1.4.1. Eccentricity calculations

When determining friction loss in an annulus, wellbore eccentricity corrections must first be determined. This equation is given by (23), wherein r_w is the radius of the annulus, r_p is the radius of the drill pipe (nominal), and δr_e is the difference between the center of the wellbore and the center of the drill pipe (degree of eccentricity).

$$Ne = \frac{\delta r_e}{r_w - r_p} \quad (23)$$

Utilizing the power law model (7), C_e (eccentricity correction factor (24)) for laminar flow is determined by using methods by Uner et al. (1989), wherein the flow rate is given by a series of equations (25)(26)(27)(28) (Mitchell & Miska, 2011).

$$C_e = (1 - R_r)^{n+1} \times \left[\frac{2E(\lambda) - \pi R_r}{F(\lambda, n, R_r)} \right]^n \quad (24)$$

$$\lambda = \delta r \frac{(1 - R_r)}{r_w - r_p} \quad (25)$$

$$E(\lambda) = \int_0^{\pi/2} \sqrt{1 - \lambda^2 \sin^2 \xi} d\xi \quad (26)$$

$$F(\lambda, n, R_r) = \int_0^\pi (\sqrt{1 - \lambda^2 \sin^2 \xi} + \lambda \cos \xi - R_r)^{2+1/n} d\xi \quad (27)$$

$$q_c = \frac{\pi r_w^3}{2} \frac{n}{2n+1} \left| \frac{dp_f}{ds} \frac{r_w}{2m} \right| \frac{(1 - R_r^2)}{(2E(\lambda) - \pi R_r)} F(\lambda, n, R_r) \quad (28)$$

Concentric pressure loss gradients can be determined through a varied equation (29) by utilizing the fanning friction factor (30) calculated from the power-law annular Reynolds number (for laminar flow, (31)), as well as fluid density and velocity. This pressure gradient technique can then be applied with the eccentricity correction factor (variation, (32)) to solve for the eccentric pressure gradient.

$$\left(\frac{dp_f}{ds} \right)_c = \frac{\rho v^2 f}{10^5 (D_a D_{dp})} \quad (29)$$

$$f = 24/N_{Re} \quad (30)$$

$$N_{Re} = \frac{(D_a - D_{dp})^n \times v^{2-n} \rho}{8^{n-1} \left[\frac{3n+1}{4n} \right]^{nm}} \quad (31)$$

$$C_e = \frac{\left(\frac{dp_f}{ds} \right)_e}{\left(\frac{dp_f}{ds} \right)_c} \quad (32)$$

This eccentric pressure gradient can then be applied along the length of an annulus (or test section) to determine expected pressure losses.

2.4.1.4.2. Slurry/Cuttings Transport and Pressure Loss

Although pressure losses can be determined through calculations in the previous section regarding the flow of non-Newtonian fluids, these equations do not consider variable concentrations of solids. Utilizing the force balance equation procedure, one can roughly determine the frictional pressure loss depending on cuttings density and concentration (33). In this equation, the frictional pressure loss (f_L) is based on hydraulic pressure gradients (i and i_L), volumetric concentrations of cuttings ' C ', annulus diameter ' D ', gravitational constant ' g ', velocity ' V ', the solid/fluid density ratio ' s '(34), and an experimental constant ' k_2 '.

$$f_L \frac{(i - i_L)}{i_L} = k_2 \frac{gDC(s - 1)}{V^2} \quad (33)$$

$$s = \rho_s / \rho_L \quad (34)$$

These equations are based off experimental data, however (given k_2 is an experimentally determined constant) and consider that the majority of cuttings are located on the bottom of the annulus, forming a cuttings bed. They do not determine the expected pressure losses of cuttings that are suspended in flow, and no repeatable correlated data has been gathered to validate any solutions to this pressure loss (Chhabra & Richardson, 2008).

2.4.1.5. Non-Newtonian Annulus Flow Modeling

Given the complexity of non-Newtonian fluid modeling summarized in the previous sections, powerful mathematical models are required to accurately predict flow in such complex

environments. Computational Fluid Dynamics modeling software is often used to adequately perform the immense level of differential calculations required when variables such as inner pipe rotation, eccentricity, varied solid drill cuttings size/concentration are considered. Thousands of iterations are often required to reach adequate convergence, and often must be performed repeatedly in transient simulations when incrementally small (0.0001 second) time-steps are considered. For the design and implementation of this flow loop, ANSYS Fluent was utilized to determine optimal inlet and outlet parameters to ensure a test section that is not affected by end effects or developing flows. Several inlet and outlet parameters will be tested in order to determine optimal flow conditions and distance to stabilized flow. When entering drilling fluid parameters into ANSYS Fluent software, the ideal calculation method will be the Hershel-Buckley, most closely models the behavior of non-Newtonian drilling fluid. The Hershel-Buckley Model is the API recommended model for drilling fluid rheological models. This model most accurately describes most drilling fluids, includes a yield stress value important for drilling hydraulics, and includes Bingham plastic and power law models as special cases (API, 2009). API RP 13D outlines drilling fluid rheology and hydraulics recommended practices. This implementation will be further discussed in the methods section.

2.4.1.6. Empirical Correlations

Although not exclusively mathematical, one method that many researchers have used to aid in the understanding of cuttings transport is through empirical correlations. This involves performing a series of tests, and determining a correlation based on varying parameters. By conducting over 700 tests on TUDRP's 5-inch flow loop, Larsen was able to develop a correlation to determine the critical deposition velocity (CDV) that would allow for no cuttings accumulation (Larsen, 1990). Larsen's studies, which were performed at angles ranging from 50°

to 90°, confirmed that at high angles, turbulent regimes are preferred for cuttings transport (Pilehvari et al., 1999).

This empirical correlation was further expanded by Jalukar in 1992 through his extensive work on an 8-inch flow loop. These models are the most commonly used correlations in today's industry, offering a good range for expected CDV based on wellbore angle (F Zhang, 2015).

The most significant downfall in empirical correlations is that they are confined to the test parameters they were developed in. In the cases of Jalukar and Larsen, although they are the most commonly used correlations in today's industry, they are bound by the properties and parameters used. Many of these flow loops, such as the TUDRP's 8-inch Low Pressure Ambient Temperature (LPAT) flow loop, are restricted to parameters such as temperature and pressure. In order to more accurately simulate downhole conditions for cuttings carrying capacity simulations, more accurate pressure and temperature parameters must be included. In the case of these correlations, Larsen's model can be used to determine the minimum flow rate required to remove cuttings, but is often used in conjunction with other models, such as Moore's slip velocity of cuttings in vertical annulus (35). In this equation, g is gravitational acceleration (m/s^2), d_s is the particle diameter, ρ_s and ρ_f represent solid density and fluid density (kg/m^3). f represents the friction factor, based off the determined Reynolds number Re . It is important to note that Larsen's empirical correlations do not apply to larger wellbores and does not adequately cover cuttings transport in large diameter wellbores.

$$V_{sl} = \frac{2}{3} \sqrt{\frac{3gd_s(\rho_s - \rho_f)}{f\rho_f}} \quad (35)$$

2.4.1.7. Critical Cuttings Transport Velocity Model

A common model for measuring cuttings transport is the minimum transport velocity model. Critical velocity (or critical flow) is the minimum annular average fluid velocity that would prevent the accumulation of cuttings on the wellbore floor, in the form of a cuttings bed (Mitchell & Miska, 2011). If this velocity can be determined, it is often possible for a rig to achieve this flow rate and eliminate the development of cuttings beds. This velocity must account for all acting forces on a drill cutting (Figure 3) and must be high enough to overcome them. This is a much more simplistic model than the Layer, transient or Computational Fluid Dynamics (CFD) model, which can be iterative in nature.

The Critical transport fluid velocity is the sum of the slip velocity and the cuttings travel velocity (36). In his 1993 study, Larsen defined cuttings traveling velocity V_c as a rate independent of the fluid flow, V_{fluid} , and V_{cpipe} as the fluid velocity minus particle slip velocity V_{sl} . In order to apply his CTFV equation, V_{cpipe} had to be equal or greater than V_c , to flush the cutting effectively.

$$CTFV = V_c + V_{sl} \quad (36)$$

Larsen also assumed that the cuttings slip velocity, V_s (54), was the representation of 4 individual terms multiplied (37). V_μ is a particle slip velocity term dependent on viscosity and derived from averaging data from 4 angles using large cuttings in unweighted drilling mud. C_{ang} , C_{size} , and C_{mwt} are all factors of change that are based on the experimental parameters that were used with respect to the V_μ variables. They describe change from pipe/wellbore angle from vertical (C_{ang}), change from cuttings size (C_{size}), and change from fluid density/mud weight (C_{mwt}) (Petersen, 2015).

$$V_{sl} = V_{\mu} \times C_{ang} \times C_{size} \times C_{mwt} \quad (37)$$

Larsen performed a large number of tests with seven drilling fluids, and developed a strong correlation, and was able to use these measurements to construct simple correlations to aid in determining minimum flow rates dependent on drilling fluid (Larsen, 1990).

Unfortunately, this method of determining ideal flow rates for cuttings transport has many issues. The CTFV model design is a theoretical system, which deals with ideal parameters such as Newtonian fluids which have a linear shear rate. Drilling fluids are generally Non-Newtonian, which may cause inaccuracies in correlation. This becomes significant in the consideration of interparticle forces, which are affected by several factors like pH, particle size/shape and ionic strength, that make drilling fluids act considerably different from Newtonian fluids (Poloski et al., 2009). With cuttings modeling it is much more difficult to account for realistic behavior and parameters in wellbores. Although collisions between particles/cuttings do not pose significant concern while being carried, these impacts can cause significant changes on initial movement of packed cuttings beds. The critical velocity model also bases cuttings size on spherical diameter, when cuttings are often oblong or obtuse in shape (F Zhang, 2015). The CTFV model also considers all particles to be of one size, when in reality, drill cuttings can range significantly in size, and can change as they travel up the wellbore (Doron & Barnea, 1993). Another significant issue with this model is its design to eliminate cuttings beds completely, through flow rate. In many extended reach operations, using the calculated flow rate to eliminate cuttings beds is not possible, often due to formation constraints (Feifei Zhang et al., 2017).

2.4.1.8. Layer Model

Layer modeling is based on the existence of multiple layers in a flow and can be applied to both steady state and transient cuttings transport applications. Although both two and three-layer models were first used to describe slurry transport (K. C. Wilson, 1970), Tomren identified similar acting layers in deviated wellbores by identifying 3 distinct layers (stationary bed, sliding bed, and heterogeneous suspension) (F Zhang, 2015).

Several researchers since have developed variations of both two and three-layer models and can vary from steady-state to transient. Steady-state models, like the one Nguyen presented, assumes no slip between the solid and fluid phases, which will affect the material balance equations (Nguyen & Rahman, 1998). He describes different variations of three-phase flow that changes as flow rates increase and turbulent eddies begin to develop. As the flow rate nears CTFV, the flow becomes a two-phase flow of dispersed and heterogeneous layer. At maximum required flow rate (CTFV), the model becomes a single-phase, as all cuttings are transported and there is no longer a need to model a cuttings bed. Figure 12 shows how this three-layer model is portrayed, and Figure 13 shows a two-layer model. Note that in both models, the gray layer is the uniform cutting bed, which can be either stationary, or in movement.

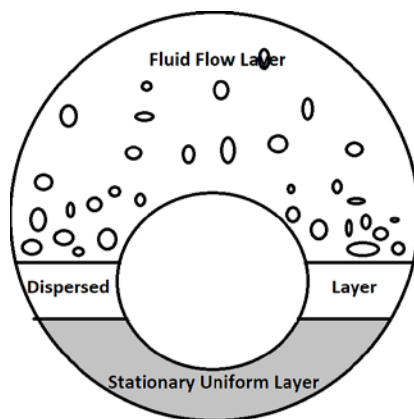


Figure 12: Three-phase flow model

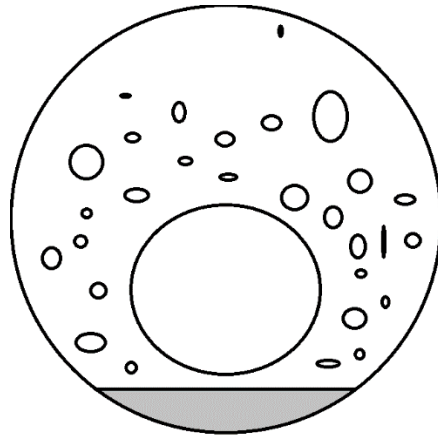


Figure 13: Two-phase flow model

Layer model equations are governed by the conservation of mass and momentum on each layer, and therefore there are differing results between steady-state calculations and transient calculations. One issue with utilizing steady-state layer modeling arises in that these models generally obtain a critical flow rate for only one well section, that has a constant hole geometry (Naganawa & Nomura, 2006). This is obviously a problem, as wellbores are often not uniform like pipe, and must be modeled differently. By utilizing transient modeling techniques with a two-layer model, Martins et al. was able to include the effects of hole instabilities, using finite volumes and a staggered mesh velocity and pressure model. This created a system of 4 differential equations (38) that are solvable for 4 unknowns; A_s/A_t ratio (α) which is the suspension area over total area, pressure (P), Suspended cuttings velocity (U_s) and cuttings bed velocity (U_b) (Martins, Santana, Gaspari, & Campos, 1998).

$$\begin{aligned}
& \frac{(1-\alpha)_{i+\frac{1}{2}}^{k+1} - (1-\alpha)_{i+\frac{1}{2}}^k}{\Delta t} + \frac{(1-\alpha)_{i+\frac{1}{2}}^{k+1} U_{Bi+1}^{k+1} - (1-\alpha)_{i+\frac{1}{2}}^k U_{Bi}^{k+1}}{\Delta x} = \frac{1}{C_B} \int_i^k \frac{G}{A_\tau} \\
& (1-\alpha)_i^{k+1} (U_{Si}^{k+1} - U_i^{k+1}) + \frac{q_T}{A_T} - U_{Si}^{k+1} = 0 \\
& \frac{U_{Bi}^{k+1} - U_{Bi}^k}{\Delta t} = -U_B \frac{\partial U_B}{\partial x} \Big|_i^k - \frac{1}{\rho_B} \left(\frac{P_{i+\frac{1}{2}}^{k+1} - P_{i-\frac{1}{2}}^{k+1}}{\Delta x} \right) - \frac{F}{A_B \rho_B} \Big|_i^k - \frac{U_B}{A_B C_B} G \Big|_i^k - \frac{\tau_B S_B}{A_B \rho_B} \Big|_i^k \\
& \quad + \frac{\tau_i S_i}{A_B \rho_B} \Big|_i^k \\
& \left(\frac{1}{\Delta t} + 2 \frac{f_B S_B}{A_B \rho_B} \Big|_i^k \right) U_{Li}^{k+1} \\
& = \left(-U_B \frac{\partial U_B}{\partial x} + \frac{\tau_B S_B}{A_B \rho_B} + \frac{\tau_i S_i}{A_B \rho_B} - g \cos \theta + \frac{U_B}{\Delta t} \Big|_i^k - \frac{1}{\rho_B \nu g_B} \Big|_i^k \frac{\partial P}{\partial x} \Big|_i^{k+1} \right)
\end{aligned} \tag{8)$$

Significant research has been done on cuttings movement using layer modeling by many researchers (Doan et al., 2003; Martins et al., 1998; Nguyen & Rahman, 1998; Song et al., 2010). Layer modeling better captures the physics and behavior of cuttings transport than the critical velocity model and has shown to be more versatile than empirical correlations. However, these complex derivatives with many unknowns also lead to convergence factors, sometimes resulting in multiple answers or none at all (F Zhang, 2015). Layer models are often better suited for pipeline slurry flow, particularly in steady-state calculations, as pipe diameter is constant. Transient layer modeling does have a better application in open hole wellbores, as it does account for hole irregularities, however the uncertainty of convergence makes this method less than ideal.

2.4.1.9. Computational Fluid Dynamics Modeling

With the increase in computing power, and the development of computational fluid dynamics programs on a commercial scale, the technology has begun to be used to study cuttings

transport in vertical and deviated wells. Bilgesu et al. was one of the first researchers to identify CFD as a viable simulation technique in studying cuttings transport through experimentation on a flow loop (H I Bilgesu, Ali, Aminian, & Ameri, 2002). These initial studies were performed with steady-state models utilizing both Newtonian and Non-Newtonian (power law) flow regimes, at various angles, and saw successful results by comparison to other models in the past on flow rate and cuttings transport efficiency. A second study performed in 2007 by Bilgesu et al. continued to run CFD simulations, testing the effects of additional parameters such as fluid velocity, cuttings size, and drill pipe rotation in addition to inclination angle. This research did not take into consideration variable diameter wellbores and drill string, however, and did not simulate large diameter wellbores, where field results have shown significant changes at the 120 and 180 RPM range.

CFD modeling generally utilizes one of two approaches for cuttings transport simulation based off the Eulerian method. The Eulerian-Eulerian model is also described as inhomogeneous, in that both the continuous (drilling mud) and dispersed (cuttings) phases are treated as continuous (Ofei, Irawan, & Pao, 2014).

The Eulerian-Lagrangian method uses the Eulerian method to describe the continuous fluid phase; however, the Lagrangian field is used to describe cuttings trajectories through either one-way coupling (low cuttings concentration) or two-way coupling (high cutting concentration) (F Zhang, 2015). This method is more commonly used in many engineering methods than the Eulerian-Eulerian method, but it does have several significant drawbacks. The Lagrangian particle is not designed to handle high solid volume fractions like the Eulerian method, and it does not account for solid particle to particle interaction with automatic turbulence inclusion (Ofei et al., 2014). The Lagrangian method is also severely limited by its sensitivity to

numerical grid resolution, with is reflected in other areas such as heat transfer, momentum exchange, etc. (Vujanović, Petranović, Edelbauer, & Duić, 2016). Given the challenges faced with modeling a large diameter wellbore (12.25-inch), and larger concentration of cuttings ($\geq 30\%$), the Eulerian-Eulerian method is the optimal method. The Lagrangian method would have difficulties handling this concentration.

Ultimately, CFD has proven to be a very useful tool in modeling cuttings flow in wellbores of various angles. Commercial CFD software can be extremely beneficial in aiding drilling engineers to troubleshoot annulus problems, with a higher degree of flexibility. With increasingly powerful computers being more readily available, CFD simulations are becoming more and more capable, while being able to handle more variables. Although this process can be time consuming, powerful hardware can allow for a more accurate modeling of cuttings movement.

2.4.2. Experimentation

Many horizontal and variable inclination flow loops have been designed and developed since the 1970's. Often funded by large oil and gas companies driven to gain a better understanding of cuttings transport, these flow loops have a wide array of parameters, and are located all over the world. These flow loops have been used for many experiments, and are often being modified to fit specific needs (Ford et al., 1990; Loureiro et al., 2004; Tomren et al., 1986). Table 1 displays current flow loops in use today and their dimensions. Further information (i.e. source) for each flow loop can be found in 8.3, however this list, displayed in Table I, was compiled by Li and Luft in a 2014 summary report (Li & Luft, 2014). It must be noted, that most of the flow loops being used today can only perform low pressure, ambient temperature (LPAT) testing. Although to simulate cuttings transport in a wellbore, primary factors involve pipe

diameter, flow rate and mud rheology, temperature and pressure can play a key role. There are currently only 2 flow loops in use today that are capable of providing HPHT simulations, and these are the 5.76 inch diameter flow loop at the University of Tulsa (Zhou et al., 2004) and the 6 inch diameter flow loop at the South West Petroleum University of China (Li & Luft, 2014). Almost all flow loops, however, are capable of having an internal drill string to simulate rotation and flow around the pipe, and some, such as Continental Oil's flow loop, has various casing string sizes ranging from 6, 8, 10 and 12 inches, and is capable of having various drill strings ranging from 3.5 to 5 inches (Thomas R Sifferman et al., 1973).

Table I: List of flow loops and their dimensions (Li & Luft, 2014)

Name	Specifications		
	Diameter (inch)	Inner Pipe Diameter (inch)	Length (feet)
BHI flow loop	5	2.375	20
BP flow loop	8	5	50
Continental Oil Co. flow loop	12/8	3.5,5/4	140
Halliburton flow loop	7	1.75	30
Heriot-Watt University flow loop	5.4	3.5	21
Institute Français du Petrole flow loop	10.625	5	16
Japan National lab flow loop	5	2	30
Middle East Technology University flow loop	2.91	1.85	21
M-I drilling fluids flow loop	4	1.9	15
Mobil flow loop	8	4.5	60
Norwegian University of Science and Technology flow loop	2.15	n/a	20
Petrobas flow loop	5	2.5	40
Rice University	8.125	4.5	60
Schlumberger	7	3.5	
Southwest Petroleum University, China HPHT flow loop	6	2.5	120
University of Alberta flow loop	3.75	1.5	30
China University of Petroleum, Beijing, flow loop	4	1.5	13
University of Tulsa- LPAT flow loop	8	4.5	100
University of Tulsa- HPHT flow loop	5.76	3.5	73
University of Tulsa- Small	2	1	12
University of Oklahoma indoor flow loop	5	2.375	20

Experimental flow loop design often incorporates variable inclination settings, such as the University of Tulsa's LPAT and advanced cuttings transport flow loop (ACTF), which can operate within a range of 0-90°. Instrumentation can range from basic mass flowmeters and gamma ray densitometers (T R Sifferman & Becker, 1992), to more complex instrumentation much like the ACTF, which contains nuclear densitometers, pressure and pressure transmitters and an air expansion tank.

Experimental studies have been used to develop and reinforce mathematical models. As cuttings transport is transient in nature, complicated mathematical models are generally small scale, and must be validated through experimentation. One study developed a 2 layer, 1 dimensional model for cuttings transport in underbalanced drilling, that considered cuttings transport as a 2-phase, solid/liquid flow (Doan et al., 2003). This model consisted of many parameters that needed to be determined through flow loop experiments, such as annulus friction factor and cuttings deposition rate. Studies were performed on the Cuttings Transport Flow Loop System (CTFLS) at the University of Tulsa, and data recovered allowed the cuttings model to be developed into a more accurate computer simulator for underbalanced drilling operations (Naganawa, Sato, & Ishikawa, 2014).

This study, along with many others, have allowed researchers to gain a better understanding of the significant role specific parameters have on the effectiveness of hole cleaning. Early studies did not consider the dynamic behavior of drill pipe rotation in downhole situations, and as such pipe was only spun on its axis (Sanchez et al., 1997). Newer flow loops are long enough and designed to recreate more realistic conditions, such as vibration and orbital whirling rotation.

Another advantage to flow loop design is to understand cuttings bed erosion and development. Khan performed a study in 2008 utilizing the University of Tulsa's LPAT and small flow loops to develop a model for cuttings bed erosion, based on transient cuttings modeling and experimentation (Khan, 2008). Although the study concluded that current modeling techniques are adequate for practical applications, it is further proof that the use of experimental flow loops are critical in confirming mathematical modeling and computer simulation techniques.

The wide design spread of these flow loops around the world all have been used to aid in the better understanding of cuttings transport and flow regimes in various wellbore deviations and sizes. Unfortunately, none of these flow loops are significantly sized or powered to perform analysis on cuttings transport changes that occur due to pipe rotation at approximately 120 and 180 RPM. Models such as the Continental Oil flow loop has a large pipe to hole area ratio (P-HAR), but it is a vertical flow loop. Other models have short test areas, or do not realistically recreate downhole well dimensions (wellbore size, drill string), making it impossible to recreate actual downhole conditions. Although rotating capability of many of these flow loops does exceed 120 RPM, studies nearing 200 RPM are not often performed (as this RPM range is often unrealistic in-field practice due to downhole equipment limits). A flow loop that accurately recreates large diameter wellbore conditions does not currently exist.

It has been observed that in these two RPM ranges (120, 180), cuttings carrying capacity increases dramatically before returning to a linear increase, although documentation of this phenomenon is not widely discussed, the step change was recognized in a Statfjord ERD well (Alfsen, Blikra, & Tjotta, 1995b). Unfortunately, other supporting documentation is not available that discusses or observes this phenomenon, and more research must be done to

confirm this effect. No flow loop is large enough to recreate these parameters in order to observe the cause of this step change presently.

2.5. Literature Review Conclusion and Recommendations

The evolution of Extended Reach Drilling has grown substantially since its initial definition. From step-outs of 5,000ft (1500m), to the world-record 49,213ft (15,000m) measured depth wells Orlan well in Northern Russia, Extended reach has grown substantially over the last 30 years. This growth has been driven by the need to produce more and more difficult to access reservoirs at a more economical rate. With the drive to access more reservoir from a single well through extended reach, operators have encountered many constraints that have pushed the limits of technology. The broad expanse of mechanical and formation related constraints have forced engineers to develop new technology and focus more energy and time into successful modeling.

Accurate modeling of torque and drag due to factors such cuttings concentration and extended reach are critical factors in assuring wells reach their intended target depth, and cuttings transport is one of the most significant constraints encountered. Only through experimental design, simulations and mathematical modeling can cuttings transport be not only understood but optimized.

Due to the ever-increasing demand for economical production, coupled with the drive to minimize environmental impact, studies must continue to find ways to better understand and optimize cuttings transport. There are currently no flow loops in existence that are specifically designed to attempt to reproduce the increases in cuttings transport efficiency in large diameter hole. The design and implementation of a large diameter horizontal flow loop that can operate with drill string rotation in excess of 180 RPM will aid in gaining a better understanding of these efficiency increases in cuttings transport that occurs around 120 and 180 RPM. This flow loop

design must incorporate sophisticated visualization and recording equipment to truly capture the flow of cuttings under various conditions.

In order to properly design this flow loop, a CFD model must first be constructed to determine optimal flow parameters (end-effects from inlet and outlet of test section). These values are critical for sizing the complete system. Once the CFD model has been constructed, the complete design and construction of the flow loop can be completed. Upon completion of the flow loop, a range of experiments can then be performed to validate the CFD model, and can then be used to develop working correlations, and real-world prediction and wellbore modeling.

The goal of this flow loop is to successfully recreate the increase in cuttings transport efficiency at both 120 and 180 RPM ranges. If this step change is better understood, it may allow for the development of new technology that can replicate this effect without the need for extremely high RPM, which is often not possible due to torque or vibration limitations.

3. Procedure and Methodology

There is currently no flow loop in operation that is capable of recreating horizontal cuttings transport in a large diameter (P-HAR greater than 3.25, (39)) wellbore with the influence of high RPM drill string rotation. Because of this, the sudden increase in cuttings transport efficiency under these conditions (P-HAR >3.25, RPM 120/180) has never been successfully recreated or studied in a controlled environment. In order to attempt to recreate this phenomenon, a purpose-built flow loop must be designed. The following section will discuss in detail the methods used to properly size this flow loop, as well as outline all components of the system.

$$P - HAR = \frac{R_H^2}{R_p^2} \quad (39)$$

3.1. Problem Identification

Prior to developing a flow loop design, a complete review of Extended Reach Drilling (ERD) was completed. This Literature review consists of the current state of ERD, what constraints are encountered in ER operations, a detailed study on cuttings transport at all inclinations, and a thorough explanation on the difficulties of modeling non-Newtonian flow. It identifies the problems associated with cuttings transport in extended reach operations and highlights the notion that drill string rotation has an important effect on cuttings transport. Further, this literature review identifies a lack of understanding in the observed step-change in cuttings transport efficiency around 120 and 180 RPM and shows that no flow loop currently in use can effectively recreate this condition for the study of this phenomenon.

3.1.1. CFD Modeling

In conclusion of the literature review, a series of detailed CFD modeling experiments were identified to mathematically model multiphase flow on a small scale. After evaluating a selection of CFD software packages, ANSYS Fluent was chosen, due to its ability to model complex multiphase flows with non-Newtonian fluid. Montana Tech already maintains several ANSYS academic licenses, which allowed for the use of a trial license of Fluent, resulting in no additional costs associated with purchase of new licenses.

3.1.1.1. Model Geometry

Prior to performing CFD simulations, both to validate existing flow loop experiments and horizontal flow loop modeling, proper geometric models were built. ANSYS Spaceclaim and DesignModeler were used to build the flow loop geometries. A detailed manual for designing basic geometric models can be found in 7.6. These flow loop designs are rudimentary, with the sole function of modeling flow. Due to these specifications, additional equipment such as flanges, bolts, fasteners and seals were not included. The results are basic solid hollow tubes, with fluid volume interiors.

The 2-inch ID vertical on-campus flow loop has pressure transducers located 42 feet apart. These dimensions were used to model the basic geometry. Inlet and outlet boundaries were identified as named selections for boundary condition initialization within the modeling software. P&ID of this geometric model can be found in 7.8.

ANSYS software allows for rigid body rotation during CFD analysis, and basic drill string designs are solid tubes, with no interior flow. Several models were created with different drill string locations to simulate varied eccentricity (Figure 14, page 90), as well as multiple drill string sizes. For determination of flow normalization within the horizontal flow loop, minimum

flow loop length was set to 40 feet from the inlet and outlet. P&ID's of these geometric models can be found in 7.9.

3.1.1.2. Meshing

Once geometric models were designed, the model was properly meshed for CFD modeling. ANSYS has meshing software that takes geometric models from Spaceclaim and DesignModeler, as well as from third-party software such as Solidworks. The internal software will often optimize the mesh dependent on the application (CFD, mechanical, electric), but must often be selected manually. Mesh size and type are very important parameters when developing a mesh for a geometry. A fine grid mesh may be more accurate but comes with the cost of much more calculation time. For simple flow CFD models, a coarse mesh may achieve the same accurate results as a fine mesh, in much less calculation time. When modeling 2-phase flow, a more refined grid required for adequate accuracy, particularly in liquid/gas models where gas expansion is a potential, or liquid/solid flow in an environment such as the horizontal flow loop. ANSYS Fluent utilizes orthogonal quality to determine the quality of a mesh, with values ranging from 0 (bad quality) to 1 (good quality). Fluent recommends having a minimal orthogonal quality of 0.01, with a significantly higher average orthogonal quality to ensure a more accurate model. Orthogonal quality is a means of determining cell quality. It is computed for individual cells by using the vector from the cell centroid to each of its faces, the corresponding face area vector, and the vector from the cell centroid to the centroids of each of the adjacent cells. Details on mesh quality of all inlet designs can be found in 7.10. It is important to note that the outlet model design is identical to the 8-inch, 90° inlet mesh, and all parameters are identical. Inlet and outlet mesh designs were inflated (more cell zones) for

increased accuracy. Vertical flow loop meshing details can be found in 7.11, and the final test section mesh details can be found in 7.12

3.1.1.3. Preprocessing - Setting up Domain

Once all of the geometric models were created and properly meshed, ANSYS Fluent requires basic domain development. During this process, mesh quality can be checked, improved, and converted to polyhedral if preferred. Within the domain setup, zones can be manipulated, separated or joined. This step is important, as models often need inlet and outlet boundaries to be manually separated. Additionally, in models with both solid and fluid geometries, interfaces must be created and assigned. These interfaces include casing wall/fluid interfaces, and drill pipe/fluid interfaces, and must be created to prevent mesh-check errors due to overlap.

3.1.1.4. Preprocessing - Setting up Physics

During preprocessing and in conjunction with setting up the domain, the simulations physics were set up. These include factors such as operating conditions (temperature, pressure, gravity, pressure reference points), material types (solid, liquid), and flow physics (energy, multiphase, discrete (injection) phase, heat transfer, etc.). Additionally, solver settings can be adjusted to be either pressure or density-based. Simulations can be run as steady-state or transient, with the ability to manipulate time steps and step-sizes. This is an important feature for post-processing, as transient time calculations are required for solution animations. Phases can also be viewed and edited within this tab.

These parameters are critical to ensure the most accurate simulations are run, and care must be taken to ensure operating conditions and fluid/solid properties are correct. At the

location of the proposed flow loop, as well as the vertical 2-inch flow loop, ambient temperature is 68°F and atmospheric pressure of 11.95 psi.

An important factor to note is that Fluent uses a modified pressure value P' (40) when calculating, which only calculates the difference in pressure, not change in hydrostatic head. This is based on knowing that there will always be a pressure field that can be easily determined through ρgy , where ' ρ ' is the fluid density, ' g ' is gravity and ' y ' is the y-axis length.

$$P' = P - \rho_0 gy \quad (40)$$

Within the setting up physics tab, cell zones can be identified, as well as boundary conditions identified. All CFD models were designed to implement a velocity inlet (calculated from given flow rates and pipe ID), and pressure outlets with predetermined outlet pressures. These boundaries can be modified and set from the boundary conditions task page, or by individual manipulation within the outline tree. If no specific boundary conditions were required for a face, boundaries were set to the default operating conditions.

Clean, uncontaminated water is used in the vertical flow loop, so no adverse fluid property modifications were required. Gas injection in the flow loop is dry air, and not an inert gas such as nitrogen. However, for horizontal flow loop simulations, fluid properties are more complex non-Newtonian fluids that must be modeled appropriately. A range of drilling fluid models were designed for optimizing inlets and outlets and determining minimum length for flow stabilization. 6 drilling fluid models were developed and implemented in Fluent using the Hershel-Buckley (14) method for non-Newtonian fluid flow, with the addition of cement for an extreme viscosity calculation. Table II shows the τ_y (55), n (56) and k (57) values used for modeling. 7.7 shows a summary of drilling fluid data used for the simulation models. These fluid models were run in comparison with a baseline of fresh water.

Table II: Drilling Mud Properties

Description	Density (ppg)	τ_y	n	K (lb/ft ² *s ⁿ)
Freshwater	8.45	0.00	1	0.00
Light WBM	9.00	9.38	0.71	0.28
Medium WBM	12.00	9.38	0.84	0.16
Light, thin OBM	9.50	3.75	0.75	0.25
Medium OBM	12.00	7.50	0.81	0.25
Heavy, thick OBM	16.00	12.20	0.81	0.37
Micronized barite OBM	12.00	1.88	0.83	0.18
Cement	16.00	6.57	0.95	0.52

3.1.1.5. User Defined Data

Within the User Defined tab, units can be manipulated and changed to output preferred units. If preferred units are not available, the program allows the input of a custom unit, based on a multiplication factor and optional offset. This is important, as ANSYS software performs all calculations in scientific notation, and these units are the default input and output.

3.1.1.6. Solving

The solving tab is where solving methods and controls are located. This is where the solution is initialized and run. Within the tab, solution methods can be determined from a range of options that Fluent offers. These methods are important and are based on the type of simulation being run. In single phase flow, the optimal method is SIMPLE, as it is good for the majority of routine incompressible flow calculations. However, the coupled method is referred to as a pressure-based solver, and should be used for compressible flow, flow where rotation is involved, and multiphase flows. When validating flow loop experiments, SIMPLE is used only for single phase calculations, and coupled is chosen for all other models.

Solution controls allow for the setting of under-relaxation factors, that help simplify the iterative process. When solution variables are updated after every iteration, only a fraction of the total change from the old value is applied. This fraction is the under-relaxation factor and can

stabilize the iterative process without affecting the outcome. These values will affect the number of iterations required, however, and can have adverse effects on run time.

Often, default settings are recommended, unless the gravity parameter is activated and natural convection is being determined. For this case, Fluent requires pressure discretization to be set to the PRESTO! Method or body force weighted option.

Within this tab, the initialization process is also performed. Fluent allows for 5 types of initialization methods, however, Hybrid initialization and standard are the most common. Hybrid is the default setting, and most recommended. However, FMC initialization is preferred for compressible flow and rotating machinery, which are 2 important scenarios that are being simulated.

3.1.1.7. Postprocessing and Results

Once solutions have been initialized and run until convergence or residual stability, vertical flow loop simulation data can be analyzed and compared to experimental data from the 6 previously recorded runs. ANSYS Fluent eliminates hydraulic head pressure loss from single phase calculations by default, so this must be manipulated within the software, or calculated manually and added post processing.

3.1.2. Experimental Data

In order to determine the accuracy of flow models within Fluent, several experimental runs were performed on the Montana Tech vertical two-inch ID flow loop. 3 separate single-phase runs were completed at volumetric water flow rates of 15 gallons per minute (gpm), 25 gpm and 35 gpm. In addition to single phase experiments, 3 multiphase runs were completed with air injection. These runs all held a steady water rate of 10 gpm, with 3 air injection rates of 15 standard cubic feet per minute (scfm), 35 scfm and 60 scfm. Validation of these models in

ANSYS Fluent is critical to ensure that the software is being properly used. Although fluid properties are different between the vertical on-campus flow loop (water, air) and the proposed horizontal flow loop (drilling fluid, solid cuttings), accurate flow modeling practices can be used to validate basic flow calculations for new models. 7.5 contains measured parameters from these tests; however, a summary of these flow experiments can be found in Table III.

Table III: Flow Loop Experiment Averages Summary

Run No.	Top Pressure (psi)	Bottom Pressure (psi)	Water Rate (gpm)	Air Rate (scfm)
1-phase 1	0	10.5	14.9	0
1-phase 2	0	11.2	24.8	0
1-phase 3	0	12.2	34.9	0
2-phase 1	1.8	6.8	9.9	14.5
2-phase 2	3.9	8.4	10.0	34.0
2-phase 3	6.6	10.7	9.6	58.5

3.1.3. Vertical Flow Loop Model

In order to properly validate experimental data from the vertical on-campus flow loop, a CDF model was created, based on the dimensions of the flow loop and the distance between pressure transducers. A 2-inch ID tube was designed with a total height of 42 feet. For the multiphase flow experimental validations, meshing was inflated to ensure accuracy. Given the simplicity of the single-phase run, no mesh inflation was necessary, as standard mesh is refined enough.

3.1.3.1. Simulation Design

Multiphase flow calculations require a significant amount more computing power and time to complete even short running simulations. Multiphase flow calculations are transient in nature, and appropriate timestep design is important in ensuring that iterations do not diverge and

offer accurate outcomes. The following section outlines the setup required for running multiphase flow.

3.1.3.1.1. Simulation Set-up

Multiphase flow is transient and complex in nature and must be approached differently than conventional steady state problems. For all the above flow rates, the following parameters were developed within Fluent.

Table IV: Fluent solver settings for multiphase flow

Solver	
Time	Transient
Type	Pressure-Based
Velocity Formulation	Absolute
Operating Conditions	
Operating Pressure	11.95 psi
Gravity	-32.2 ft/s ²
Operating Density	0.0765 lbm/ft ³

Table IV outlines the solver settings for all multiphase flow simulations. Operating conditions are based on actual values recorded at the vertical flow loop. When selecting the VOF model, the solver settings automatically default to transient time solving (steady is not possible).

Table V: Fluent model settings for multiphase flow

Models	
Multiphase	
Model	Volume of Fluid (VOF)
Number of Eulerian Phases	2
Formulation	Explicit
Volume Fraction Cutoff	1e-06 (Default)
Courant Number	0.25
Body Force Formulation	Implicit Body Force
Interface Modeling Type	Sharp
Viscous Model	
Model	k-epsilon (2 eqn)
k-epsilon model	Realizable
Near-Wall Treatment	Scalable Wall Functions
Model Constants	Default

Table V outlines the parameters for the multiphase and viscous properties for the simulation. The courant number is a dimensionless value (41)(Courant, Lewy, & Friedrichs, 1928) and must remain below 1 or the solution will grow as time continues. It is important to continuously observe the current courant number (output at the beginning of every timestep) to ensure it is still low.

$$Co = \alpha \frac{\Delta t}{\Delta x} \quad (41)$$

Table VI: Fluent phase settings for multiphase flow

Phases	
Air	Primary Phase
Water	Secondary Phase
Velocity Formulation	Absolute
Phase Interaction	
Surface Tension	
Surface Tension Force Modeling	Yes
Model	Continuum Surface Force
Adhesion Options	Wall Adhesion
Surface Tension Coefficients	Constant, 0.072

Table VII: Fluent boundary properties for multiphase flow

Zone Boundary Properties	
Pipe Outlet	Pressure Outlet (Pressure based on experimental data)
Water Inlet	
Phase	Mixture
Velocity Magnitude	0.981-1.017 ft/s Reference Frame - Absolute
Phase	Water
Volume Fraction	1 (Constant)
Air Inlet	
Phase	Mixture
Velocity Magnitude	12.5-45 ft/s
Phase	Water
Volume Fraction	0 (Constant)

Table VI and Table VII detail the phase assignments and properties for both the fluids used and inlets. The model used for multiphase flow is slightly different than the single phase,

and the design introduces a gas stream to the water stream through a second inlet. As such, volume fraction inputs are important (they must always be 0 or 1).

Some of the most important settings for multiphase flow to ensure proper modeling are the solution methods and initialization/calculation data. When performing multiphase flow calculations, the coupled method is the most effective for most scenarios. Many discretization calculations should be changed to second order, for a more accurate outcome (often this is recommended when “check case” is selected in Fluent).

When setting time steps and initializing any transient problem, it is important to ensure a small enough time step that will not cause solution divergence. A good method of checking the quality of the time step size is the courant number. Initial values should optimally be below 0.05, particularly early in the calculations. Most complications in calculation occur within the first few time steps, so ensuring a low courant number during this time is critical. All model simulations run began with courant numbers below 0.05. Table VIII outlines a summary of input parameters for the solution methods, as well as initialization and calculation settings.

Table VIII: Fluent solver settings for multiphase flow

Solution Methods	
Pressure-Velocity Coupling Scheme	Coupled
Spatial Discretization Gradient	Least Squares Cell Based
Spatial Discretization Pressure	PRESTO!
Spatial Discretization Momentum	Second Order Upwind
Spatial Discretization Volume Fraction	Geo-Reconstruct
Spatial Discretization Turbulent Kinetic Energy	Second Order Upwind
Spatial Discretization Turbulent Dissipation Rate	Second Order Upwind
Transient Formulation	First Order Implicit
Initialization & Calculation	
Initialization Method	Hybrid
Time Step Size	0.001 (Start Point)
No. of Time Steps	45,000 (Based on Initial Step Size, to allow water to flow from bottom to top of pipe)
Maximum Iterations per Time Step	20
Total Simulation Time	45 Seconds
Maximum Allowable Courant Number	0.25
Optimal Courant Range	0.02-0.09

Given the transient nature of these solutions, it is important that simulations be run so that the fluids entering at the inlets at the beginning of the simulation run exit the outlet. This will ensure that the flow has become uniform and complete throughout the solution. Given the minimum linear velocity of water in these multiphase simulations (~1.0 ft/s), and the distance from water inlet to outlet (45 ft.), the simulation must be run to a minimum of 45 seconds. Based on initial timestep value of 0.001 seconds, a minimum of 45,000 timesteps must occur.

This number can increase greatly if an increase in courant number is seen, or flow become more extreme. Higher flow rates (35 scfm, 60 scfm) will cause higher chance of divergence, and smaller timesteps are required. Average iterations per time step range from 10 to 40, requiring upwards of 1,800,000 iterative calculations based on initial time step values. This results in simulations lasting upwards of one week on a standalone machine.

3.1.4. Horizontal Flow Loop Model

The importance of software validation with experimental data is a critical step towards developing a robust model for the horizontal flow loop. This will allow for greater certainty when developing a model for the horizontal flow loop.

The design of the horizontal flow loop will require several stages of CFD modeling, prior to a final simulation set up for experimental validation.

3.1.4.1. Inlet and Outlet Design

These fluid models are used to determine optimal inlet and outlet angles (45° or 90°) for predetermined inlet and outlet ID. These CFD runs also determine when flow normalization occurs, allowing conclusive minimum length for the flow loop, based on flow properties. To ensure pipe eccentricity will not play an adverse role, the flow normalization simulations are also run at three eccentricities (Figure 14), once optimal angle has been determined. Upon completion of these flow simulations, the scenario requiring the longest length for normalization is modified with the largest expected drill string (5.875"), to ensure appropriate minimum length is determined.

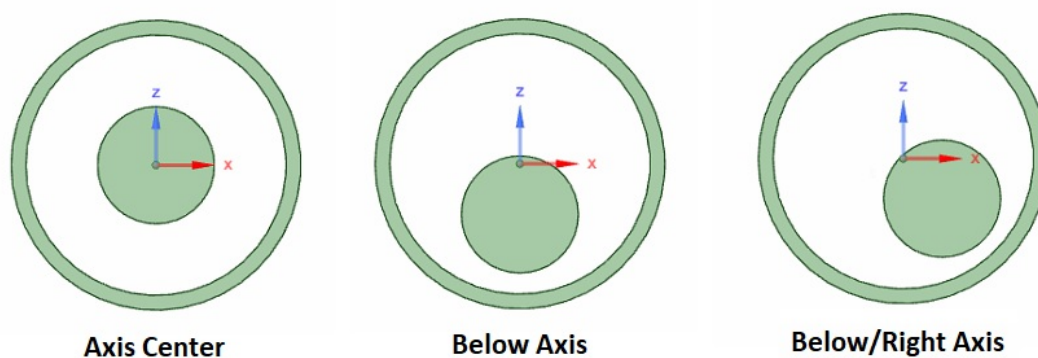


Figure 14: Eccentricity Test Run Locations

Flow visualizations will be combined with iso-surface pressure and velocity plots to identify normalized flow. As it is unlikely full flow normalization may occur with inner drill string rotation, the parameters for flow normalization from the inlet will be based on no irrational flow resulting in flow from the smaller inlet. End effects from the outlet at the end of the test section will be evaluated similarly.

3.1.4.2. Test Section Dimensions

Alongside fluid-based end-effects calculations, internal drill string selection and basic orbital motion analysis is considered as a secondary means for sizing minimal flow loop test section length. Utilizing results from end-effects calculations and drill pipe selection, an appropriate observation window is selected, where all visualization and analysis devices are located. During this evaluation, a high-level cost-benefit analysis is performed to outline the final length of the flow loop. This analysis is required to determine whether flow loop length will be based on flow normalization, or free pipe movement. This differentiation is important to determine whether the act of natural drill pipe eccentric motion based on RPM is a main driver in changes in cuttings efficiency, or if this eccentricity can be simulated by drill string inlet and outlet placement to recreate the same effects. Although the final CFD model design will host a rigid body of rotation, and will not include eccentric or orbital motion, it is an important characteristic to consider within the design.

Upon completion of inlet and outlet parameters, adequate test-section size is determined. These dimensions are utilized in appropriate sizing of power unit, pumping unit and fluid storage components.

3.1.4.3. Test Section Design

The final CFD model design will replicate the test observation window previously determined. This model will incorporate particle dispersion and rotating drill pipe parameters. 3 separate models will be designed, with various drill pipe locations, to test the effect of drill pipe location on cuttings transport under various RPM.

3.2. Flow Loop Design

3.2.1. Overview

The final flow loop design will consist of several components. The test section, power section, cuttings management, fluid management, data acquisition and monitoring systems and control systems. These components all require unique design parameters that are discussed in the following sections.

Given the size of the flow loop test section, and the high flow rates expected, the optimal design is a closed-loop test section that would circulate the same volume of fluid and cuttings continuously. Contrary to open-loop systems which separate the cuttings from the circulation fluid after leaving the test section, a closed-loop system will circulate the same volume of fluid and cuttings indefinitely until the test is complete, reducing experimental uncertainty. There are many benefits to this design, but a notable advantage is the ability to use markers within the circulation system for multiple circulations. Many systems introduce cuttings for a single circulation before being separated and transported to an injection tank for reintroduction at a given time.

3.2.1.1. Test Section

The closed-loop test section will consist of a pumping system, test section, return system, and drain. It is important that the pump chosen can produce annular velocity rates

ranging from 150 ft/min to 300 ft/min, while additionally being able to handle variable solid cuttings concentrations. It is expected that experimental conditions will contain upwards of 40% cuttings concentration within the test section, and the type and size of pump chosen must be able to properly handle a high solids concentration.

The test section will be a length of casing with the minimum ID of 12.25 inches. The length of this test section will be determined by the CFD model optimization of both inlet and outlet angles and sizes (3.1.4.1). The test section will also house a viewing window that will display a centralized tool joint, with a minimum of one half-length of drill pipe on each side of the connection for observation. Given the average length of a joint of drill pipe is 30 feet, minimum test-length will be 30 feet.

The test section will have the ability to house various sizes of drill pipe strings for testing, with a potential range of 4.5-inch OD drill pipe to 5.875-inch OD drill pipe. The drill string will be mounted on both ends of the flow loop test section in a manner that they can handle being rotated at high RPM's via the power section and can be anchored at different locations of the test section (Figure 14). Optimal design length of the test section will ensure that pipe sag due to length is not a considerable factor in drill string position within the test section, and experimental control of drill string position is maintained. The minimum length of the flow loop test section should also allow for some natural drill string eccentricity at higher rotations.

End caps for the test section will allow for drill pipe accommodation and rotation via bearing or seal assembly, as well as adjustability via one plane. This flange can be bolted in a variety of patterns to allow drill string position to be adjusted in both a horizontal and vertical manner.

The return system will connect to the test section inlet and outlet and will also contain the pump. This return system must be large enough to prevent plugging due to solids contamination and must also be designed to optimize pump operation if minimum head is required.

The return system will also have both inlets and outlets connecting to the fluid and cuttings management systems, allowing for cuttings separation and drainage.

3.2.1.2. Test Section Pump

Proper pump selection is a critical component to the operation of the flow loop. Several parameters must be considered during pump evaluations and will be discussed in detail in the following sections. The pump must be optimally sized to handle the flow rates expected, as well as ideally designed for the range of fluid properties expected.

There is a wide variety of pump types, and each design has its own optimal operating conditions. The following sections will outline the selection parameters and determine flow loop requirements for each.

3.2.1.2.1. Pump Selection Parameters

When selecting the correct pump, there are a list of factors that must be considered:

1. The nature of the fluid being pumped
2. Required capacity (volume flow rate)
3. Inlet (suction) and outlet (discharge) conditions
4. Total head on the pump
5. The type of system that the pump is delivering to
6. The type of power source powering the motor
7. Space, weight, and/or position limitations
8. Environmental conditions
9. Cost of pump purchase, installation, and operation
10. Governing codes and standards

3.2.1.2.2. Nature of Fluid

The flow loop will be designed to handle a moderately wide range of drilling fluids, from water-based drilling fluids that can have increased corrosive behavior, to synthetic based muds which can be damaging to seals. Additionally, these fluids will be a calculated range of densities and viscosities, all dependent on experimental procedures.

One of the most critical factors of the nature of the fluid being pumped is its contamination factor. Given the nature of the flow loop, and its closed-loop experiment design, it is expected that cuttings will be a phase of the fluid being pumped at any given time. This means that any pump design chosen must be able to handle a variation of solid cuttings concentrations (0-50%) reliably. This will adversely affect the density and flow properties and is

a crucial consideration in pump design. Additionally, the significant increase in risk of fouling, blockage, or premature wear can significantly decrease operating efficiency and pump life, leading to increased costs. Part of the pump selection process will be to determine whether cuttings will be injected prior to the main pump or supplemented into the flow stream by a secondary pump on the discharge line. Additional considerations that must be factored in at this point are ensuring that flow rates are adjusted to ensure test section flow is correct.

Table IX displays the expected range of fluid properties that will be encountered on this flow loop.

Table IX: Expected Fluid Property Ranges

Fluid Type	Water-Based	Diesel-Based	Synthetic-Based
Density Range (ppg)	8.3 - 16	6.9 - 16	7.2 - 16
Dynamic Viscosity (cP)	1-30	14-30	1-30
Solids Contamination (%)	0-50	0-50	0-50

3.2.1.2.3. Required Capacity

In drilling operations, flow rate is a critical component to cuttings transport. Particularly in high inclination, big hole conditions ($P\text{-HAR} > 3.25$), annular velocity is expected to be above 200 ft/min. However, in some cases, 150 ft/min can be considered as a minimum for efficient hole cleaning. Any rate below this can potentially lead to hole cleaning problems and barite sag. Volume flow rate is calculated using (42). When calculating expected volume flow rate for the pump, the largest area within the flow range must be used.

$$\text{Fluid Velocity} \times \text{Flow Area} = \text{Volume Flow Rate} \quad (42)$$

The ID of the flow loop test section is designed to be 12.25 inches. Its internal flow area will be determined by the OD of the drill string installed, ranging from 4.5 inches to 5.875. The return section ID is 8 inches. These diameters are used to calculate minimum fluid velocities based on volumetric flow rates. Table X shows expected approximate fluid velocities calculated from flow rates ranging from 750 gpm to 1200 gpm in the flow loop test section, as well as the return section. It is critical that with the smallest expected diameter drill pipe installed, minimum fluid velocity still exceeds 200 ft/min to prevent significant cuttings bed accumulation. With 4.5-inch OD drill string installed, a 1200 gpm flow rate will exceed this requirement at 225 ft/min.

Table X: Flow Loop Test Section Flow Ranges

	800 gpm	1000 gpm	1200 gpm
12.25" Test Section Fluid Velocity (ft/min) (5.875" OD Drill Pipe)	170	210	250
12.25" Test Section Fluid Velocity (ft/min) (4.5" OD Drill Pipe)	151	190	225
8" Return Section Fluid Velocity (ft/min)	305	385	460

This table shows that the pump selected must be able to efficiently pump within a range of 800 to 120 gpm, in order to maintain minimum hole cleaning velocity of 150 ft/min) in the flow loop test section with the smallest expected drill string.

3.2.1.2.4. Inlet Conditions

As mentioned in a previous section, the injection of cuttings is considered on the inlet side of the pump, as this closed system will require the pump to be continuously pumping fluid contaminated with solids. When calculating inlet conditions, the general energy equation is used (43).

$$\frac{p_1}{\gamma} + z_1 + \frac{v_1^2}{2g} + h_A - h_R - h_L = \frac{p_2}{\gamma} + z_2 + \frac{v_2^2}{2g} \quad (43)$$

It is expected that the suction will be pulling from either an open tank with atmospheric conditions during experimental setup but become a closed loop during trials. This will create two different pumping situations. However, a small positive displacement pump can be utilized for test section filling purposes, prior to closing the system for a centrifugal pump to perform. It is also important to note that due to experimental conditions being closed-loop, different conditions exist, and pumps do not see adverse effects from static pressure, and do not have to overcome elevation-related head pressures. These pumps must simply overcome frictional losses within the system, as well as ensure that the system does not fall below vapor pressure (McLoone, 2018).

3.2.1.2.5. Cuttings Injection in Inlet

When considering a flow path in which the drilled cuttings are introduced on the suction end of the pump, it is paramount that the pump chosen can reliably handle a multiphase flow system (solid and liquid). Many industrial applications see the use of slurry pumps, from mining, to the oil and gas field to even the food industry.

There are 3 main type of pump designs that can handle multiphase fluid regimes. Lobe pumps and peristaltic hose pumps are positive displacement style pumps, and centrifugal pumps are kinetic.

3.2.1.2.6. Lobe Pumps

Lobe pumps act on the principle of creating positive displacement by cavitation caused rotation of 2 or more rotors within lobes. Lobe pumps are considered reliable when pumping

both high viscosity fluids as well as compressible solids, corrosive materials and fine, abrasive particles, due to the lack of physical contact between rotors. Other advantages to lobe pumps are that they offer pulse-free flow, unlike others such as rod and piston pumps, that require pulsation dampening. Lobe pumps can pass medium sized solids, have no metal to metal contact, and can be designed to pump at high rates (2,500+ gpm). Disadvantages to lobe pumps are their lower operating pressures (<200 psi max operating pressure), adequate timing gears and the requirement for multiple seals. The lower maximum operating pressures are the most significant drawback for flow loop application, where pressures could exceed 200 psi.

3.2.1.2.7. Peristaltic Hose Pumps

Peristaltic hose pumps are another form of pump that able to handle slurries and high viscosity fluids. They operate by trapping a fluid within a flexible tube that is routed between rotating rollers and a fixed housing. As the rotating rollers move, they trap a section a fluid in the tube. As the rotation continues, the fluid is expelled in the discharge line. The hose properties can be specifically designed to handle a wide range of fluid chemical properties.

Significant disadvantages to peristaltic hose pumps are their inability to provide high flow rates (35 gpm max), at low operating pressures (50 psi), making this type of pump inadequate for the flow loop demands.

3.2.1.2.8. Centrifugal Pumps

A centrifugal pump is a form of kinetic pump, in that energy is added to a fluid by a rotating impeller. The centrifugal pump is the most common type of kinetic pump and is used in a wide range of applications. Kinetic pumps are significantly different from positive displacement pumps in that there is a significant dependency between pump capacity and pressure. A positive displacement pump, efficiency is determined to be either volumetric, based

on the ratio of volume flow rate provided compared to theoretical expectations (usually within the 90-100% range) or overall, which measures the ratio of power delivered to the fluid to the power delivered to the pump. This varies significantly from kinetic pumps, where performance curves are most often based on total head ' h_a ' from the energy equation (2), and discharge.

This total head is the amount of energy added to a unit weight of fluid as it passes through the pump. If the capacity of the pump increases, head will decrease as less power can be delivered to a single unit from the impeller.

Basic centrifugal pump performance curves display a correlation between pump capacity and total head. As pump capacity increases, total head begins to decrease, until no more energy is transferred to the fluid (Figure 15).

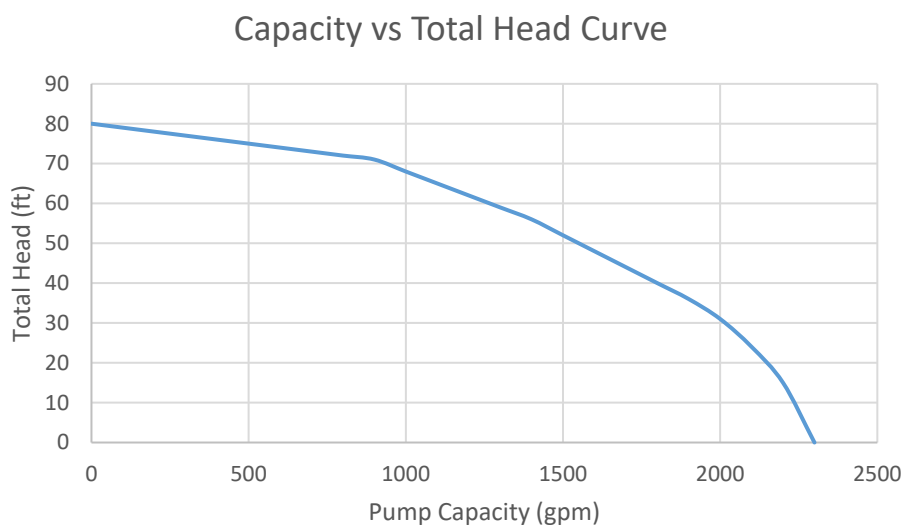


Figure 15: Centrifugal Performance Curve (Capacity vs. Total Head)

However, additional parameters are considered with centrifugal pumps that play into ideal pump selection and operating parameters. Pump power, often denoted in horsepower, and pump efficiency are used to size pumps properly. Unlike positive displacement pumps, kinetic

centrifugal pumps often see optimal operating range efficiencies between 60% and 80%, shortly before efficiency and total head drop off (Figure 16).

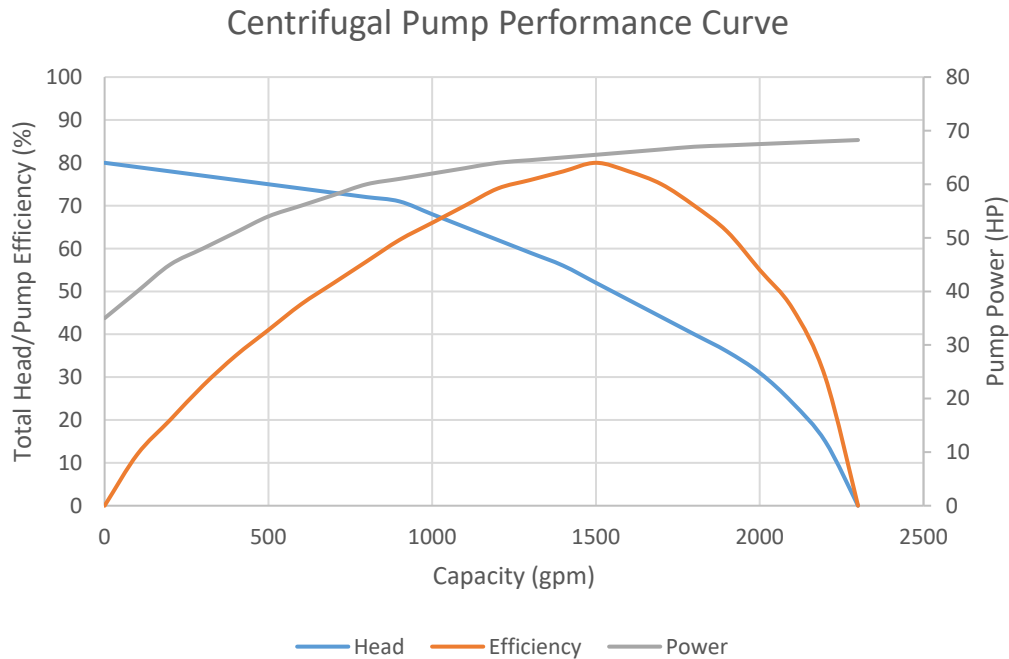


Figure 16: Centrifugal Performance and Efficiency Curve

There are 2 sets of affinity laws that determine the relationship between capacity, total head, and power required for centrifugal pumps. One is based on impeller speed ‘N’, and the other is based on impeller diameter D. Each set consists of 2 relationships. When based on impeller speed, (44)(45)(46) are used. When based on impeller diameter, (47)(48)(49) are used.

$$\frac{Q_1}{Q_2} = \frac{N_1}{N_2} \quad (44)$$

$$\frac{h_{a1}}{h_{a2}} = \left(\frac{N_1}{N_2}\right)^2 \quad (45)$$

$$\frac{P_1}{P_2} = \left(\frac{N_1}{N_2}\right)^3 \quad (46)$$

$$\frac{Q_1}{Q_2} = \frac{D_1}{D_2} \quad (47)$$

$$\frac{h_{a1}}{h_{a2}} = \left(\frac{D_1}{D_2}\right)^2 \quad (48)$$

$$\frac{P_1}{P_2} = \left(\frac{D_1}{D_2}\right)^3 \quad (49)$$

When selecting centrifugal pump, it is crucial to understand the expected total head and flow rate (capacity) in order to maximize operational efficiency, as well as select the adequate drive motor.

One final operating parameter that is important to proper centrifugal pump selection is net positive suction head required (NPSH_R). This design characteristic is important to ensure there is sufficient pressure to provide adequate flow on the inlet side of the pump. If the NPSH is insufficient, pump pressure is too low and vapor bubbles can form and enter the pump, severely degrading pump efficiency. This number is designated by the manufacturer and is pump specific. When designing a flow system, it is vital to ensure that NPSH is above manufacturers minimum allowable value (NPSH_R) through proper fluid reservoir location and design, as well as head loss from piping system (50). This equation subtracts head loss in the suction piping system h_f and vapor pressure head of the liquid at pumping temperature ($h_{vp} = p_{vp}/\gamma$) from the static pressure head ($h_{sp} = p_{sp}/\gamma$). If the elevation of the reservoir h_s from the

pump centerline is below the pump, this value is also subtracted; if it is above the pump, it is added.

$$NPSH_A = h_{sp} \pm h_s - h_f - h_{vp} \quad (50)$$

When considering total friction losses in the $NPSH_A$ equation, friction losses from the piping system may be significantly more complex in a system where cuttings enter the inlet. Cuttings will be added to the system prior to experimental trials, done via either auger, or injection pump outside of the test section; however, these cuttings could potentially increase friction losses that could adversely affect h_f .

Centrifugal pumps that are capable of handling slurries are called rotodynamic centrifugal slurry pumps and undergo unique design dependent on slurry concentrations and type. Several factors outside of basic flow requirements are taken into consideration during design, such as cuttings concentration and solids density, as slurries are often very abrasive and inadequate designs can shorten pump life and lead to premature failure.

3.2.1.3. Power Section

The power section will consist of the drive motor that will rotate various drill strings at speeds ranging from 60 RPM to in excess of 200 RPM. The motor selected will be required to maintain accurate, consistent and sustainable drill string speeds for a range of drill pipe sizes and masses. Additionally, it is important that feedback from the motor can be precisely and accurately recorded to observe any changes caused by experimental variable changes. This motor ideally must be compact and be electric to minimize footprint, maintenance and eliminate liquid fuel consumption.

A critical component of the flow loop test section is the drive motor that will rotate the drill pipe. It is important to properly select a motor that will give the precise control required, as well as offer feedback in torque fluctuations due to different RPM speeds, fluid properties, cuttings concentration and flow rates.

The motor type chosen to power drill string rotation is an asynchronous induction motor, due to its compact design, level of control, and torque and power delivery. AC induction motors generally offer a more simplified design over other options (DC, combustion), at a lower cost. These motors also are very reliable and have less parts. It is expected that high torque levels will not be required over a long period of time (rotational torque will be at maximum during acceleration of drill string), however small torque fluctuations may occur during changes in RPM, or adverse flow regimes brought on by changes in rotation. Therefore, maximum torque requirements were based on initial torque to arrive to maximum RPM (200) in as little time as possible (1 second). This torque calculation is described in equations (51) and (52) where T is torque, WK^2 is the moment of inertia, ΔN is change in speed (RPM), t is time in seconds, m is mass and R_i and R_o are respective internal and external radii. These equations were applied for both 5.875" drill string and 4.5" drill string. Table XI displays the results based on acceleration from 0 to 200 RPM in 1 second for both 5.875-inch OD drill strings and 4.5-inch drill strings. Drill pipe data can be found in 7.14.

$$T = \frac{(WK^2)\Delta N}{308t} \quad (51)$$

$$WK^2 = \frac{1}{2} m(R_i^2 + R_o^2) \quad (52)$$

Table XI: Expected Torque Values

	WK²	Mass, m (lb/ft)	Torque, T (ft*lb)
4.5" Drill Pipe	60.3	16.6	39.2
5.875" Drill Pipe	164.3	26.3	107

3.2.1.4. Cuttings Management

The cuttings management section will allow for both efficient separation of cuttings and drilling fluid, as well as introduction of cuttings to the test section. Cuttings will be introduced from a settling tank into the fluid management section via auger to introduce cuttings to the test section. In-line pigging stations will also be located on the fluids management system to allow for “marker” cuttings to be introduced in the test section for tracking.

Cuttings-laden fluid from the test section or from circulation will be separated from fluid by optimized solids control. Cuttings will then be deposited into a storage tank for future injection if needed, or disposal. As the test section will be closed-loop, constant injection of cuttings is not needed, and therefore auger fouling is less likely.

3.2.1.5. Fluids Management

The fluids management system will consist of a storage section, mixing equipment and circulation system, and will be driven by independent positive-displacement pumps. This system will be used to prepare fluid properties, fill the flow loop test section, and aid in the introduction and circulation of drill cuttings and markers. It will also aid in the transport and separation of cuttings upon completion of any experiments.

The fluids storage tank will be large enough to contain 1.5 the volume of the flow loop test section and circulation system combined. This will ensure an adequate surplus of fluids and allow for a range of cuttings concentrations in experimentation, with a respectable safety factor.

The fluid storage system will contain a chemical mixing station, as well as independent tank agitators, to allow for fluid property manipulation. This station will allow for the introduction of chemicals and additives in a safe and effective manner. A small pump will allow for the mixing and circulation of drilling fluids within the tank storage system.

The fluids management system will be driven by one positive displacement circulation pump. This pump will have duties including filling the test section with mud (cuttings will be injected into the flow stream), as well as flush the complete system of cuttings post-experiment. In addition, this pump will allow for bypass circulation of drilling mud through the fluids management system.

The cuttings management system will be integrated into the fluids system to allow for introduction of cuttings to the test section, as well as a means of transporting cuttings for separation post-trials.

The fluids management system must also have pressure-bypass systems built in to prevent over pressurization of the circulation system due to potential plugs from cuttings.

3.2.1.6. Data Acquisition, Monitoring and Controls Systems

It is critical that adequate visualization techniques are selected to model cuttings and fluid movement. Identifying proper equipment is a critical part the design process, as it will help collect and validate experimental data. Data acquisition systems must include collection and interpretation software packages, pressure transducers, visualization hardware and software, as well as flow meters and control systems.

The control systems that are a part of the flow loop design must be designed to precisely control variable parameters such as flow rate, cuttings concentration via auger, and internal drill pipe rotation. Given that the test section is a closed-loop system, a predetermined volume of

cuttings would be calculated to ensure expected solids concentrations would remain the same throughout the entire test section; however, these cuttings would need to be introduced through an automated and controlled auger system within the fluid circulation system. As discussed previously, the closed loop system will allow for the implementation of markers to track solids movement within the test section. These markers will require recording devices throughout the test section and return line, to ensure adequate tracking.

In addition to markers within the system, other visualization techniques and equipment must be evaluated, such as three charge-coupled device (3CCD) cameras (for increased resolution through individual color filter ranges) and particle image velocimetry (PIV). PIV is a form of optical measurement using non-intrusive lasers, and is available in standard (two velocity components), stereo (three velocity components), volumetric velocimetry (three velocity components) or time resolved PIV, and use one or more CCD or complementary metal-oxide semiconductor (CMOS – another image sensor comparable to CCD) cameras.

A viewing window or clear casing section centralized in the test section is also an important design feature that will allow for visual confirmation of any experimental procedure, and must be designed on a scale large enough to encapsulate a tool joint and reasonable length on either side of the pipe connection, to evaluate any considerable effects the diameter change may have on fluid and cuttings flow at variable drill pipe RPM.

Pressure changes are also a significant variable that must be monitored, and due to the variable pipe location, as well as changing flow conditions due to flow rates and varied pipe rotation, pressure transducers should be installed throughout the test section, on both horizontal and vertical axis' to detect potential pressure differences around the circumference of the casing.

Data monitoring software is a key component to the flow loop design, and an appropriately designed software package (or multiple if required) must be efficiently designed to handle large incoming volumes of data from pressure transducers, visualization hardware, torque and power readings from the power section, and flow rates at various stages. In addition to software capability, adequate internal storage must be planned for to handle the large volumes of real-time data per experiment.

4. Results

4.1. Experimental Results

The following section details the results of the experimental modeling of the vertical flow loop on campus. A total of six experiments were designed. 3 single-phase experiments (water flow rates set to 15 gpm, 25 gpm and 35 gpm) and 3 multiphase experiments (15 scfm, 35 scfm and 60 scfm air rate with 10 gpm water constant rate). Although all single-phase models were successfully run using a standalone machine, multiphase simulations require more capable HPC (High-Performance Computing) equipment to adequately perform all multiphase simulations to completion. A detailed breakdown of all parameters is outlined in 4.1.2.

4.1.1. Single Phase Results

When modeling single-phase fluid flow, ANSYS Fluent automatically omits any head loss due to elevation changes. However, frictional head losses are still calculated, and simple hand calculations can confirm the results from CFD modeling.

Additional calculations are performed to compare expected fluid loss due to elevation change. However, actual single-phase results (7.5) show negative pressure at the upper transducer, indicating a potential vacuum and issue with the transducer. This inaccuracy forced alternative methods to attempt to validate the simulation results.

4.1.1.1. Simulation Results

Table XII below displays the results from all 3 single-phase simulation runs, displaying flow rate, corresponding linear velocity, and bottom and top pressures.

Table XII: Single Phase Simulation Results

Flow Rate (GPM)	Linear Velocity (ft/s)	Bottom Pressure (psi)	Top Pressure (psi)	Pressure Difference (psi)
15	1.53	0.144	0.109	0.103
25	2.54	0.195	0.132	0.243
35	3.57	0.177	0.100	0.444

Figure 17 also displays all three simulations associated static pressure drops, in which data was pulled from a center line of the flow area.

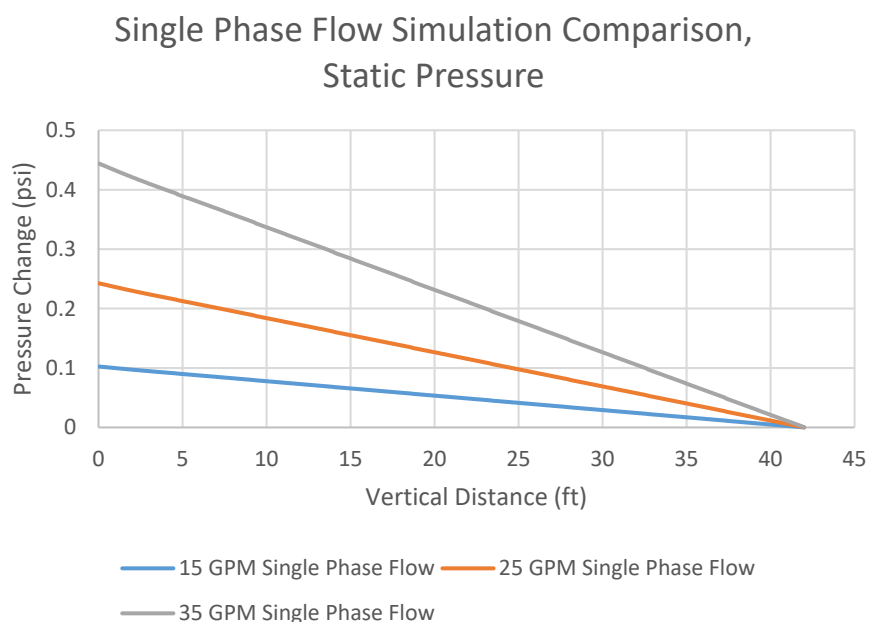


Figure 17: Single phase simulations pressure drop

In order to validate this pressure loss (excluding head loss), manual friction loss calculations were performed using the Hazen and Williams empirical formula for head loss (53). In this equation, the Hazen-Williams Coefficient, “C”, was set to 140 to represent smooth pipe. Table XIII shows the results of these calculations.

$$h_L = L \times Q^{1.852} / C^{1.852} / d^{4.87} \quad (53)$$

Table XIII: Calculated results, single-phase

Flow Rate (GPM)	Linear Velocity (ft/s)	Reynolds Number Re	Flow Type	Friction factor	ΔP_f , psi	Fluent/ Calculated ΔP_f , psi
15	1.53	24,200	Turbulent	0.02478	0.104	0.001
25	2.54	40,178	Turbulent	0.02204	0.268	0.025
35	3.57	56,470	Turbulent	0.02045	0.499	0.055

The comparison of the simulated and calculated data shows a difference in psi ranging between 0.001 and 0.055 psi (Table XIII). ANSYS Fluent utilizes the energy and momentum equations in determining pressure loss, and the numerical errors and difference to the Hazen-Williams equation are likely due to grid resolution and boundary/wall interaction.

4.1.1.2. Hardware and Simulation Time

All single-phase simulations were run on a standalone machine. The specifications of this machine are outline in Table XIV.

Table XIV: Standalone computer specifications

System	
Manufacturer	Dell
Processor	Intel® Core™ i7-3770 CPU @ 3.40 GHz
Installed memory (RAM)	16.0 GB
System Type	64-bit Operating System, x64 based processor

Additionally, average simulation time ranged between approximately 3 and 17 minutes. Single simulation run times (500 iteration) are displayed in Table XV.

Table XV: Simulation run times

Simulation	Time (sec)
8-inch, 90°	179.039
8-inch, 45°	220.654
5-inch, 90°	978.650
5-inch, 45°	150.667
8-inch, reverse 45°	819.780
8-inch, dual-90°	271.141
8-inch, 90° outlet	

4.1.2. Multiphase Results

In contrast to single-phase simulations, where in steady state flow can be considered and simulations do not require transient modeling, multiphase flows are considerably more complicated and require substantial computing time to model. Table XVI summarizes the results from the three trials. It is important to note that all values presented are average values taken over a period (varied for each trial).

Table XVI: Multiphase flow experiment results

Water Rate (GPM)	Linear Velocity (ft/s)	Air Flow Rate (scfm)	Bottom Pressure (psi)	Top Pressure (psi)
9.947	0.981	15.875	1.761	6.808
9.955	1.017	35.463	3.908	8.402
9.604	0.981	60.340	6.641	10.746

Figure 18, Figure 19 and Figure 20 display the bottom pressure, top pressure and air flow rate fluctuations for the time of each test.

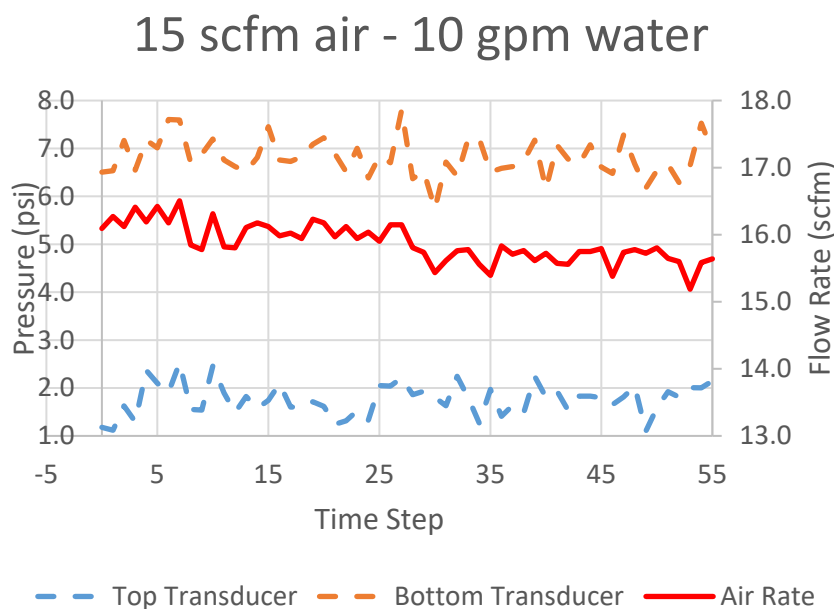


Figure 18: Experimental results, 15 scfm air and 10 gpm water rates

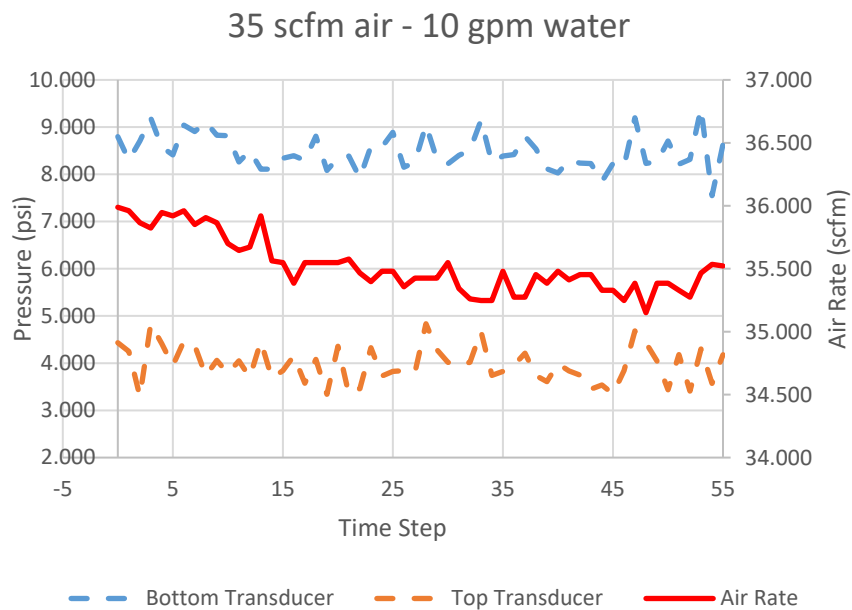


Figure 19: Experimental results, 35 scfm air and 10 gpm water rates

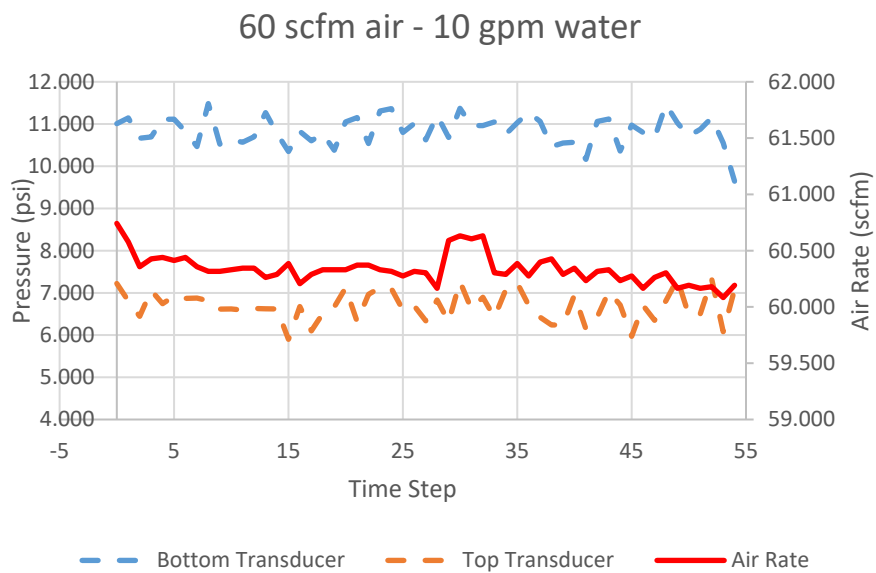


Figure 20: Experimental results, 60 scfm air and 10 gpm water rates

4.1.2.1. Hardware and Simulation Time

Multiphase simulations cannot be performed reasonably on a standalone machine, due to the transient solving methods required and size of timestep often used to avoid solution divergence. Montana Tech has one HPC cluster and an additional copper server. The cluster contains 1 management node, 22 compute nodes and 2 NFS storage systems. Table XVII outlines the specifications of the cluster and copper server.

Table XVII: Montana Tech cyberinfrastructure

Head Node		Copper Server		Other Specs	
CPU	Dual E5-2660 (2.2 GHz, 8-cores)	CPU	Dual E5-2643 v3 (3.4 GHz, 6-cores)	CPU	nfs0- 25 TB nfs1- 66 TB
RAM	64 GB	RAM	128 GB	Network	Ethernet 40 Gbps Infiniband
Disk	450 GB	Disk	1 TB		
14 Compute Nodes		6 Compute Nodes		2 GPU Nodes	
CPU	Dual E5-2660 (2.2 GHz, 8-cores)	CPU	Dual E5-2660 (2.2 GHz, 8-cores)	CPU	Dual E5-2660 (2.2 GHz, 8-cores)
RAM	64 GB	RAM	64 GB	RAM	128 GB
Disk	450 GB	Disk	450 GB	Disk	450 GB
Nodes	n0-n-11, n13, n14	Nodes	n12, n15-n19	GPU	Three nVidia Tesla K20
				Nodes	N20, n21

Given the dimensions and input parameters of performing a multiphase flow simulation to replicate experiments on the Montana Tech flow loop, the current accessible cyberinfrastructure is inadequate, and future benchmarking must be performed to determine minimum HPC requirements.

4.2. Flow Test Section

The flow loop test section was divided into 3 separate areas. The flow inlet, the flow outlet, and the test window. In order to determine adequate flow loop test section length, flow normalization parameters needed to be determined via CFD modeling for both inlet and outlets. This modeling involved several simulations with parameter variables such as inner drill pipe location, inlet and outlet angle, and fluid properties. This was done in order to determine which

variable had the most significant effect on flow normalization distance. Data points were recorded over vertical and horizontal planes, as well as centralized lines on both the horizontal and vertical planes at the half way point between the interior drill pipe and casing wall. These simulations were run on steady-state solver settings, with a minimum of 500 iterations.

The flow loop test window is defined as the area of the test section where experimental data will be recorded. It will have no adverse effects from either inlet or outlet conditions and provide a suitable window for data acquisition.

4.2.1. Flow Inlet

In order to determine optimal inlet design, the flow junction was tested at four different angles (dual 90°, 90°, reverse 45° and 45°) (Figure 21). The inlet ID for the single 90° and 45° designs was also varied at 5 and 8 inches for a total of six trials.

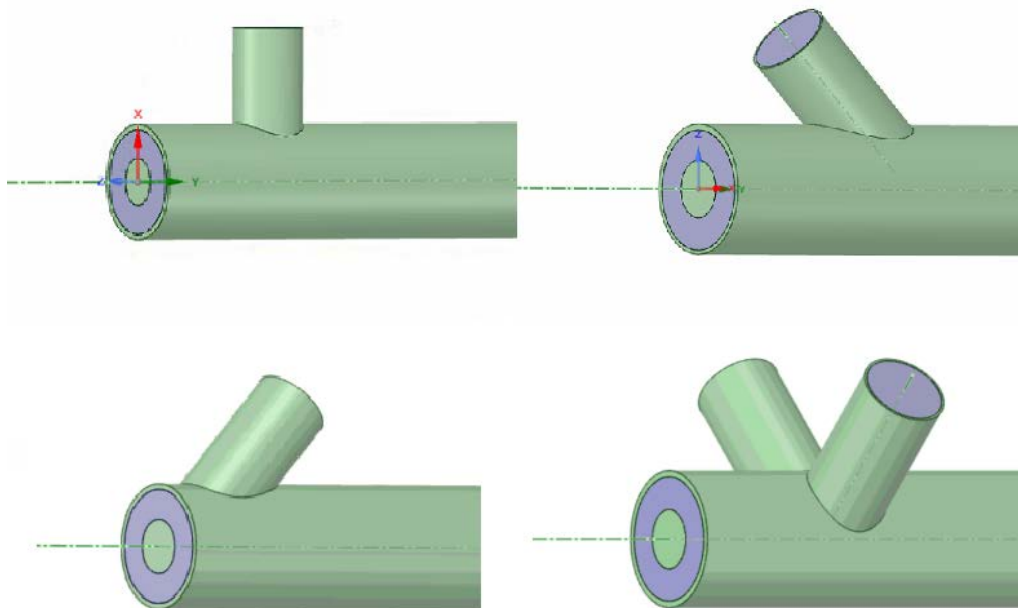


Figure 21: Flow Loop Test Section Inlet Designs (45°, reverse 45°, 90° and dual 90°) with 8-inch ID

In order to determine the longest expected velocity normalization distance based on fluid parameters, 3 separate runs were performed on the 45°, 8-inch model. The fluids chosen for these runs were water, light water-based mud, and heavy, thick oil-based mud. Properties for these fluids are detailed in Table II of the Preprocessing - Setting up Physics section. Figure 22 displays data from an x-plane line from all three trials, showing that fresh water requires the most distance to reach a steady flow, approximately 30-40 feet. The wavy pattern of the water velocity is due to the low viscosity, and more turbulent flow of water. Flow was determined to be steady based on two factors. The velocity line appears to be relatively unchanged and is within the expected range of the calculated flow rate based on inlet velocity. A complete water velocity plot (run to 60 feet) can be found in 7.13, but it must be noted normalization occurs at approximately 40 feet.

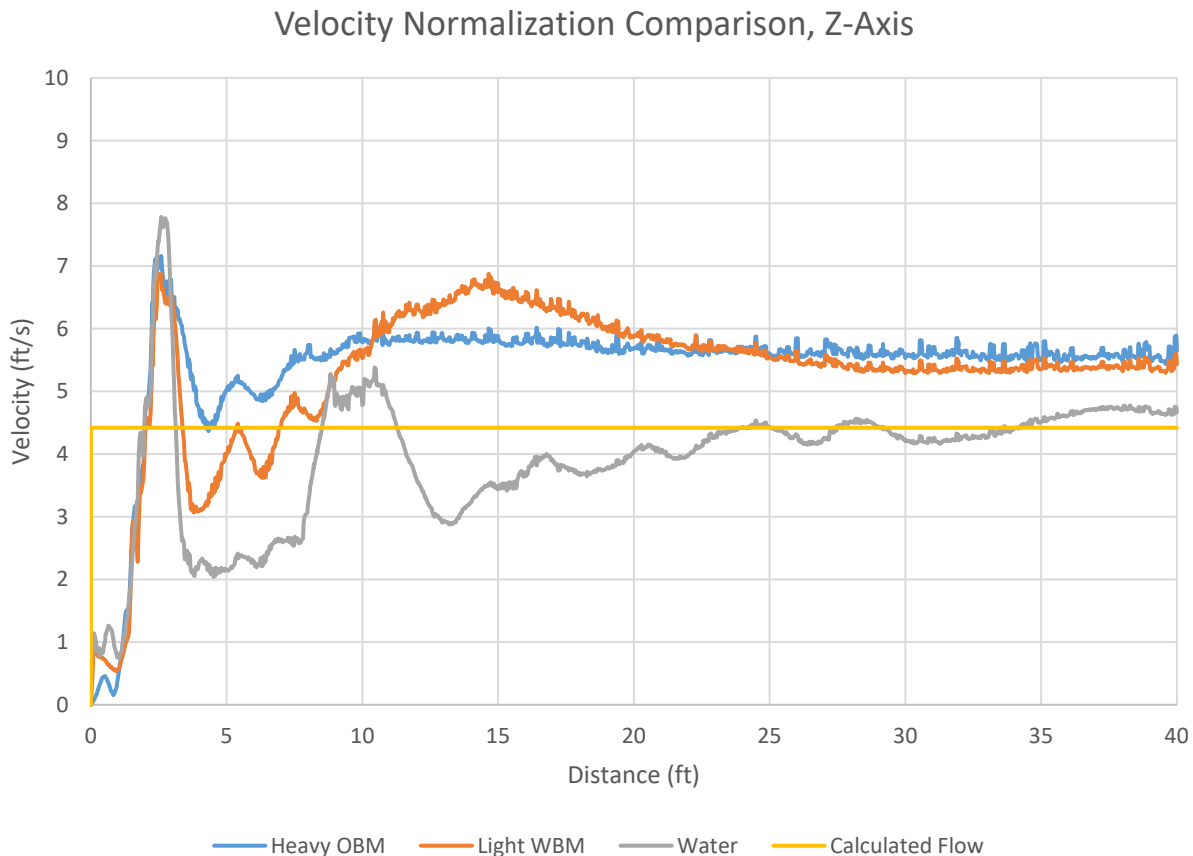
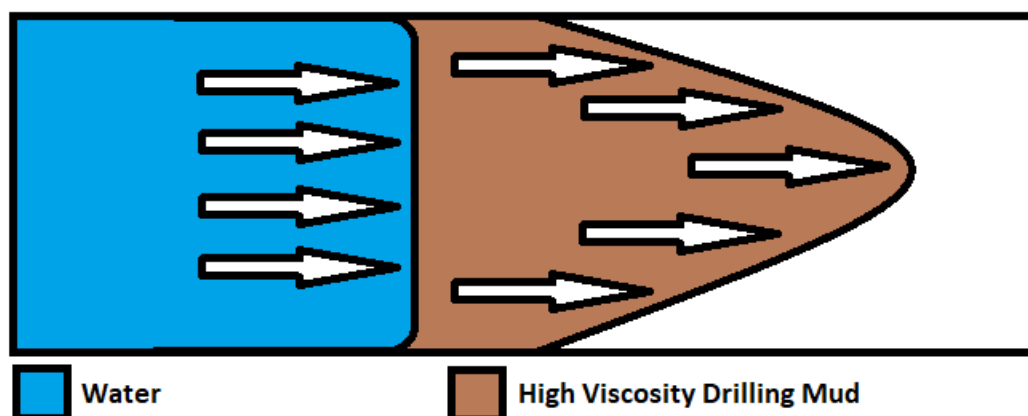


Figure 22: Flow Normalization by Fluid Characteristics (45°, 8-inch inlet)

Table XVIII displays expected flow loop fluid velocities and inlet velocities used for Fluent modeling. The results illustrate that a higher linear velocity is seen in both drilling muds, as compared to the water. This is due to the higher viscosity of the drilling fluids, causing more resistance to flow along both the casing and the drill pipe. This resistance results in flow channeling and an increased velocity at the test points. Figure 23 displays the difference between flow regimes of water vs. drilling fluid.

Table XVIII: Summary of Fluid Velocities

	5-inch inlet	8-inch inlet
Inlet velocity (ft/s)	20.426	7.979
Expected flow loop velocity (ft/s)	4.416	4.419
Actual flow loop velocity (ft/s)	4.6-4.8	4.4-4.8

**Figure 23: Varied Shear Between Fluids**

The 90° and 45° inlet design, with both 8-inch and 5-inch ID's were chosen for volume handling capability and sort distance to steady flow conditions. Given that this flow loop will be a closed system, it was important to consider the minimum dimensions for handling a reasonable volume of cuttings (~30% of total volume) as well as fluid to maintain adequate flow in such a large diameter test section.

The inlet angle design focuses on determining if pressure and velocity normalization is adversely affected by changing the angle. After running 4 tests with the largest expected drill string (5.875" OD), it was determined that there was a significant difference between inlet angle and velocity normalization (Figure 24 vs. Figure 25 for 8-inch, Figure 26 vs. Figure 27 for 5-inch). In both cases, the 45° inlet required 10-15 additional feet to reach expected fluid velocity. When running simulations for inlet size, however, there was no noticeable difference in velocity

normalization between the 8-inch inlet ID and 5 inch inlet ID (Figure 24 vs. Figure 26). This data identifies that inlet angle is a significant factor in determining minimum length of the flow loop.

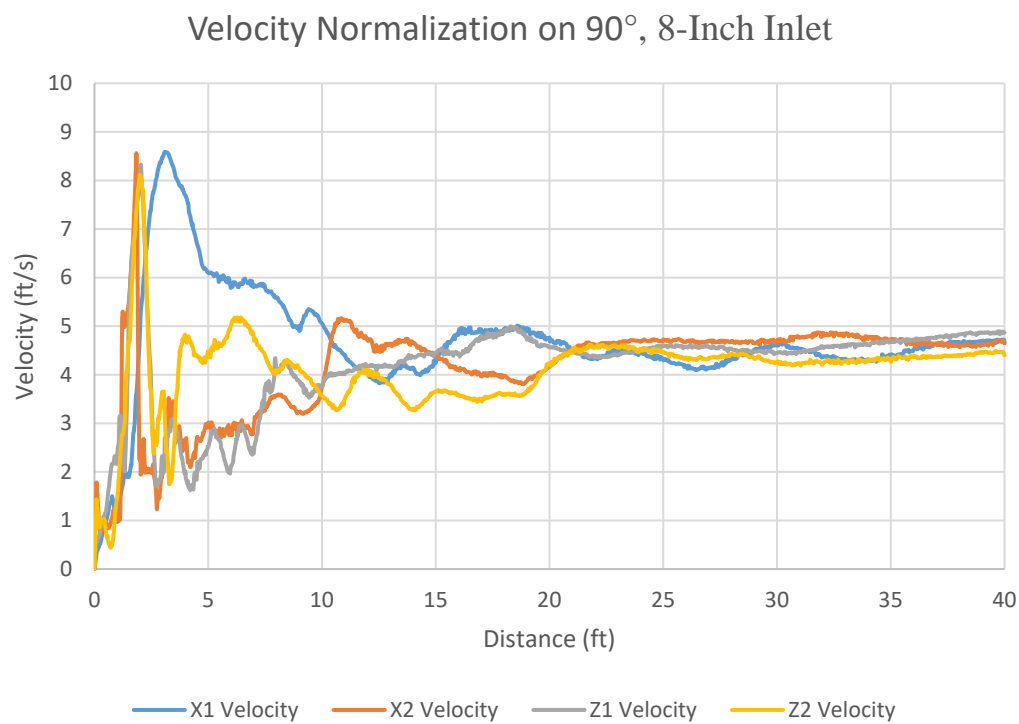


Figure 24: Velocity Normalization on 90° inlet (8 inch)

Velocity Normalization on 45°, 8-Inch Inlet

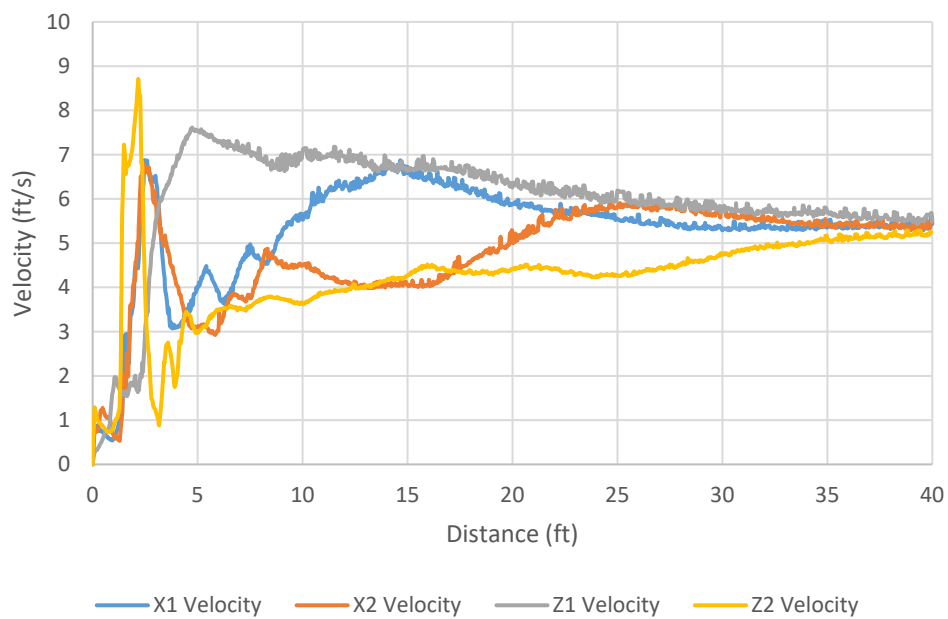


Figure 25: Velocity Normalization on 45° inlet (8 inch)

Velocity Normalization on 90°, 5-Inch Inlet

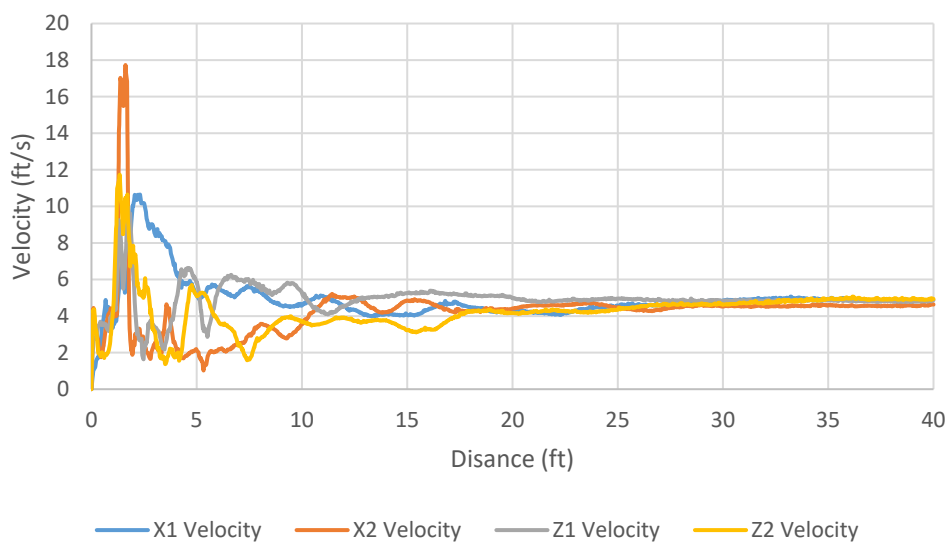


Figure 26: Velocity Normalization on 90° inlet (5 inch)

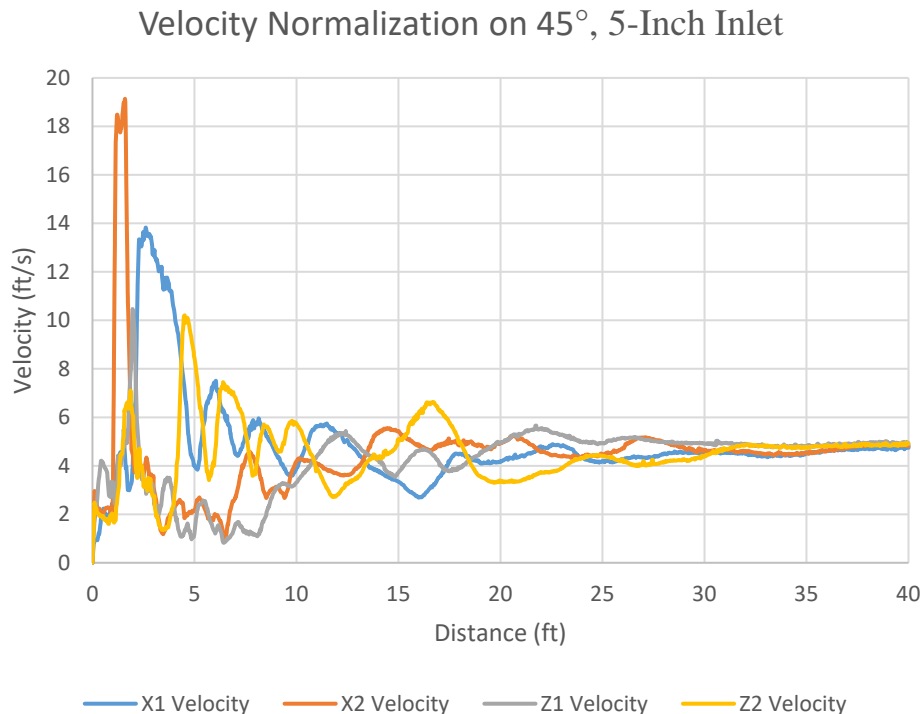


Figure 27: Velocity Normalization on 45° inlet (5 inch)

Both the reverse 45° inlet and dual 90° designs were developed to compare against the 90° inlet design, to determine if further optimization could occur. Figure 28 and Figure 29 display the results of these simulations. There is high turbulence seen in the initial 15 feet of the reverse 45° model, however flow does not reach steady state until approximately 40 feet. In reviewing the results from the dual-90° inlet simulation, there is much lower initial velocities (due to lower velocities required by doubling inlets), however steady state flow is not achieved until approximately 35 feet.

Velocity Normalization on Reverse 45°, 8-Inch Inlet

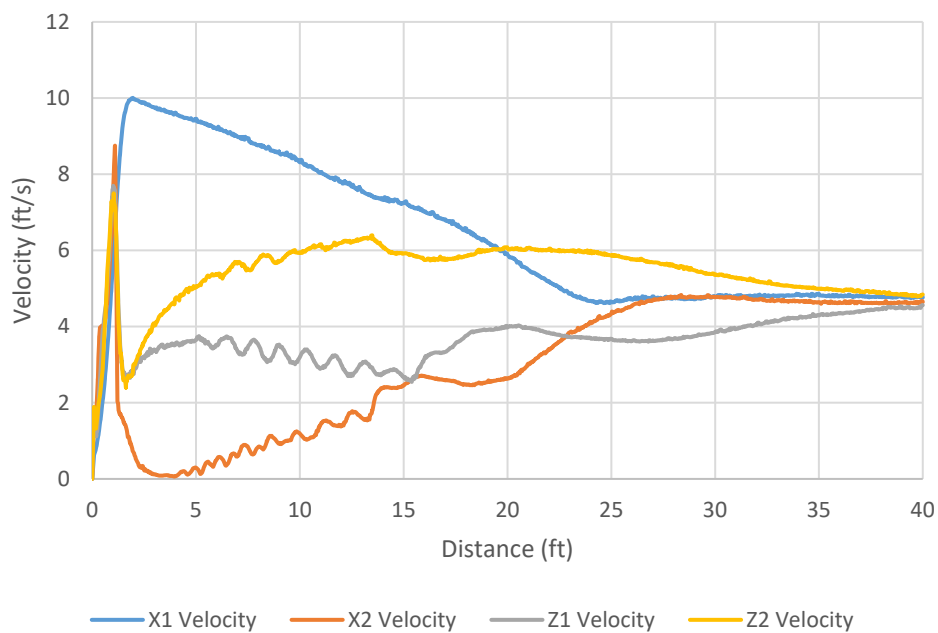


Figure 28: Velocity Normalization on reverse 45° inlet (8-inch)

Velocity Normalization on Dual-90°, 8-Inch Inlet

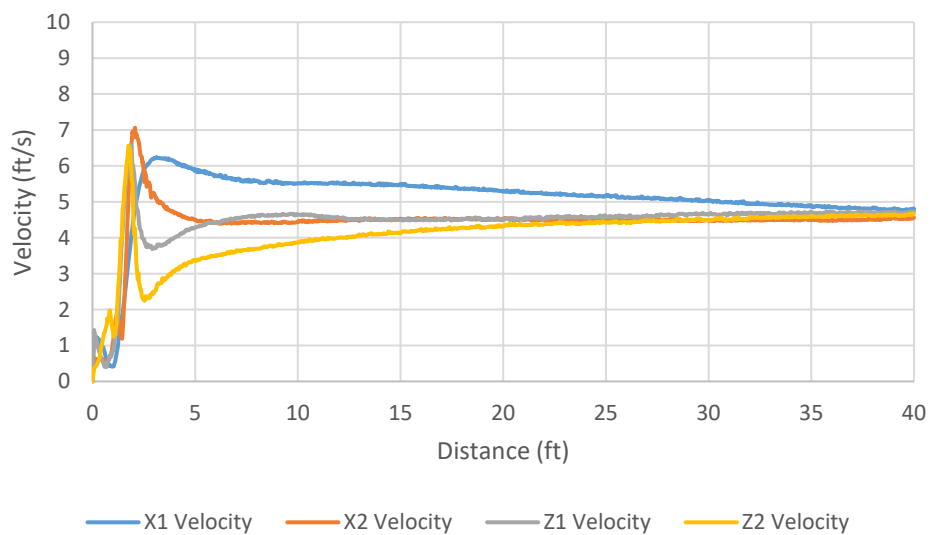


Figure 29: Velocity Normalization on dual-90° inlet (8-inch)

Given the results of these CFD model simulations, the optimal inlet design is a single 90° inlet. An 8-inch, 90° inlet was selected for interchangeability (outlet design discussed in future sections). The results of these trials show that the minimum required distance from the inlet until flow normalization is approximately 30 feet, based on fresh water. This number is multiplied by a 20% safety factor, resulting in a minimum inlet distance to normalization of 36 feet. As the average drill pipe length is 30 feet, inlet design has been set to 45 feet, incorporating 1.5 joints and ensuring minimum distance from tool joint is ensured (50% safety factor). Table XIX displays a summary of inlet design characteristics developed through simulations run with water. Water was proven to require the most distance to reach steady flow (Figure 19).

Table XIX: Inlet Parameter Summary

Inlet ID (in)	8.0
Inlet angle (°)	90
Inlet length (no safety factor) (ft)	30
Safety factor (%)	50
Inlet length (total) (ft)	45

4.2.2. Flow Outlet

Flow outlet design considerations involved gravitational assist, and volumetric efficiency. Outlet ID was set to 8 inches, to carry the combined cuttings and fluid volume without experiencing a significantly higher velocity based on 1250 gpm flow rate (~5.0 fps in 8 inch). The outlet design was placed downward, to allow for gravitational drainage post-experiment.

No additional model designs were considered, and this model was run to determine drainage end effects for minimum sizing using the same 3 different fluid characteristics tested on

the inlet (Table II). The results of these three simulations are displayed in Figure 30, Figure 31 and Figure 32, and these figures show that there is little back pressure present, causing little to no end-effects. However, it is important to note that these simulations were run without solids contamination. Although drilled cuttings within the flow should not be adversely affected (minimum carrying speed is maintained), this could cause a build-up of cuttings at the outlet. The outlet center is located 8.5 inches from the end plate

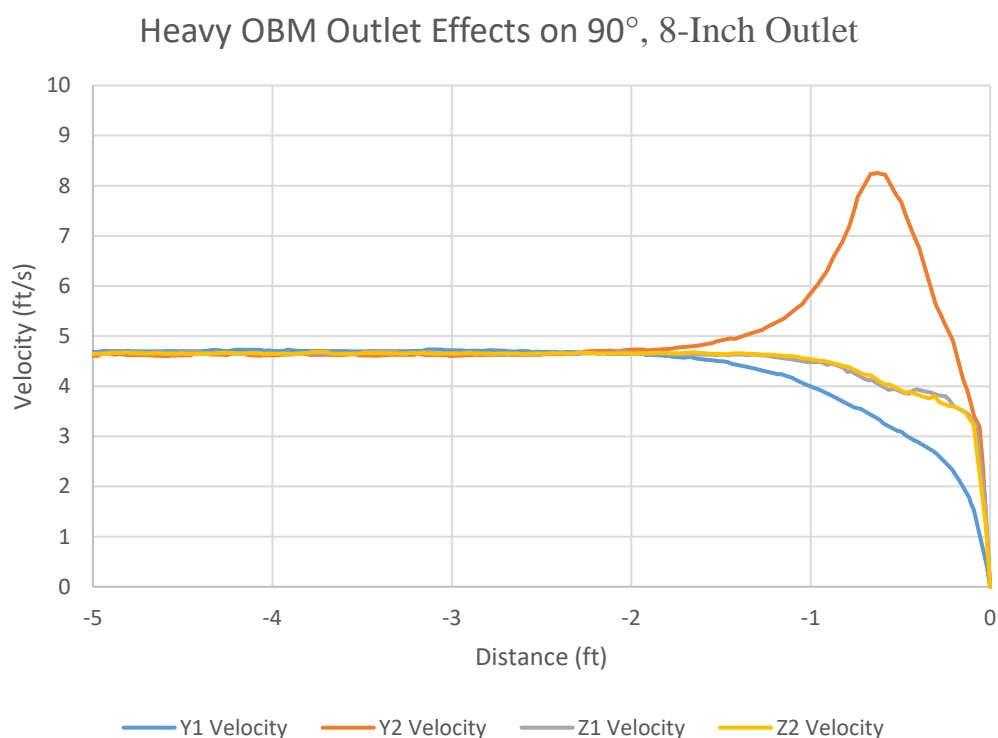


Figure 30: End-effects, heavy OBM, 90° outlet (8-inch)

Light WBM Outlet Effects on 90°, 8-Inch Outlet

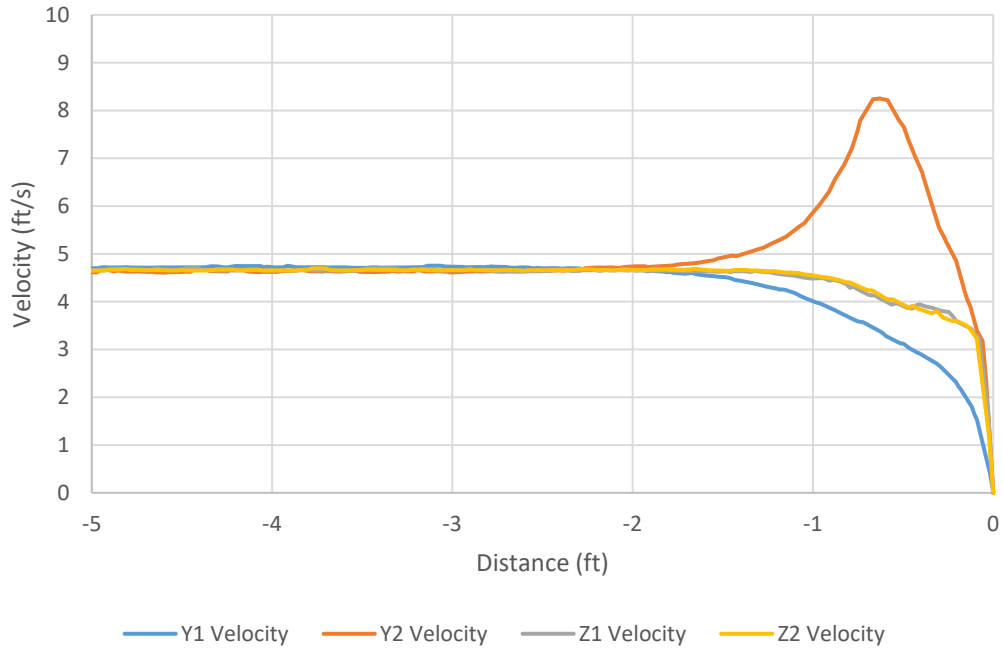


Figure 31: End-effects, light WBM, 90° outlet (8-inch)

Water Outlet Effects on 90°, 8-Inch Outlet

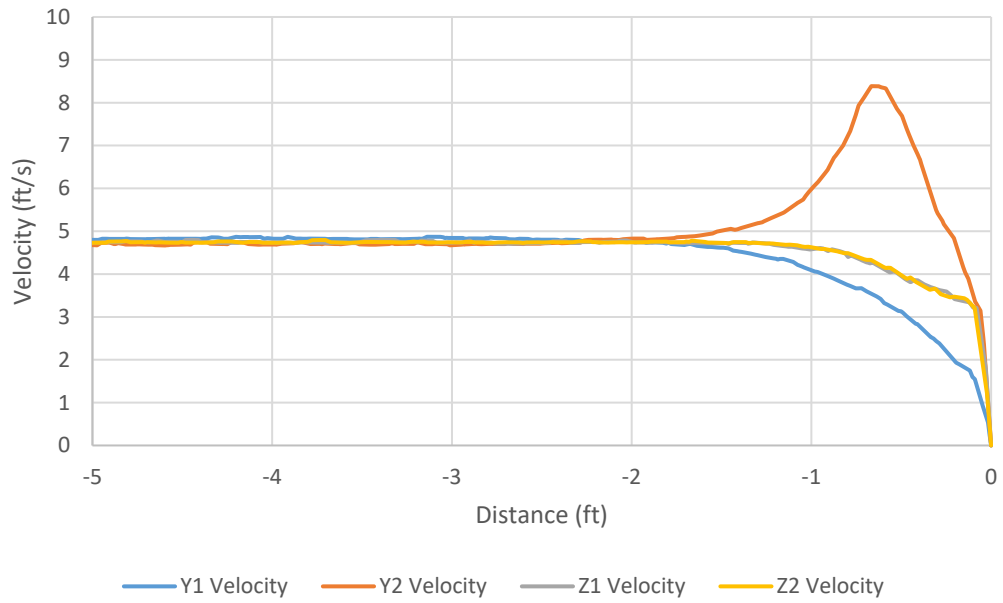


Figure 32: End-effects, water, 90° outlet (8-inch)

In reviewing the results of these tests, and considering adverse effects that cuttings build up may have, a significant safety factor (5x) is implemented to ensure no adverse effects on the test window. This results in an outlet length of 15 feet. Table XX displays a summary of outlet parameters.

Table XX: Outlet Parameter Summary

Outlet ID (in)	8.0
Outlet angle (°)	90
Outlet length (no safety factor) (ft)	3
Safety factor (%)	500
Outlet length (total) (ft)	15

4.2.3. Test Window

The test window section is in place to allow a section for experimental data acquisition, based on specified experimental trials. Although this section may not necessarily consist of a physical “window”, the above term is used to describe the section of the flow loop that is unaffected by inlet and outlet flow. The optimal parameters for this section would include a viewing window or clear Lexan tubing for 360 degree viewing and be long enough to host a minimum of 1 drill pipe tool joint, with reasonable distance on either side of the tool joint (30 ft).

It is extremely important to note that although it is possible that the orbital motion of a drill string within an extended reach horizontal wellbore (and its tendency to “walk up” the wellbore side as RPM increases) may play an important factor in cuttings transport, the unpredictability of this phenomenon makes it unviable for experimental recreation. Additionally, with an extended length of flow loop, the ability to vary pipe eccentricity becomes severely limited, as drill pipe will likely rest on the bottom of the flow loop due to gravitational forces. Therefore, the decision to have a test window that is large enough to contain a minimum of one tool joint is made, with a maximum of three. This will allow suitable experimental

viewing of the effects surrounding a tool joint on cuttings transport, but will also not limit the ability to vary pipe eccentricity through manipulation of end caps on the test section (see 4.3). The optimal design characteristics will allow for maximum viewing window, even including visualization before flow stabilizes. However, inlet and outlet designs will require welded inlets and outlets, as well as the ability to bolt flanges to the ends.

4.2.4. Test Window Length

Within the test section, a viewing window and observation area must be designed that is not adversely affected by inlet and outlet flows. In order to properly study the effects of drill string rotation on cuttings transport efficiency, it is also important that both drill pipe body and tool joint are positioned in this window. The test window design will have a minimum of two tool joints with a minimum of one half-length of pipe on both the inlet and outlet side to allow for recording of any changes caused by pipe connections. Given the average range of drill pipe length manufactured is approximately 30 feet (with exceptions for some strings designed specifically for large rigs) and the minimum required length from flow inlet to normalization, it is expected that 1.5 joints are required to surpass the inlet (with safety factor) to reach the test window. Based on minimum viewing requirements previously outlined, this results in 2 joints within the test window to satisfy all criteria. The minimum distance from the outlet to the test section is 15 feet (with safety factor), or approximately 0.5 drill pipe joints. Table XXI displays the minimum distances required, and tool joints required to complete the flow loop test section. This table shows that the minimum length of the flow loop test section is 120 feet.

Table XXI: Test section length summary

Inlet length (ft)	45
Outlet length (ft)	15
Test Section (ft)	60
Joints Required	4
Total Length	120

4.3. Return Line

Based on inlet and outlet design, and negating pump design parameters (discussed later), return line on the closed system of the flow loop will be approximately the same length as the test section, at 120 ft. Additional parameter such as outlet to return, and return to inlet, are an additional 16 ft., for a total of 136 ft. of 8-inch ID return line. Table XXII outlines return line sections and lengths. Figure 33 highlights the elbows identified in the table.

Table XXII: Return line specifications

Inlet to elbow (a) (ft)	2
Elbow (a) to elbow (b) (ft)	2
Elbow (b) to elbow (c) (ft)	6
Return line (ft)	120
Elbow (d) to elbow (e) (ft)	3
Elbow (e) to outlet (ft)	3
Total return line length (ft)	136

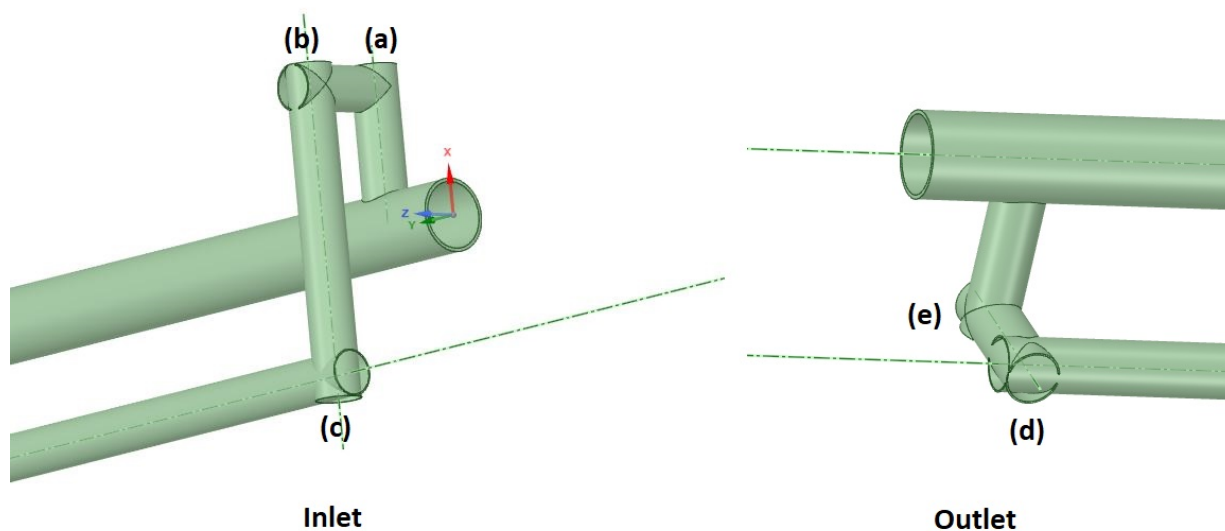


Figure 33: Inlet and outlet elbow identification

4.4. Flow Loop Volume Requirements

Considering the total lengths of both the test window, inlet, outlet and return section, total internal volume (without drill pipe) is approximately 26 bbl. Table XXIII shows a breakdown of volume by section.

Table XXIII: Flow loop volume summary

Test section volume (bbl)	17.5
Inlet to elbow (a) (bbl)	0.125
Elbow (a) to elbow (b) (bbl)	0.125
Elbow (b) to elbow (c) (bbl)	0.373
Return line (bbl)	7.46
Elbow (d) to elbow (e) (bbl)	0.187
Elbow (e) to outlet (bbl)	0.187
Total volume (bbl)	26

4.5. Test Section Ends

One critical component of the flow loop design is the ability to house a variety of drill string sizes within the flow loop, with the capability of maintaining a seal during high RPM rotation. Additionally, the ability to adjust wellbore position (centralized, low side, simulated walk-up) is an important component. These end plates must also be able to connect to the power section efficiently, in order to rotate the drill string.

4.6. Flow Loop Pumps

4.6.1. Test Section Pump

In reviewing the operating parameters for a variety of pump styles, the optimal pump selection for a multi-phase flow at high capacity is a rotodynamic centrifugal slurry pump.

These pumps are extremely durable and often used in drilling applications and can be optimally

sized to operate at the required conditions. Additionally, these slurry pumps can be modified via impeller size and RPM to further expand operating range. The application of this pump is to provide a high flow rate, with lower demanded pressures. As positive displacement pumps often offer high flow rates with accompanying high pressures, they are less suited to be an inline pump for the flow loop. However, as discussed in the next section, a large positive displacement pump is the optimal choice for the ancillary system pump. This will allow for an open-loop style of experimentation.

Due to the unique and abrasive characteristics of slurries, the Hydraulic Institute implemented ANSI/HI 12.1-12.6: The American National Standard for Rotodynamic (Centrifugal) Slurry Pumps to aid in the design of slurry pumps by application. Section 12.3 was used to design the minimum requirements for the flow loop test section.

Identifying the slurry characteristics expected is a key component of pump design, and there are several methods outlined. Given that drilled cuttings are often not corrosive but can erode pump equipment if not accounted for. As cuttings used for experimental trials will likely be a variety of formation types (sandstone, limestone, etc.), their abrasiveness must be considered. Drilled cuttings are also classified as settling and can form stationary beds when slurry velocity is below a minimum rate or stationary. Given the complex nature of drilling fluids, there are characteristics of non-settling (clay suspension) and settling (cuttings beds) that may occur within the flow loop test section, as well as the returns section where the pump will be located. It is important to account for both factors in pump design.

Settlings slurries have deposit velocity (minimum settling velocity) that when reached will cause solids to drop out of flow and form a stationary bed. As Table VI shows, minimum expected experimental velocity within the test section is 150 ft/min, which is when cuttings will

likely begin to form stationary beds along the bottom of the pipe. As discussed in previous sections (2.4.1.8), layer modeling is often used in calculating steady state slurry flow but can have adverse outcomes. Studies (summarized in (Pilehvari et al., 1999)) identified that minimum transport velocities required to carry cuttings in horizontal wellbores ranges between 4 and 6 ft/s (240-360 ft/min) in experimental settings, however indicated that many large wellbores (12+ inch ID) are effectively cleaned at much lower rates (2-3 ft/s, 120-180 ft/min) with assistance of drill string rotation. Although this 150 ft/min fluid velocity is the minimum acceptable velocity, it is important to note, that within the smaller diameter return section, a 300 ft/min velocity is expected, which is much higher than cuttings deposit velocity.

Pump performance is derated in connection with increase in slurry properties, such as cuttings concentration and fluid viscosity. Given that experimental fluids will be both viscous and may contain higher cuttings concentrations, it is expected that significant decreases will be expected in pump head, and increased power over a conventional centrifugal pump will be required. Drilling fluid exhibits non-Newtonian flow, which makes standard derating approximations from ANSI/HI 9.6.7. inaccurate, and consultation with pump manufactures is the most optimal method for determining these derating values.

Wetted materials (parts of the pump exposed to slurry flow) must be chosen appropriately. Table XXIV (Institute, 2011) from ANSI/HI 12.3 indicates that for this flow loop, optimal wetted material choice should be ductile iron, as moderate abrasiveness is expected with no corrosion.

Table XXIV: General Suitability of Wetted Materials

Wetted Material	Abrasive characteristics of pumpage	Applicable wear service class	Corrosive characteristics of pumpage
Grey cast iron	Very mild, fine particles	1	Noncorrosive
Ductile iron	Moderate	2	Noncorrosive
White irons	Severe	4	Mildly corrosive
Martensitic stainless steel	Moderate	3	Mildly corrosive
Austenitic stainless steel	Mild	1	Corrosive
Duplex stainless steel	Moderate	2	Corrosive
Super-duplex stainless steel	Moderate	2	Highly corrosive
Elastomers	Severe, fine particles	3 ^a	Mildly corrosive

The return line of the flow loop test section has an ID of 8 inches; however, it is possible that this diameter may be modified to fit an optimal pump. Most centrifugal slurry pumps have a larger suction end, and a smaller discharge. Large ID pumps often have minimal operating conditions that are equivalent to the low end of experimental flow rates (800 gpm), which would make them inefficient for the design. Swages can be properly designed to accommodate a smaller pump that would be more appropriate. Table XXV summarizes the required parameters of the pump selection.

Table XXV: Flow loop pump requirements

Pump style	Centrifugal
Flow rate range (gpm)	800-1300
Wetted material	Ductile iron
Power	Electric
Inlet/Outlet (in)	6/4 - 8/6
Solids Handling	Moderate abrasive, non-corrosive
Head Pressure	Based on circulation system design (closed loop test section)

4.6.2. Fluid circulation pump

An additional pump will be in operation that will allow for the filling of the flow loop, and complete circulation of the flow loop system to and from the storage tanks. This pump will be installed directly on the suction of the fluid storage tank, much like a conventional premix or mud tank. This pump will be a positive displacement, triplex design which will allow for high volumetric flow rates required to both fill the flow loop with fluid and cuttings and circulate the system in an open-loop.

The fluid circulation pump will be tasked with the ability to fill the flow loop test section with fluid and cuttings; however, this pump will not handle cuttings in the suction, but rather provide an active flow in which cuttings will be injected via auger (discussed in a later section) further down the discharge line, prior to entering the flow loop test section.

In addition, this pump will be able to provide high enough fluid velocity to successfully carry cuttings (minimum 150-200 ft/s) in order to successfully carry cuttings from the flow loop test section and return to the solids control equipment.

Secondary functions of this pump may include facilitating the return of cuttings from solids control to the cuttings injection tank, and to aid in moving cuttings through the auger system into the circulation line. These functions may however be controlled by the mixing pump located in the mixing station (discussed in a later section).

4.7. Power Sections

4.7.1. Pipe Rotation

After determining minimum torque requirements, Northwest Motion was contacted in order to size an appropriate motor. Most electric motors are capable of high rotating RPM (upwards of 3000) but begin to lose power and torque as RPM increase. However, installing a drive motor that is overpowered is inefficient and not cost-effective. Additionally, with overpowered motors, gearing is often a requirement, which can adversely affect torque readings. Given that one key parameter of this flow loop will be the ability to detect minor changes in torque from fluid flow changes and drill string rotation, the ideal motor must not be geared. Additional hardware, such as a torque-load cell may also be required, as many motors will display torque to one decimal, but often have a margin of error.

After discussion with distributors, the optimal drive motor for this application was determined to be a Bosch-Rexroth IndraDrive M HMS01 motor. This air-cooled motor is an electric drive, powered by 480-volt AC current. It has a maximum usable speed of 3000 RPM, however, can comfortably supply required power and torque at lower RPM. Maximum torque value is 395 Newton-meters (Nm), and continuous torque supply of 179.84 Nm. This motor will be paired with an integrated brake transistor and resistor, to further increase torque measurement accuracy.

Northwest Motion includes free software for PC's for control of the drive motor, as well as data read-outs and acquisition. They can also develop software that will integrate additional parameters (pump rate, cuttings injection, data management) for an additional fee, however at this time, individual software packages will be sufficient in order to maintain low costs.

A full description of the Indradrive motor can be found in 7.15.

4.7.2. Pipe Assembly/Disassembly

Given that this flow loop is designed to handle various sizes of drill strings, a means of assembling, disassembling, and torquing drill pipes must be determined. The American Petroleum Institute (API) recommended practice 7G outlines recommended make-up torque for drill pipe (API, 2004), and for the range of drill pipe expected within this flow loop, Table XXVI outlines expected make-up torque requirements. API does not list minimum make-up torque for 5.875" drill pipe, however for reference, NOV manufactures a 5.875" range 2 drill pipe with a minimum make-up torque of 47,200 ft-lb.

Table XXVI: API Make-up torque recommendations

Drill Pipe Nominal Size (in.)	New Tool Joint Make-up Torque (ft-lb)	Premium Tool Joint Make-up Torque (ft-lb)	Class 2 Make-up Torque (ft-lb)
4.5" 16.60 lb/ft	20,620-26,969	11,590-21,230	10,072-18,367
4.5" 20.00 lb/ft	30,620-34,520	13,815-25,569	12,085-21,914
5" 19.50 lb/ft	22,361-43,328	15,776-28,737	14,082-24,645
5" 25.60 lb/ft	26,674-47,230	20,127-35,446	17,127-30,943
5.5" 21.90 lb/ft	33,412-52,059	19,172-35,446	17,127-30,943
5.5" 24.70 lb/ft	33,412-52,059	22,294-38,901	19,172-33,180
6.875" 25.20 lb/ft	43,934-65,012	26,810-48,204	24,100-42,312

In reviewing all expected torque requirements for a variety of drill strings, the torque range required for assembling drill strings is between 10,000-65,000 ft-lb.

The most common method for torquing drill string components in a shop-setting is a stroking unit. These units are capable of torquing connections within a large range (200-200,000 ft-lb), and often have fixed headstock and traveling tailstock to allow for the movement of joints. Several options are available on the market, from vendors such as Forum Energy Services, and Enerquip. Forum offers a fully rotational torque machine that would comfortably satisfy the requirements of this flow loop. Figure 34 displays this unit, and additional information can be found in 7.16.



Figure 34: FORUM Energy Services fully rotational torque machine

4.8. Fluids Management System

4.8.1. Storage and Mixing Equipment

The storage and mixing facility design must be large enough to accommodate a minimum of double the volume of the flow loop, to allow for adequate filling, and flushing of the flow loop, as well as storage of the entirety of the flow loop volume pre and post-experimental trials. Conventional premix tanks are often a minimum of 200 bbl and have excessive capacity for what is required. Conventional mud tanks allow for the housing of solids control equipment (a requirement discussed further in this document) but are designed to handle even larger volumes (1000+ bbl).

Previous calculations confirmed that flow loop fluid requirements total approximately 26 bbl, plus additional surface line volume. Adequate fluid storage design would be a small storage tank with a minimum of 3 separate compartments for different fluid mixtures. These compartments must be individually accessible for both mixing and pumping to the flow loop and much like a conventional mud tank, one compartment would be set up to handle solids control

equipment, receiving drilling fluid separated from cuttings. The additional 2 compartments must contain some form agitators or paddle mixers to ensure no settling occurs. These tanks must also be designed with enough capacity to store the maximum volume required to fill the entire system, while remaining above the suction inlet.

In order to maintain minimum suction pressure on the suction line located at the bottom of conventional premix tanks, an excess volume must always remain in the tank. Table XXVII summarizes minimum capacity for the fluid storage tank, based on fluid storage capability of both a testing fluid (drilling mud) and a flushing fluid (likely water).

Table XXVII: Minimum tank capacity

Compartment 1	Compartment 2	Compartment 3	Total tank capacity
50	50	50	150

A conventional mixing room is a key requirement and must contain a mud mixer-hopper. Mixing hoppers are most commonly a venture-type jet mixer (Figure 35) that allows solids to be integrated into a high-speed liquid flow. This fluid velocity is obtained using a centrifugal mixing pump. This mixing pump must be designed with adequate power to circulate the entirety of the fluids storage system.

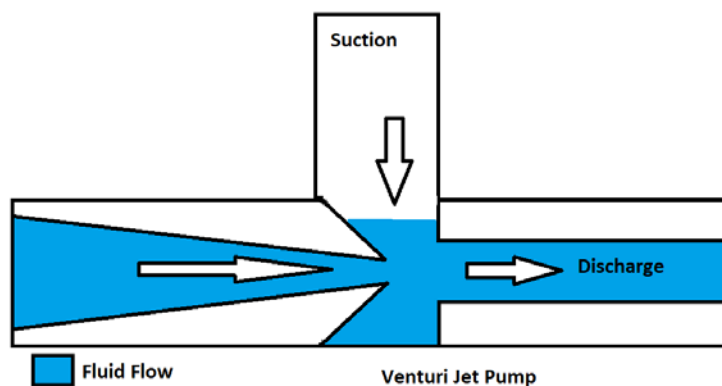


Figure 35: Venturi jet pump design

4.8.2. Flow and circulation lines

The flow and circulation system design will allow for the circulation of fluids throughout the entire flow loop system. This includes the storage tank, flow loop test and return section, and cuttings injection tank. The circulation system can be divided into 2 primary sections; the drain system and the filling/circulation system.

4.8.2.1. Drain System

The drain system component of the circulation system will consist of the lines connecting the flow loop return line to the solids control equipment. This line be 8 inches ID to match the return line system and will be a direct line to the solids control system located on the fluid storage tanks. Although exact dimensions and pipe specifications have been allocated to future work, Figure 36 and Figure 37 display the direct line from the flow loop return line to the solids control equipment. The drain lines and solids control equipment are highlighted in orange, coming off the inlet/power section of the flow loop test section and connecting to the fluid storage tank (in green).

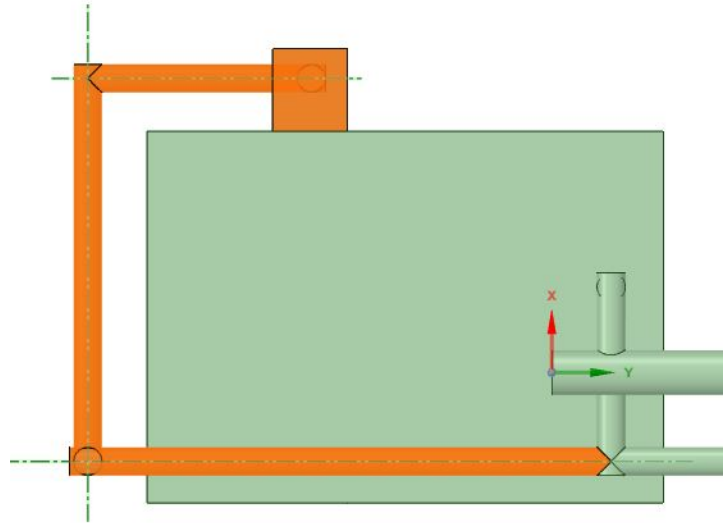


Figure 36: Drain line front view

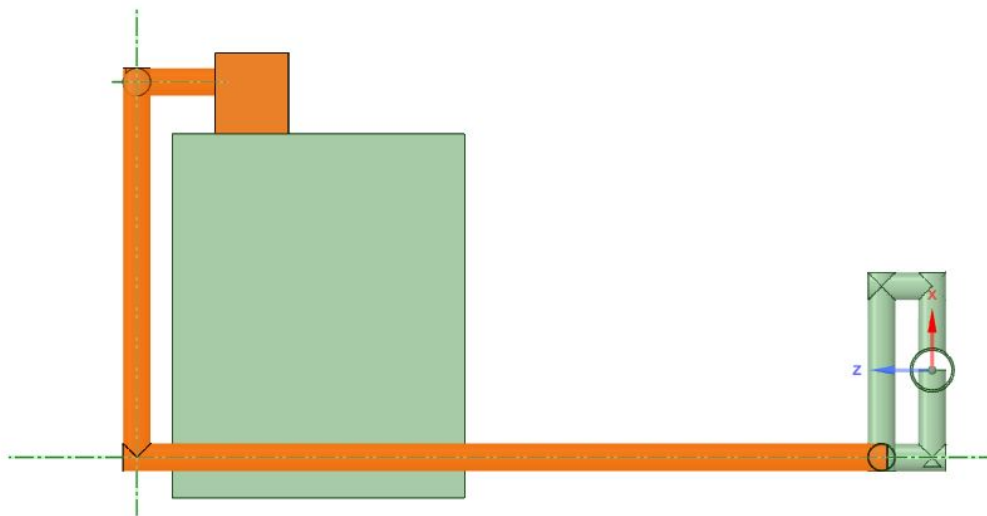


Figure 37: Drain line side view

4.8.2.2. Filling/Circulation System

The filling and circulation system is considerably more complex in design in comparison to the drain system and consists of circulation lines from the storage tank to the flow loop test section. This filling system will also house the fluid circulating pump (discussed in 4.6.1), which will be used for filling the flow loop for experimentation, providing a means for transportation of cuttings being injected to the test section, and providing fluid to adequately flush the flow loop test section after experimentation.

In order to prepare the flow loop test section for experimentation, flow will travel from the fluid storage tanks in a direct line to the flow loop inlet (Figure 38, Figure 39, highlighted in orange). Future work will entail dimensions, pipe specifications, and any additional fill lines to the flow loop system. However, initial design parameters include either 5-inch or 8-inch ID pipe, as the piping must be large enough to transport cuttings with low risk of plug-off, but not too large as to require a large flow rate to overcome settling velocity of cuttings.

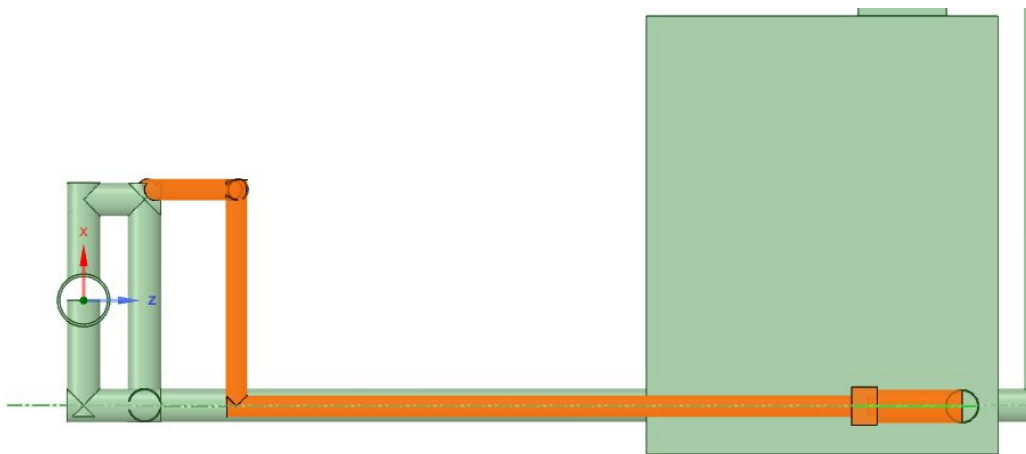


Figure 38: Side view, fill line to inlet

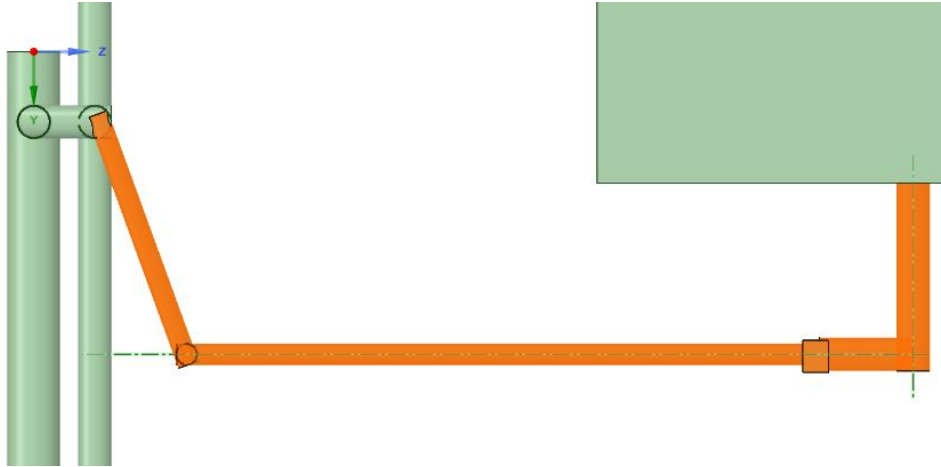


Figure 39: Top view, fill line to inlet

The fill line will also be fitted with both a return circulation and pressure relief bypass system, located prior to the cuttings auger that will allow for the recirculation of fluid to the storage tank in the event cuttings clog the circulation line.

Additional circulation and bypass lines may be required for functions such as flushing of the flow loop system, assistance in cuttings transport from solids control to the injection tank, and fluid injection into the cuttings injection tank.

4.9. Cuttings Management System

4.9.1. Cuttings Separation

In order to adequately separate the cuttings from drilling fluid post-experimental runs, several options were considered and graded on feasibility. Given that drilling fluids will not be subjected to additional fines during experimentation, primary solids control is all that is required for this flow loop (no centrifuges, degassers, mud conditioners, etc.). Shale shaker technology is the most common for separating cuttings from drilling fluid, however other options such as the Mudcube™ were also considered. After a high-level comparison between conventional shale shaker technology and the Mudcube (Table XXVIII), the second was a more optimal fit. The

Mudcube has a reduced weight/footprint and contained design minimizing exposure to fumes and drilling mud splashing. Additional benefits include increased solid removal efficiency and less fluids contamination.

Table XXVIII: Shale shaker vs Mudcube

Specification	Mudcube	NOV King Cobra Shale shaker
Dimensions (L/W/H) (in)	104.6/84.3/70.4	120.25/66.375/66
Weight (lb)	3637	4800
Hydraulic capacity (gpm)	1100	<1000, dependent on fluid/angle
Vacuum Pump Airflow (cfm)		706
Vibration	None	High, 2 vibra-motors, linear or elliptical
Noise	Low	High
Fume Exposure	None	High
Splashing of fluids	None/low	Medium

Technical data of the MudCube unit can be found in Table XXIX, and it is important to note that hydraulic capacity is 1100 gpm, which will exceed the minimum fluid velocity to ensure cuttings removal in the 8 inch inlet of 200 ft/min. Solids control will only be used post-experimental procedures, and maximum flow rates are not required. Table XXX outlines fluid velocities based on high and low flow rate ranges. It can be confirmed that at no time will fluid velocity will drop below minimum 200 ft/min required velocity to transport cuttings within the 8-inch return line.

Table XXIX: Mudcube specifications

MudCube Specifications	Imperial Values
Unit dimensions (L/W/H, in)	104.6/84.3/70.4
Weight (lb)	3637
Hydraulic capacity (gpm)	1100
Vacuum Pump Airflow (cfm)	706
Body material	316 L Stainless steel
Electrical Power Supply 440 (690 VAC, 50/60 Hz)	2+15
Air Supply	230 cfm @ 87 psig

Table XXX: Fluid velocities summary

	Linear velocity based on 1250 gpm flow rate (ft/min)	Linear velocity based on 1100 gpm flow rate (ft/min)	Linear velocity based on 800 gpm flow rate (ft/min)
12.25" ID	265	233	170
8" ID	480	421	305

The additional advantages of installing a Mudcube is to allow rapid separation of cuttings from drilling fluid, if an open-loop experiment is performed. However, if time is not a factor, the cuttings laden slurry can be routed to a steel-mesh bottomed drainage tank, allowing for slow filtering of drilling fluid to a secondary tank over an extended period. The capacity of this tank must be a minimum of 40 bbl.

4.9.2. Cuttings Storage and Injection

An important component of the flow loop design is the successful implementation of cuttings into the flow stream, and this can most effectively be achieved using an auger system. This auger system will be run in-line with the fluid circulation system leading to the flow loop and will allow for the introduction of cuttings to the flow stream immediately prior to entering the flow loop test section. Basic grain auger systems can be implemented, although careful design must be taken to ensure auger blade is large enough to prevent plugging. Cuttings concentration can be calculated based on auger size and speed, allowing for the proper solids concentration to be achieved within the test section prior to experiments.

Upon separation from drilling fluids via solids control, or upon initial storage of cuttings for experimentation, cuttings are to be stored in a vented, hopper-style tank. The hopper design will allow cuttings to funnel to the auger at the bottom outlet through gravity assist, lessening the likelihood of auger failure. This tank must be large enough to contain enough drilled cuttings to supply the flow loop with in excess of 50% cuttings concentration by volume (13 bbl equivalent) with an approximate 50% overage as a safety factor. Drilled cuttings will likely need to be transported via pumping after separation from drilling fluid and will be mixed with a small

concentration of drilling fluid. This overage in design will allow the addition of drilling fluids to the cuttings, and aid in injection of cuttings to the flow line.

Table XXXI displays overall design characteristics of the cuttings system, including solids control, injection method and storage tank specifications.

Table XXXI: Cuttings management system specifications

Solids control	Mudcube
Cuttings injection style	Auger system
Cuttings storage tank type	Hopper
Tank volume (bbl)	30
Vented tank?	Yes
Outlets	2 (drain, auger)
Inlets	2 (cuttings, fluid)

4.10. Data Acquisition, Monitoring and Controls systems

One of the most critical components of the flow loop design is the data monitoring and acquisition system. In order to ensure confirmation of experiments, enough data collection and monitoring must be installed. In addition, a centralized control system must be designed to allow synchronous functionality of the flow loop in both open-loop and closed-loop setup. The following section describes in detail these ancillary systems.

4.10.1. Monitoring Systems

Several parameters within the flow loop must always be monitored. Some are relevant to experimental procedure, others to generalized operation of the flow loop. The scope of this thesis is focused solely on data monitoring systems on the flow loop test section.

Monitoring systems include flow meters, pressure transducers, visualization methods (cameras) and tracking systems such as PIV.

1. Pressure monitoring: Pressure changes and variations are an important measurement that must be recorded throughout the flow loop test section, at various intervals. It is recommended that pressure transducers be placed not only along the length of the

flow loop test section, but at multiple locations along the vertical plane of the casing to identify pressure drops seen by channeling of high viscosity fluid and drill string location. Pressure transducers sets, consisting of 4 units placed on the vertical plane (top of casing, bottom of casing, and both sides of casing, Figure 40, orange) will identify pressure differential between pipe zones. These sets should be at locations along the test window, ensuring pressure monitoring is occurring at regular intervals and observes pressure over both pipe body and pipe tool joints. Table XXXII indicates recommended spacing of pressure transducers, based on overall length of the test window (60 ft.). Most pressure transducers can be implemented to record information in real-time and display on an interface with additional parameters.

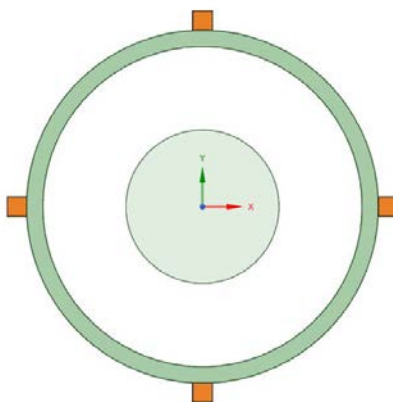


Figure 40: Transducer locations on casing

Table XXXII: Pressure transducer set location along test window

Pressure Transducer Set	Location on Test Window
1 (pipe body)	0
2 (tool joint)	15
3 (pipe body)	30
4 (pipe body)	60

2. Flow measurement: Another important component to ensuring proper testing is the measurement of flow. It is important that an appropriate flow measurement tool is

- selected to ensure accurate readouts. It is possible due to the solids concentration of some experiments, some flow meters such as orifice meters, turbines and vortex flow meters may become clogged and inaccurate. Ultrasonic or Doppler-type flow meters are non-invasive, do not restrict flow (no observable pressure drop from measurement), and are ideal for measuring slurry. It is recommended that one ultrasonic flow meter be installed on both the test section (at the beginning of the test window), and one on the discharge side of the return pump to measure flow rates in both lines. In addition, a mass flow rate meter should be installed on the inlet, to monitor mass flow of the test. This will facilitate monitoring cuttings concentration. This data can also be recorded and displayed on a centralized interface.
3. Visualization and recording: Another important attribute for monitoring cuttings transport within this flow loop is visualization and observation of individual cuttings. Basic HD video recording devices will be implemented to visualize cuttings movement and changes in transport efficiency based on factors such as drill pipe RPM and flow rate, but more complex methods of recording should also be installed, such as radioactive tracers. Transit time of radioactive tracers can be measured externally through the use of a radioisotope tracer or tracers located along the flow path (Turtiainen, 1986). Particle Image velocimetry measurement can be used in conjunction with multiple CCD (charged coupled device) cameras, to record velocity of cuttings. One field-based method for utilizing radioactive tracers in completions is Core Laboratories Spectra Stim technology, which consists of non-soluble tracer metals to ceramic proppants. Additional information on this technology can be found in 7.17.

Table XXXIII summarizes all data monitoring systems recommended for installation within this flow loop.

Table XXXIII: Summary of data monitoring systems

Monitoring Type	Number of systems
Pressure transducer (set of 4)	4
Flowmeters	2 (ultrasonic) 1 mass flow
HD video camera	1 (mobile)
Tracer System	1 injection port 5 Radioisotope tracers (1/15 ft)
PIV System	1 Stereo type (3-velocity) 2 CCD or CMOS image sensor

5. Discussions and Conclusions

The knowledge obtained through flow loop experimentation has been proven through various studies referenced in this document, and the oil and gas industry has seen many advantages and breakthroughs thanks in part to these past studies. However, there is still much that is not understood surrounding drill string rotation on cuttings transport in non-Newtonian flow, and no flow loop has been able to successfully recreate the industry-recognized increase in cuttings transport efficiency observed at both 120 and 180 RPM ranges. The continued development, completion and installation of this flow loop will allow greater access to the understanding of effects of drill pipe rotation on cuttings transport in large diameter horizontal wellbores.

Many studies have identified the relevance and importance of drill string rotation on cuttings transport, but none conclusively determine cause and effect. This flow loop will be the first of its kind that can manipulate both drill string sizes and drill string position within the test section, while being able to rotate at speeds in excess of 200 rpm. This will vastly increase its operating and research capabilities.

5.1. Design Implications

The advantages of designing a large diameter horizontal flow loop capable of high flow rates, high drill string RPM, drill string interchangeability, and variable drill string centralization will offer a large expanse of research opportunities. This flow loop will exhibit all the characteristics required to recreate the step-changes in cuttings transport efficiency, and with the ideal data acquisition and monitoring equipment installed, quantifiable solutions may be obtained leading to real world predictive models and working correlations. In addition, a robust and

refined version of the CFD model completed for this thesis will aid in the validation of experimental procedures.

Additional benefits from this research expand out from the initial scope of the thesis. The design of a flow loop model calibrated to the current on-campus vertical 2-inch flow loop can be used with several single and multiphase flow regimes to validate experimental procedures. This model can be used to assist in validating future experiments involving multiphase (gas/water) flow, and the current parameters will be transferrable to model both the on-campus 0.75-inch and 0.5-inch flow loops, once operational.

5.2. Flow Loop Design Summary

The result of this research and development is a high-level flow loop design that identifies optimal testing section size requirements, pump requirements, fluid handling capability, cuttings management and power systems, as well as data monitoring and acquisition systems. The design presented in this thesis will provide the framework for the continued development of a final flow loop design. Table XXXIV provides a summary of the flow loop parameters, in tabular form.

Table XXXIV: Flow loop design parameters summary

Flow Loop Test Section	
Test section ID (in)	12.25
Test section length (ft)	120
Test section maximum volume (bbl)	17.5
Return line ID (in)	8.0
Return line length, including elbows (ft)	136
Return line maximum volume (bbl)	8.5
Maximum flow loop capacity (Test section/return) (bbl)	26
Pump type	Rotodynamic centrifugal slurry
Optimized flow rate range (gpm)	800-1300
Fluid Circulation System	
Pump type	Centrifugal
Minimum pump displacement (gpm)	600
Drain/discharge line ID (in)	8
Circulating line minimum ID (in)	5
Additional design requirements	Return circulation line Pressure relief line
Power Components	
Drill string motor type	Bosch-Rexroth MAD electric
Drive series	IndraDrive M HMS01
Main voltage	480 V
Drill string torque equipment	Fully rotational torque machine
Fluids Management System	
Storage tank compartments	3
Storage tank total capacity	150
Mixing equipment	Mixing hopper 60 hp (min) mixing pump Paddle mixers for 2 of 3 compartments Mixing gun line
Cuttings Management System	
Solids Control	Mudcube
Cuttings storage	30 bbl Hopper-style vented tank
Cuttings injection equipment	Sealed grain-auger
Data Acquisition, Monitoring and Control Equipment	
Pressure transducer (set of 4)	4
Flowmeters	2 (ultrasonic) 1 mass flow
HD video camera	1 (mobile)
Tracer System	1 injection port 5 Radioisotope tracers (1/15 ft)
PIV System	1 Stereo type (3-velocity) 2 CCD or CMOS image sensor

The development of this flow loop required substantial computer modeling utilizing ANSYS Fluent CFD software in order to properly identify flow normalization at both the inlet and outlet. Several designs were developed and compared to determine optimal sizes and angles. In addition, several base models of a flow loop test section were developed, utilizing realistic drill pipe dimensions. These models can exhibit axial drill string rotation, and 3 models were constructed. These models differ from one another through the location of the centerline of the drill string within the flow loop section to recreate real downhole conditions. All flow loop models were developed as single-phase, non-Newtonian flow models using field-based drilling fluid numbers, and can be further modified to incorporate two-phase, liquid/solid flow.

In order to validate these CFD models, simulations were designed and tested against the current on-campus vertical flow loop. This resulted in several flow loop designs modeling the 2-inch vertical flow loop. These designs are unique, based on the number of phases modeled. The single phase CFD models host only one inlet/outlet, wherein the multiphase models host two inlets (one for each phase), and a slightly longer length to ensure pressure comparisons can still be validated. This allows for the injection of air into the water stream, and more accurately represents the physical flow loop design.

Table XXXV outlines the high-level design parameters for each CFD model.

Table XXXV: CFD Models summary

CFD Modeling Software	
CFD software	ANSYS Fluent
License type	Academic (Trial)
Vertical Flow Loop (single phase)	
Length (ft)	42
Tube ID (in)	2
Tube OD (in)	2.325
Inlet type	Velocity
Outlet type	Pressure
Refined mesh?	NO
Vertical Flow Loop (multiphase)	
Length (ft)	42
Tube ID (in)	2
Tube OD (in)	2.325
Inlet type	Velocity
Outlet type	Pressure
Refined mesh?	YES
Phases	Water Air
Mixture Simulation type(s)	VOF Mixture Eulerian
Horizontal Flow Loop Test Section	
Length (ft)	60
Outer casing ID (in)	12.25
Outer casing OD (in)	13.5
Inner drill pipe OD (in)	5.5
Inner drill pipe tool joint OD (in)	5.875
Inlet type	Velocity
Outlet type	Pressure
Refined mesh?	YES
Multiphase? (liquid/solid)	NO
Drill Pipe Location(s)	Centered Bottom Low side

5.3. Future Work

The design proposal and CFD models outlined in this thesis are a groundwork for several future projects outline below. This work can be subdivided into two categories: flow loop design and CFD model refinement. The following sections outline a detailed dissection of future work that is required for each category.

5.3.1. Flow Loop Design Refinement

The flow loop design presented in this thesis outlines minimum dimensions, volumes, flow rates and power requirements. Armed with these parameters, future development will include refinements on several areas.

5.3.1.1. Equipment Design and Selection

Although this thesis outlines generalized dimensions for many sections of the flow loop (Table XXXIV), this design requires refinement and finalized product selection and pricing. Several component properties must be also determined, highlighted in the following sections.

Table XXXVI outlines the areas that require future development, and the following sections will discuss in more detail these areas.

Table XXXVI: Summary of future design work for flow loop

Pipe and Casing	
Test section	<ul style="list-style-type: none"> • Pipe classification • Test window material • Pipe connections
Circulation system	<ul style="list-style-type: none"> • Pipe classification • Pipe ID • Pipe connections • Pipe flow path
End Caps	<ul style="list-style-type: none"> • Complete design allowing pipe rotation and axial location adjustment
Pumps	
Test section pump	<ul style="list-style-type: none"> • Finalize pump design with manufacturer
Circulation pump	<ul style="list-style-type: none"> • Design inlet, outlet and head requirements based on circulation system design
Mixing pump	<ul style="list-style-type: none"> • Select optimal mixing pump for mixing and storage tank
Fluid Storage	
Storage tanks	<ul style="list-style-type: none"> • Finalize dimensions of tanking system • Determine mixing system • Design fluid circulation system • Design installation of Mudcube
Cuttings Management	
Solids control	<ul style="list-style-type: none"> • Implementation of Mudcube in mud tank design
Cuttings storage and injection	<ul style="list-style-type: none"> • Hopper tank dimensions finalized • Auger system design • Cuttings return system
Centralized controls	
Power supply	<ul style="list-style-type: none"> • Develop central control board for pumps, motors, auger
Controls Equipment	<ul style="list-style-type: none"> • Select optimal equipment to measure pressure, flow • Identify ideal location for PIV, CCD, HD Camera • Design data management software • Design data storage mainframe
Additional Equipment	
Pipe Equipment	<ul style="list-style-type: none"> • Pipe handling equipment (crane, forklift) • Pipe storage
Shipping and receiving	<ul style="list-style-type: none"> • Bay access for shipping and receiving of materials and equipment • Supplemental storage for fluids and solids for premix
Facility design	<ul style="list-style-type: none"> • Facility capable of housing all equipment • Temperature controlled • Adequate power and ventilation
Spill mitigation	<ul style="list-style-type: none"> • Proper spill containment, sump
Operational/HSE	
Operations Manual	<ul style="list-style-type: none"> • Design of complete operations manual • ERP plan design • Maintenance schedule • Hazardous materials handling procedures

5.3.1.1.1. Pipe and Casing

Although dimensions for the flow loop test section, return, and fluid circulation systems have been identified, material and classification of all piping is still required. In addition, refinement is required in the circulation system to ensure optimal performance for filling and draining the flow loop. Optimal circulation line diameters must also be determined and are directly related to final pump selection dimensions.

5.3.1.1.2. Flow Loop End Caps

A crucial component of the flow loop are the end caps that will allow for the adjustment of drill pipe location within the casing, while maintaining a seal during high RPM rotation. Although basic design requirements have been laid out in this thesis, further research and design must be completed to develop optimal end plates.

5.3.1.1.3. Fluid Pumps

Pump design and selection must be finalized, based on flow specifications for the flow loop test section, flow circulation system and mixing equipment. The flow loop test section pump parameters have been adequately calculated and this information can directly be translated to vendors for pump recommendations. However, additional development must be undertaken to select the proper fluid circulation system pump, as its requirements will be based on the final circulation system design. In addition, the mixing pump design will be incorporated into the complete fluid storage and mixing tank assembly.

5.3.1.1.4. Fluid Storage

The minimum fluid handling capacity of the fluid storage facility has been determined, as well as minimum required handling compartments. Continued design into optimal dimensions of this fluid storage tank must be completed, to optimize use of space, hydraulic head supply (for

circulation pump) and installation and handling of solids control equipment. This final design will include dimensions, internal piping (including flow lines for mixing and circulating), mixing and agitating equipment, volume monitoring equipment and safeguards (railings, etc.).

5.3.1.1.5. Cuttings Management

The optimal solids control equipment has been determined for this flow loop, however the dimensions of the Mudcube must be referenced directly in the design of the fluids storage tank, circulation and return system, and cuttings tank/auger combination.

The cuttings storage and injection system (auger) must be further developed, and a means of returning cuttings to the tank from solids control must also be determined. In addition, a closed-system auger must be selected and designed in such a way that it can precisely introduce cuttings to the flow regime in a controlled manner and be accessible for maintenance and clearing of any fouling/clogging.

5.3.1.1.6. Centralized Controls System

It is important that all powered equipment is designed to run from a central control panel (480V preferred), that is easily accessible and shielded. This centralized control panel will be responsible for powering pipe handling equipment, drive motors, pumps, solids control equipment and any additional power requirements.

A computer mainframe system must also be designed and developed in order to handle the many functions required for the flow loop. This computer system must also have a customized software package that can monitor the high volume of data (pressure transducers, flow rates, CCD/PIV information and displaying it in a fashion that is understandable. Several software packages can perform this task, such as FLO-CAL, LabView (by National Instruments),

and MyOpenLab. Software design and development must be an integral part of the data acquisition and monitoring refinement.

Further research must be undertaken to determine the location and installation of data acquisition methods on the flow loop test section.

5.3.1.1.7. Additional Equipment

Additional equipment required to effectively operate the flow loop in a safe manner must be designed, developed or selected upon completion of the flow loop design. This includes equipment such as pipe handling and storage, spill mitigation and drains, facilities, and environmental management (fluid and cuttings storage and disposal techniques).

5.3.1.2. Operating Guidelines, HSE

Alongside the development of the physical flow loop model, general operating practices must be developed to ensure safe operation of all components of the flow loop. This includes experimental procedure, experimental preparation, and maintenance and draining of the flow loop. It is important that detailed work guidelines are in place to ensure safe practices are always adhered to during operation.

Maintenance schedules must also be developed in conjunction with equipment supplier guidelines.

5.3.2. CFD Model Refinement

The most important step that will be required in order to continue to develop and refine all previously discussed flow models will be the purchase of a minimum of one professional or academic license of ANSYS Fluent. The entirety of the CFD modeling performed during this thesis was completed on a time-dependent trial-license, which will no longer be active after the release of this document. For future work, this license will be required. Montana Tech currently

owns licenses to Workbench, SpaceClaim, Meshing and several other ANSYS programs, but Fluent is the modeling software use for these models and is required for future work.

Upon obtaining Fluent license(s), development can continue on both the vertical flow loop and horizontal flow loop designs.

5.3.2.1. Vertical Flow Loop Models

Although the initial models for both single-phase and multiphase flow are complete, continued refinement can be continuously developed on both ends. For single phase modeling, additional wall interface manipulation can occur to ensure more accurate representation of wall slip is occurring during simulations. In addition, research can be performed into enabling the display of head loss due to elevation change, a parameter that is automatically disabled by Fluent in single-phase flow.

For multiphase flow models, primary focus is to appoint a dedicated computer for simulation runs. As discussed in 4.1.2, transient simulation models require a very large amount of computing time and power to model, and given the dimensions of the flow loop and flow rate, considerable time is spent running one single simulation to reach completion. In addition, significant memory storage is required to provide detailed data throughout the simulation.

Continued refinement into the utilization of the Eulerian, VOF (volume of fluid) and mixture models must be explored as VOF is the only multiphase model regime explored during this thesis. There are several variable parameters within each of these calculation methods, and Eulerian is by far the most complex. Multiphase models completed during this thesis are basic representations of 3 different multiphase flows, and the results comparison to actual experimental data indicate that these models require more refining. Optimal multiphase model boundaries can also be further developed, based on phase-boundaries (bubble, slug, churn, mist),

as some models are more effective than others. Table XXXVII displays a broad recommendation for modeling techniques for flow regimes.

Table XXXVII: Multiphase method assignments

Flow Regime	Multiphase Model
Bubble	Mixture
Slug	VOF
Churn	Mixture or Eulerian
Droplet/Mist	Eulerian

5.3.2.2. Horizontal Flow Loop Models

Continued development must occur for refining the current horizontal flow loop models and can be subdivided into pre and post flow loop construction. Additional development of fluid properties, material definitions and boundary conditions will allow for more accurate results, as non-Newtonian fluids exhibit vastly different shear characteristics than Newtonian fluids, and fluid/wall interfaces can adversely affect outcomes if not properly designed. Current models use default steel parameters for both drill string and casing walls.

All horizontal flow loop models must incorporate multiphase flow regimes through the incorporation of drilled solids. This solid/liquid multiphase model is entirely different than previously modeled gas/liquid mixtures and requires a different approach. This multiphase flow model recommendation may vary drastically from liquid/gas models, and entirely dependent on solids properties (granular vs. non-granular).

Drilling fluid models utilized for the modeling in this thesis did not take into consideration enthalpy, and the complete energy equation was not used for calculations. Future work would entail developing additional parameters for these fluid models, allowing them to exhibit realistic reactions to temperature and additional energy changes if heat transfer is a parameter required for future experiments.

Upon completion of the physical flow loop, these complete models can then be compared to experimental data, further refined, and used to begin to develop working correlations to be used for real-world predictions and advanced wellbore modeling.

6. References Cited

- Agbaji, A. L. (2011). Optimizing the Planning, Design and Drilling of Extended Reach and Complex Wells. Society of Petroleum Engineers. <https://doi.org/10.2118/149099-MS>
- Ahmed, R. M. (2001). *Mathematical Modeling and Experimental Investigation on Solids and Cuttings Transport*. Norwegian University of Science and Technology.
- Alfsen, T. E., Blikra, H. (SPE), & Tjotta, H. (Statoil A. (1995a). *Pushing the Limits for Extended Reach Drilling: New World Record from Platform Statfjord C, Well C2. SPE Drilling & Completion*.
- Alfsen, T. E., Blikra, H., & Tjotta, H. (Statoil A. (1995b). Pushing the Limits for Extended Reach Drilling: New World Record From Platform Statfjord C, Well C2. *SPE Drilling & Completion*, (June), 71–76.
- Allen, F., Tooms, P., Conran, G., Lesso, B., & Slijke, P. Van De. (1997). Extended-Reach Drilling : Breaking the 10-km Barrier. *Oilfield Review, Winter*, 32–47.
- API. (2004). *Recommended Practice for Drill Stem Design and Operating Limits*.
- API. (2009). *API Recommended Practice 13D - Rheology and hydraulics of oil-well drilling fluids*.
- Bhalla, K. (1996). Achieving Extended Reach. Society of Petroleum Engineers. <https://doi.org/10.2118/36347-MS>
- Bilgesu, H. I., Ali, M. W., Aminian, K., & Ameri, S. (2002). Computational Fluid Dynamics (CFD) as a Tool to Study Cutting Transport in Wellbores. Society of Petroleum Engineers. <https://doi.org/10.2118/78716-MS>
- Bilgesu, H. I., Mishra, N., & Ameri, S. (2007). Understanding the Effect of Drilling Parameters on Hole Cleaning in Horizontal and Deviated Wellbores Using Computational Fluid Dynamics. Society of Petroleum Engineers. <https://doi.org/10.2118/111208-MS>
- BOEM. (2017). Hilcorp Alaska LLC.
- Bogdanov, S., Deliya, S., Latsin, D., Akhmetov, M., Gagaev, Y., & Udodov, A. (2012). Drilling world-class ERD wells in the North Caspian Sea. Society of Petroleum Engineers. <https://doi.org/10.2118/162099-MS>
- BP Exploration, A. (2007). *Liberty Development Project - Development and Production Plan*.
- Britannica, E. (2018). Shear Stress. Retrieved September 9, 2018, from <https://www.britannica.com/science/shear-stress>

- Brown, N. P., Bern, P. A., & Weaver, A. (1989). Cleaning Deviated Holes: New Experimental and Theoretical Studies. Society of Petroleum Engineers. <https://doi.org/10.2118/18636-MS>
- Cai, J., Gao, Y., Zhang, M., Cui, L., & Guo, H. (2014). Solution to Cement Integrity Evaluation in Long Extended Reach Wells: New Record in South China Sea. Offshore Technology Conference. <https://doi.org/10.4043/25027-MS>
- Cameron, C. (2001). Drilling Fluids Design and Management for Extended Reach Drilling. Society of Petroleum Engineers. <https://doi.org/10.2118/72290-MS>
- Chen, X., & Gao, D. (2016). Mega-Extended-Reach Drilling to Deepwater Target: What is the Well's Maximum Allowable Measured Depth While Drilling? Society of Petroleum Engineers. <https://doi.org/10.2118/183025-MS>
- Cheung, E., Takach, N., Ozbayoglu, E., Majidi, R., & Bloys, J. B. (2012). Improvement of Hole Cleaning Through Fiber Sweeps. Society of Petroleum Engineers. <https://doi.org/10.2118/154759-MS>
- Chhabra, R. P., & Richardson, J. F. (2008). *Non-Newtonian Flow and Applied Rheology* (2nd ed.). Oxford: Butterworth-Heinemann.
- Clark, R. K., & Bickham, K. L. (1994). A Mechanistic Model for Cuttings Transport. Society of Petroleum Engineers. <https://doi.org/10.2118/28306-MS>
- Cocking, D. A., Bezant, P. N., & Tooms, P. J. (1997). Pushing the ERD Envelope at Wytch Farm. Society of Petroleum Engineers. <https://doi.org/10.2118/37618-MS>
- Coley, C. (BP). (2015). *2015 Oil Field Industry Drilling Envelope*.
- Courant, R., Lewy, H., & Friedrichs, K. (1928). About the Partial Difference Equations of Mathematical Physics. *Mathematical Annals*, 756.
- Devenish, G. (Baker H. I., Dirksen, R. (Halliburton), Dow, B. (Schlumberger), & Maingot, C. (Weatherford). (2015). Directional Drilling. In C. (Cobalt I. E. Butler, B. (Cobalt I. E. Gabourie, C. (Consultant) McCartney, & L. L. (Schlumberger) Vieira (Eds.), *IADC Drilling Manual* (12th ed., p. 36). Houston: IADC.
- Dewangan, S. K., & Sinha, S. L. (2016). On the effect of eccentricity and presence of multiphase on flow instability of fully developed flow through an annulus. *Journal of Non-Newtonian Fluid Mechanics*, 236, 35–49. <https://doi.org/https://doi.org/10.1016/j.jnnfm.2016.08.008>
- Doan, Q. T., Oguztoreli, M., Masuda, Y., Yonezawa, T., Kobayashi, A., Naganawa, S., & Kamp, A. (2003). Modeling of Transient Cuttings Transport in Underbalanced Drilling (UBD).

<https://doi.org/10.2118/85061-PA>

- Dodge, D. W., & Metzner, A. B. (1959). Turbulent flow of non-Newtonian systems. *AIChE Journal*, 5(2), 189.
- Doron, P., & Barnea, D. (1993). A three-layer model for solid-liquid flow in horizontal pipes. *International Journal of Multiphase Flow*, 19(6), 1029–1043.
[https://doi.org/https://doi.org/10.1016/0301-9322\(93\)90076-7](https://doi.org/https://doi.org/10.1016/0301-9322(93)90076-7)
- Duan, M., Miska, S. Z., Yu, M., Takach, N. E., Ahmed, R. M., & Zettner, C. M. (2006). Transport of Small Cuttings in Extended-Reach Drilling. <https://doi.org/10.2118/104192-PA>
- Duan, M., Miska, S. Z., Yu, M., Takach, N. E., Ahmed, R. M., & Zettner, C. M. (2008). Transport of Small Cuttings in Extended Reach Drilling. Society of Petroleum Engineers. <https://doi.org/10.2118/104192-MS>
- Egenti, N. B. (2014). Understanding Drill-cuttings Transportation in Deviated and Horizontal Wells. Society of Petroleum Engineers. <https://doi.org/10.2118/172835-MS>
- Escudier, M. P., Oliveira, P. J., & Pinho, F. T. (2002). Fully developed laminar flow of purely viscous non-Newtonian liquids through annuli, including the effects of eccentricity and inner-cylinder rotation. *International Journal of Heat and Fluid Flow*, 23(1), 52–73.
[https://doi.org/https://doi.org/10.1016/S0142-727X\(01\)00135-7](https://doi.org/https://doi.org/10.1016/S0142-727X(01)00135-7)
- Ettehadi Osgouei, R., Ozbayoglu, M. E., Ozbayoglu, M. A., & Yuksel, E. (2010). Flow Pattern Identification Of Gas-Liquid Flow Through Horizontal Annular Geometries. Society of Petroleum Engineers. <https://doi.org/10.2118/129123-MS>
- Ford, J. T., Peden, J. M., Oyeneyin, M. B., Gao, E., & Zarrouh, R. (1990). Experimental Investigation of Drilled Cuttings Transport in Inclined Boreholes. Society of Petroleum Engineers. <https://doi.org/10.2118/20421-MS>
- Foster, B., & Krepp, T. (2007). Redefining the Offshore ERD Envelope: Techniques and Technologies Necessary for an Expanding Frontier. Offshore Technology Conference. <https://doi.org/10.4043/19064-MS>
- Glebov, E., Shokarev, I., Boroday, A., Grigoryev, M., Gulov, A., Zhudov, A., ... Gainullin, M. (2014). Drilling Record ERD Wells at Yamal Region. Society of Petroleum Engineers. <https://doi.org/10.2118/171328-MS>
- Gupta, V. P., Sanford, S. R., Mathis, R. S., DiPippo, E. K., & Egan, M. J. (2013). Case History

- of a Challenging Thin Oil Column Extended Reach Drilling (ERD) Development at Sakhalin. Society of Petroleum Engineers. <https://doi.org/10.2118/163487-MS>
- Gupta, V. P., Yeap, A. H. P., Fischer, K. M., Mathis, R. S., & Egan, M. J. (2014). Expanding the Extended Reach Envelope at Chayvo Field, Sakhalin Island. Society of Petroleum Engineers. <https://doi.org/10.2118/168055-MS>
- Hareland, G., Lyons, W. C., Baldwin, D. D., Briggs, G. M., & Bratli, R. K. (1998). Extended-Reach Composite-Materials Drillpipe. <https://doi.org/10.2118/37646-PA>
- Hilcorp. (2017). *Liberty DPP, Amended*.
- Husband, F. J., Bitar, G., & Quinlan, M. (2007). Extended Reach: New Generation Frontier Drilling Rigs. Offshore Technology Conference. <https://doi.org/10.4043/19067-MS>
- Institute, H. (2011). *American National Standard for Rotodynamic (Centrifugal) Slurry Pumps*. Parsippany: Hydraulic Institute.
- Jaffe, L., Maidla, E., Irrgang, R., & Janisch, W. (1997). Casing Design for Extended Reach Wells. Society of Petroleum Engineers. <https://doi.org/10.2118/38617-MS>
- Jellison, M. J., Chandler, R. B., Payne, M. L., & Shepard, J. S. (2007). Drillstring Technology Vanguard for World-Class Extended-Reach Drilling. Offshore Technology Conference. <https://doi.org/10.4043/18512-MS>
- Jellison, M. J., Payne, M. L., Shepard, J. S., & Chandler, R. B. (2003). Next Generation Drill Pipe for Extended Reach, Deepwater and Ultra-deep Drilling. Offshore Technology Conference. <https://doi.org/10.4043/15327-MS>
- Jerez, H., Dias, R., & Tilley, J. (2013). Offshore West Africa Deepwater ERD: Drilling Optimization Case History. Society of Petroleum Engineers. <https://doi.org/10.2118/163485-MS>
- Kamaruddin, S., Md Zin Che'apos;, L., Sering, L., Good, A., & Khun, L. H. (2000). Pushing the Envelope - Extending the Limits of Current Drilling Technology. Society of Petroleum Engineers. <https://doi.org/10.2118/64696-MS>
- Kefayati, G. H. R., Tang, H., & Chan, A. (2018). Immersed Boundary-Finite Difference Lattice Boltzmann method through fluid–structure interaction for viscoplastic fluids. *Journal of Fluids and Structures*, 83, 238–258. <https://doi.org/https://doi.org/10.1016/j.jfluidstructs.2018.09.007>
- Khan, M. U. (University of T. (2008). *Transient Cuttings Transport Focused on Bed Erosion for*

Horizontal Wells. University of Tulsa.

- Knott, D. (1998, January). BP Completes Record Extended Reach Well. *Oil & Gas Journal*. Retrieved from <http://www.ogj.com/articles/print/volume-96/issue-3/in-this-issue/drilling/bp-completes-record-extended-reach-well.html>
- Krueger, S., Sharpe, R., Attridge, W., & Ruzska, J. (2017). Introduction of New Drilling Technology Provides Continuous High Build Rate Capability in Complex Corkscrew Well Trajectory, Accessing Unswept Reserves in the North Sea. Society of Petroleum Engineers. <https://doi.org/10.2118/184639-MS>
- Larsen, T. I. (1990). *A Study of the Critical Fluid Velocity in Cuttings Transport*. University of Tulsa.
- Li, J., & Luft, B. (2014). Overview of Solids Transport Studies and Applications in Oil and Gas Industry - Experimental Work. Society of Petroleum Engineers. <https://doi.org/10.2118/171285-MS>
- Li, J., & Walker, S. (1999). Sensitivity Analysis of Hole Cleaning Parameters in Directional Wells. Society of Petroleum Engineers. <https://doi.org/10.2118/54498-MS>
- Lockett, T. J., Richardson, S. M., & Worraker, W. J. (2000). The Importance of Rotation Effects for Efficient Cuttings Removal During Drilling. Society of Petroleum Engineers. <https://doi.org/10.2118/25768-MS>
- Loureiro, B. V., Paula, R. S., Serafim, M., & Martins, A. L. (2004). Experimental Evaluation of the Effect of Drill String Rotation in the Suspension of a Cuttings Bed. Society of Petroleum Engineers. <https://doi.org/10.2118/122071-MS>
- Martin, M., Georges, C., Bisson, P., & Konirsch, O. (1987). Transport of Cuttings in Directional Wells. Society of Petroleum Engineers. <https://doi.org/10.2118/16083-MS>
- Martins, A. L., Sa, C. H. M., Lourenco, A. M. F., Freire, L. G. M., & Campos, W. (1996). Experimental Determination of Interfacial Friction Factor in Horizontal Drilling With a Bed of Cuttings. Society of Petroleum Engineers. <https://doi.org/10.2118/36075-MS>
- Martins, A. L., Santana, M., Gaspari, E., & Campos, W. (1998). Evaluating the Transport of Solids Generated by Shale Instabilities in ERW Drilling. Society of Petroleum Engineers. <https://doi.org/10.2118/50380-MS>
- Mason, C. J., & Judzis, A. (1998). Extended-Reach Drilling -- What is the Limit? Society of Petroleum Engineers. <https://doi.org/10.2118/48943-MS>

- McLoone, J. (2018). Closed Loop Systems. Retrieved from <http://fluidflowinfo.com/closed-loop-systems/>
- Meader, T., Allen, F., & Riley, G. (2000). To the Limit and Beyond - The Secret of World-Class Extended-Reach Drilling Performance at Wytch Farm. Society of Petroleum Engineers. <https://doi.org/10.2118/59204-MS>
- Mims, M. G., Krepp, A. N., & Williams, H. A. (2007). *Drilling Design and Implementation for Extended Reach and Complex Wells* (3rd ed.). Houston: K&M Technology Group.
- Mishra, P., & Tripathi, G. (1971). Transition from laminar to turbulent flow of purely viscous non-Newtonian fluids in tubes. *Chemical Engineering Science*, 26(6), 915–921. [https://doi.org/https://doi.org/10.1016/0009-2509\(71\)83051-8](https://doi.org/https://doi.org/10.1016/0009-2509(71)83051-8)
- Mitchell, R. F. (Halliburton), & Miska, S. Z. (University of T. (2011). *Fundamentals of Drilling Engineering* (1st ed.). Richardson: Society of Petroleum Engineers.
- Modi, S., Mason, C. J., Tooms, P. J., & Conran, G. (1997). Meeting the 10km Drilling Challenge. Society of Petroleum Engineers. <https://doi.org/10.2118/38583-MS>
- Mohammadesalehi, M. (Iranian C. O. C., & Malekzadeh, N. (Iranian C. O. C. (2001). Optimizat on of Hole Cleaning and Cutting Removal in Vertical, Deviated and Horizontal Wells.
- Mohammadesalehi, M. (Iranian C. O. C., & Malekzadeh, N. (Iranian C. O. C. (2011). Optimization of Hole Cleaning and CUtting Removal in Vertical, Deviated and Horizontal Wells. In *SPE Asia Pacific Oil and Gas Conference and Exhibition* (p. 8). Jakarta.
- Mott, R. L. (2006). *Applied Fluid Mechanics*. (D. Yarnell, Ed.) (Sixth). New Jersey: Pearson Education.
- Naganawa, S., & Nomura, T. (2006). Simulating Transient Behavior of Cuttings Transport over Whole Trajectory of Extended Reach Well. Society of Petroleum Engineers. <https://doi.org/10.2118/103923-MS>
- Naganawa, S., Oikawa, A., Masuda, Y., Tetsuo, Y., Hoshino, M., & Acuna, P. (2002). Cuttings Transport in Directional and Horizontal Wells While Aerated Mud Drilling. Society of Petroleum Engineers. <https://doi.org/10.2118/77195-MS>
- Naganawa, S., Sato, R., & Ishikawa, M. (2014). Cuttings Transport Simulation Combined With Large-Scale Flow Loop Experiment and LWD Data Enables Appropriate ECD Management and Hole Cleaning Evaluation in Extended-Reach Drilling. Society of Petroleum Engineers.

- <https://doi.org/10.2118/171740-MS>
- Nguyen, D., & Rahman, S. S. (1998). A Three-Layer Hydraulic Program for Effective Cuttings Transport and Hole Cleaning in Highly Deviated and Horizontal Wells. <https://doi.org/10.2118/51186-PA>
- Nixon, J. U., Nims, D., Rodman, D. W., & Swietlik, G. (1996). Extended Reach Drilling Limitations - A Shared Solution. Offshore Technology Conference. <https://doi.org/10.4043/8153-MS>
- Oates, K. M. N., Krause, W. E., Jones, R. L., & Colby, R. H. (2006). Rheopexy of synovial fluid and protein aggregation. *Journal of the Royal Society Interface*, 3(6), 167–174. <https://doi.org/10.1098/rsif.2005.0086>
- Ofei, T. N., Irawan, S., & Pao, W. (2014). CFD Method for Predicting Annular Pressure Losses and Cuttings Concentration in Eccentric Horizontal Wells. *Journal of Petroleum Engineering*. <https://doi.org/10.1155/2014/486423>
- Okrajni, S., & Azar, J. J. (1986). The Effects of Mud Rheology on Annular Hole Cleaning in Directional Wells. <https://doi.org/10.2118/14178-PA>
- Osório, L., Arevalo, H., Velho, M., Flores, V., Carrois, F., France, V., & Biddle, N. (2013). Achieving Brazilian Extended Reach Drilling Records on Polvo Project With Ultra-High Torque Connection. Offshore Mediterranean Conference.
- Paes, P., Ajikobi, F., & Chen, D. -K. (2005). Challenges in Drilling in Campos Basin. Society of Petroleum Engineers. <https://doi.org/10.2118/95418-MS>
- Payne, M. L., Cocking, D. A., & Hatch, A. J. (1994). Critical Technologies for Success in Extended Reach Drilling. Society of Petroleum Engineers. <https://doi.org/10.2118/28293-MS>
- Peden, J. M., Ford, J. T., & Oyeneyin, M. B. (1990). Comprehensive Experimental Investigation of Drilled Cuttings Transport in Inclined Wells Including the Effects of Rotation and Eccentricity. Society of Petroleum Engineers. <https://doi.org/10.2118/20925-MS>
- Petersen, J. (2015). Determining the Cuttings Critical Transport Fluid Velocity using Simple Geometrical Approximations. Society of Petroleum Engineers. <https://doi.org/10.2118/173843-MS>
- Philip, Z., Sharma, M. M., & Chenevert, M. E. (1998). The Role of Taylor Vortices in the Transport of Drill Cuttings. Society of Petroleum Engineers. <https://doi.org/10.2118/39504-MS>

MS

- Pigott, R. J. S. (1941). *Mud Flow In Drilling*. American Petroleum Institute.
- Pilehvari, A. A., Azar, J. J., & Shirazi, S. A. (1999). State-of-the-Art Cuttings Transport in Horizontal Wellbores. *SPE Drilling & Completion*, 14(3), 196–200.
<https://doi.org/10.2118/57716-PA>
- Poloski, A. ., Adjins, H. E., Abrefah, J., Casella, A. M., Hohimer, R. E., Nigl, F., ... Yokuda, S. T. (2009). *Deposition Velocities of Newtonian and Non-Newtonian Slurries in Pipelines*. Richland.
- Riglogix. (2017). Offshore Rig Day Rates. Retrieved from
<http://market.rigzone.com/data/dayrates/>
- Rolovic, R., Weng, X., Hill, S., Robinson, G., Zemlak, K., & Najafov, J. (2004). An Integrated System Approach to Wellbore Cleanouts With Coiled Tubing. Society of Petroleum Engineers. <https://doi.org/10.2118/89333-MS>
- Roque, J. L., & Maidla, E. E. (1995). Casing Cost Optimization for Complex Loading Situations. <https://doi.org/10.2118/28224-PA>
- Rubiandini R.S., R. (2008). Extended Reach Drilling (ERD) Design in Deepwater Application. Society of Petroleum Engineers. <https://doi.org/10.2118/115286-MS>
- Rudman, M., Blackburn, H. M., Graham, L. J. W., & Pullum, L. (2004). Turbulent pipe flow of shear-thinning fluids. *Journal of Non-Newtonian Fluid Mechanics*, 118(1), 33–48.
<https://doi.org/https://doi.org/10.1016/j.jnnfm.2004.02.006>
- Ryan, N. W., & Johnson, M. . (1959). Transition from laminar to turbulent flow in pipes. *AIChE Journal*, 5(4), 433.
- Saeverhagen, E., Thorsen, A. K., Gard, S., & Jones, R. D. (2008). Troll West Oilfield Development—How a Giant Gas Field Became the Largest Oil Field in the NCS Through Innovative Field and Technology Development. Society of Petroleum Engineers.
<https://doi.org/10.2118/112616-MS>
- Sanchez, R. A., Azar, J. (University of T., Bassal, A. (Gear H. A., & Martins, A. (Petrobas). (1997). The Effect of Drill Pipe Rotation on Hole Cleaning During Directional Well Drilling (p. 9). Amsterdam: SPE.
- Sanchez, R. A., Brown, C. F., & Adams, W. (2012). Casing Centralization in Horizontal and Extended Reach Wells. Society of Petroleum Engineers. <https://doi.org/10.2118/150317->

MS

- Sapru, A. (University of T. (2001). *Study of Effect of Drill Pipe Rotation on Cuttings Bed Erosion in Horizontal Wells*. University of Tulsa.
- Sifferman, T. R., & Becker, T. (SPE/Mobil R. C. (1992). *Hole Cleaning in Full-Scale Inclined Wellbores*.
- Sifferman, T. R., & Becker, T. E. (1992). Hole Cleaning in Full-Scale Inclined Wellbores.
<https://doi.org/10.2118/20422-PA>
- Sifferman, T. R., Myers, G. M., Haden, E. L., & Wahl, H. A. (1973). Drill Cutting Transport in Full Scale Vertical Annuli. *APA*. <https://doi.org/10.2118/4514-PA>
- Song, X. Z., Li, G. S., Huang, Z. W., Wang, H. Z., Tian, S. C., & Shi, H. Z. (2010). Experimental study on horizontal wellbore cleanout by rotating jets. *Journal of Petroleum Science and Engineering*, 75(1), 71–76.
<https://doi.org/https://doi.org/10.1016/j.petrol.2010.10.015>
- Stockwell, L. L., Zambrano, S., Bezerra, F., & Arevalo, Y. I. (2010). BC-10 Brazil: Successful Deepwater 3D ERD Directional-Drilling Strategy Using Seismic Inversion and Point-the-Bit Rotary-Steerable System. Society of Petroleum Engineers.
<https://doi.org/10.2118/139328-MS>
- Suggett, J. C., & Smith, T. (2005). Performing Extended-Reach-Drilling Operations With Limited Rig Capability. International Petroleum Technology Conference.
<https://doi.org/10.2523/IPTC-10509-ABSTRACT>
- Surjaatmadja, J. B., & Rosine, R. S. (2005). An Effective Sweep--Cleaning Out of Large Deviated Wellbores Using Small Coiled-Tubing Systems. Society of Petroleum Engineers.
<https://doi.org/10.2118/94102-MS>
- Tomren, P. (SPE & S., Iyoho, A. (SPE & D. S., & Azar, J. (SPE & U. of T. (1986). Experimental Study of Cuttings Transport in Direcitonal Wells. In *SPE Drilling Engineering* (pp. 43–56).
- Turtiainen, H. (1986). *Flow-rate measurement using radioactive tracers and transit time method*. Finland. Retrieved from http://inis.iaea.org/search/search.aspx?orig_q=RN:18013974
- van Oort, E., Lee, J., Friedheim, J., & Troups, B. (2004). New Flat-Rheology Synthetic-Based Mud for Improved Deepwater Drilling. Society of Petroleum Engineers.
<https://doi.org/10.2118/90987-MS>
- Vujanović, M., Petranović, Z., Edelbauer, W., & Duić, N. (2016). Modelling spray and

- combustion processes in diesel engine by using the coupled Eulerian–Eulerian and Eulerian–Lagrangian method. *Energy Conversion and Management*, 125(Supplement C), 15–25. <https://doi.org/https://doi.org/10.1016/j.enconman.2016.03.072>
- Walker, M. W. (2012). Pushing the Extended-Reach Envelope at Sakhalin: An Operator. Society of Petroleum Engineers. <https://doi.org/10.2118/151046-MS>
- Walker, S., & Li, J. (2000). The Effects of Particle Size, Fluid Rheology, and Pipe Eccentricity on Cuttings Transport. Society of Petroleum Engineers. <https://doi.org/10.2118/60755-MS>
- Williams Jr., C. E., & Bruce, G. H. (1951). Carrying Capacity of Drilling Muds. *Petroleum Transactions, AIME*, 192. <https://doi.org/10.2118/951111-G>
- Wilson, A. (2015). Optimization Leads to Successful Deepwater Extended-Reach Drilling Offshore West Africa. *JPT*, (May), 89–90. <https://doi.org/10.2118/0515-0089-JPT>
- Wilson, K. C. (1970). Slip Point of Beds in Solid-Liquid Pipeline Flow. *Journal of the Hydraulics Division*, 96(1), 1–12.
- Yoho, A. W. (1980). *Drilled-cuttings transport by non-newtonian drilling fluids through inclined eccentric annuli*. University of Tulsa.
- Zadvornov, D., Truba, A., Petrakov, Y., Sobolev, A., Pavlov, V., Dymov, S., ... Zhudov, A. (2015). Record Erd Senomanian wells on Yamal. Society of Petroleum Engineers. <https://doi.org/10.2118/176619-MS>
- Zamora, M., Broussard, P. N., & Stephens, M. P. (2000). The Top 10 Mud-Related Concerns in Deepwater Drilling Operations. Society of Petroleum Engineers. <https://doi.org/10.2118/59019-MS>
- Zarrouh, R. (1991). *Drilled Cuttings Transport in Deviated Wells*. Heriot-Watt University.
- Zeidler, U. H. (1972). An Experimental Analysis of the Transport of Drilled Particles. *Transactions*, 253. <https://doi.org/10.2118/3064-PA>
- Zhang, F. (2015). *Numerical Simulation and Experimental Study of Cuttings Transport in Intermediate Inclined Wells*. University of Tulsa. Retrieved from <https://books.google.com/books?id=0SHyjcEACAAJ>
- Zhang, F., Filippov, A., Miska, S., & Yu, M. (2017). Hole Cleaning and ECD Management for Drilling Ultra-Long-Reach Laterals. Society of Petroleum Engineers. <https://doi.org/10.2118/183786-MS>
- Zhou, L., Ahmed, R. M., Miska, S. Z., Takach, N. E., Yu, M., & Pickell, M. B. (2004).

Experimental Study and Modeling of Cuttings Transport with Aerated Mud in Horizontal Wellbore at Simulated Downhole Conditions. Society of Petroleum Engineers.

<https://doi.org/10.2118/90038-MS>

7. Appendix

7.1. Rig Pricing

Table XXXVIII: Floating Rig Price Estimates

Rig Type	Floating Rigs				
	Drillship (= 3,999')	Drillship (4,000'+)	Semisub (= 1,499')	Semisub (1,500'+)	Semisub (4,000'+)
Day Rate	\$204,000	\$443,000	\$382,000	\$294,000	\$291,000
1	\$204,000	\$443,000	\$382,000	\$294,000	\$291,000
2	\$408,000	\$886,000	\$764,000	\$588,000	\$582,000
3	\$612,000	\$1,329,000	\$1,146,000	\$882,000	\$873,000
4	\$816,000	\$1,772,000	\$1,528,000	\$1,176,000	\$1,164,000
5	\$1,020,000	\$2,215,000	\$1,910,000	\$1,470,000	\$1,455,000
6	\$1,224,000	\$2,658,000	\$2,292,000	\$1,764,000	\$1,746,000
7	\$1,428,000	\$3,101,000	\$2,674,000	\$2,058,000	\$2,037,000
8	\$1,632,000	\$3,544,000	\$3,056,000	\$2,352,000	\$2,328,000
9	\$1,836,000	\$3,987,000	\$3,438,000	\$2,646,000	\$2,619,000
10	\$2,040,000	\$4,430,000	\$3,820,000	\$2,940,000	\$2,910,000
11	\$2,244,000	\$4,873,000	\$4,202,000	\$3,234,000	\$3,201,000
12	\$2,448,000	\$5,316,000	\$4,584,000	\$3,528,000	\$3,492,000
13	\$2,652,000	\$5,759,000	\$4,966,000	\$3,822,000	\$3,783,000
14	\$2,856,000	\$6,202,000	\$5,348,000	\$4,116,000	\$4,074,000
15	\$3,060,000	\$6,645,000	\$5,730,000	\$4,410,000	\$4,365,000
16	\$3,264,000	\$7,088,000	\$6,112,000	\$4,704,000	\$4,656,000
17	\$3,468,000	\$7,531,000	\$6,494,000	\$4,998,000	\$4,947,000
18	\$3,672,000	\$7,974,000	\$6,876,000	\$5,292,000	\$5,238,000
19	\$3,876,000	\$8,417,000	\$7,258,000	\$5,586,000	\$5,529,000
20	\$4,080,000	\$8,860,000	\$7,640,000	\$5,880,000	\$5,820,000
21	\$4,284,000	\$9,303,000	\$8,022,000	\$6,174,000	\$6,111,000
22	\$4,488,000	\$9,746,000	\$8,404,000	\$6,468,000	\$6,402,000
23	\$4,692,000	\$10,189,000	\$8,786,000	\$6,762,000	\$6,693,000
24	\$4,896,000	\$10,632,000	\$9,168,000	\$7,056,000	\$6,984,000
25	\$5,100,000	\$11,075,000	\$9,550,000	\$7,350,000	\$7,275,000
26	\$5,304,000	\$11,518,000	\$9,932,000	\$7,644,000	\$7,566,000
27	\$5,508,000	\$11,961,000	\$10,314,000	\$7,938,000	\$7,857,000
28	\$5,712,000	\$12,404,000	\$10,696,000	\$8,232,000	\$8,148,000
29	\$5,916,000	\$12,847,000	\$11,078,000	\$8,526,000	\$8,439,000
30	\$6,120,000	\$13,290,000	\$11,460,000	\$8,820,000	\$8,730,000
31	\$6,324,000	\$13,733,000	\$11,842,000	\$9,114,000	\$9,021,000
32	\$6,528,000	\$14,176,000	\$12,224,000	\$9,408,000	\$9,312,000
33	\$6,732,000	\$14,619,000	\$12,606,000	\$9,702,000	\$9,603,000
34	\$6,936,000	\$15,062,000	\$12,988,000	\$9,996,000	\$9,894,000
35	\$7,140,000	\$15,505,000	\$13,370,000	\$10,290,000	\$10,185,000
36	\$7,344,000	\$15,948,000	\$13,752,000	\$10,584,000	\$10,476,000
37	\$7,548,000	\$16,391,000	\$14,134,000	\$10,878,000	\$10,767,000
38	\$7,752,000	\$16,834,000	\$14,516,000	\$11,172,000	\$11,058,000
39	\$7,956,000	\$17,277,000	\$14,898,000	\$11,466,000	\$11,349,000
40	\$8,160,000	\$17,720,000	\$15,280,000	\$11,760,000	\$11,640,000

Table XXXIX: Jack up Rig Price Estimates

Rig Type	Jackup Rigs							
	Jackup (< 250' IC)	Jackup (< 250' IS)	Jackup (200' + MC)	Jackup (200' + MS)	Jackup (250' IC)	Jackup (300' IC)	Jackup (300' + IC)	Jackup (300' + IS)
Day Rate	\$72,000	\$57,000	\$56,000	\$56,000	\$65,000	\$85,000	\$123,000	\$48,000
1	\$72,000	\$57,000	\$56,000	\$56,000	\$65,000	\$85,000	\$123,000	\$48,000
2	\$144,000	\$114,000	\$112,000	\$112,000	\$130,000	\$170,000	\$246,000	\$96,000
3	\$216,000	\$171,000	\$168,000	\$168,000	\$195,000	\$255,000	\$369,000	\$144,000
4	\$288,000	\$228,000	\$224,000	\$224,000	\$260,000	\$340,000	\$492,000	\$192,000
5	\$360,000	\$285,000	\$280,000	\$280,000	\$325,000	\$425,000	\$615,000	\$240,000
6	\$432,000	\$342,000	\$336,000	\$336,000	\$390,000	\$510,000	\$738,000	\$288,000
7	\$504,000	\$399,000	\$392,000	\$392,000	\$455,000	\$595,000	\$861,000	\$336,000
8	\$576,000	\$456,000	\$448,000	\$448,000	\$520,000	\$680,000	\$984,000	\$384,000
9	\$648,000	\$513,000	\$504,000	\$504,000	\$585,000	\$765,000	\$1,107,000	\$432,000
10	\$720,000	\$570,000	\$560,000	\$560,000	\$650,000	\$850,000	\$1,230,000	\$480,000
11	\$792,000	\$627,000	\$616,000	\$616,000	\$715,000	\$935,000	\$1,353,000	\$528,000
12	\$864,000	\$684,000	\$672,000	\$672,000	\$780,000	\$1,020,000	\$1,476,000	\$576,000
13	\$936,000	\$741,000	\$728,000	\$728,000	\$845,000	\$1,105,000	\$1,599,000	\$624,000
14	\$1,008,000	\$798,000	\$784,000	\$784,000	\$910,000	\$1,190,000	\$1,722,000	\$672,000
15	\$1,080,000	\$855,000	\$840,000	\$840,000	\$975,000	\$1,275,000	\$1,845,000	\$720,000
16	\$1,152,000	\$912,000	\$896,000	\$896,000	\$1,040,000	\$1,360,000	\$1,968,000	\$768,000
17	\$1,224,000	\$969,000	\$952,000	\$952,000	\$1,105,000	\$1,445,000	\$2,091,000	\$816,000
18	\$1,296,000	\$1,026,000	\$1,008,000	\$1,008,000	\$1,170,000	\$1,530,000	\$2,214,000	\$864,000
19	\$1,368,000	\$1,083,000	\$1,064,000	\$1,064,000	\$1,235,000	\$1,615,000	\$2,337,000	\$912,000
20	\$1,440,000	\$1,140,000	\$1,120,000	\$1,120,000	\$1,300,000	\$1,700,000	\$2,460,000	\$960,000
21	\$1,512,000	\$1,197,000	\$1,176,000	\$1,176,000	\$1,365,000	\$1,785,000	\$2,583,000	\$1,008,000
22	\$1,584,000	\$1,254,000	\$1,232,000	\$1,232,000	\$1,430,000	\$1,870,000	\$2,706,000	\$1,056,000
23	\$1,656,000	\$1,311,000	\$1,288,000	\$1,288,000	\$1,495,000	\$1,955,000	\$2,829,000	\$1,104,000
24	\$1,728,000	\$1,368,000	\$1,344,000	\$1,344,000	\$1,560,000	\$2,040,000	\$2,952,000	\$1,152,000
25	\$1,800,000	\$1,425,000	\$1,400,000	\$1,400,000	\$1,625,000	\$2,125,000	\$3,075,000	\$1,200,000
26	\$1,872,000	\$1,482,000	\$1,456,000	\$1,456,000	\$1,690,000	\$2,210,000	\$3,198,000	\$1,248,000
27	\$1,944,000	\$1,539,000	\$1,512,000	\$1,512,000	\$1,755,000	\$2,295,000	\$3,321,000	\$1,296,000
28	\$2,016,000	\$1,596,000	\$1,568,000	\$1,568,000	\$1,820,000	\$2,380,000	\$3,444,000	\$1,344,000
29	\$2,088,000	\$1,653,000	\$1,624,000	\$1,624,000	\$1,885,000	\$2,465,000	\$3,567,000	\$1,392,000
30	\$2,160,000	\$1,710,000	\$1,680,000	\$1,680,000	\$1,950,000	\$2,550,000	\$3,690,000	\$1,440,000
31	\$2,232,000	\$1,767,000	\$1,736,000	\$1,736,000	\$2,015,000	\$2,635,000	\$3,813,000	\$1,488,000
32	\$2,304,000	\$1,824,000	\$1,792,000	\$1,792,000	\$2,080,000	\$2,720,000	\$3,936,000	\$1,536,000
33	\$2,376,000	\$1,881,000	\$1,848,000	\$1,848,000	\$2,145,000	\$2,805,000	\$4,059,000	\$1,584,000
34	\$2,448,000	\$1,938,000	\$1,904,000	\$1,904,000	\$2,210,000	\$2,890,000	\$4,182,000	\$1,632,000
35	\$2,520,000	\$1,995,000	\$1,960,000	\$1,960,000	\$2,275,000	\$2,975,000	\$4,305,000	\$1,680,000
36	\$2,592,000	\$2,052,000	\$2,016,000	\$2,016,000	\$2,340,000	\$3,060,000	\$4,428,000	\$1,728,000
37	\$2,664,000	\$2,109,000	\$2,072,000	\$2,072,000	\$2,405,000	\$3,145,000	\$4,551,000	\$1,776,000
38	\$2,736,000	\$2,166,000	\$2,128,000	\$2,128,000	\$2,470,000	\$3,230,000	\$4,674,000	\$1,824,000
39	\$2,808,000	\$2,223,000	\$2,184,000	\$2,184,000	\$2,535,000	\$3,315,000	\$4,797,000	\$1,872,000
40	\$2,880,000	\$2,280,000	\$2,240,000	\$2,240,000	\$2,600,000	\$3,400,000	\$4,920,000	\$1,920,000

7.2. Additional Mixture Velocity Equations

$$v_s = v_{sa}(1 - \lambda_p^2) - v_{sp}\lambda_p^2$$

$$V_{sa} = V_1(c, Re_p, v'_{sa})$$

$$v_{sp} = V_s(v'_{sp}, Y_a)$$

$$v'_{sa} = \sqrt{\frac{4d_s g(\rho_s - \rho)}{3\rho C_D}} \quad (54)$$

$$v'_{sp} = \cos \phi \sqrt{\frac{4}{\rho C_D} \left\{ \frac{d_s g(\rho_s - \rho)}{3} - \pi \tau_y \right\}}$$

7.3. Velocity Ratio Data

RPM	Ang Vel	Velocity Ratio, ξ		
		5-Inch	5.5-Inch	5.875 inch
0	0	0	0	0
10	1.047	0.049	0.054	0.058
20	2.094	0.099	0.109	0.116
30	3.142	0.148	0.163	0.174
40	4.189	0.197	0.217	0.232
50	5.236	0.247	0.272	0.290
60	6.283	0.296	0.326	0.348
70	7.330	0.346	0.380	0.406
80	8.378	0.395	0.434	0.464
90	9.425	0.444	0.489	0.522
100	10.472	0.494	0.543	0.580
110	11.519	0.543	0.597	0.638
120	12.566	0.592	0.652	0.696
130	13.614	0.642	0.706	0.754
140	14.661	0.691	0.760	0.812
150	15.708	0.741	0.815	0.870
160	16.755	0.790	0.869	0.928
170	17.802	0.839	0.923	0.986
180	18.850	0.889	0.978	1.044
190	19.897	0.938	1.032	1.102
200	20.944	0.987	1.086	1.160

7.4. Flow Loop Data

Table XL: Flow Loop Sources

Name	Source
BHI flow loop	(Li & Walker, 1999)
BP flow loop	(Brown, Bern, & Weaver, 1989)
Continental Oil Co. flow loop	(Thomas R Sifferman et al., 1973)
Halliburton flow loop	(Surjaatmadja & Rosine, 2005)
Heriot-Watt University flow loop	(Zarrouh, 1991)
Institute Français du Petrole flow loop	(Martin et al., 1987)
Japan National lab flow loop	(Naganawa et al., 2002)
Middle East Technology University flow loop	(Ettehad Osgouei, Ozbayoglu, Ozbayoglu, & Yuksel, 2010)
M-I drilling fluids flow loop	(F Zhang, 2015)
Mobil flow loop	(T.R. Sifferman & Becker, 1992)
Norwegian University of Science and Technology flow loop	(F Zhang, 2015)
Petrobras flow loop	(Martins, Sa, Lourenco, Freire, & Campos, 1996)
Rice University	(Zeidler, 1972)
Schlumberger	(Rolovic et al., 2004)
Southwest Petroleum University, China HPHT flow loop	(F Zhang, 2015)
University of Alberta flow loop	(F Zhang, 2015)

China University of Petroleum, Beijing, flow loop	(Song et al., 2010)
University of Tulsa- LPAT flow loop	(Larsen, 1990)
University of Tulsa- HPHT flow loop	(Zhou et al., 2004)
University of Tulsa- Small	(Cheung, Takach, Ozbayoglu, Majidi, & Bloys, 2012)
University of Oklahoma indoor flow loop	(F Zhang, 2015)

7.5. Vertical Flow Loop Experimental Data

15 GPM Water Rate - No Air							
Time Stamp	Loop 1 Top Pressure	Loop 1 Bottom Pressure	water flow rate	air flow control (scfm)	air flow rate (scfm)	Water Flow Command	Pressure Differential
1/11/2019 13:46	-0.285	10.631	14.966	90	1.608	15	10.917
1/11/2019 13:47	-0.285	10.610	14.970	90	1.613	15	10.895
1/11/2019 13:47	-0.285	10.601	14.974	90	1.613	15	10.886
1/11/2019 13:47	-0.285	10.632	14.979	90	1.544	15	10.918
1/11/2019 13:47	-0.285	10.582	14.979	90	1.585	15	10.867
1/11/2019 13:48	-0.285	10.640	14.958	90	1.613	15	10.925
1/11/2019 13:48	-0.285	10.663	14.977	90	1.626	15	10.948
1/11/2019 13:48	-0.285	10.582	14.989	90	1.585	15	10.867
1/11/2019 13:48	-0.285	10.569	14.991	90	1.625	15	10.855
1/11/2019 13:48	-0.285	10.587	14.991	90	1.625	15	10.872
1/11/2019 13:49	-0.285	10.550	14.964	90	1.640	15	10.835
1/11/2019 13:49	-0.285	10.541	14.961	90	1.558	15	10.826
1/11/2019 13:49	-0.285	10.541	14.961	90	1.599	15	10.826
1/11/2019 13:49	-0.285	10.548	14.985	90	1.558	15	10.833
1/11/2019 13:49	-0.285	10.549	14.953	90	1.599	15	10.834
1/11/2019 13:50	-0.285	10.503	14.951	90	1.572	15	10.788
1/11/2019 13:50	-0.285	10.540	14.976	90	1.596	15	10.825
1/11/2019 13:50	-0.285	10.512	14.945	90	1.613	15	10.797
1/11/2019 13:50	-0.285	10.503	14.991	90	1.599	15	10.788
1/11/2019 13:50	-0.285	10.520	14.967	90	1.640	15	10.805
1/11/2019 13:50	-0.285	10.520	14.967	90	1.585	15	10.805
1/11/2019 13:51	-0.285	10.500	14.958	90	1.596	15	10.785
1/11/2019 13:51	-0.285	10.526	14.991	90	1.606	15	10.811
1/11/2019 13:51	-0.285	10.511	14.961	90	1.613	15	10.796
1/11/2019 13:51	-0.285	10.532	14.953	90	1.585	15	10.817
1/11/2019 13:52	-0.285	10.507	14.946	90	1.626	15	10.791
1/11/2019 13:52	-0.285	10.510	14.940	90	1.550	15	10.795
1/11/2019 13:52	-0.285	10.513	14.939	90	1.544	15	10.798
1/11/2019 13:52	-0.285	10.513	14.976	90	1.572	15	10.798
1/11/2019 13:52	-0.285	10.514	14.930	90	1.544	15	10.799
1/11/2019 13:53	-0.285	10.498	14.948	90	1.675	15	10.782
1/11/2019 13:53	-0.285	10.498	14.948	90	1.626	15	10.782
1/11/2019 13:53	-0.285	10.490	14.960	90	1.688	15	10.775
1/11/2019 13:53	-0.285	10.510	14.964	90	1.585	15	10.795
Average	-0.285	10.545	14.965	90	1.600	15	10.830

25 GPM Water Rate - No Air							
Time Stamp	Loop 1 Top Pressure	Loop 1 Bottom Pressure	water flow rate	air flow control (scfm)	air flow rate (scfm)	Water Flow Command	Pressure Differential
1/11/2019 13:55	-0.285	11.276	24.183	90	1.613	25	11.561
1/11/2019 13:55	-0.285	11.116	24.280	90	1.572	25	11.401
1/11/2019 13:56	-0.285	11.170	24.399	90	1.626	25	11.455
1/11/2019 13:56	-0.285	11.267	24.399	90	1.626	25	11.552
1/11/2019 13:56	-0.285	11.149	24.570	90	1.585	25	11.434
1/11/2019 13:56	-0.285	11.137	24.707	90	1.599	25	11.422
1/11/2019 13:56	-0.285	11.137	24.707	90	1.654	25	11.422
1/11/2019 13:56	-0.285	11.154	24.720	90	1.585	25	11.439
1/11/2019 13:56	-0.285	11.163	24.860	90	1.585	25	11.447
1/11/2019 13:56	-0.285	11.163	24.860	90	1.654	25	11.447
1/11/2019 13:57	-0.285	11.172	24.814	90	1.585	25	11.456
1/11/2019 13:57	-0.285	11.174	24.888	90	1.613	25	11.459
1/11/2019 13:57	-0.285	11.151	24.830	90	1.613	25	11.436
1/11/2019 13:57	-0.285	11.148	24.891	90	1.558	25	11.433
1/11/2019 13:57	-0.285	11.144	24.918	90	1.613	25	11.429
1/11/2019 13:58	-0.285	11.142	24.921	90	1.623	25	11.427
1/11/2019 13:58	-0.285	11.177	24.948	90	1.626	25	11.462
1/11/2019 13:58	-0.285	11.161	24.952	90	1.572	25	11.446
1/11/2019 13:58	-0.285	11.161	24.952	90	1.585	25	11.446
1/11/2019 13:58	-0.285	11.151	24.925	90	1.558	25	11.435
1/11/2019 13:59	-0.285	11.141	24.921	90	1.613	25	11.426
1/11/2019 13:59	-0.285	11.139	24.933	90	1.544	25	11.424
1/11/2019 13:59	-0.285	11.139	24.906	90	1.571	25	11.424
1/11/2019 13:59	-0.285	11.141	24.928	90	1.572	25	11.426
1/11/2019 13:59	-0.285	11.141	24.928	90	1.626	25	11.426
1/11/2019 14:00	-0.285	11.149	24.933	90	1.585	25	11.434
1/11/2019 14:00	-0.285	11.154	24.915	90	1.640	25	11.439
1/11/2019 14:00	-0.285	11.154	24.915	90	1.640	25	11.439
1/11/2019 14:00	-0.285	11.127	24.936	90	1.572	25	11.411
1/11/2019 14:00	-0.285	11.141	24.894	90	1.572	25	11.425
1/11/2019 14:01	-0.285	11.150	24.935	90	1.613	25	11.435
1/11/2019 14:01	-0.285	11.152	24.946	90	1.572	25	11.437
1/11/2019 14:01	-0.285	11.152	24.884	90	1.572	25	11.437
1/11/2019 14:01	-0.285	11.126	24.909	90	1.640	25	11.410
1/11/2019 14:01	-0.285	11.148	24.918	90	1.654	25	11.432
1/11/2019 14:02	-0.285	11.149	24.906	90	1.585	25	11.433
1/11/2019 14:02	-0.285	11.149	24.942	90	1.613	25	11.433
1/11/2019 14:02	-0.285	11.132	24.921	90	1.599	25	11.417
1/11/2019 14:02	-0.285	11.131	24.927	90	1.640	25	11.416
1/11/2019 14:02	-0.285	11.154	24.927	90	1.558	25	11.439
1/11/2019 14:02	-0.285	11.152	24.930	90	1.640	25	11.436
1/11/2019 14:02	-0.285	11.149	24.933	90	1.585	25	11.434
Average	-0.285	11.154	24.834	90	1.601	25	11.439

35 GPM Water Rate - No Air							
Time Stamp	Loop 1 Top Pressure	Loop 1 Bottom Pressure	water flow rate	air flow control (scfm)	air flow rate (scfm)	Water Flow Command	Pressure Differential
1/11/2019 14:06	-0.285	12.150	34.851	90	1.640	35	12.435
1/11/2019 14:06	-0.285	12.178	34.821	90	1.599	35	12.462
1/11/2019 14:06	-0.285	12.178	34.882	90	1.599	35	12.462
1/11/2019 14:07	-0.285	12.172	34.854	90	1.621	35	12.457
1/11/2019 14:07	-0.285	12.169	34.897	90	1.626	35	12.454
1/11/2019 14:07	-0.285	12.169	34.897	90	1.654	35	12.454
1/11/2019 14:07	-0.285	12.167	34.912	90	1.628	35	12.452
1/11/2019 14:07	-0.285	12.185	34.915	90	1.604	35	12.470
1/11/2019 14:08	-0.285	12.195	34.882	90	1.585	35	12.479
1/11/2019 14:08	-0.285	12.195	34.918	90	1.585	35	12.479
1/11/2019 14:08	-0.285	12.169	34.940	90	1.573	35	12.454
1/11/2019 14:08	-0.284	12.166	34.943	90	1.572	35	12.451
1/11/2019 14:08	-0.284	12.166	34.943	90	1.599	35	12.451
1/11/2019 14:08	-0.284	12.171	34.909	90	1.585	35	12.456
1/11/2019 14:08	-0.284	12.174	34.961	90	1.654	35	12.458
1/11/2019 14:08	-0.284	12.174	34.943	90	1.613	35	12.458
1/11/2019 14:09	-0.284	12.140	35.007	90	1.623	35	12.424
1/11/2019 14:09	-0.284	12.167	34.958	90	1.626	35	12.452
1/11/2019 14:09	-0.284	12.167	34.976	90	1.626	35	12.452
1/11/2019 14:09	-0.284	12.181	34.958	90	1.544	35	12.465
1/11/2019 14:09	-0.284	12.168	34.909	90	1.635	35	12.453
1/11/2019 14:10	-0.284	12.161	34.897	90	1.640	35	12.445
1/11/2019 14:10	-0.284	12.161	34.897	90	1.654	35	12.445
1/11/2019 14:10	-0.284	12.166	34.958	90	1.572	35	12.450
1/11/2019 14:10	-0.284	12.170	34.956	90	1.640	35	12.455
1/11/2019 14:10	-0.284	12.175	34.955	90	1.585	35	12.459
1/11/2019 14:11	-0.284	12.179	34.927	90	1.613	35	12.463
1/11/2019 14:11	-0.284	12.179	34.927	90	1.572	35	12.463
1/11/2019 14:11	-0.284	12.168	34.976	90	1.599	35	12.452
1/11/2019 14:11	-0.284	12.157	34.934	90	1.585	35	12.441
1/11/2019 14:11	-0.284	12.149	34.976	90	1.613	35	12.434
1/11/2019 14:11	-0.284	12.149	34.921	90	1.599	35	12.434
1/11/2019 14:12	-0.284	12.169	34.936	90	1.637	35	12.453
1/11/2019 14:12	-0.284	12.170	34.946	90	1.640	35	12.455
1/11/2019 14:12	-0.284	12.149	34.946	90	1.558	35	12.434
1/11/2019 14:12	-0.284	12.159	34.954	90	1.599	35	12.443
1/11/2019 14:12	-0.284	12.166	34.961	90	1.572	35	12.451
1/11/2019 14:12	-0.284	12.166	34.961	90	1.613	35	12.451
1/11/2019 14:13	-0.284	12.156	34.912	90	1.605	35	12.440
1/11/2019 14:13	-0.284	12.191	34.958	90	1.599	35	12.476
1/11/2019 14:13	-0.284	12.152	34.973	90	1.599	35	12.436
1/11/2019 14:13	-0.284	12.156	34.903	90	1.544	35	12.441
1/11/2019 14:13	-0.284	12.158	34.946	90	1.613	35	12.442
1/11/2019 14:14	-0.284	12.163	34.958	90	1.572	35	12.447
Average	-0.284	12.168	34.931	90	1.605	35	12.452

15 SCFM Air Rate - 10 GPM Water Rate							
Time Stamp	Loop 1 Top Pressure	Loop 1 Bottom Pressure	water flow rate	air flow control (scfm)	air flow rate (scfm)	Water Flow Command	Pressure Differential
1/11/2019 14:26	1.178	6.507	9.973	15	16.093	10	5.329
1/11/2019 14:26	1.120	6.536	9.973	15	16.272	10	5.416
1/11/2019 14:27	1.625	7.168	9.912	15	16.121	10	5.542
1/11/2019 14:27	1.296	6.549	9.887	15	16.409	10	5.252
1/11/2019 14:27	2.369	7.172	9.887	15	16.189	10	4.803
1/11/2019 14:27	2.101	7.011	10.003	15	16.423	10	4.911
1/11/2019 14:27	1.907	7.604	9.903	15	16.175	10	5.697
1/11/2019 14:28	2.524	7.593	9.939	15	16.505	10	5.069
1/11/2019 14:28	1.551	6.698	9.939	15	15.846	10	5.146
1/11/2019 14:28	1.539	6.881	9.954	15	15.777	10	5.342
1/11/2019 14:28	2.459	7.195	9.961	15	16.313	10	4.736
1/11/2019 14:28	1.896	6.759	9.961	15	15.819	10	4.862
1/11/2019 14:28	1.485	6.622	10.006	15	15.805	10	5.137
1/11/2019 14:29	1.823	6.521	9.954	15	16.107	10	4.698
1/11/2019 14:29	1.576	6.814	9.957	15	16.175	10	5.238
1/11/2019 14:29	1.742	7.454	9.912	15	16.121	10	5.712
1/11/2019 14:29	2.089	6.760	9.961	15	15.983	10	4.671
1/11/2019 14:29	1.603	6.730	9.912	15	16.025	10	5.127
1/11/2019 14:29	1.603	6.825	9.912	15	15.942	10	5.223
1/11/2019 14:30	1.714	7.086	9.939	15	16.230	10	5.372
1/11/2019 14:30	1.617	7.224	9.942	15	16.175	10	5.607
1/11/2019 14:30	1.243	6.889	9.942	15	15.970	10	5.646
1/11/2019 14:30	1.315	6.511	9.912	15	16.121	10	5.196
1/11/2019 14:30	1.524	7.003	10.003	15	15.942	10	5.478
1/11/2019 14:30	1.329	6.386	10.009	15	16.038	10	5.057
1/11/2019 14:31	2.051	6.840	9.973	15	15.901	10	4.789
1/11/2019 14:31	2.039	6.702	9.906	15	16.148	10	4.663
1/11/2019 14:31	2.213	7.803	9.906	15	16.148	10	5.590
1/11/2019 14:31	1.859	6.368	9.930	15	15.807	10	4.509
1/11/2019 14:31	1.933	6.526	9.985	15	15.736	10	4.593
1/11/2019 14:32	1.803	5.738	9.906	15	15.434	10	3.935
1/11/2019 14:32	1.629	6.715	9.906	15	15.613	10	5.085
1/11/2019 14:32	2.245	6.422	9.970	15	15.762	10	4.177
1/11/2019 14:32	1.796	7.204	9.924	15	15.777	10	5.408
1/11/2019 14:32	1.268	7.204	9.939	15	15.558	10	5.936
1/11/2019 14:32	1.969	6.509	9.985	15	15.393	10	4.540
1/11/2019 14:32	1.409	6.585	9.961	15	15.832	10	5.176
1/11/2019 14:32	1.637	6.623	9.961	15	15.709	10	4.986
1/11/2019 14:33	1.481	6.738	9.884	15	15.764	10	5.256
1/11/2019 14:33	2.239	7.174	9.912	15	15.613	10	4.935
1/11/2019 14:33	1.807	6.154	10.006	15	15.723	10	4.347
1/11/2019 14:33	1.936	7.069	9.945	15	15.572	10	5.132
1/11/2019 14:33	1.537	6.778	9.914	15	15.558	10	5.241
1/11/2019 14:34	1.829	6.677	9.912	15	15.750	10	4.848
1/11/2019 14:34	1.829	7.076	9.912	15	15.750	10	5.248
1/11/2019 14:34	1.796	6.613	9.968	15	15.791	10	4.816
1/11/2019 14:34	1.652	6.480	9.973	15	15.379	10	4.828
1/11/2019 14:34	1.813	7.278	10.003	15	15.736	10	5.465
1/11/2019 14:34	2.041	6.675	9.945	15	15.777	10	4.633
1/11/2019 14:35	1.096	6.171	9.939	15	15.723	10	5.075
1/11/2019 14:35	1.583	6.540	9.939	15	15.805	10	4.958
1/11/2019 14:35	1.923	6.664	9.976	15	15.647	10	4.741
1/11/2019 14:35	1.809	6.289	9.988	15	15.599	10	4.481
1/11/2019 14:35	2.007	6.646	9.970	15	15.187	10	4.639
1/11/2019 14:35	2.002	7.526	10.003	15	15.585	10	5.523
1/11/2019 14:36	2.145	6.942	9.942	15	15.640	10	4.796
Average	1.761	6.808	9.947	15	15.875	10	5.047

35 SCFM Air Rate - 10 GPM Water Rate							
Time Stamp	Loop 1 Top Pressure	Loop 1 Bottom Pressure	water flow rate	air flow control (scfm)	air flow rate (scfm)	Water Flow Command	Pressure Differential
1/11/2019 14:37	4.434	8.798	9.982	35	35.988	10	4.364
1/11/2019 14:37	4.249	8.298	9.982	35	35.961	10	4.049
1/11/2019 14:37	3.297	8.707	9.936	35	35.865	10	5.411
1/11/2019 14:37	4.834	9.189	9.945	35	35.824	10	4.356
1/11/2019 14:38	4.413	8.579	9.909	35	35.947	10	4.166
1/11/2019 14:38	3.946	8.411	9.912	35	35.920	10	4.464
1/11/2019 14:38	4.466	9.041	9.970	35	35.961	10	4.575
1/11/2019 14:38	4.371	8.907	9.970	35	35.851	10	4.536
1/11/2019 14:38	3.734	9.108	9.939	35	35.906	10	5.374
1/11/2019 14:38	4.059	8.828	9.948	35	35.865	10	4.769
1/11/2019 14:38	3.782	8.816	9.954	35	35.700	10	5.034
1/11/2019 14:38	4.048	8.261	9.954	35	35.645	10	4.213
1/11/2019 14:39	3.701	8.499	10.022	35	35.673	10	4.798
1/11/2019 14:39	4.463	8.109	10.000	35	35.920	10	3.646
1/11/2019 14:39	3.679	8.109	10.000	35	35.563	10	4.430
1/11/2019 14:39	3.842	8.338	9.939	35	35.549	10	4.496
1/11/2019 14:39	4.153	8.393	9.939	35	35.384	10	4.239
1/11/2019 14:40	3.573	8.297	9.939	35	35.549	10	4.724
1/11/2019 14:40	4.079	8.807	9.939	35	35.549	10	4.728
1/11/2019 14:40	3.341	8.083	9.939	35	35.549	10	4.742
1/11/2019 14:40	4.357	8.348	9.939	35	35.549	10	3.991
1/11/2019 14:40	3.344	8.386	9.967	35	35.576	10	5.042
1/11/2019 14:40	3.459	7.921	9.912	35	35.467	10	4.462
1/11/2019 14:41	4.327	8.594	9.967	35	35.398	10	4.267
1/11/2019 14:41	3.728	8.576	9.942	35	35.480	10	4.848
1/11/2019 14:41	3.825	8.890	9.988	35	35.480	10	5.064
1/11/2019 14:41	3.841	8.151	9.930	35	35.357	10	4.310
1/11/2019 14:41	3.802	8.257	9.939	35	35.425	10	4.455
1/11/2019 14:41	4.834	9.047	9.939	35	35.425	10	4.213
1/11/2019 14:42	4.285	8.322	9.973	35	35.425	10	4.037
1/11/2019 14:42	4.018	8.221	9.957	35	35.549	10	4.203
1/11/2019 14:42	3.949	8.400	9.957	35	35.343	10	4.451
1/11/2019 14:42	4.019	8.513	9.988	35	35.260	10	4.494
1/11/2019 14:42	4.673	9.147	9.881	35	35.247	10	4.474
1/11/2019 14:42	3.739	8.253	9.939	35	35.247	10	4.514
1/11/2019 14:43	3.826	8.386	9.967	35	35.480	10	4.560
1/11/2019 14:43	3.954	8.418	9.967	35	35.275	10	4.464
1/11/2019 14:43	4.212	8.803	9.967	35	35.275	10	4.591
1/11/2019 14:43	3.738	8.540	9.935	35	35.453	10	4.801
1/11/2019 14:43	3.609	8.116	9.924	35	35.384	10	4.507
1/11/2019 14:44	3.989	8.029	9.973	35	35.480	10	4.040
1/11/2019 14:44	3.835	8.294	9.973	35	35.412	10	4.460
1/11/2019 14:44	3.746	8.238	9.987	35	35.453	10	4.492
1/11/2019 14:44	3.448	8.230	9.988	35	35.453	10	4.781
1/11/2019 14:44	3.536	7.847	9.988	35	35.329	10	4.311
1/11/2019 14:44	3.347	8.232	9.909	35	35.329	10	4.885
1/11/2019 14:44	3.841	8.172	9.988	35	35.247	10	4.331
1/11/2019 14:44	4.684	9.196	9.951	35	35.384	10	4.512

1/11/2019 14:45	4.428	8.232	9.961	35	35.151	10	3.804
1/11/2019 14:45	4.047	8.265	9.970	35	35.384	10	4.218
1/11/2019 14:45	3.437	8.707	9.970	35	35.384	10	5.270
1/11/2019 14:45	4.180	8.214	9.954	35	35.329	10	4.034
1/11/2019 14:45	3.409	8.317	9.948	35	35.275	10	4.908
1/11/2019 14:46	4.301	9.400	9.994	35	35.467	10	5.099
1/11/2019 14:46	3.571	7.548	9.994	35	35.535	10	3.978
1/11/2019 14:46	4.177	8.635	9.939	35	35.522	10	4.458
1/11/2019 14:46	3.189	8.294	9.942	35	35.686	10	5.105
1/11/2019 14:46	3.182	7.804	9.942	35	35.576	10	4.622
1/11/2019 14:46	4.337	8.458	9.988	35	35.673	10	4.120
1/11/2019 14:47	3.809	7.940	9.950	35	35.590	10	4.131
1/11/2019 14:47	3.402	8.825	9.950	35	35.590	10	5.423
1/11/2019 14:47	4.300	8.628	9.933	35	35.632	10	4.328
1/11/2019 14:47	4.019	8.765	9.881	35	35.645	10	4.746
1/11/2019 14:47	3.468	7.961	9.961	35	35.590	10	4.494
1/11/2019 14:47	4.006	7.816	9.939	35	35.686	10	3.809
1/11/2019 14:48	4.348	8.718	9.957	35	35.535	10	4.370
1/11/2019 14:48	4.375	8.614	9.939	35	35.425	10	4.239
1/11/2019 14:48	4.264	9.410	9.881	35	35.425	10	5.145
1/11/2019 14:48	3.953	8.313	9.960	35	35.563	10	4.359
1/11/2019 14:48	4.273	8.700	9.973	35	35.494	10	4.427
1/11/2019 14:48	4.367	8.383	9.942	35	35.576	10	4.016
Average	3.908	8.402	9.955	35	35.463	10	4.494

60 SCFM Air Rate - 10 GPM Water Rate							
Time Stamp	Loop 1 Top Pressure	Loop 1 Bottom Pressure	water flow rate	air flow control (scfm)	air flow rate (scfm)	Water Flow Command	Pressure Differential
1/11/2019 14:49	7.221	11.010	9.955	60	60.742	10	3.789
1/11/2019 14:49	6.807	11.145	9.970	60	60.577	10	4.337
1/11/2019 14:50	6.444	10.665	9.945	60	60.358	10	4.221
1/11/2019 14:50	7.058	10.695	10.000	60	60.426	10	3.637
1/11/2019 14:50	6.742	11.112	9.930	60	60.440	10	4.370
1/11/2019 14:50	6.922	11.115	9.909	60	60.413	10	4.193
1/11/2019 14:50	6.869	10.827	9.994	60	60.440	10	3.958
1/11/2019 14:50	6.878	10.466	9.955	60	60.358	10	3.588
1/11/2019 14:50	6.811	11.484	9.948	60	60.317	10	4.673
1/11/2019 14:50	6.614	10.522	9.985	60	60.317	10	3.908
1/11/2019 14:51	6.619	10.626	9.947	60	60.331	10	4.006
1/11/2019 14:51	6.592	10.569	9.912	60	60.344	10	3.977
1/11/2019 14:51	6.629	10.698	9.912	60	60.344	10	4.069
1/11/2019 14:51	6.621	11.270	9.976	60	60.262	10	4.648
1/11/2019 14:51	6.618	10.776	10.003	60	60.289	10	4.157
1/11/2019 14:52	5.900	10.348	9.951	60	60.385	10	4.448
1/11/2019 14:52	6.677	10.826	9.951	60	60.207	10	4.150
1/11/2019 14:52	6.100	10.602	10.011	60	60.289	10	4.502

1/11/2019 14:52	6.510	10.773	10.019	60	60.330	10	4.263
1/11/2019 14:52	6.664	10.379	9.939	60	60.330	10	3.715
1/11/2019 14:52	7.118	11.050	9.912	60	60.330	10	3.932
1/11/2019 14:53	6.318	11.151	9.939	60	60.372	10	4.834
1/11/2019 14:53	6.964	10.538	10.000	60	60.372	10	3.574
1/11/2019 14:53	7.128	11.308	9.939	60	60.330	10	4.180
1/11/2019 14:53	7.100	11.364	9.939	60	60.317	10	4.264
1/11/2019 14:53	6.595	10.800	9.939	60	60.275	10	4.205
1/11/2019 14:53	6.691	11.011	9.939	60	60.317	10	4.320
1/11/2019 14:54	6.337	10.625	9.939	60	60.303	10	4.288
1/11/2019 14:54	6.832	11.207	9.970	60	60.166	10	4.375
1/11/2019 14:54	6.317	10.681	9.970	60	60.591	10	4.364
1/11/2019 14:54	7.268	11.374	9.995	60	60.632	10	4.106
1/11/2019 14:54	6.612	10.962	9.997	60	60.605	10	4.350
1/11/2019 14:54	6.897	10.962	9.997	60	60.632	10	4.065
1/11/2019 14:55	6.418	11.048	9.976	60	60.303	10	4.630
1/11/2019 14:55	7.075	10.757	9.973	60	60.289	10	3.682
1/11/2019 14:55	7.233	11.033	9.912	60	60.385	10	3.800
1/11/2019 14:55	6.705	11.273	9.942	60	60.275	10	4.567
1/11/2019 14:55	6.424	11.060	9.942	60	60.399	10	4.636
1/11/2019 14:56	6.241	10.466	9.942	60	60.426	10	4.226
1/11/2019 14:56	6.241	10.549	9.942	60	60.289	10	4.309
1/11/2019 14:56	6.950	10.569	9.972	60	60.344	10	3.619
1/11/2019 14:56	6.145	10.164	9.976	60	60.234	10	4.019
1/11/2019 14:56	6.431	11.060	9.957	60	60.317	10	4.628
1/11/2019 14:56	7.030	11.119	9.968	60	60.330	10	4.089
1/11/2019 14:56	6.715	10.359	9.970	60	60.234	10	3.644
1/11/2019 14:56	5.972	10.974	9.970	60	60.275	10	5.002
1/11/2019 14:57	6.704	10.801	9.912	60	60.166	10	4.097
1/11/2019 14:57	6.348	10.672	10.031	60	60.262	10	4.323
1/11/2019 14:57	6.812	11.463	9.924	60	60.303	10	4.651
1/11/2019 14:57	7.325	11.026	9.963	60	60.166	10	3.701
1/11/2019 14:57	6.470	10.716	9.979	60	60.193	10	4.246
1/11/2019 14:58	6.505	10.876	9.945	60	60.166	10	4.371
1/11/2019 14:58	7.328	11.150	9.881	60	60.179	10	3.822
1/11/2019 14:58	6.081	10.552	9.973	60	60.083	10	4.471
1/11/2019 14:58	7.082	9.646	0.031	60	60.193	10	2.564
1/11/2019 14:58	4.166	5.508	0.031	60	60.495	10	1.342
Average	6.641	10.746	9.604	60	60.340	10	4.106

7.6. SpaceClaim User Manual

The Following outlines a basic procedure for creating basic geometries for CFD simulations. They are meant to be an outline, and for more detailed instruction please consult the ANSYS Learning Hub. This Learning Hub contains both live and self-paced lectures for SpaceClaim.

All analysis systems should be built in Workbench, which allows for a step by step process from Geometry (SpaceClaim/DesignModeler or third party), Mesh, Setup (Fluent), Solution and Results (CFD Post). This tutorial is designed to be followed from the Workbench Project Schematic.

Prior to designing a model, open Workbench. Click and drag “Fluid Flow (Fluent)” from the Analysis System Toolbox to the project schematic window (Figure 41). Spaceclaim, Design Modeler, or uploading of a third-party geometric model can be completed by right-clicking on the geometry tab.

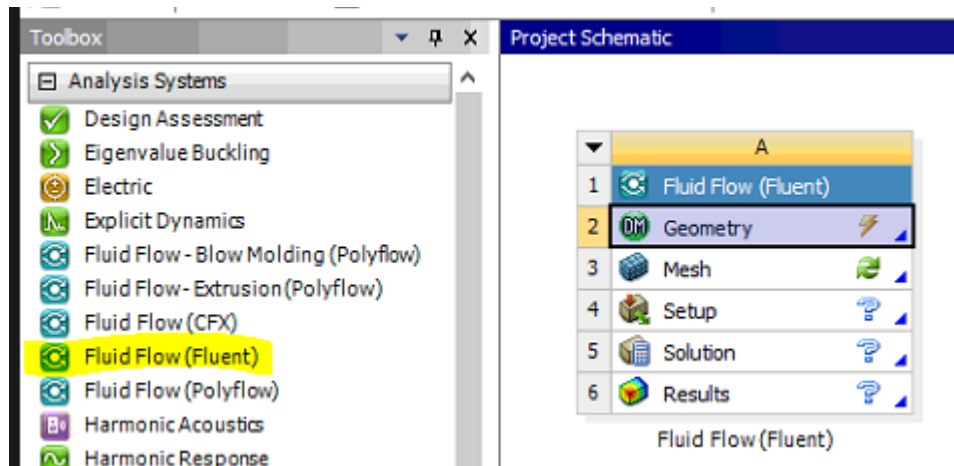


Figure 41: Workbench Window

When designing basic cylindrical models, be aware of your sketch plane and the axis directions. When inputting values such as gravity in Fluent, axis can be chosen. Therefore, it is not necessary to always assign X, Y and Z axis' traditionally (Figure 42).

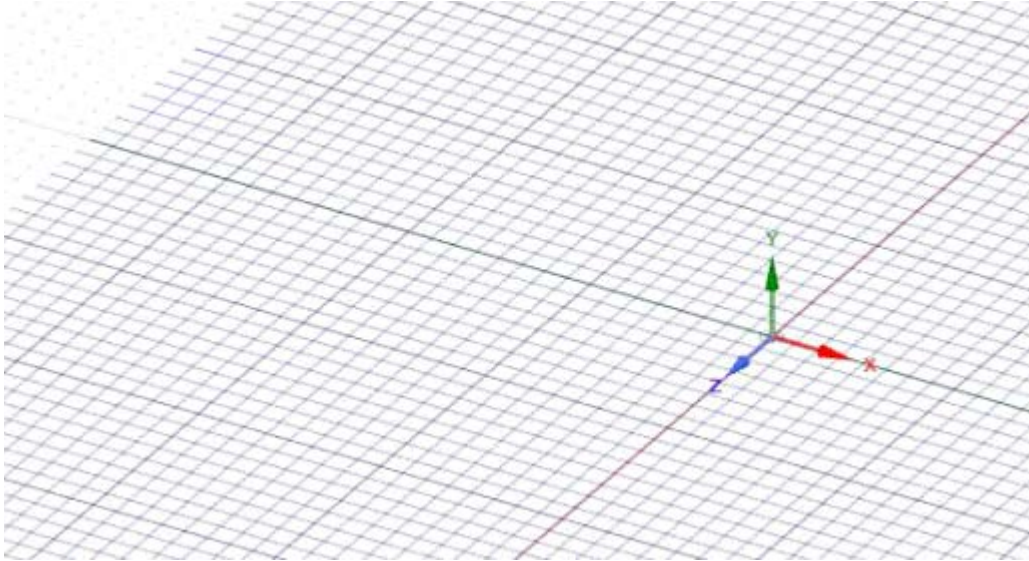


Figure 42: SpaceClaim Default Sketch Plane

Prior to beginning any design modeling, it is important to ensure that all units are set to the preferred configuration (SI, Imperial). This is available in the Spaceclaim Options menu, found in the “File” dropdown tab (Figure 43).

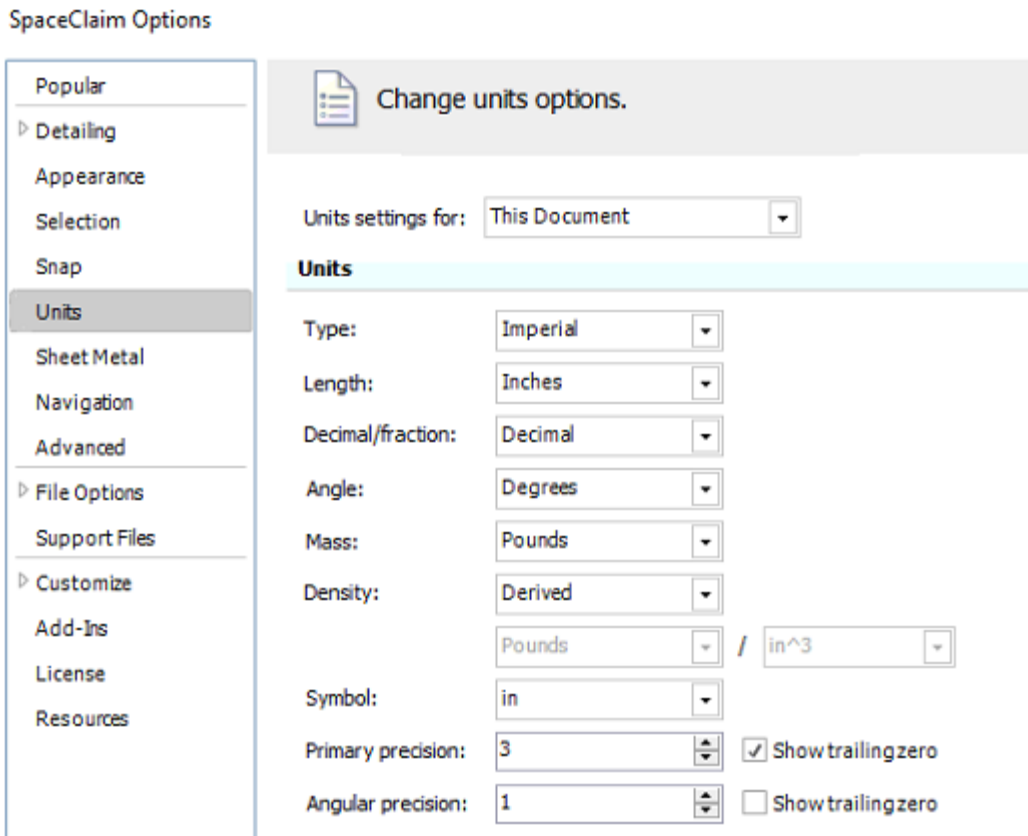


Figure 43: SpaceClaim Options Menu

To begin designing a hollow cylinder, select the “circle” function on the design tab, or press (C) on the keyboard as a shortcut. It is best to start the circle at the axis origin; however, it is possible to utilize the “cartesian dimensions button in the “structure/options-sketch” window to measure a distance from a selected point to start the circle. Circles can be sized by dragging to the preferred diameter, or by manually inputting the circle size (type the preferred value into the dimension box \emptyset) (Figure 44). If an error is made, simply press “Esc” on the keyboard to cancel the circle. This method can be repeated to create both the ID and OD of the pipe geometry being modeled.

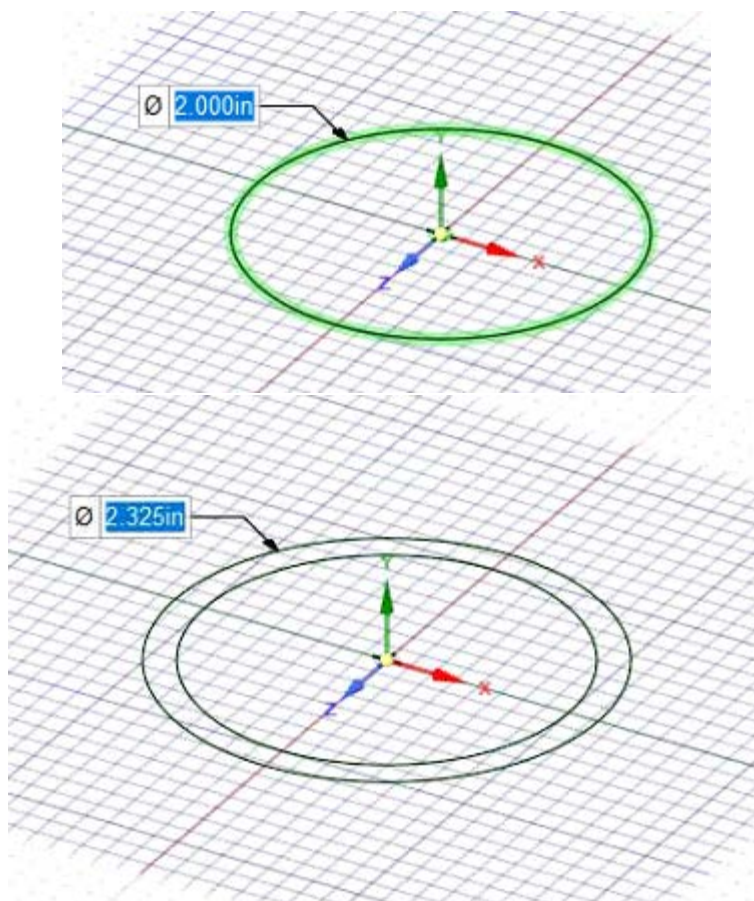


Figure 44: Circle Sketch, 2-inch ID, 2.325 OD

In order to convert the circles to a tube, the “Pull” function is selected from the Edit section of the Design tab (Figure 45). Click on the cylinder encased by the original OD and ID circles and begin to drag. Hit the space bar to allow for manual entry of the length of pull, if the length is expected to be outside of the window.

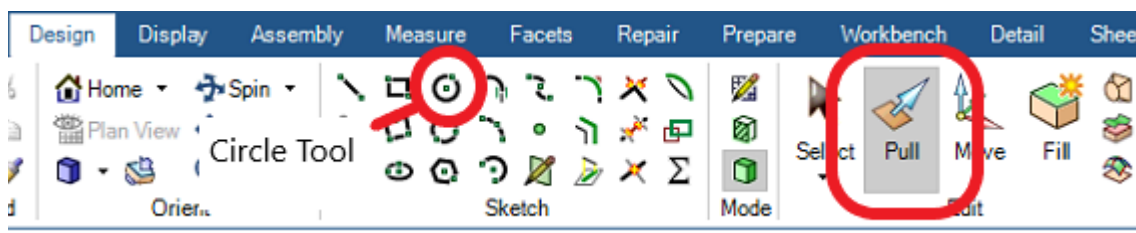


Figure 45: Design Tab

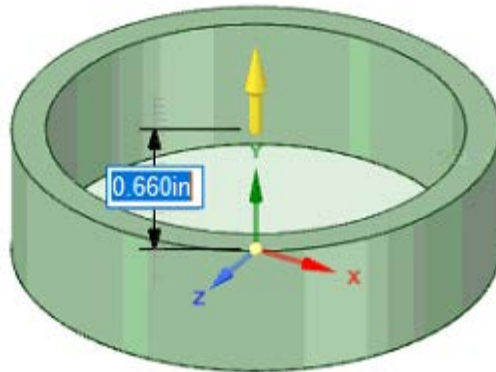


Figure 46: Cylinder pull

You can choose to delete the Surface from the Design Structure or maintain it as a cap or other type of face for CFD simulation later.

In order to obtain a volume from the cylinder, the volume extract tool must be used from the Prepare tab. Given the nature of the model, select edge loops that enclose on both ends of the cylinder, and the seed face, which is the ID surface of the cylinder. Then hit the check mark (Figure 47).

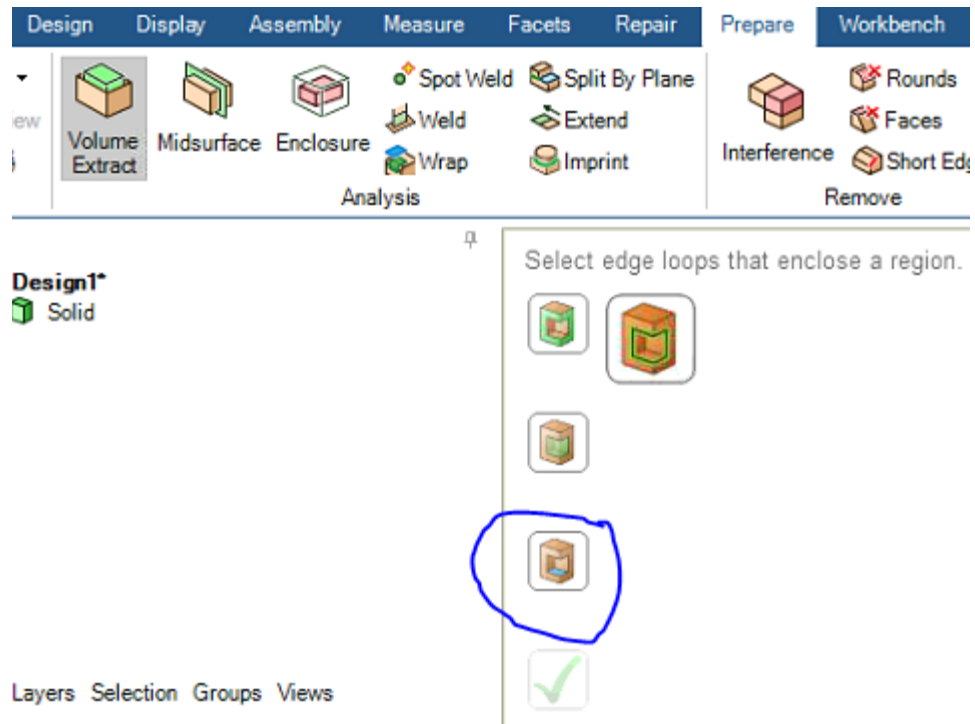


Figure 47: Volume extract tool

Material types can be assigned in either Spaceclaim, DesignModeler, or Fluent, however it is easiest to do in DesignModeler, prior to Meshing. This can be done by saving the model in Spaceclaim and closing the program to return to the Workbench window. Right click on the geometry tab and select “Edit in DesignModeler”. In the Tree Outline window, right click on the Import sub topic and select “Generate” (F5). This will import the model designed in SpaceClaim and allow for material identification. Under the parts and bodies sub-topic, both the cylinder and generated volume can be selected, and the details window below allows for the selection of either fluid or solid (Figure 48).

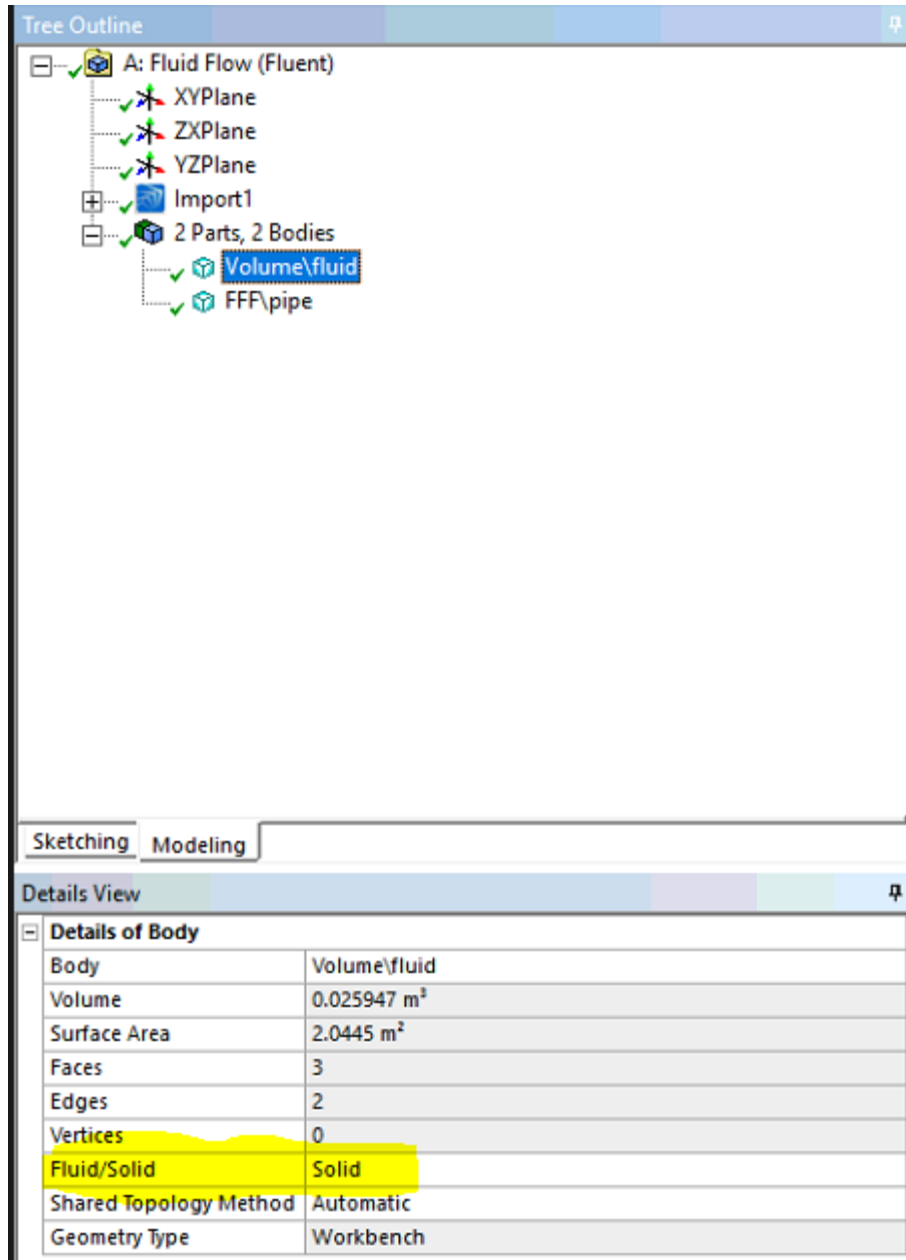


Figure 48: Material Assignment

7.7. Supplemental Drilling Fluid Data

Table XLI: Drilling Fluid Rheometer Data

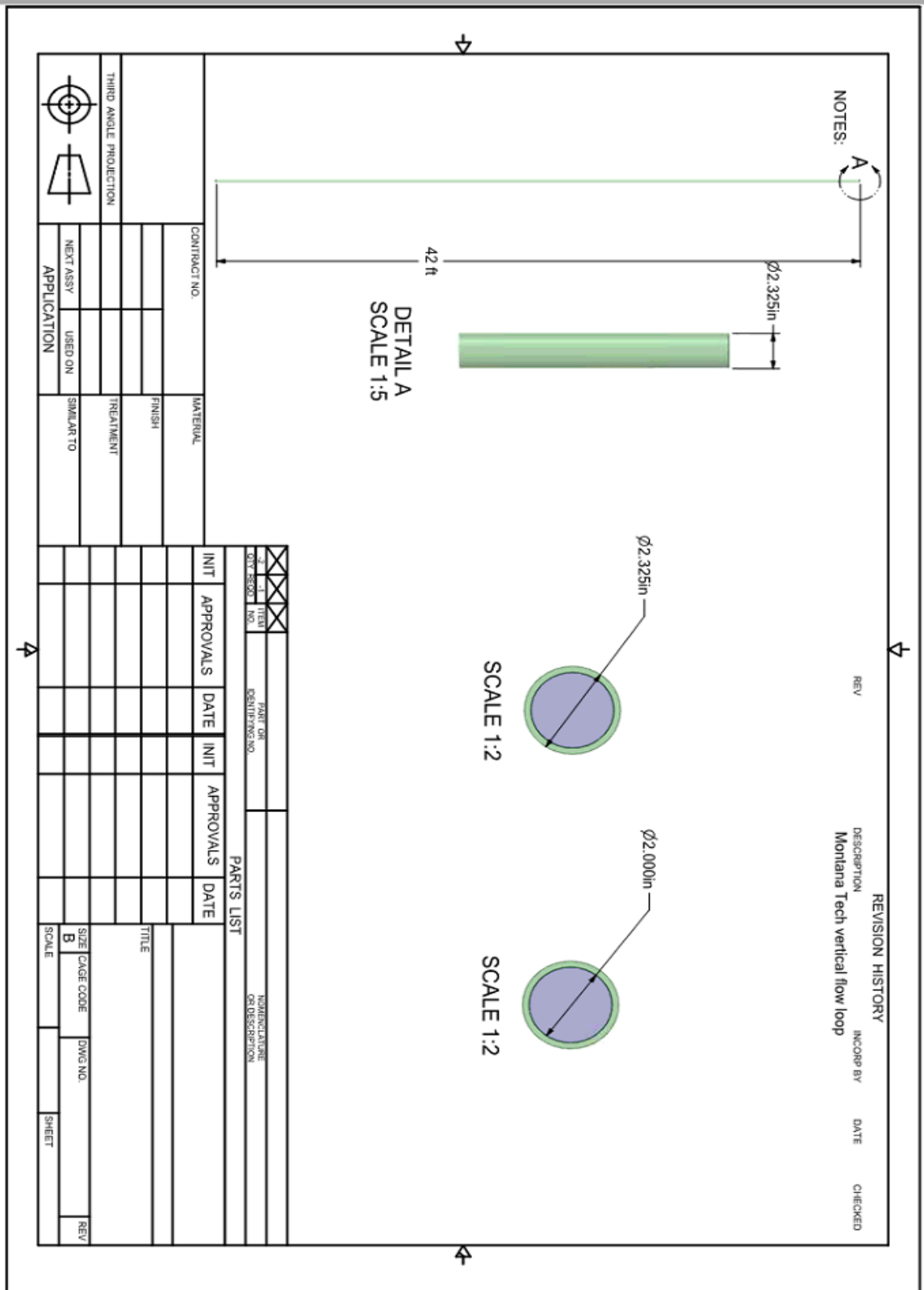
Descript.	P Temp (F)	Rheo Temp (F)	RPM 600 (°)	RPM 300 (°)	RPM 200 (°)	RPM 100 (°)	RPM 6 (°)	RPM3 (°)
Water	75	75	2.0	1.0	0.67	0.33	0.02	0.01
Light WBM	75	120	47.0	33.0	27.0	21.0	12.0	11.0
Medium WBM	75	120	63.0	40.0	32.0	22.0	12.0	11.0
Light, thin OBM	75	120	51.0	32.0	25.0	17.0	8.0	6.0
Medium OBM	75	120	74.0	46.0	35.0	4.0	0.0	.0
Heavy, thick OBM	75	120	114.0	71.0	55.0	7.0	5.0	4.0
Micronized Barite OBM	75	120	57.0	33.0	24.0	5.0	.0	.0
Cement	75	120	381.0	201.0	140.0	7.0	5.0	5.0

$$\tau_y = 2 \times \left(\frac{RPM3}{1.066} \right) - \left(\frac{RPM6}{1.066} \right) \quad (55)$$

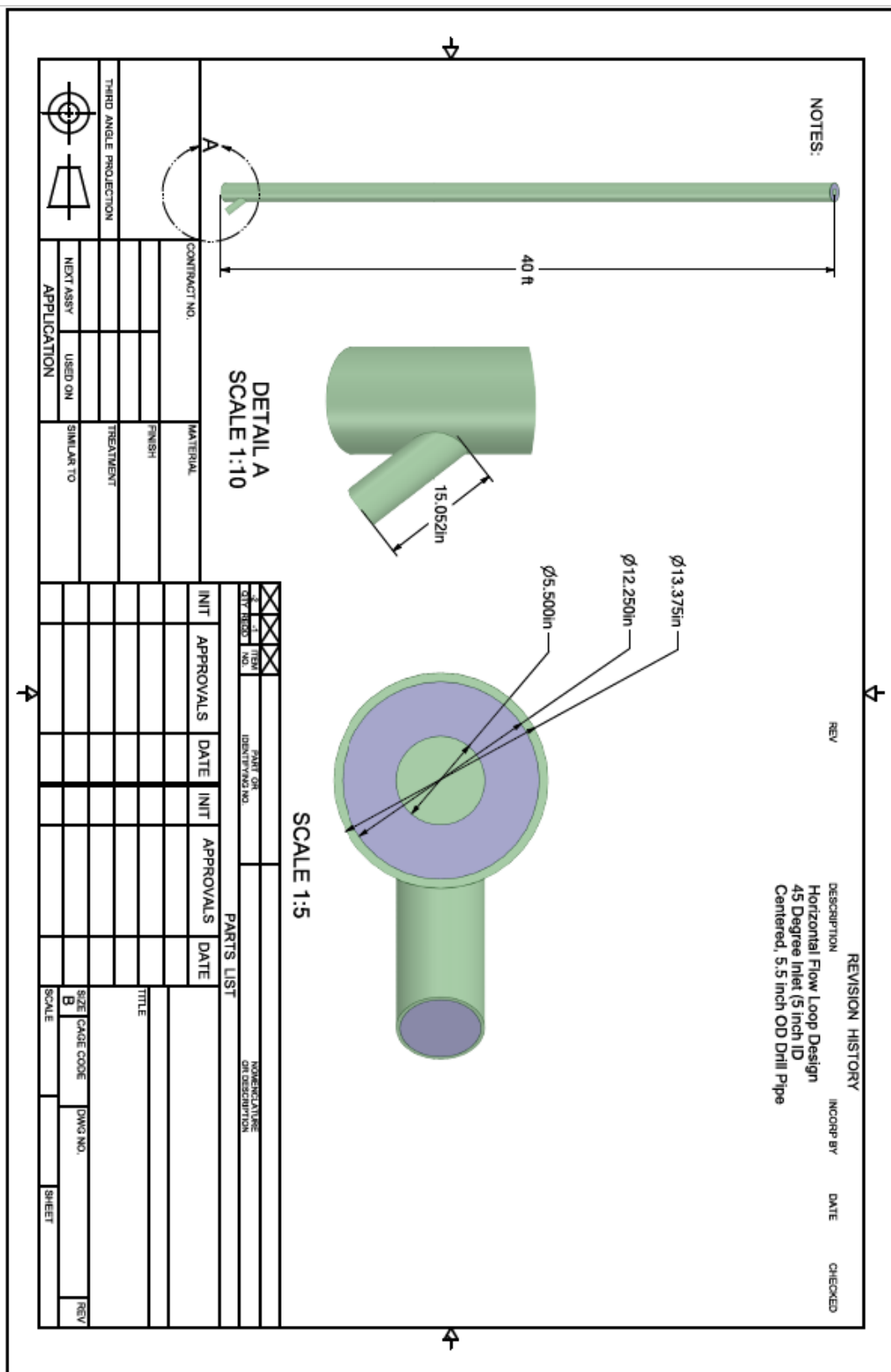
$$n = 3.32 \log_{10} \left(\left(\frac{RPM600}{1.066} - \frac{\tau_y}{1.066} \right) / \left(\frac{RPM300}{1.066} - \tau_y \right) \right) \quad (56)$$

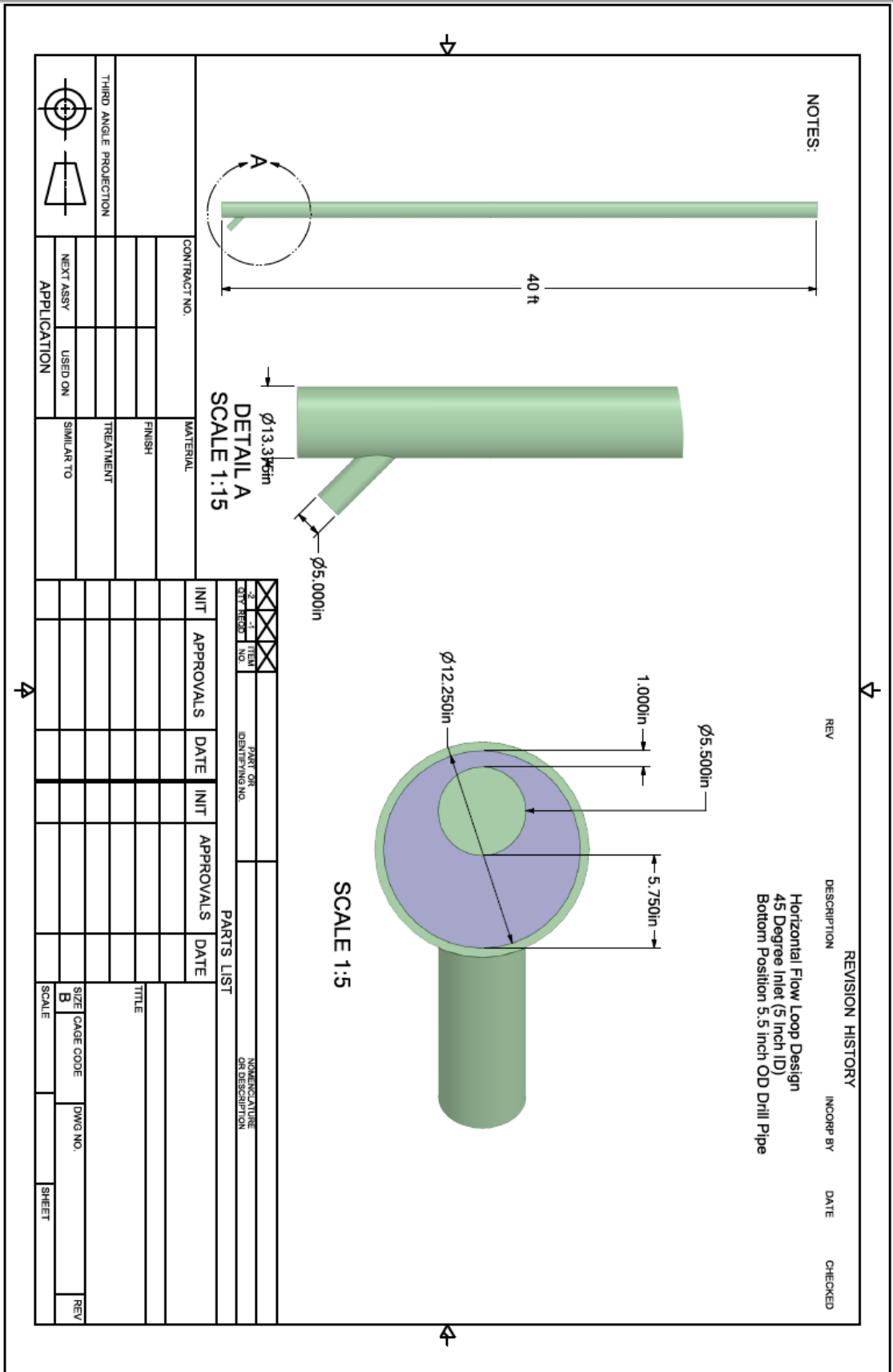
$$k = \frac{RPM300 / 1.066 - \tau_y}{511^n} \times 1.066 \quad (57)$$

7.8. Montana Tech Flow Loop Spaceclaim P&ID



7.9. Horizontal Flow Loop Inlet Spaceclaim P&ID's





7.10. Inlet/Outlet Mesh Data

First Saved	Wednesday, February 27, 2019
Last Saved	Wednesday, February 27, 2019
Product Version	19.2 Release
Save Project Before	
Solution	No
Save Project After	
Solution	No

Mechanical_Report_Files/Figure0001.png

Contents

Units

Model (A3, B3, C3)

Geometry

Parts

Materials

Coordinate

Systems

Connections

Contacts

Contact Regions

Mesh

Mesh Controls

Units

TABLE 1

Unit System	U.S. Customary (ft, lbm, lbf, s, V, A) Degrees rad/s Fahrenheit
Angle	Degrees
Rotational Velocity	rad/s
Temperature	Fahrenheit

Model (A3, B3, C3)

Geometry

TABLE 2

Model (A3, B3, C3) > Geometry

Object Name	Geometry
-------------	----------

State	Fully Defined	
Definition		
Source	D:\Users\drathgeber\ANSYS\Flow Normalization Tests\8-inch outlet tests_files\dp0\FFF-4\DM\FFF-4.agdb	
Type	DesignModeler	
Length Unit	Meters	
Bounding Box		
Length X	2.0677 ft	
Length Y	40. ft	
Length Z	1.1354 ft	
Properties		
Volume	40.863 ft ³	
Scale Factor Value		1
Statistics		
Bodies		3
Active Bodies		3
Nodes		151220
Elements		380584
Mesh Metric	None	
Update Options		
Assign Default		
Material	No	
Basic Geometry		
Options		
Parameters	Independent	
Parameter Key		
Attributes	Yes	
Attribute Key		
Named Selections	Yes	
Named Selection		
Key		
Material Properties	Yes	
Advanced		
Geometry Options		
Use Associativity	Yes	
Coordinate		
Systems	Yes	
Coordinate System		
Key		
Reader Mode		
Saves Updated File	No	
Use Instances	Yes	
Smart CAD Update	Yes	
Compare Parts On		
Update	No	

Analysis Type	3-D
Clean Bodies On Import	No
Stitch Surfaces On Import	No
Decompose Disjoint Geometry	Yes
Enclosure and Symmetry Processing	No

TABLE 3

Model (A3, B3, C3) > Geometry > Parts

Object Name	Volume\fluid	Flow Loop 40 ft 90 outlet 8 inch center drill pipe\casing	Flow Loop 40 ft 90 outlet 8 inch center drill pipe\drill pipe
State	Meshed		
Graphics Properties			
Visible	Yes		
Transparency		0.1	1
Definition			
Suppressed	No		
Coordinate System	Default Coordinate System		
Behavior	None		
Reference Frame	Lagrangian		
Material Assignment			
Fluid/Solid	Defined By Geometry (Fluid)	Defined By Geometry (Solid)	
Bounding Box			
Length X	2.0104 ft	2.0677 ft	0.45833 ft
Length Y	40. ft		
Length Z	1.0208 ft	1.1354 ft	0.45833 ft
Properties			
Volume	26.495 ft ³	7.769 ft ³	6.5995 ft ³
Centroid X	1.3664e-002 ft	2.6697e-003 ft	-4.4582e-018 ft
Centroid Y	19.747 ft	19.98 ft	20. ft
Centroid Z	-1.0131e-006 ft	7.485e-006 ft	-1.7956e-017 ft
Statistics			
Nodes		96675	13327
Elements		305296	39704
Mesh Metric	None		41218
			35584

CAD Attributes
 Color:143.143.175
 Color:143.175.143

Coordinate
 Systems

TABLE 4
 Model (A3, B3, C3) > Coordinate Systems > Coordinate System

Object Name	Global Coordinate System
State	Fully Defined
Definition	
Type	Cartesian
Coordinate System ID	0
Origin	
Origin X	0. ft
Origin Y	0. ft
Origin Z	0. ft
Directional Vectors	
X Axis Data	[1. 0. 0.]
Y Axis Data	[0. 1. 0.]
Z Axis Data	[0. 0. 1.]

Connections

TABLE 5
 Model (A3, B3, C3) > Connections

Object Name	Connections
State	Fully Defined
Auto Detection	
Generate	
Automatic	
Connection On	
Refresh	Yes
Transparency	
Enabled	Yes

TABLE 6
 Model (A3, B3, C3) > Connections > Contacts

Object Name	Contacts	
State	Fully Defined	
Definition		
Connection Type	Contact	
Scope		
Scoping Method	Geometry Selection	
Geometry	All Bodies	
Auto Detection		
Tolerance Type	Slider	
Tolerance Slider		0
Tolerance Value	0.10017 ft	
Use Range	No	
Face/Face	Yes	
Face Overlap		
Tolerance	Off	
Cylindrical Faces	Include	
Face/Edge	No	
Edge/Edge	No	
Priority	Include All	
Group By	Bodies	
Search Across	Bodies	
Statistics		
Connections		2
Active Connections		2

TABLE 7

Model (A3, B3, C3) > Connections > Contacts > Contact Regions

Object Name	Contact Region	Contact Region 2
State	Fully Defined	
Scope		
Scoping Method	Geometry Selection	
Contact	2 Faces	1 Face
Target	2 Faces	1 Face
Contact Bodies	Volume\fluid Flow Loop 40 ft 90 outlet 8 inch center drill pipe\casing	Flow Loop 40 ft 90 outlet 8 inch center drill pipe\drill pipe
Target Bodies		
Protected	No	
Advanced		
Small Sliding	Program Controlled	
Mesh		

TABLE 8
Model (A3, B3, C3)
> Mesh

Object Name	Mesh
State	Solved
Display	
Display Style	Use Geometry Setting
Defaults	
Physics Preference	CFD
Solver Preference	Fluent
Element Order	Linear
Element Size	Default (2.0035 ft)
Export Format	Standard
Export Preview	
Surface Mesh	No
Sizing	
Use Adaptive Sizing	No
Growth Rate	Default (1.2)
Max Size	Default (4.0069 ft)
Mesh Defeaturing	Yes
Defeature Size	Default (1.0017e-002 ft)
Capture Curvature	Yes
Curvature Min Size	Default (2.0035e-002 ft)
Curvature Normal Angle	Default (18.0°)
Capture Proximity	No
Bounding Box	
Diagonal	40.069 ft
Average Surface Area	32.602 ft ²
Minimum Edge Length	1.4399 ft
Quality	
Check Mesh	
Quality	Yes, Errors
Target Skewness	Default (0.900000)
Smoothing	Medium
Mesh Metric	None
Inflation	
Use Automatic Inflation	
Inflation	None
Inflation Option	Smooth Transition

Transition Ratio		0.272
Maximum Layers		5
Growth Rate		1.2
Inflation Algorithm	Pre	
View Advanced Options	No	
Assembly Meshing Method	None	
Advanced		
Number of CPUs for Parallel Part Meshing	Program Controlled	
Straight Sided Elements		
Rigid Body Behavior	Dimensionally Reduced	
Triangle Surface Mesher	Program Controlled	
Topology Checking	Yes	
Pinch Tolerance	Default (1.8031e-002 ft)	
Generate Pinch on Refresh	No	
Statistics		
Nodes		151220
Elements		380584

TABLE 9

Model (A3, B3, C3) > Mesh > Mesh Controls

Object Name	Automatic Method	Inflation
State	Fully Defined	
Scope		
Scoping Method	Geometry Selection	
Geometry Definition	1 Body	
Suppressed	No	
Method	Automatic	
Element Order	Use Global Setting	
Boundary Scoping Method		Geometry Selection
Boundary		1 Face
Inflation Option		Smooth Transition
Transition Ratio		Default (0.272)
Maximum Layers		5

Growth Rate
Inflation Algorithm

Pre

1.2

7.11. Vertical Flow Loop Mesh Data

Project

First Saved	Friday, January 25, 2019
Last Saved	Tuesday, January 29, 2019
Product Version	19.2 Release
Save Project Before Solution	No
Save Project After Solution	No

Mechanical_Report_Files
/Figure0001.png

Contents

Units

Model (B3)
Geometry
Parts
Materials
Coordinate Systems
Connections
Contacts
Contact Region
Mesh
Mesh Controls

Units

TABLE 1

	U.S. Customary (ft, lbm, lbf, s, V, A)
Unit System	Degrees rad/s Fahrenheit
Angle	Degrees
Rotational Velocity	rad/s
Temperature	Fahrenheit

Model (B3)

Geometry

TABLE 2

Model (B3) > Geometry

Object Name	Geometry	
State	Fully Defined	
Definition		
Source	D:\Users\drathgeber\ANSYS\Vertical Loop Files\Run 7 Injection design\Work Bench Base_files\dp0\FFF-1\DM\FFF-1.scdoc	
Type	SpaceClaim	
Length Unit	Meters	
Bounding Box		
Length X	0.43021 ft	
Length Y	43. ft	
Length Z	0.19375 ft	
Properties		
Volume	1.2698 ft ³	
Scale Factor Value		1
Statistics		
Bodies		3
Active Bodies		3
Nodes		158383
Elements		591406
Mesh Metric	None	
Update Options		
Assign Default Material	No	
Basic Geometry Options		
Solid Bodies	Yes	
Surface Bodies	Yes	
Line Bodies	Yes	
Parameters	Independent	
Parameter Key		
Attributes	Yes	
Attribute Key		
Named Selections	Yes	
Named Selection Key		
Material Properties	Yes	
Advanced Geometry Options		
Use Associativity	Yes	
Coordinate Systems	Yes	
Coordinate System Key		
Reader Mode Saves		
Updated File	No	
Use Instances	Yes	

Smart CAD Update	Yes
Compare Parts On Update	No
Analysis Type	3-D
Mixed Import Resolution	None
Clean Bodies On Import	No
Stitch Surfaces On Import	No
Decompose Disjoint Geometry	Yes
Enclosure and Symmetry Processing	No

TABLE 3
Model (B3) > Geometry > Parts

Object Name	pipe-body	FFF\pressure-face
State	Meshed	
Graphics Properties		
Visible	Yes	
Transparency		1
Definition		
Suppressed	No	
Coordinate System	Default Coordinate System	
Behavior	None	
Reference Frame	Lagrangian	
Thickness		0. ft
Thickness Mode		Refresh on Update
Offset Type		Middle
Material Assignment		
Fluid/Solid	Solid	Fluid
Bounding Box		
Length X	0.43021 ft	0.16667 ft
Length Y	43. ft	0. ft
Length Z	0.19375 ft	0.16667 ft
Properties		
Volume	0.33033 ft ³	0. ft ³
Centroid X	5.4529e-004 ft	-4.4225e-020 ft
Centroid Y	21.453 ft	1. ft
Centroid Z	7.6062e-007 ft	-8.4701e-019 ft
Surface Area(approx.)		2.1817e-002 ft ²
Statistics		
Nodes	78691	55

Elements		235070	45
Mesh Metric	None		
CAD Attributes			
PartTolerance:		0.00000001	
Color:143.175.143			
Color:143.143.175			

Coordinate Systems

TABLE 4
 Model (B3) > Coordinate Systems > Coordinate System

Object Name	Global Coordinate System	
State	Fully Defined	
Definition		
Type	Cartesian	
Coordinate System ID		0
Origin		
Origin X	0. ft	
Origin Y	0. ft	
Origin Z	0. ft	
Directional Vectors		
X Axis Data	[1. 0. 0.]	
Y Axis Data	[0. 1. 0.]	
Z Axis Data	[0. 0. 1.]	

Connections

TABLE 5
 Model (B3) > Connections

Object Name	Connections
State	Fully Defined
Auto Detection	
Generate Automatic	
Connection On Refresh	Yes
Transparency	
Enabled	Yes

TABLE 6
 Model (B3) > Connections
 > Contacts

Object Name	Contacts	
State	Fully Defined	
Definition		
Connection Type	Contact	
Scope		
Scoping Method	Geometry Selection	
Geometry	All Bodies	
Auto Detection		
Tolerance Type	Slider	
Tolerance Slider		0
Tolerance Value	0.10751 ft	
Use Range	No	
Face/Face	Yes	
Face Overlap Tolerance	Off	
Cylindrical Faces	Include	
Face/Edge	No	
Edge/Edge	No	
Priority	Include All	
Group By	Bodies	
Search Across	Bodies	
Statistics		
Connections		1
Active Connections		1

TABLE 7

Model (B3) > Connections > Contacts > Contact Regions

Object Name	Contact Region
State	Fully Defined
Scope	
Scoping Method	Geometry Selection
Contact	2 Faces
Target	2 Faces
Contact Bodies	pipe-body
Target Bodies	Volume\Volume
Protected	No
Advanced	
Small Sliding	Program Controlled

Mesh

TABLE 8

Model (B3) > Mesh

Object Name	Mesh	
State	Solved	
Display		
Display Style	Use Geometry Setting	
Defaults		
Physics Preference	CFD	
Solver Preference	Fluent	
Element Order	Linear	
Element Size	Default (2.1501 ft)	
Export Format	Standard	
Export Preview Surface		
Mesh	No	
Sizing		
Use Adaptive Sizing	No	
Use Uniform Size		
Function For Sheets	No	
Growth Rate		1.2
Max Size	Default (4.3003 ft)	
Mesh Defeaturing	Yes	
Defeature Size	Default (1.0751e-002 ft)	
Capture Curvature	Yes	
Curvature Min Size	Default (2.1501e-002 ft)	
Curvature Normal Angle	Default (18.0°)	
Capture Proximity	No	
Bounding Box Diagonal	43.003 ft	
Average Surface Area	5.4925 ft ²	
Minimum Edge Length	0.2618 ft	
Quality		
Check Mesh Quality	Yes, Errors	
Target Skewness	Default (0.900000)	
Smoothing	Medium	
Mesh Metric	None	
Inflation		
Use Automatic Inflation	None	
Inflation Option	Smooth Transition	
Transition Ratio		0.272
Maximum Layers		5
Growth Rate		1.2
Inflation Algorithm	Pre	
View Advanced Options	No	
Assembly Meshing		
Method	None	

Advanced		
Number of CPUs for Parallel Part Meshing	Program Controlled	
Straight Sided Elements		
Rigid Body Behavior	Dimensionally Reduced	
Triangle Surface Mesher	Program Controlled	
Topology Checking	Yes	
Pinch Tolerance	Default (1.9351e-002 ft)	
Generate Pinch on Refresh	No	
Sheet Loop Removal	No	
Statistics		
Nodes		158383
Elements		591406

TABLE 9
Model (B3) > Mesh >
Mesh Controls

Object Name	Automatic Method	Inflation	
State	Fully Defined		
Scope			
Scoping Method	Geometry Selection		
Geometry Definition	1 Body		
Suppressed	No		
Method	Automatic		
Element Order	Use Global Setting		
Boundary Scoping Method		Geometry Selection	
Boundary		1 Face	
Inflation Option		Smooth Transition	
Transition Ratio		Default (0.272)	
Maximum Layers			5
Growth Rate			1.2
Inflation Algorithm		Pre	

7.12. Test Section Flow Loop Mesh Data

First Saved	Tuesday, March 5, 2019
Last Saved	Wednesday, April 3, 2019
Product Version	19.2 Release

Save Project Before Solution No
 Save Project After Solution No

Mechanical_Report_Files/Figure0001.png

Contents

Units

Model (A3)

- Geometry
- Parts
- Materials
- Coordinate Systems
- Connections
- Contacts
- Contact Regions
- Mesh
- Mesh Controls

Units

TABLE 1

	U.S. Customary (ft, lbm, lbf, s, V, A) Degrees
Unit System	rad/s Fahrenheit
Angle	Degrees
Rotational Velocity	rad/s
Temperature	Fahrenheit

Model (A3)

Geometry

TABLE 2

Model (A3) > Geometry

Object Name	Geometry
State	Fully Defined
Definition	
Source	D:\Users\drathgeber\ANSYS\Hz Flow Loop\Test Section_files\dp0\FFF\DM\FFF.scdoc

Type	SpaceClaim	
Length Unit	Meters	
Bounding Box		
Length X	1.1104 ft	
Length Y	89.266 ft	
Length Z	1.1104 ft	
Properties		
Volume	86.143 ft ³	
Scale Factor Value		1
Statistics		
Bodies		4
Active Bodies		4
Nodes		142141
Elements		252580
Mesh Metric	None	
Update Options		
Assign Default Material	No	
Basic Geometry Options		
Solid Bodies	Yes	
Surface Bodies	Yes	
Line Bodies	Yes	
Parameters	Independent	
Parameter Key		
Attributes	Yes	
Attribute Key		
Named Selections	Yes	
Named Selection Key		
Material Properties	Yes	
Advanced Geometry Options		
Use Associativity	Yes	
Coordinate Systems	Yes	
Coordinate System Key		
Reader Mode Saves		
Updated File	No	
Use Instances	Yes	
Smart CAD Update	Yes	
Compare Parts On Update	No	
Analysis Type	3-D	
Mixed Import Resolution	None	
Clean Bodies On Import	No	
Stitch Surfaces On Import	No	

Decompose Disjoint
 Geometry Yes
 Enclosure and Symmetry
 Processing No

TABLE 3
 Model (A3) > Geometry
 > Parts

Object Name	Drill Pipe\pipe	Casing\casing	FFF\pipe
State	Meshed		
Graphics Properties			
Visible	Yes		
Transparency		1	
Definition			
Suppressed	No		
Coordinate System	Default Coordinate System		
Thickness	0. ft		0. ft
Thickness Mode	Refresh on Update		Refresh on Update
Offset Type	Middle		Middle
Behavior	None		
Reference Frame	Lagrangian		
Material			
Assignment			
Fluid/Solid	Defined By Geometry (Solid)		
Bounding Box			
Length X	0.48958 ft	1.1104 ft	0.48958 ft
Length Y	44.633 ft	88.953 ft	44.633 ft
Length Z	0.48958 ft	1.1104 ft	0.48958 ft
Properties			
Volume	0. ft ³	13.339 ft ³	0. ft ³
Centroid X	1.8474e-009 ft	5.8371e-018 ft	-3.9543e-009 ft
Centroid Y	37.76 ft	60.138 ft	82.24 ft
Centroid Z	2.1767e-006 ft	1.5802e-016 ft	1.6155e-006 ft
Surface Area(approx.)	64.288 ft ²		64.288 ft ²
Statistics			
Nodes		15673	23478
Elements		15667	14508
Mesh Metric	None		
CAD Attributes			

PartTolerance: 0.00000001
 Color:143.175.143
 Color:143.143.175

Coordinate Systems

TABLE 4

Model (A3) > Coordinate Systems > Coordinate System

Object Name	Global Coordinate System	
State	Fully Defined	
Definition		
Type	Cartesian	
Coordinate System ID		0
Origin		
Origin X	0. ft	
Origin Y	0. ft	
Origin Z	0. ft	
Directional Vectors		
X Axis Data	[1. 0. 0.]	
Y Axis Data	[0. 1. 0.]	
Z Axis Data	[0. 0. 1.]	

Connections

TABLE 5

Model (A3) >
 Connections

Object Name	Connections
State	Fully Defined
Auto Detection	
Generate Automatic	
Connection On Refresh	Yes
Transparency	
Enabled	Yes

TABLE 6

Model (A3) >
 Connections > Contacts

Object Name	Contacts
State	Fully Defined

Definition	
Connection Type	Contact
Scope	
Scoping Method	Geometry Selection
Geometry	All Bodies
Auto Detection	
Tolerance Type	Slider
Tolerance Slider	0
Tolerance Value	0.2232 ft
Use Range	No
Face/Face	Yes
Face Overlap Tolerance	Off
Cylindrical Faces	Include
Face/Edge	No
Edge/Edge	No
Priority	Include All
Group By	Bodies
Search Across	Bodies
Statistics	
Connections	2
Active Connections	2

TABLE 7
Model (A3) > Connections > Contacts > Contact Regions

Object Name	Contact Region	Contact Region 2
State	Fully Defined	
Scope		
Scoping Method	Geometry Selection	
Contact	2 Faces	1 Face
Target	2 Faces	1 Face
Contact Bodies	Drill Pipe\pipe	Casing\casing Volume\Volume
Target Bodies	FFF\pipe	
Contact Shell Face	Program Controlled	
Target Shell Face	Program Controlled	
Protected	No	
Advanced		
Small Sliding	Program Controlled	
Mesh		

TABLE 8
Model (A3) > Mesh

Object Name	Mesh	
State	Solved	
Display		
Display Style	Use Geometry Setting	
Defaults		
Physics Preference	CFD	
Solver Preference	Fluent	
Element Order	Linear	
Element Size	Default (4.464 ft)	
Export Format	Standard	
Export Preview Surface		
Mesh	No	
Sizing		
Use Adaptive Sizing	No	
Use Uniform Size		
Function For Sheets	No	
Growth Rate	Default (1.2)	
Max Size	Default (8.928 ft)	
Mesh Defeaturing	Yes	
Defeature Size	Default (2.232e-002 ft)	
Capture Curvature	Yes	
Curvature Min Size	Default (4.464e-002 ft)	
Curvature Normal Angle	Default (18.0°)	
Capture Proximity	No	
Bounding Box Diagonal	89.28 ft	
Average Surface Area	43.92 ft ²	
Minimum Edge Length	1.4294 ft	
Quality		
Check Mesh Quality	Yes, Errors	
Target Skewness	Default (0.900000)	
Smoothing	Medium	
Mesh Metric	None	
Inflation		
Use Automatic Inflation	None	
Inflation Option	Smooth Transition	
Transition Ratio		0.272
Maximum Layers		5
Growth Rate		1.2
Inflation Algorithm	Pre	

View Advanced Options	No	
Assembly Meshing		
Method	None	
Advanced		
Number of CPUs for Parallel Part Meshing	Program Controlled	
Straight Sided Elements		
Rigid Body Behavior	Dimensionally Reduced	
Triangle Surface Mesher	Program Controlled	
Topology Checking	Yes	
Pinch Tolerance	Default (4.0176e-002 ft)	
Generate Pinch on Refresh	No	
Sheet Loop Removal	No	
Statistics		
Nodes		142141
Elements		252580

TABLE 9
Model (A3) > Mesh >
Mesh Controls

Object Name	Automatic Method	Inflation
State	Fully Defined	
Scope		
Scoping Method	Geometry Selection	
Geometry Definition	1 Body	
Suppressed	No	
Method	Automatic	
Element Order	Use Global Setting	
Boundary Scoping Method		Geometry Selection
Boundary		1 Face Smooth Transition
Inflation Option		Default (0.272)
Transition Ratio		
Maximum Layers		5
Growth Rate		1.2
Inflation Algorithm		Pre

7.13. Flow Normalization Plot, 60 ft.

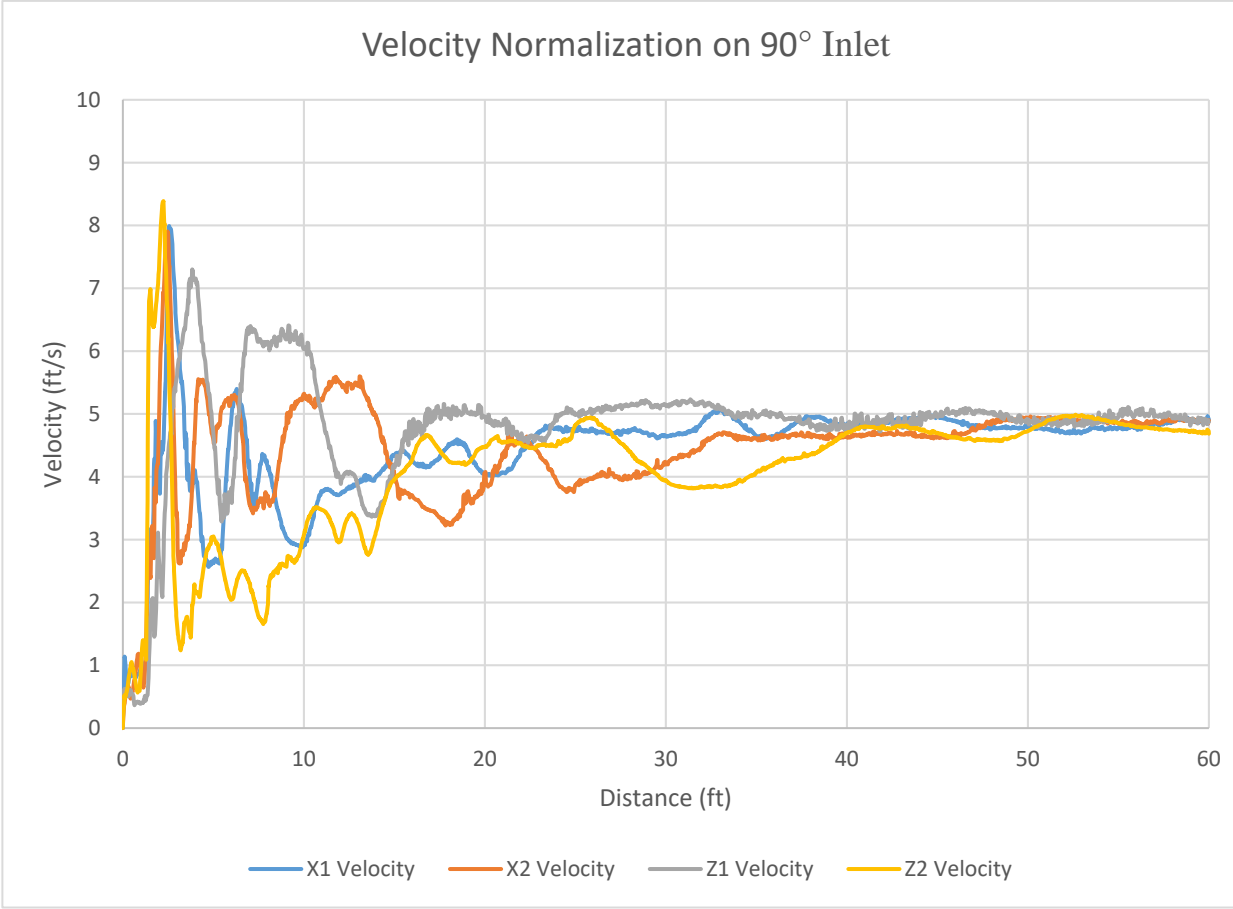


Figure 49: Velocity Normalization on 90° inlet (8-inch, 60 ft.)

7.14. Drill Pipe Data Table

Size (OD) in.	Nominal Weight (lb/ft)	Grade and Upset Type	Torsional Yield Strength ft-lb	Tensile Yield Strength lb	Wall Thickness in.	Nominal ID in.
4.5	16.6	E-75 IEU	30800	330600	0.337	3.826
4.5	16.6	E-75 EU	30800	330600	0.337	3.826
4.5	16.6	X-95 IEU	39000	418700	0.337	3.826
4.5	16.6	X-95 EU	39000	418700	0.337	3.826
4.5	16.6	G-105 IEU	43100	462800	0.337	3.826
4.5	16.6	G-105 EU	43100	462800	0.337	3.826
4.5	16.6	S-135 IEU	55500	595000	0.337	3.826
4.5	16.6	S-135 EU	55500	595000	0.337	3.826
4.5	16.6	Z-140 IEU	57500	617000	0.337	3.826
4.5	16.6	Z-140 EU	57500	617000	0.337	3.826
4.5	16.6	V-150 IEU	61600	661100	0.337	3.826
4.5	16.6	V-150 EU	61600	661100	0.337	3.826
4.5	20	E-75 IEU	36900	412400	0.43	3.64
4.5	20	E-75 EU	36900	412400	0.43	3.64
4.5	20	X-95 IEU	46700	522300	0.43	3.64
4.5	20	X-95 EU	46700	522300	0.43	3.64
4.5	20	G-105 IEU	51700	577300	0.43	3.64

4.5	20	G-105 EU	51700	577300	0.43	3.64
4.5	20	S-135 IEU	66400	742200	0.43	3.64
4.5	20	S-135 EU	66400	742200	0.43	3.64
4.5	20	Z-140 IEU	68900	769700	0.43	3.64
4.5	20	Z-140 EU	68900	769700	0.43	3.64
4.5	20	V-150 IEU	73800	824700	0.43	3.64
4.5	20	V-150 EU	73800	824700	0.43	3.64
5	19.5	E-75 IEU	41200	395600	0.362	4.276
5	19.5	E-75 EU	41200	395600	0.362	4.276
5	19.5	X-95 IEU	52100	501100	0.362	4.276
5	19.5	X-95 EU	52100	501100	0.362	4.276
5	19.5	G-105 IEU	57600	553800	0.362	4.276
5	19.5	G-105 EU	57600	553800	0.362	4.276
5	19.5	S-135 IEU	74100	712100	0.362	4.276
5	19.5	S-135 EU	74100	712100	0.362	4.276
5	19.5	Z-140 IEU	76800	738400	0.362	4.276
5	19.5	Z-140 EU	76800	738400	0.362	4.276
5	19.5	V-150 IEU	82300	791200	0.362	4.276
5	19.5	V-150 EU	82300	791200	0.362	4.276
5	25.6	E-75 IEU	52300	530100	0.5	4
5	25.6	E-75 EU	52300	530100	0.5	4
5	25.6	X-95 IEU	66200	671500	0.5	4
5	25.6	X-95 EU	66200	671500	0.5	4
5	25.6	G-105 IEU	73200	742200	0.5	4

5	25.6	G-105 EU	73200	742200	0.5	4
5	25.6	S-135 IEU	94100	954300	0.5	4
5	25.6	S-135 EU	94100	954300	0.5	4
5	25.6	Z-140 IEU	97500	989600	0.5	4
5	25.6	Z-140 EU	97500	989600	0.5	4
5	25.6	V-150 IEU	104500	1050300	0.5	4
5	25.6	V-150 EU	104500	1060300	0.5	4
5.5	21.9	E-75 IEU	50700	437100	0.361	4.778
5.5	21.9	E-75 EU	50700	437100	0.361	4.778
5.5	21.9	X-95 IEU	64200	553700	0.361	4.778
5.5	21.9	X-95 EU	64200	553700	0.361	4.778
5.5	21.9	G-105 IEU	71000	612000	0.361	4.778
5.5	21.9	G-105 EU	71000	612000	0.361	4.778
5.5	21.9	S-135 IEU	91300	786800	0.361	4.778
5.5	21.9	S-135 EU	91300	786800	0.361	4.778
5.5	21.9	Z-140 IEU	94700	816000	0.361	4.778
5.5	21.9	Z-140 EU	94700	81600	0.361	4.778
5.5	21.9	V-150 IEU	101400	874200	0.361	4.778
5.5	21.9	V-150 EU	101400	874200	0.361	4.778
5.5	24.7	E-75 IEU	56600	497200	0.415	4.67
5.5	24.7	E-75 EU	56600	497200	0.415	4.67
5.5	24.7	X-95 IEU	71700	629800	0.415	4.67
5.5	24.7	X-95 EU	71700	629800	0.415	4.67
5.5	24.7	G-105 IEU	79200	696100	0.415	4.67

5.5	24.7	G-105 EU	79200	696100	0.415	4.67
5.5	24.7	S-135 IEU	101800	895000	0.415	4.67
5.5	24.7	S-135 EU	101800	895000	0.415	4.67
5.5	24.7	Z-140 IEU	105600	928100	0.415	4.67
5.5	24.7	Z-140 EU	105600	928100	0.415	4.67
5.5	24.7	V-150 IEU	113100	994400	0.415	4.67
5.5	24.7	V-150 EU	113100	994400	0.415	4.67
5.875	23.4	E-75 IEU	58600	469000	0.361	5.153
5.875	23.4	X-95 IEU	74200	594100	0.361	5.153
5.875	23.4	G-105 IEU	82000	656600	0.361	5.153
5.875	23.4	S-135 IEU	105500	844200	0.361	5.153
5.875	23.4	Z-140 IEU	109400	875500	0.361	5.153
5.875	23.4	V-150 IEU	117200	938000	0.361	5.153
5.875	26.3	E-75 IEU	65500	533900	0.415	5.045
5.875	26.3	X-95 IEU	83000	676300	0.415	5.045
5.875	26.3	G-105 IEU	91700	747400	0.415	5.045
5.875	26.3	S-135 IEU	117900	961000	0.415	5.045
5.875	26.3	Z-140 IEU	122300	996600	0.415	5.045
5.875	26.3	V-150 IEU	131000	1067800	0.415	5.045

7.15. Drive Motor Specifications



IndraSize

Output Report 15-03-2019 13:30

Software for Sizing Drives

Version 06.04.20181026

Project data

Project name: Unnamed Axis name: Unnamed

	User adress	Ordering adress
Name:		Northwest Motion
Contact:		Patrick OConnell
Street:		815 7th Ave NW
ZIP-Code:		98027
City:		Issaquah, WA
Country:		USA
Phone number:		425-837-9150
Fax number:		425-837-9154
E-Mail adress:		poconnell@nwmotion.com

Additional text:

Application

Direct drive selection



Selected drive

Drive series	IndraDrive M HMS01	Motor family	IndraDyn A MAD
Drive type	HMS01.1N-W0054-_-_-_-	Motor type	MAD130D-0050-_-_-_-0-_-
Supply unit	IndraDrive M HMV01.1R	Mains Choke	HNL01.1R
Main voltage	3 x AC 480 V (-5%)	PWM-frequency	4 [kHz]
Maximum torque	395.64 [Nm]	Cont. torque	179.84 [Nm]
Cooling mode of motor	forced ventilation	Motor mounting:	100K
Maximum NC usable speed	3000.00 [1/min]	Motor inertia	0.1640000 [kgm ²]
Brake holding torque	0.00 [Nm]	Brake inertia	0.0000000 [kgm ²]

Inserted working points

Rotation speed	Torque	Condition
200.00	150.00	<= Mcont
0.00	0.00	<= Mmax
0.00	0.00	<= Mmax
0.00	0.00	<= Mmax

- 1 -

The Software IndraSize is a license free version. Use it at your own risk.
 IndraSize has been developed and tested with the highest possible diligence, but nonetheless, the occurrence of defects cannot be completely eliminated.
 Rexroth will not be liable for any defects that occur by the usage of this software.

IndraSize

Output Report 15-03-2019 13:30

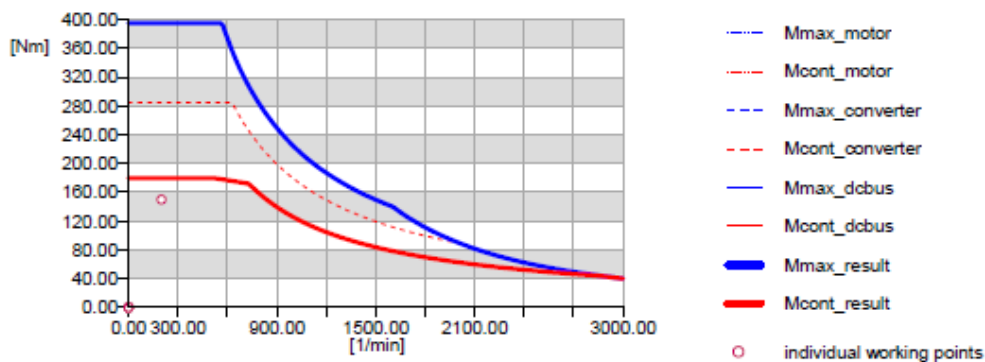
Software for Sizing Drives

Version 06.04.20181026

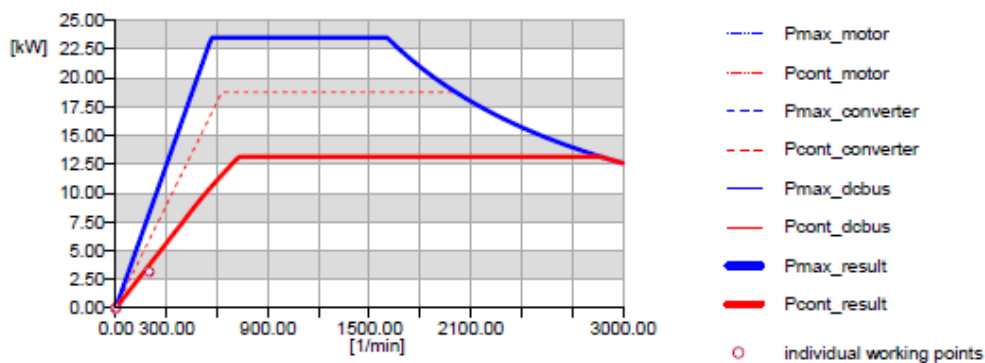
0.00	0.00	<= Mmax
0.00	0.00	<= Mmax

Drive characteristics with working points

Speed-Torque Diagram



speed-power diagram



7.16. Fully Rotational Torque Bucking Machine

Smart Solutions. Powerful Products.



Fully Rotational Torque Bucking Machine



Forum Energy Technologies' AMC fully rotational torque (RT) bucking machine is a self-contained, free-standing, hydraulically powered unit designed for fast and accurate makeup and breakout of premium and non-premium threaded tubular equipment. The machine can handle up to a maximum torque of 200,000 ft-lb tracking thread, and run in from as low as 200 ft-lb.

The unit consists of a fixed headstock and a traversing tailstock. The tailstock is available with a hinged, top-opening feature to assist with loading tools safely and efficiently. Both heads feature hydraulically controlled clamp cylinders that can go from 2 3/8 to 48 in. OD, or up to the machine's maximum diameter, without the need to change jaws between sizes. This can reduce downtime, while minimizing safety hazards associated with changing jaws manually.

The RT unit features a fully floating tail and headstock option for offset torque connections, which is available on machines up to 100,000 ft-lb and 22-in. working OD. The hydraulic system works at low working pressures, eliminating the need for high-pressure hoses and fittings; thus, reducing costs to the customer and helping ensure a safer working environment.

The RT unit is also available with other options, such as extension beams with lifting jacks to help support the tool without the use of slings, cranes or forklifts; a hinged push/pull; and an in-house designed torque control system (TCS). Specifically developed to meet industry standards, the Forum TCS provides PDF graph reports on threaded makeups, which records the accuracy and history of each makeup.

All machines are delivered with a one-year OEM warranty for peace-of-mind operation. The system is robust enough to withstand virtually every environment, including extreme heat and cold temperatures for extended and prolonged workshop use.

Forum's service parts and calibration equipment are kept in stock at strategically placed locations around the world, which allows its highly trained team of engineers and technicians to immediately respond to customer needs and support operations.

For more information, contact your nearest local Forum representative.

Smart Solutions. Powerful Products.



Fully Rotational Torque Bucking Machine

BENEFITS

- Reduces nonproductive time (NPT) with increased OD clamping range
- Increases versatility with nonmarking soft jaws for Cr connections (up to 25,000 ft-lb)
- Increases reliability since tailstock travel is driven by two rack and pinion hydraulic motors versus a chain drive system
- Decreases HSE risks since jaws do not need to be changed for varying pipe diameters, and no manual handling is required

FEATURES

- Fully floating head and tailstock to accommodate offset connections
- Forum TCS provides accurate graph reports on threaded makeups for full authentication and traceability
- Calibrated to thread manufacturers' guidelines and tolerances, in accordance with BS 7882:2008
- Oil cooler fitted as standard
- Full OEM 12-month warranty

ADDITIONAL SAFETY FEATURES

- High-visibility hose chain houses all hydraulic hoses and electric cabling
- Low-pressure working hydraulic system
- No manual changing of jaws between varying pipe diameters
- Remote clamping
- Electronic sensor fitted to open locking pin; disengages machines hydraulic clamps until pin is fully engaged

OTHER OPTIONS

- Top-open tailstock option for ease of loading
- Extensive choice of accessories
- Tailored machine layouts are available
- Customer-specific coatings

FORUM DRILLING TECHNOLOGIES

10344 Sam Houston Park Drive, Suite 300, Houston, TX 77064
1.844.525.3500 [t] / f-e-t.com/drilling / ForumDP.Sales@f-e-t.com

DRL 1094.05.2017

Protechnics



SPECTRATM is a proppant tracing technology that involves the precise injection of uniquely identifiable ZeroWash[®] tracers. Engineered for maximum diagnostic value, SPECTRATM tracers are designed to target specific stages or segments and different proppant or fluid types in hydraulic fracture and other completion operations.

ZeroWash tracers are the only means to accurately pinpoint completion placement. A post-stimulation spectral gamma ray log is run to precisely identify and quantify the ZeroWash tracer placement in the completion operation.

SPECTRATM provides direct measurements to develop and refine completion procedures and processes to optimize production.

SPECTRATM is a proven diagnostic tool in the following applications:

- Hydraulic Fracturing Treatments
- Acid Treatments
- Cementing (Channel Identification, Squeeze Coverage, Top of Cement)
- Horizontal Well Completions
- Mechanical Integrity Tests
- Conformance Control
- Polymer Treatments
- Gravel and Frac Pack Treatments
- Pre-Frac Diagnostic Testing
- Staging Performance and Efficiency
- Mechanical Integrity (Internal and External)
- Wellbore/Fracture Connectivity
- Fracture Orientation Signature (Transverse/Longitudinal)
- Perforation Cluster Strategy and Effectiveness
- Interwell/Offset Fracture Communication

SPECTRATM is essential in determining:

- Fracture Height
- Staging Performance and Efficiency
- Mechanical Integrity (Internal and External)
- Wellbore/Fracture Connectivity
- Fracture Orientation Signature (Transverse/Longitudinal)
- Perforation Cluster Strategy and Effectiveness
- Interwell/Offset Fracture Communication

ZeroWash tracers are manufactured using a patented process that fixes the non-water-soluble tracer metal into the matrix of a high strength ceramic particle. Independently tested and certified to perform in the most extreme downhole environments.

ZeroWash tracers are so effectively formed with no potential for wash-off they are:

- Client HSE Preferred
- US Nuclear Regulatory Commission (NRC) Approved
- Safe to Transport, Handle, Store and Dispose



Isotope Table

Isotope	Symbol	Form	Half Life Days	Energy Spectrum (million electron volts)	Maximum Representative Concentration	Disposal Method
Iridium 192	Ir-192	ZW, ZW/LD	74 days	0.311, 0.468, 0.609	10	ID, OD, CII
Scandium 46	Sc-46	ZW, ZW/LD	83.8 days	0.889, 1,121	10	ID, OD, CII
Antimony 124	Sb-124	ZW	60.2 days	0.603, 0.720, 1.691	7	ID, CII

ID= In-Situ Decay OD= Offshore Disposal CII= Class II Disposal

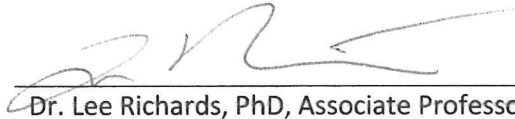
Tracer Properties and Usage

Tracer Form	Description	Mesh Size	Specific Gravity	Crush Strength (psi)	Color	Application	Concentration (mCi)
Zero Wash (ZW)	Intermediate strength bead with voids on the surface of the isotope	40/70 mesh	2.65	>8000	Various shades of grey	Designed to emulate particulate material. Primarily used to trace completion materials. Used to trace proppant, gravel, sand, and other materials.	35 to 6 mCi per 1,000 gal or 1,000 lb
Zero Wash LD (ZWLD)	Low density voided form of the isotope	40/70 mesh	1.3-1.48	1,500-2,000	Dark green to brown	Designed to emulate particulate material. Primarily used to trace completion materials. Used to trace proppant, gravel, sand, and other materials.	3 to 1 mCi per 1,000 gal or 1,000 lb
Cobalt Wire	1/8 in. wire approximately 2 cm long	N/A	N/A	N/A	N/A	Depth control cement hardware, non-ferrous tubulars, completion	1 microcurie



SIGNATURE PAGE

This is to certify that the thesis prepared by David Clifford Rathgeber entitled "Horizontal Flow Loop Design for the Study of Drill String Rotation Effects on Cuttings Transport" has been examined and approved for acceptance by the Department of Petroleum Engineering, Montana Technological University, on this 26th day of April, 2019.



Dr. Lee Richards, PhD, Associate Professor
Department of Petroleum Engineering
Chair, Examination Committee



Dr. Peter Lucon, PhD, Associate Professor
Department of General Engineering
Member, Examination Committee



Dave Nugent, Associate Professor
Department of Petroleum Engineering
Member, Examination Committee



Brandon Foster, Industry Professional
TD Unlimited
Member, Examination Committee